Brain intracellular pH in neonatal encephalopathy

Dr Cristina Uria-Avellanal

Submitted to University College London (UCL),

for the degree of Doctor of Philosophy

Department of Neonatology, EGA Institute for Women's Health

June 2022

I, Cristina Uria, confirm that the work presented in this thesis is my own. Where information has been derived from other sources, I confirm that this has been indicated in the thesis.

Abstract

Neonatal encephalopathy following hypoxia-ischaemia occurs in 1-3 per 1000 term births in the UK. Despite therapeutic hypothermia only around 30% survive with normal neurodevelopmental function. Novel, safe, and effective therapies to optimise neuroprotection following neonatal brain injury are needed.

The aim of the studies undertaken by the author is to improve the understanding of the role of brain intracellular pH (pHi) in the pathophysiology of brain injury in neonatal encephalopathy to further develop neuroprotective therapies. The first study (*Chapter 3*) analyses localised deep grey matter (DGM) pHi using phosphorus-31 spectroscopy, obtained within the first two weeks of life in 43 newborn infants with neonatal encephalopathy who underwent cooling. We observed that brain alkalosis is associated with other prognostic factors, such as severity of brain injury on magnetic resonance imaging (MRI), amplitude electroencephalography (aEEG) background pattern, seizure burden measured from raw EEG, and peak-area ratio Lactate+Threonine to N-acetyl aspartate (LacT/NAA) calculated from thalamic proton magnetic resonance spectroscopy (MRS) – current biomarker of outcome. We observed an association between an alkaline DGM pHi on day 2-15 and seizure burden. Previous research in a rodent model showed that both seizure burden and outcome improved when this rebound alkalosis was avoided (e.g., graded restoration of normocapnia or blocking the Na^+/H^+ exchangers). In a sub-study (*Chapter 4*), we also observed a trend of increased DGM perfusion (measured using pseudo-continuous arterial spin labelling (pCASL)) and DGM alkaline pHi between day 4-15 in 23 infants.

‘Luxury perfusion’ may be one of the mechanisms leading to brain alkalosis and neuronal damage. A third study (*Chapter 5*), in a pre-clinical model of neonatal encephalopathy, showed an association between the lowest level of brain tissue acidosis during hypoxia-ischaemia, the duration of acidosis under a certain threshold and its rate of recovery over the first hour after the insult and energy metabolite ratios at 1h after the insult.

Impact Statement

Neonatal encephalopathy (NE) represents a significant global burden. It is the second leading cause of neonatal mortality. Despite the introduction of therapeutic hypothermia, almost half of infants still develop adverse neurological sequelae.

The primary aim of this thesis is to to improve the understanding of the role of brain intracellular pH (pHi) in the pathophysiology of brain injury in NE to further develop neuroprotective therapies. Brain pHi can be used as a predictor of outcome in NE, but no studies have analysed this since the introduction of cooling. Furthermore, it is the first time that the relationship between brain pHi and seizures is addressed in infants with NE. This association can lead to new neuroprotective therapies alongside hypothermia, like the administration of sodium-proton exchangers inhibitors.

Recently, there has been progress in quantifying cerebral blood flow using Arterial Spin Labelling (ASL) in infants with neonatal encephalopathy secondary to hypoxia-ischaemia. Regional cerebral blood flow can be used as an additional biomarker of outcome. The aim of the second sub-study is to investigate the association between brain pHi and cerebral blood flow measured in the first two weeks of life in neonatal encephalopathy. This hasn't been explored previously and would contribute to a better understanding of the pathophysiology of NE.

Lastly, this thesis explores the impact of acidosis, its severity, duration, and recovery rate, in oxidative brain metabolism. The third study uses a well-established translational piglet model of neonatal encephalopathy to deliver a

reproducible, standardised HI injury. The availability of MR scanning throughout the hypoxic-ischaemic insult and for one-hour post-insult, allows novel insights into the pathophysiology of acidosis and secondary energy failure.

Acknowledgements

I would like to express my gratitude to my primary supervisor Prof Nicola J Robertson for the support, guidance, and encouragement throughout my PhD project. I am grateful for her expertise and constructive feedback on my thesis. I would like to thank Prof Xavier Golay for his contributions to the project, his advice and sharing his knowledge and experience. They inspired me to achieve the best I could. Without their scientific, emotional, and financial support, this work wouldn't have been completed. I am very grateful to the Buffini and the Barrington families who donated towards the purchase of the neonatal phosphorus coil used in this study. I am indebted to the medical physics team at UCLH – Dr Alan Bainbridge, David Price, Dr Magdalena Sokolska and Dr Patxi Torrealdea, for their continuous support, assistance, and encouragement. I was very fortunate to undertake this work in the neonatal unit in University College London Hospital (UCLH). I owe a huge gratitude to all doctors and nurses in this unit. I have received an incredible support from the team, particularly from Dr Giles Kendall, Dr Sean Mathieson, Dr Angela Huertas-Ceballos, Prof Neil Marlow, Dr Roxanna Gunny, Mary Dinan, Dr Subha Mitra and all UCLH neonatal imaging team members, who have directly contributed to my work in different ways. A very special thank you to all the families who consented to carry on this research on their babies. Finally, I would like to thank my family and friends for their constant support and encouragement; my parents who always believe in me no matter what, my husband and Sofia, an endless source of energy. I genuinely wouldn't have been able to go through this journey without you.

Publications resulting from this work to date

Outcome following neonatal seizures. **Uria-Avellanal C**, Marlow N, Rennie JM. Semin Fetal Neonatal Med. **2013;** 18 (4): 224-232.

Na^+/H^+ Exchangers and pHi in Neonatal Brain Injury. **Uria-Avellanal C**, Robertson NJ. Transl Stroke. Res. **2014;** 5 (1): 79-98.

Brain perfusion imaging in neonates: an overview. Proisy M, Mitra S, **Uria-Avellanal C**, Sokolska M, Robertson NJ, Le Jeune F, Ferre JC. AJNR Am J Neuroradiol **2016** Apr 14

Proton MRS thalamic Lac+Thr/tNAA peak area ratio acquired within 2 weeks of birth at 3T accurately predicts motor, cognitive and language outcome at 2 years in neonatal encephalopathy treated with therapeutic hypothermia. Mitra S, Kendall GS, Dinan M, **Uria-Avellanal C**, McKinnon K, Bainbridge A, Sokolska M, Price D, Gunny R, Huertas-Ceballos A, Golay X, Robertson NJ. Arch Dis Child Fetal Neonatal Ed. May **2018**.

Conference proceedings

Increased seizure burden in babies with deep grey matter alkalosis following neonatal encephalopathy. **Uria-Avellanal C**, Price D, Sokolska M, Mitra S, Bainbridge A, Golay X, Robertson N. EAP. Geneva, Oct **2016**.

Association between seizure burden and deep grey matter alkalosis following neonatal encephalopathy: possibility for a novel therapy for seizures? **Uria-Avellanal C**, Price D, Sokolska M, Mitra S, Golay X, Robertson N. Anglo-French Neonatal Societies Summer Meeting. Cambridge, June **2016**. (**Best oral presentation**)

An increase seizure burden is associated with deep gray matter alkalosis in babies with neonatal encephalopathy following hypoxia-ischaemia. **Uria-Avellanal C**, Price D, Sokolska M, Mitra S, Bainbridge A, Golay X, Robertson N. PAS, Baltimore. April **2016**.

Severity and duration of brain acidosis during hypoxia-ischemia correlates with recovery of brain oxidative metabolism at 1h. **Uria-Avellanal C**, Bainbridge A, Sokolska A, Ezzati M, Golay X, Robertson NJ. PAS, Baltimore. April **2016**.

Cerebral deep grey matter alkalosis in babies with neonatal encephalopathy is associated with an increased seizure burden. **Uria-Avellanal C**, Price D, Sokolska M, Mitra S, Bainbridge A, Golay X, Robertson N. ESPR/jENS, Budapest. September **2015**.

Increased ratio Taurine/Total Creatine on brain Magnetic Resonance Spectroscopy can be a predictor in Neonatal Encephalopathy. **Uria-Avellanal C**, Bainbridge A, Hassell J, Proisy M, Kendall G, Cady E, Golay X and Robertson NJ. ESPR Meeting, October **2013**

Imaging pH changes in the piglet brain after acute hypoxia-ischemia using APT-MRI. Rega M, Torrealdea F, Bainbridge A, Price D, Broad K, Fierens I, Ezzati M, Oliver-Taylor A, **Uria-Avellanal C**, Robertson N, Walker-Samuel S, Thomas D, Golay X. ESPR Meeting, October **2013**

Characterization of cerebral White Matter damage in Neonatal Encephalopathy using ^{1}H MRS, Diffusion weighted MR imaging and T2 Relaxometry. Proisy M, Kendall G, **Uria-Avellanal C**, Bainbridge A, Melbourne A, Ourselin S, Huertas A, Golay X and Robertson N. ESPR Meeting, October **2013**

And not presented by me:

Assessing brain damage after perinatal hypoxia-ischaemia using an automated protocol for combined regional analysis of the cerebral Blood Flow and MR Spectroscopy. Sokolska M, **Uria-Avellanal C**, Cardoso MJ, Proisy M, Bainbridge A, Ourselin S, Thomas D, Robertson N, Golay X. ISMRM, Toronto (Canada). May **2015**.

Combined use of arterial spin labeling and MRS to determine the severity of injury in neonates with hypoxic-ischaemic encephalopathy. Sokolska MJ, Proisy M, **Uria-Avellanal C**, Bainbridge A, Cady E, Thomas D, Robertson N, and Golay X. ISMRM Meeting **2014**.

3-tesla Proton Magnetic Resonance Spectroscopy in neonatal encephalopathy: Lactate/N-acetyl-aspartate prognosis. Badii S, **Uria-Avellanal C**, Bainbridge A, Price D, Dinan M, Kendall G, Robertson NJ. Perinatal Meeting, Harrogate (UK). June **2014**.

Predictors of Outcome in babies with Neonatal Encephalopathy treated with Therapeutic Hypothermia. Bonifacio SL, Uria-Avellanal C, Glass HC, Gunny RS, Huertas A, Barkovich J, Ferriero DM, Robertson NJ, deVries LS, Groendaal F. (Annual PAS Meeting 2013, Boston. Platform Session on Neonatal HIE. May **2013**).

Predictors of Death and Death/Withdrawal of care in an international Cohort of neonates treated with Therapeutic Hypothermia. Bonifacio SL, Uria-Avellanal C, Glass HC, Gunny RS, Barkovich J, Ferriero DM, Robertson NJ, deVries LS, Groendaal F. (Annual PAS Meeting 2012, Boston. Platform Session on Neonatal HIE: clinical aspects. April 30th, 2012)

Table of Contents

Index of Figures

Index of Tables

List of Abbreviations

ADP	Adenosine di-phosphate
aEEG	Amplitude integrated electroencephalogram
AMP	Adenosine monophosphate
ASL	Arterial spin labelling
ATP	Adenosine triphosphate
BBB	Blood Brain Barrier
BGT	Basal ganglia thalami
BS	Burst suppression
Ca^{2+}	Calcium
CBF	Cerebral blood flow
CFM	Cerebral function monitor
Cho	Choline
CLV	Continuous Low Voltage
CNV	Continuous Normal Voltage
CO2	Carbon dioxide
Cr	Creatine
CrUSS	Cranial ultrasound
CSI	Chemical shift imaging
DGM	Deep grey matter
DNV	Discontinuous Normal Voltage
DWI	Diffusion weighted imaging
EEG	Electroencephalography

EIPA	N-ethyl-N-isopropyl amiloride
EPP	Exchangeable phosphate pool
FID	Free induction decay
FiO2	Fraction of inspired oxygen
GABA	Gamma-Aminobutyric Acid
GM	Grey matter
GPC	Glycerophosphocholine
GPE	Glycerophosphoethanolamine
H^+	Proton
^1H	Proton
Hb	Hemoglobin
H_3PO_4	Phosphoric acid
HI	Hypoxia ischemia
HIE	Hypoxic ischemic encephalopathy
H_2O	Water
ISIS	Image selected in vivo
KH_2PO_4	Monopotassium phosphate
K_2PO_4	Potassium phosphate
Lac	Lactate
MIA	N-methyl-isobutyl-amiloride
mI	Myo-inositol
MRI	Magnetic resonance imaging
MRS	Magnetic resonance spectroscopy

Na^+	Sodium
NAA	N-acetyl aspartate
NaCl	Sodium chloride
NADH	Nicotinamide adenine dinucleotide
NE	Neonatal encephalopathy
NHE	Sodium-proton exchanger
NIRS	Near infrared spectroscopy
$NiSO_4$	Nickel sulphate
NMDA	N-methyl d-aspartate
NMR	Nuclear Magnetic Resonance
NO	Nitric oxide
NOE	Nuclear Overhauser Enhancement
NOS	Nitric oxide synthetase
NTP	Nucleotide triphosphate
O2	Oxygen
^{31}P	Phosphorus
PaCO2	Partial pressure arterial carbon dioxide
PaO2	Partial pressure arterial oxygen
PC	Phosphocholine
PCr	Phosphocreatine
PDA	Patent ductus arteriosus
PDE	Phosphodiesters
PEA	Phosphoryl-ethanolamine

PET	Positron emission tomography
Pet	Phosphoethanolamine
pHi	Intracellular pH
PID	Peri-infarct depolarizations
Pi	Inorganic orthophosphate
PLD	Post labelling delay
PLIC	Posterior limb of internal capsule
PME	Phosphomonoesters
PRESS	Point resolved spectroscopy
RI	Resistance index
ROI	Region of interest
ROS	Reactive oxygen species
RNS	Reactive nitrogen species
SEF	Secondary energy failure
SWC	Sleep-wake cycling
TE	Echo time
TH	Therapeutic hypothermia
TR	Repetition time

Chapter 1: General introduction

Part 1: Motivation and Thesis overview

Neonatal encephalopathy (NE) is the clinical manifestation of an abnormal neurological condition in a newborn infant associated with significant mortality and morbidity. Encephalopathy following hypoxia-ischaemia occurs in 1-3 per 1000 term births in the UK. Despite therapeutic hypothermia, only around 30% survive with normal neurodevelopmental function (1, 2). Novel, safe, and effective therapies to optimise neuroprotection following neonatal brain injury are needed.

The **motivation** of this PhD is to improve the understanding of the role of brain intracellular pH (pHi) in the therapeutic hypothermia era. This could bring new neuroprotective therapy targets. To achieve this, the following steps were undertaken:

1. Systematic literature review (*Chapter 1*), especially on brain pHi and sodium-proton exchangers.
2. Setting up the Baby Brain Study and developing the sequence to be used with a new birdcage neonatal Phosphorus coil, that allowed to measure localised deep grey matter pHi (*Chapter 2*).
3. Investigation of the relationship between localised deep grey matter (DGM) pHi measured within the first 2 weeks of life in infants with neonatal encephalopathy who underwent therapeutic hypothermia and

outcome (and other predictors of outcome); and between DGM pHi and seizure burden (*Chapter 3*).

4. Investigation of the relationship between cerebral blood flow within the first 2 weeks of life in infants with neonatal encephalopathy who underwent therapeutic hypothermia and DGM pHi (*Chapter 4*).
5. Understanding, in a preclinical model of perinatal hypoxia-ischaemia, the association between the severity, duration and rate of recovery of brain acidosis over the first hour after the insult and brain energy metabolite ratios at 1h after the insult (*Chapter 5*).

The key take-aways from the literature review in Chapter 1 were that rebound brain alkalosis was described in infants with a poor prognosis following hypoxia-ischaemia (3), but no studies have been performed in infants since the introduction of therapeutic hypothermia; that sodium-proton exchangers (NHE) have a key role in this rebound alkalosis and research both in vivo and in vitro support their potential as neuroprotectors (paper published with this literature review (4)); and that a relationship between brain pHi and seizures has been described in a rodent model of asphyxia (5), hence, the potential role for NHE inhibitors. This relationship between seizures and brain pHi hasn't been described before in neonates. Hence, my hypothesis for the study in 43 neonates in Chapter 3 was that a more alkalotic DGM pHi was associated with a more severe outcome in infants with NE who underwent therapeutic hypothermia; and that those with a more alkalotic pHi had a higher seizure burden.

I also reviewed the literature on brain perfusion following perinatal hypoxia-ischaemia and how brain perfusion can be measured using arterial spin labelling (ASL) in neonates (6). Although some studies have been done using ASL in newborn infants following hypoxia ischaemia (7, 8), it was unknown whether brain alkalosis is associated with a higher brain perfusion to certain areas. Understanding this was the aim of the sub-study of 23 infants within Baby Brain Study presented in *Chapter 4*. My hypothesis was that 'luxury perfusion' would be associated with a more alkalotic DGM pHi.

In *Chapter 2*, I discuss the preparations I had to undertake to set up the clinical research study: writing up the study protocol, application and obtaining Ethics approval and NHS approval, having a neonatal purpose-made birdcage Phosphorus-31 coil ordered, and then developing the sequence together with a Physicist from the Physics Department at UCLH. The challenges I encountered during data analysis are also discussed and how I addressed those.

Part 2: Acute hypoxic-ischaemic perinatal brain injury in the term infant

Neonatal encephalopathy (NE) is the clinical manifestation of an abnormal neurological condition in a newborn infant. It consists of an abnormal mental status (subnormal level of consciousness), abnormal tone (hypo- or hypertonia), abnormal reflexes, respiratory difficulties and often seizures (9). There are

different causes of NE with similar clinical signs at presentation: hypoxia-ischaemia, neonatal sepsis, congenital infections, metabolic conditions, neuronal migration disorders, congenital myotonic disorders, lung or airway disorders, extracranial trauma causing significant blood loss and/or pressure, genetic disorders associated with thrombotic or thrombophilic abnormalities (10). If the aetiology of encephalopathy is perinatal asphyxia, this is known as hypoxic-ischaemic encephalopathy (HIE).

Hypoxic-ischaemic encephalopathy occurs in 1-3 per 1,000 term births in the UK. It remains one of the most devastating neurologic processes throughout the world, causing morbidity and mortality, with great impact in lives and families and entailing huge financial burdens for society (11).

The decrease of oxygen supply in the blood (hypoxia) and the decreased amount of blood perfusion to the brain (ischaemia) are the causes of brain injury. The latter plays a more important role in neuronal injury, since it not only causes oxygen deprivation but it also results in deprivation of glucose, essential in cerebral metabolism (12). Hypoxia-ischaemia is commonly associated with maternal factors (hypotension or severe hypoxia), cord factors (prolapsed or occlusion), placental factors (insufficiency and abruption) and uterine factors (rupture), which are commonly known as “sentinel events” of perinatal brain injury (13). Events occurring in the postnatal period such as shock, respiratory or cardiac arrest (postnatal collapse) can also lead to hypoxic-ischaemic injury.

Evidence of intrapartum asphyxia can be found in up to 30% of the cases of HIE in developed countries (14, 15). There have been efforts since 1996 to address

the diagnosis of intrapartum asphyxia. The American College of Obstetrics and Gynaecology (2003) published the following markers of intrapartum asphyxia:

- Metabolic acidosis (pH < 7.0 and base deficit >12 mmol/L)
- Moderate or severe encephalopathy
- Cerebral palsy of spastic quadriplegia or dyskinetic type
- Exclusion of other pathologies of cerebral palsy
- Sentinel event
- Abrupt change in foetal heart rate
- Apgar score < 3 beyond 5 minutes
- Multisystemic failure within 72 hours of birth
- Imaging evidence.

The current criteria we use in clinical practice to diagnose HIE are the treatment criteria developed by the Toby (TOtal Body hYpothermia) cooling trial (16, 17), which include:

A. Infants ≥36 completed weeks gestation admitted to the neonatal unit with at least one of the following:

- Apgar score of ≤5 at 10 minutes after birth
- Continued need for resuscitation at 10 minutes after birth, including endotracheal or mask ventilation
- Acidosis within 60 minutes of birth (defined as any occurrence of umbilical cord, arterial or capillary pH < 7.00)
- Base Deficit ≥ 16 mmol/L in umbilical cord or any blood sample (arterial, venous, or capillary) within 60 minutes of birth

B. Seizures or moderate to severe encephalopathy, consisting of:

- Altered state of consciousness (reduced response to stimulation or absent response to stimulation) and
- Abnormal tone (focal or general hypotonia, or flaccid) and
- Abnormal primitive reflexes (weak or absent suck or Moro response)

C. At least 30 minutes duration of amplitude integrated electroencephalogram (aEEG) recording that shows: moderately abnormal or suppressed background aEEG activity or seizures (classifications of aEEG will be defined further below in *Part 3*).

Serious consequences follow moderate to severe NE. Therapeutic hypothermia is now the standard clinical care for moderate to severe NE in the UK and developed countries, based on 2 decades of evidence from laboratory studies (18-26), clinical trials (1, 27-31) and the endorsement from regulatory bodies (16). The first reports of hypothermia being used by clinicians in the treatment of neonatal asphyxia dates back to the 1960s and early 1970s (32-35), but was delegated to medical history for three decades due to reports of adverse effects (e.g. subcutaneous fat necrosis (36)) and the findings of increased mortality rates in preterm infants when hypothermic (37-40). In the 90s there was an increased interest in therapies aiming to prevent neuronal injury in newborn infants with signs of HIE. Wagner et al (41) present an elegant review of the pertinent animal studies that specifically address the efficacy of hypothermia in improving the outcome of perinatal asphyxia. Subsequently, meta-analysis (1, 2) of three large

pragmatic trials in newborn infants (27-29) show that therapeutic hypothermia reduces the combined rate of death and severe disability at 18 months of age with a risk ratio of 0.81 (95% CI 0.71-0.93) and a number needed to treat of 9. The outcomes at 18-24 months of age from these major therapeutic hypothermia studies are listed in *table 1-0-1*.

Follow-up data at school-age (6-8 years old) confirmed that the improved outcome of cooled babies seen at 18 months of age, was consistently seen in childhood (see *table 1-0-2)* (42-44). The Toby trial (43) showed that whole body moderate hypothermia after perinatal asphyxia resulted in improved neurocognitive outcomes in middle childhood (52% of children in the hypothermia group survived with an IQ>85 at 6-7 years of age, compared to 39% of children in the standard care group, p=0.04), and more children survived without neurologic abnormalities. They had reduced risk of cerebral palsy and of moderate-severe disability, as well as having significant better motor-function scores. The NICHD (44) showed that whole body hypothermia reduced the rate of the combined end point of death or IQ score of less than 70 at 6 - 7 years of age, compared to the children undergoing usual care but no cooling (47% vs 62%, respectively), but the differences were not significant. However, hypothermia resulted in lower death rates (28% vs 44%) and did not increase rates of severe disability among survivors (35% vs 38%).

	Coolcap (27) (N=116)	**Toby** (29) (N=163)	**NICHD** (45) (N=102)		**ICE** (30) (N=110)	**Neo-nEURO network** (31) (N=53)	
			Moderate HIE	Severe HIE			
Died or severe disability at 18 months	55% (59/108)	45% (74/163)	42% (43/102)		51% (55/107)	51% (27/53)	
						32% (6/19)	62% (21/34)
Died	33% (36/108)	26% (42/163)	24% (24/100)		25% (2/108)	38% (20/53)	
			13% (9/69)	47% (15/32)			
Severe neuromotor disability	19% (14/72)	27% (32/120)	24% (19/78)		35% (28/80)		
Bayley MDI<70	30% (21/70)	24% (28/115)	25% (19/75)		26% (19/73)		
			21% (12/57)	41% (7/17)			
Bayley PDI<70	30% (21/69)	24% (27/114)	27% (20/74)		23% (17/73)	21% (7/33)	
Cerebral palsy	32% (23/72)	28% (33/120)	19% (15/79)		27% (19/73)	13% (4/32)	
			14% (8/57)	41% (7/17)			
Bilateral cortical visual impairment	10% (7/72)	7% (8/119)	7% (5/75)		1% (1/78)	3% (1/32)	
			5% (3/60)	13% (2/15)			
Bilateral sensori-neural hearing loss	8% (5/64)	4% (4/114)	4% (3/75)		3% (2/79)	0% (0/30)	
			2% (1/50)	12% (2/17)			
Epilepsy	15% (11/72)	10% (12/116)	17% (13/77)		8% (6/79)	n/a	
			15% (9/60)	24% (4/17)			
Survival without neurologic abnormality	n/a	44% (71/163)	32% (32/100)		40% (42/97)	n/a	
			39% (26/67)	16% (5/31)			

Table 1-0-1: Outcome at 18-24 months of age in trial populations from major therapeutic hypothermia studies. This table shows the outcome for those babies who received hypothermia in the following trials: Coolcap (234 term infants with moderate to severe neonatal encephalopathy and an abnormal aEEG were assigned to either head cooling for 72h within 6h of birth with rectal temperature maintained at 34-35^{o}C (n=116) or conventional care (N=118); and primary outcome was death or severe disability at 18m)**, Toby trial** (325 infants of at least 36 weeks gestational age with perinatal asphyxial encephalopathy were randomised to either intensive care plus cooling within 6h of birth to 32.5^{o}C for 72h (n=163) or intensive care alone (n=162); and primary outcome was death or severe disability at 18m), **NICHD** (208 infants with HI encephalopathy randomised to whole body hypothermia (n=102) or control (n=106); and primary outcome was death or disability at 18-22m), **ICE** (221 infants of at least 35 weeks gestational age with peripartum HI and moderate to severe clinical encephalopathy randomised to either hypothermia to 32.5^{o}C within 6h for 72h (n=110) or standard care (n=111); and primary outcome was death or major sensorineural disability at 2 years of age), **Neo-nEURO.network** (129 term infants with clinical and EEG evidence of HI encephalopathy randomised to either whole body hypothermia to 32.5^{o}C within 6h for 72h (n=53) or control (n=37); and primary outcome was death or severe disability at 18-21m of age).

	Toby(43) (N=163)	**NICHD**(44) (N=102)
Died or severe disability at 6-7 years	48% (68/143)	41% (38/93)
Died	32% (47/145)	28% (27/97)
Moderate-severe disability	21% (21/96)	35% (24/69)
IQ score <70	n/a	27% (19/70)
IQ score <85	23% (23/98)	n/a
Attention and executive function score <70	n/a	4% (2/48)
Visuospatial score <70	n/a	4% (2/53)
Cerebral palsy	21% (21/98)	17% (12/69)
Blindness	1% (1/98)	1% (1/67)
Hearing impairment	4% (4/98)	5% (3/63)
Epilepsy	n/a	10% (7/67)
Survival without disability	68% (65/96)	41% (28/69)

Table 1-0-2: Outcome at 6-7 years of age in trial populations from two of the major therapeutic hypothermia studies. This table shows the outcome for those babies who received hypothermia in the following trials: Toby trial (325 infants of at least 36 weeks gestational age with perinatal asphixial encephalopathy were randomised to either intensive care plus cooling within 6h of birth to 32.5^{o}C for 72h (n=163) or intensive care alone (n=162); and primary outcome was survival with an IQ>85 at 6-7 years of age), **NICHD** (208 infants with HI encephalopathy randomised to whole body hypothermia (n=102) or control (n=106); and primary outcome was death or disability at 18-22m),

Part 3: Pathophysiology of hypoxia-ischaemia

From research performed in animal models of hypoxia-ischaemia, we know that within 10 min there is a decrease in pO_2 values, increase in pCO_2 and pH falls from 7.3 to 6.8 (46, 47). Physiologically the fetus will try to preserve cerebral oxygenation as much as possible and minimize energy consumption during an

acute event of hypoxia-ischaemia. The distribution of blood flow to the different foetal organs during hypoxia has been described in a sheep model (48). Blood flow tends to maintain a constant supply of oxygen to the central nervous system, heart, and adrenal glands despite hypoxia initially. When hypoxic levels become more severe, an abrupt decrease of blood flow to some viscera (e.g., kidneys and digestive tract) and to the skeletal muscle occurs. If hypoxia is maintained, lactate levels increase due to anaerobic glycolysis in the muscles. The final stage of foetal hypoxia involves a decrease of oxygen supply to all organs, including the brain and heart.

1.3.1 Mechanisms of brain injury

I have reviewed both preclinical and clinical research studies that have led to a better understanding of the pathophysiology and metabolic pathways following an acute hypoxic-ischaemic perinatal event, causing cell death and brain injury (49). Once the different mechanisms of brain injury following hypoxia-ischaemia are better understood, new targets for neuroprotection can be investigated at the different stages and pathways of neuronal injury.

Following a decrease in cerebral blood flow (CBF), various processes related to cerebral homeostasis gradually fail (50). There are reported CBF threshold levels – varying between different animal model used, the length and type of ischaemia, medications used and others – below which the brain becomes ischaemic, with the cessation of electrical function, tissue acidosis and accumulation of lactate (51).

Five main mechanisms of injury are described: energy failure and brain pH changes, release of excitatory aminoacids, calcium influx, reactive oxygen and nitrogen species, and inflammation (10, 12).

Energy failure and brain pH changes are two of the mechanisms I will focus on further in the next sections as they are at the core of these studies.

Magnetic Resonance Spectroscopy (MRS) has made a significant contribution to the understanding of the evolution of energy failure and pHi changes following hypoxia-ischaemia (52).

In infants with adverse outcome, despite adequate oxygenation and circulation, there is a decline in energy metabolites as manifested by low phosphocreatine (PCr) and nucleotide triphosphate (NTP, mainly ATP in newborn infants), and an increase in Pi, in the first days of life (53-56). An acidotic shift in brain intracellular pH (pHi) as measured by the chemical shift of Pi (see further explanations in next section) has been related with neuronal death. However, following the initial acidotic period, phosphorus-31 (^{31}P) MRS has evidenced an interesting alkaline shift in brain pHi in babies who didn't undergo therapeutic hypothermia (57). It was described that newborn infants presenting with a more severe injury pattern on brain magnetic resonance imaging (MRI) had a more alkaline brain pHi on ^{31}P MRS (3). Post-asphyxia brain alkalosis is likely to play an important role in cell death in a more delayed phase.

During the acute insult, oxidative phosphorylation metabolism is converted into anaerobic glycolysis, leading to depletion of energy molecules – such as ATP and phosphocreatine (PCr) – together with lactic acid accumulation. If the duration

and severity of ischaemia is short enough (generally described as less than 10 min of complete ischaemia although it varies depending on maturation, substrate availability, body temperature, concomitant inflammation/infection, etc.), most of the metabolic alterations are reversible (58), with restoration of metabolic levels and function. However, if the reperfusion occurs following a longer period of ischaemia, there may be an initial restoration of metabolite level, only to be followed by an additional cytotoxic cascade, the so called 'secondary energy failure' (52) over the subsequent 24-48 hours (59). This secondary energy failure process leads to irreversible changes and neuronal loss, infarction, and gliosis, characterized on MRS with low N-acetyl aspartate (NAA) levels. The neurotoxic cascade of events include breakdown of cellular function, cell swelling/lysis (secondary to a failure of the ATP-dependent Na^+/K^+ pump and hence Na^+, Cl^- and H_2O influx), passive influx of calcium (secondary to increased glutamate release and to a failure of the ATP-dependent Ca^{2+} pump to extrude calcium), release of excitatory neurotransmitters such as glutamate and aspartate from ischaemic cells, and activation of free fatty acids and free radicals, leading to acidosis and cellular necrosis occurring typically at 24-48 hours (10). Following cell death occurring during the secondary phase, there is often a chronic or tertiary phase of further progressive cell death, repair, astrogliosis, and remodelling (60, 61) during weeks or months following the initial acute brain injury.

See in *figure 1-0-1* the representation of ion transporters that regulate cytoplasmatic pH, calcium influx and the ATP production in aerobic and

anaerobic condition (49). The mechanisms of cell death may be more delayed (apoptosis) or necrosis.

The Na^+/H^+ exchangers (NHE) are a family of ion membrane transport proteins involved in maintaining a normal intracellular pH (pHi) and cell volume in many mammalians cell types, by extruding protons from, and taking up sodium ions into cells in an electroneutral manner. Excessive activation of NHE is likely to lead to alkaline shifts in pHi and increased cell death via Na^+ overload which promotes intracellular Ca^{2+} entry. A whole section reviewing the role of NHE in hypoxia-ischaemia and the evidence in neuroprotection in animal models has been included, and the important observation in a preclinical model of the association between alkaline brain pHi and seizures is discussed.

Anaerobic glycolysis during hypoxia-ischaemia will occur generating lactic acidosis (*figure 1-0-1*). Initially, this accumulation of lactate and protons (H^+) won't be detrimental, as ATP will be produced from PCr and CBF will increase because of the acidosis effect on the smooth muscle. However, if acidosis progresses it is known to contribute to brain injury by direct tissue necrosis/neuronal injury, by a further decrease in ATP (secondary to phosphofructokinase inhibition) and by loss of autoregulation (10, 12).

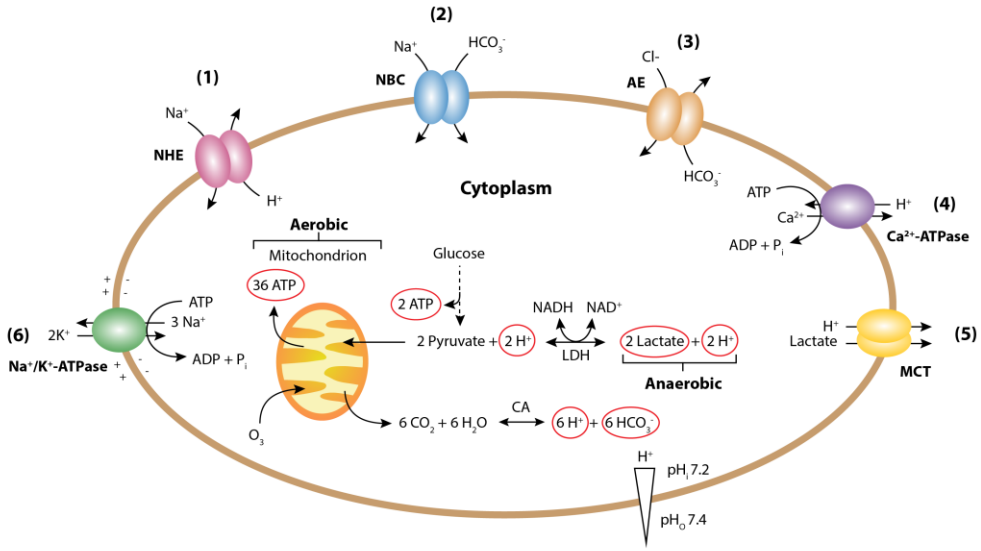

Figure 1-0-1: Ion transporters that regulate cytoplasmatic pHi
There is a tendency to acidification of the cytoplasm due to the activity of the anaerobic metabolism producing lactate from glucose and aerobic metabolism (oxidative phosphorylation in mitochondria that produce CO_2). The main transporters regulating cytosolic pH are the plasma membrane Na^+/ H^+ exchangers (NHEs) (1) and the Na^+ / HCO_3^- co-transporters (NBCs) (2). The plasma membrane Cl^-/HCO_3^- or anion exchangers (AE) (3) counterbalance these mechanisms by acidifying the cell; and plasma membrane Ca^{2+}-ATPases (4) also acidify the cytosol by exchanging cytosolic Ca^{2+} for extracellular H^+ when intracellular Ca^{2+} is elevated. Importantly in the brain after hypoxia-ischaemia, the monocarboxylate-H^+ co-transporters (MCTs) will alkalinize the cell (5). The Na^+/K^+-ATPase pumps (6) establish an inward electrochemical Na^+ gradient. CA – Carbonic anhydrase, LDH – lactate dehydrogenase, pHi: intracellular or cytosolic pH; pHo: extracellular or outside pH. Taken from (49).

The mechanisms by which intracellular calcium contributes to cell death are: i) proteases stimulation (contributing to cell membrane breakdown and to the production of proinflammatory molecules such as prostaglandins, leukotrienes and oxygen radical free), ii) lipases stimulation (caspase cascade activation, leading to cellular apoptosis), iii) activation of calcium-dependent isoforms of NOS (nitric oxide synthetase), iv) activation of ATP-dependent Ca^{2+} transporters systems, and v) calcium mediated uncoupling of oxidative phosphorylation (10).

During hypoxia-ischaemia and reperfusion, reactive oxygen and nitrogen species (ROS, RO free radicals, RNS, NO) are produced (62). Activation of new radical free can cause irreversible injury (e.g., by means of fatty acids peroxidation) and cell necrosis.

Many inflammatory pathways are activated following hypoxia-ischaemia and recent studies postulated that blood inflammatory markers, such as IL-6 and IL-16, could be used as markers of injury severity used in combination with other clinical predictors (63). It has also been well described in animal models (64, 65) that an ongoing inflammation/infection setting may aggravate brain injury.

Whether cell death is apoptotic or necrotic may depend on the severity of the insult (and its duration) (66). Necrosis generally occurs in the acute phase due to an abnormality of membrane integrity and permeability, and apoptosis is more frequent in the delayed phases of brain injury. However, a study in a rodent model of hypoxia-ischaemia explores the idea that there are not completely different pathways of cell death but there may be a "continuum" phenotype of cell death (67).

In *part 5,* I will review the loss of autoregulation occurring following hypoxia-ischaemia with increased cerebral blood flow.

Part 4: Neuromonitoring and prognostic tools in hypoxia-ischaemia

Understanding the fundamental mechanisms underlying brain injury in the newborn brain at term has rapidly advanced in recent years, providing better biomarkers of outcome. Some of the following techniques to assess brain damage have been used for decades and they still have a very relevant role (e.g., neurological clinical examination, cranial US scans, electroencephalography (EEG)). However, in the last three decades, advances in magnetic resonance imaging and spectroscopy have made a significant contribution in finding more accurate early biomarkers and helping in the understanding of mechanisms of injury.

1.4.1 Neurological examination

Clinical signs of neonatal encephalopathy typically evolve with time. Sarnat and Sarnat (68) described a scoring system of the neurological abnormalities presented by infants following hypoxia-ischaemia. The evolution of the score during the first seven days of life would be a prognostic tool. Several modifications have been published, being the Thompson score (69) largely used in the UK as part of the Toby criteria for therapeutic hypothermia trial and for daily clinical assessments during the first 4 days of life. Sedation is a limitation for these scoring systems. Cooling is standard of care currently, bringing the infant's core temperature – as soon as possible within the first 6 hours of life – to 33-

34^0C with a servo-control device (rectal temperature being monitored continuously) for 72 hours. Then slow gradual rewarming (0.25-0.5^{0}C every hour) until temperature is brought back within the normal physiological range (rectal temperature between 37-37.5^{0}C) (16). Thoresen et al. (70) reported that mild hypothermia for 24 h was not protective after hypoxia-ischaemia in unsedated piglets, although there is controversy with other animal studies (71). It is a common practice in neonatal units to sedate (plus muscle relaxant medication at times) during therapeutic hypothermia.

Once the sedative medication is stopped, it is crucial to determine the degree of neurological impairment with a full neurological examination assessing tone, posture, reflexes, respiratory thrive and feeding abilities. Dubowitz et al (72) published a comprehensive guide for neurological examination.

There are good clinical predictors of outcome, such as having attained full oral feeding by 1 week after hypothermia (73)).

1.4.2 Cranial Ultrasound scan

This technique has been in use for around fifty years and is still valuable as a bed-side tool to rule other structural causes of neonatal encephalopathy (e.g., brain abnormalities, cystic changes, or calcifications in infection), to detect early changes in brain echogenicity (e.g., oedema / areas of haemorrhage or infarction) and its evolution. In terms of imaging, the level of structural detail reached by MR imaging has relegated cranial ultrasound to a second plane (74).

Pourcelot introduced in 1976 the cerebral resistance index (RI) (75). A RI below the cut-off of 0.55 was found to predict adverse outcome in over 80% of newborn infants with hypoxic-ischaemic encephalopathy in the pre-cooling era (76). However, a low RI is significantly less predictive of poor outcome during hypothermia than normothermia (77, 78).

A low RI reflects vasodilatation or hypovolaemia, due to a loss of the brain's ability to autoregulate cerebral blood flow (CBF) (79, 80). An increased CBF is found in babies who have suffered a more severe insult. It may be that hypothermia induces cerebral vasoconstriction and hence increases RI.

1.4.3 Amplitude integrated EEG (aEEG)

Following a decrease in cerebral blood flow (CBF), various processes related to cerebral homeostasis gradually fail (50). Below a certain CBF threshold level – variable between different subjects and conditions – the brain becomes ischaemic, with cessation of electrical function, accumulation of lactate and tissue acidosis (51). If the duration and severity of ischaemia is short enough there may be restoration of the function.

Integrated amplitude electroencephalography (aEEG) – a single or two-channel EEG filtered signal rectified, smoothed and amplitude-integrated before it is written out in a semilogarithmic scale at slow speed (6cm/h) – is especially helpful at assessing the degree of insult severity and also for prognostication (81-84). The classification of the background activity can be done based on the

voltage criteria (85) or the pattern classification (86) (see *figure 1-0-2* with examples of the different patterns):

- Severe aEEG:
    - *Voltage classification*: Severely abnormal voltage (upper margin below 10 µV and lower margin below 5 µV)
    - *Pattern classification*: Flat trace (all activity below 5 µV) or Continuous Low Voltage (CLV: upper margin below 10 µV and lower margin below 5 µV)
- Moderate aEEG:
    - *Voltage classification*: Moderately abnormal voltage (upper margin above 10 µV and lower margin below or equal to 5 µV)
    - *Pattern classification*: Burst Suppression (BS: baseline activity below 10 µV with spikes up to 25 µV) or Discontinuous Normal Voltage (DNV: upper margin above 10 µV and lower margin mostly above 5 µV, with wide band and no sleep-wake cycling)
- Normal aEEG:
    - *Voltage classification*: normal voltage (upper margin above 10 µV and lower margin above 5 µV)
    - *Pattern classification*: Continuous Normal Voltage (upper margin above 10 µV and lower margin above 5 µV). A normal aEEG will also show variability with sleep-wake cycling (SWC).

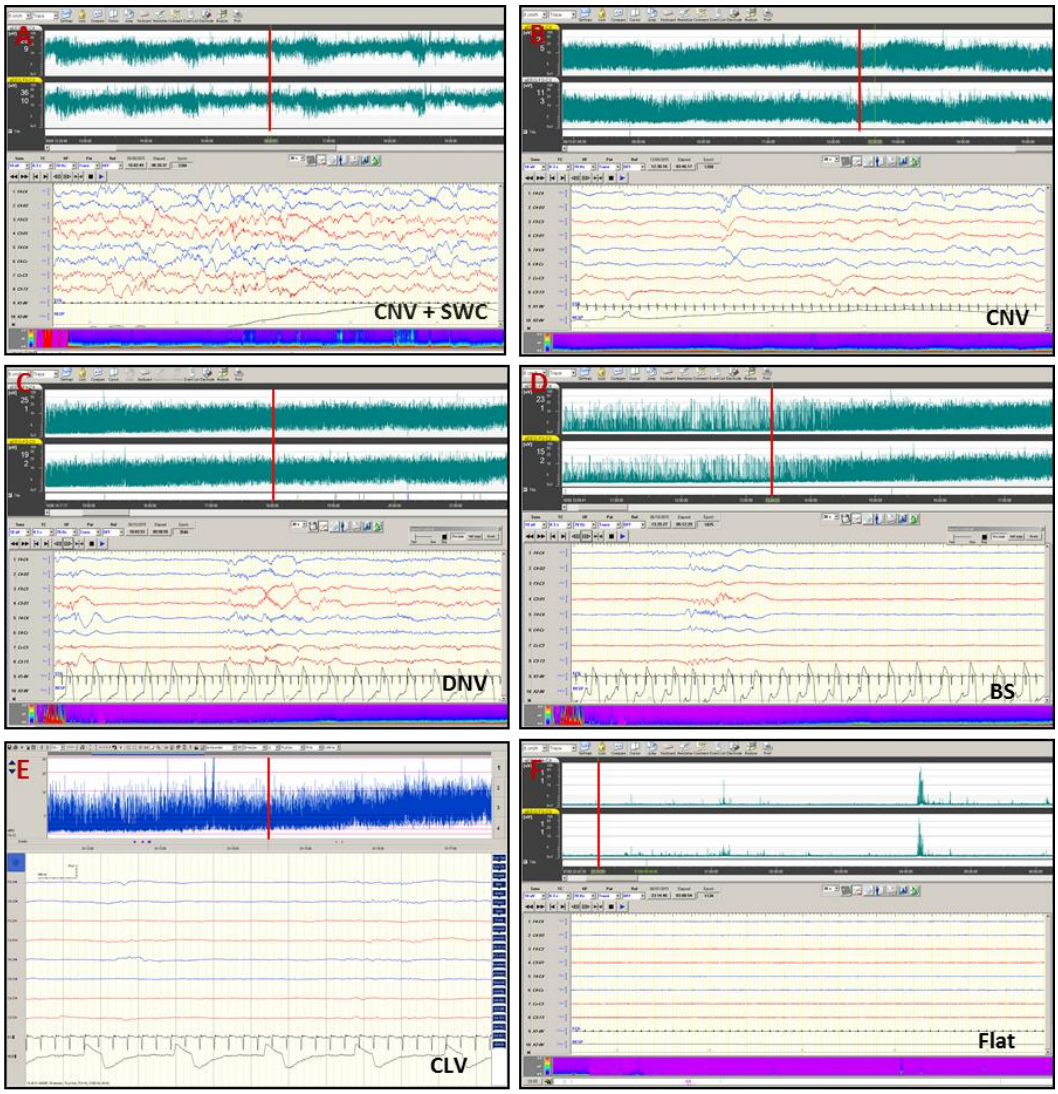

Figure 1-0-2: aEEG classification based on pattern criteria. A: Continuous Normal Voltage (CNV) with sleep wave cycling (SWC). In infants with neonatal encephalopathy generally it is not found such a well-defined pattern even at the end of cooling, not only because of the abnormal electrical activity secondary to hypoxia-ischaemia but also due to sedative medication. **B:** CNV immature or returning. This is more typically seen in infants with neonatal encephalopathy when they are normalising the EEG activity. **C:** Discontinuous Normal Voltage (DNV). **D:** Burst Suppression (BS). **E:** Continuous Low Voltage (CLV). **F:** Flat trace or isoelectric EEG. **A, B, C, D and F** are aEEG recording with the Nihon-Kohden® system (Japan) and **E** is using NicoletOne® (Care Fusion, UK). Both allow 12 lead EEG recording. On the top are, aEEG bands are found, which show the patterns classified. The red vertical line on the aEEG shows the time-period for which the machine is showing raw EEG in the bottom of the screen.

Electrical seizures can be detected even in the absence of clinical seizures. They appear as a sudden elevation of both the lower and the upper margin of the aEEG or as a paroxysmal episode of brain dysfunction of at least 10-20 seconds.

Examples of neonatal seizures from the patients included in this study can be found in *figure 1-0-3.*

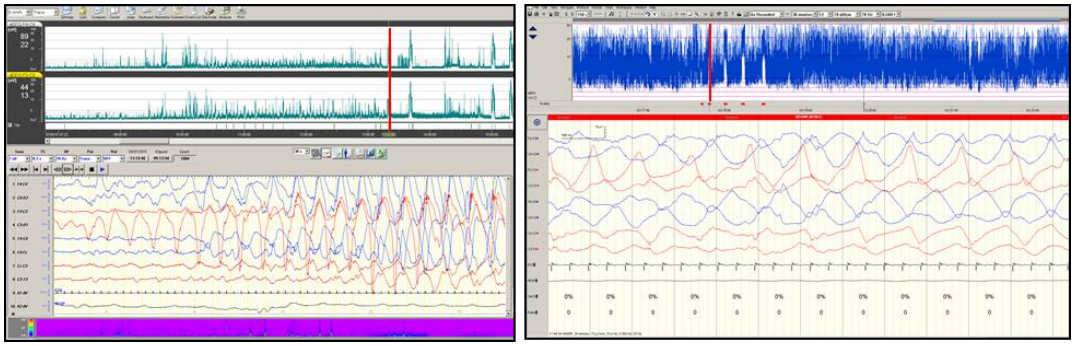

Figure 1-0-3: Examples of neonatal seizures. (Left) Start of a seizures with stereotypical sharp-waves, rythmic, recorded with the Nihon-Kohden system; and (Right) and ongoing seizure, recorded with the NicoletOne system.

For further details, there is a paper I contributed in where we describe in detail outcomes in infants with neonatal encephalopathy depending on the background pattern and on whether they had seizures or not (87). The interictal pattern of background aEEG data has been shown to correlate well with outcome (88). It is a dynamic tool contributing to assess the evolution of electrical activity at bedside in real-time, as opposed to other very specific techniques such as MR which require generally being differed a few days. Generally, the background activity will be suppressed following a significant hypoxic-ischaemic event. The rate of improvement of the background EEG is a useful prognostic tool. A fast normalisation of background activity and return to sleep-wake cycle at around 36 hours of age are considered to be associated with a good prognosis (12). It is harder to predict with aEEG in the grey/mid-area of infants with moderate HIE, but it is rare to find significant adverse neurodevelopmental disabilities when the background activity is normal. A

persistently abnormal background activity (BS, CLV or Flat trace) increases the likelihood of a poor outcome.

With the introduction of therapeutic hypothermia, it has been shown that infants with neonatal encephalopathy can take longer to normalise background patterns. If a normal background returns before or at 48 hours of life, the child is still likely to have a good prognosis (84).

Seizures have been associated with long-term effects (89). There is evidence that seizures are associated with increased risk of mortality and morbidity (90), suggesting that untreated electrical seizures may either induce neuronal injury or exacerbate existing brain injuries (91). Therapeutic hypothermia appears to reduce seizure burden (92).

When predicting outcome, it is always a matter of gathering the information from the different prognostic tools available, such as background EEG, seizure burden, neuroimaging results, and clinical examination.

1.4.4 Near Infrared Spectroscopy (NIRS)

Cerebral NIRS is another neuromonitoring tool that can be used combined with aEEG/EEG. It can continuously monitor cerebral blood flow (CBF), oxygenation, and metabolism at cot-side from the early stages after birth for a prolonged time, with the potential to provide information on the severity of the evolving injury and outcome.

NIRS uses the near infrared (NIR) region of light (700–1,000 nm) through the relatively transparent biological tissue (93), detected on electrodes (optodes)

stuck to the baby's forehead. The thinner skin and skull of newborn infants, compared to adults or older children, allows a better brain tissue depth penetration. Hemoglobin is one of the compounds (chromophores) in the human body that absorbs light. The absorption spectra of oxygenated and de-oxygenated hemoglobin (HbO2 and HHb) are different in the near-infrared region, allowing changes in concentration to be individually monitored using NIRS. Total hemoglobin (HbT = HbO2 + HHb) and hemoglobin difference (HbD = HbO2-HHb) are derived parameters and have been used to represent changes in cerebral blood volume (CBV) and cerebral oxygenation, respectively. Most commercially available NIRS systems measure cerebral oxygenation or tissue saturation (StO2, rScO2, TOI, rSO2), which is the percentage ratio of HbO2 to HbT (HbO2/ HbO2 + HHb); these systems are often referred to as brain oximeters, with different manufactures implementing different NIRS techniques to derive brain tissue saturation. At UCLH, the broadband NIRS system developed by the Engineers and Physicists at the BORL (Biomedical Optics Research Laboratory) allows to monitor changes in cytochrome C oxidase (CCO) during and after neonatal hypoxic ischaemic injury. This work is part of the doctoral thesis works of Dr Subhabratra Mitra and Dr Gemma Bale (94, 95).

In section 1.4.6, the changes in cerebral energy metabolism following hypoxia-ischaemia, during the different stages of energy failure, are discussed in detail using phosphorus spectroscopy (PMRS). Part 7 presents the changes in brain perfusion and cerebral blood flow following a significant hypoxic-ischaemic event.

1.4.5 Pattern of brain Injury on conventional MRI

MR imaging provides important information about the localization, extent, and severity of brain injury, as well as aetiology. It has been shown to be a helpful prognostic tool (96).

Patterns of hypoxic-ischaemic brain injury were previously described in pathology studies. With magnetic resonance imaging (MRI) they are now illustrated in great detail and resolution in vivo in newborn infants (97, 98).

In the 1950s-1970s the two main patterns of injury on MRI were described in a primate model: the injury pattern associated with acute total asphyxia (99) and with chronic partial asphyxia (46, 100). These two main patterns are described below *(Figure 1-0-4).*

The pattern of injury can predict neurodevelopmental outcome. MRI changes, on conventional imaging (T1 and T2-weighted images), are at their most obvious between 1 and 2 weeks from birth. Very early imaging during the first week may be useful to make management decisions in ventilated neonates. However, brain abnormalities may still be subtle during the first few days of life using conventional sequences. In these early days, it is crucial to use the Diffusion-weighted imaging (DWI) to detect ischaemic tissue in the neonatal brain, with decreased mean diffusivity (MD) ratios in the ischaemic areas within the first 7 days of life (96). In infants who underwent therapeutic hypothermia, the return of MD to normal (pseudo-normalization) occurred after the tenth day as compared to 6–8 days in the pre-cooling group**.** Infants with the most severe

injury demonstrated greater reduction in MD, but no difference in time to pseudo-normalization (101).

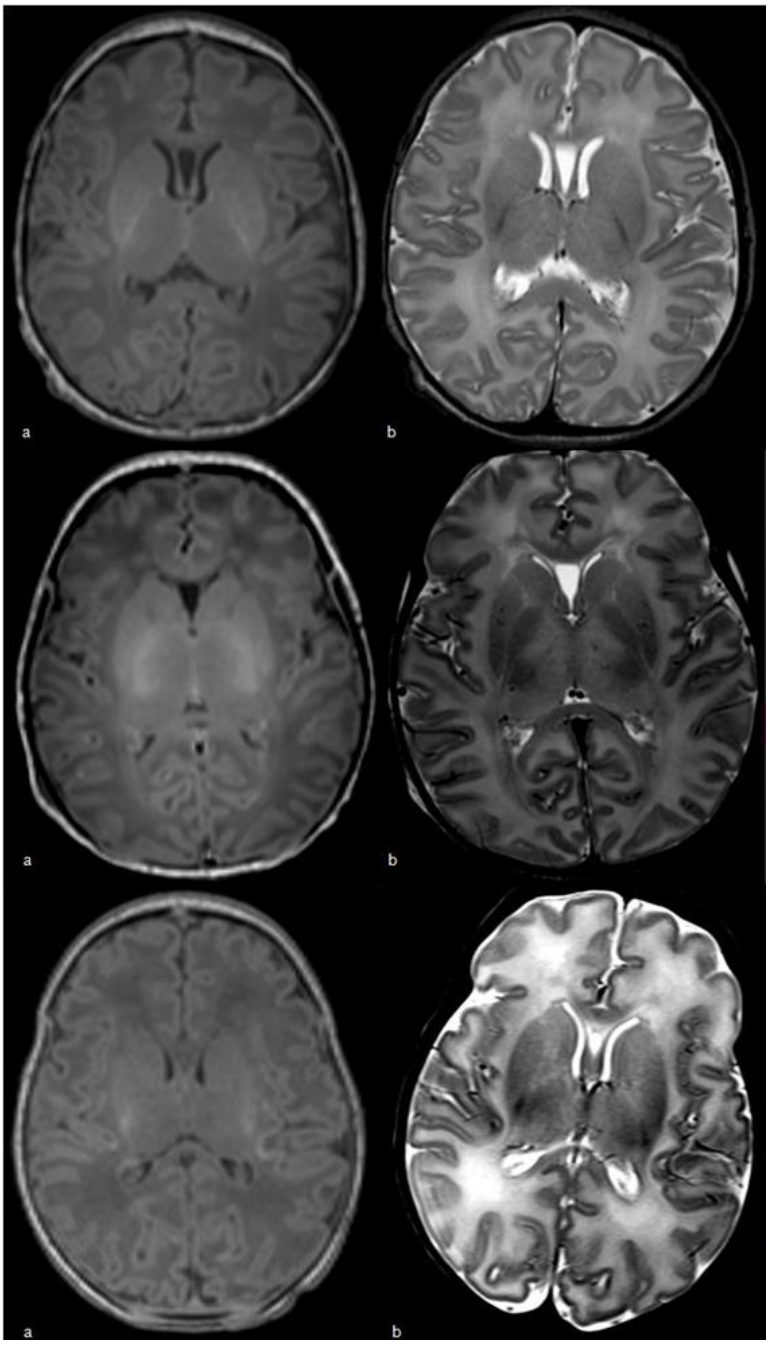

Figure 1-0-4: Patterns of brain injury

First row: infant with normal intracranial appearances on day 5 of age after mild HIE (3-Tesla Philips®): a) Axial T1-weighted (w) MPRAGE image; and b) Axial T2-w 2D 3mm image.

Second row (3-Tesla Philips®): 2-day-old infant with a predominant BGT pattern of brain injury (infarctions of basal ganglia, thalami and perirolandic cortices) with a) Axial T1-w MPRAGE; and b) Axial T2-w 2D 3mm.

Third row (1.5-Tesla Philip Philips®): 4-day-old infant with a predominant watershed injury pattern following HIE (areas of cerebral cortical infarction affecting the insular cortices, frontal, temporal occipital lobes, some of which is in anterior and posterior arterial watershed territory): a) Axial T1-w; b) Axial T2-w axial 2D 3mm. Thalamus is relatively preserved.

Predominant basal ganglia–thalamus pattern (BGT) is the most frequent pattern in 'acute near-total asphyxia', affecting bilaterally the central grey nuclei (ventrolateral thalami and posterior putamina) and peri-rolandic cortex. The hippocampus and brainstem can also be involved. As described in the first section, this pattern of injury is most often seen following an acute sentinel event, such as uterine rupture, placental abruption or prolapsed cord (13). The high metabolic rate and increased concentration of NMDA receptors in the BGT make these structures very susceptible to acute perinatal HI injury (102). Injury to the BGT will be more likely to lead to motor problems (e.g. cerebral palsy) and others (visual and hearing impairment, later seizures, behavioural difficulties and cognitive impairment) described elegantly by Martinez-Biarge et al (103). The severity of the BGT lesions is the best predictor of motor problems. The signal intensity of the PLIC (posterior limb of the internal capsule) is the best predictor of the ability to walk at 2 years of age.

Watershed predominant pattern of injury typically follows 'prolonged partial asphyxia'. The areas susceptible to injury are vascular watershed zones – border zones between the major cerebral arteries: anterior–middle cerebral artery and posterior–middle cerebral artery; and at the depth of the sulci. This will affect white matter and in more severe cases the overlying cortex. The lesions can be uni- or bilateral, anterior and/or posterior. The loss of the cortical ribbon can be detected on conventional MRI (104, 105). These lesions may become cystic, atrophic or develop gliosis (106). Hypotension, infection, and hypoglycaemia can be associated as aetiological factors (107). Cognitive deficits are associated

predominantly with a watershed pattern of injury – often without functional motor deficits. Cognitive impairments include memory difficulties, visual–motor or visual–perceptive dysfunction, or increased hyperactivity (108-112).

Global pattern of injury typically follows a very severe neonatal encephalopathy, and the condition tends to be fatal. MRI can show subcortical white matter and cortex involvement.

1.4.6 Cerebral energy metabolism following perinatal hypoxia-ischaemia

Magnetic Resonance Spectroscopy (MRS) has been used to study brain energy metabolism non-invasively. Phosphorus-31 (^{31}P) and proton (^{1}H) MRS have contributed with unique information over the last thirty years on cerebral energy metabolism during the evolution of brain injury following hypoxia-ischaemia in the newborn infant (54), neonatal rat (113) and the newborn piglet (52, 114) (*Figure 1-0-5 and 1-0-6)*.

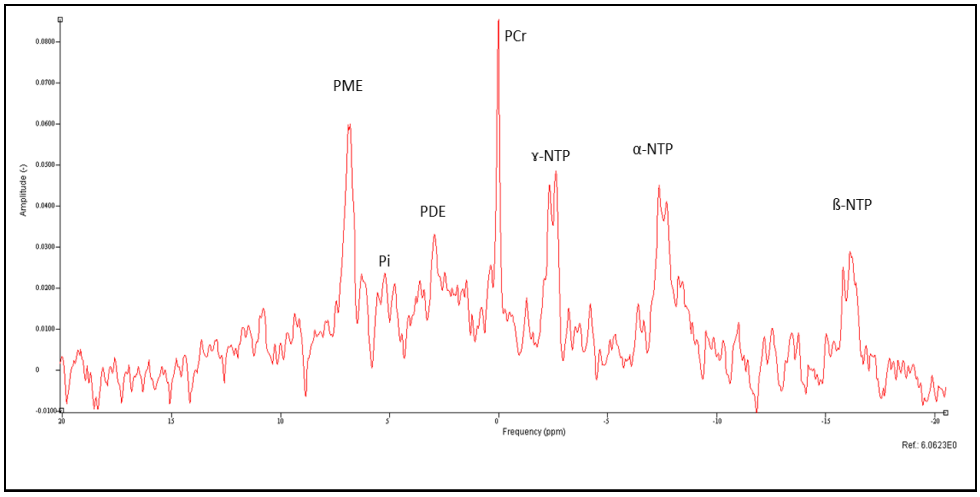

Figure 1-0-5: 31P MRS spectra from deep grey matter of a newborn infant following mild HIE. It provides in vivo information on tissue bioenergetics and pH. The metabolites are: **PME:** Phosphomonoesters (PEt: phosphoethanolamine and PC: phosphocholine); **Pi**: inorganic phosphate (product of ATP breakdown and generally a summed peak of HPO_4^- and $H_2PO_4^-$); **PDE**: phosphodiesters (**GPC:** glycerophosphocholine and **GPE**: glycerophosphoethanolamine); **PCr**: phosphocreatine (high energy buffer compound); **NTP**: nucleotide triphosphate (mainly ɣ-, α- and ß-ATP, central intermediate of energy metabolism).

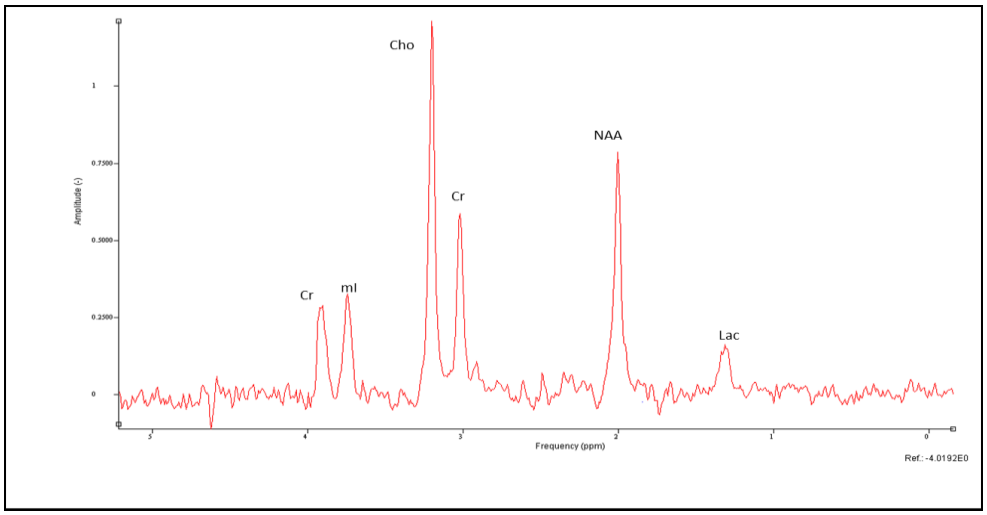

Figure 1-0-6: 1H MRS Spectra (PRESS, TE 288ms) on the left thalamus of the BGT of a newborn infant following mild HIE. It provides in vivo information on tissue metabolism and neuronal death. The metabolites are: mI: **myo-inositol** (glial cell marker and osmolyte hormone receptor mechanisms); **Cho:** choline (cell membrane marker); **Cr**: creatine (energy metabolism); **NAA**: N-acetyl aspartate (main neuronal marker); **Lac:** Lactate (product of anaerobic glycolysis). The water suppression technique is used with PRESS pulse sequence addition (PointRESolved SpectroScopy, which refocuses the spins with a 180° RF pulse like a spin echo).

Proton (^{1}H) MRS has been used in neonates since the early 1990s (115, 116). Due to the greater sensitivity of the ^{1}H nucleus, compared to ^{31}P, data can be obtained from smaller regions of the brain using proton spectroscopy. Using long echo times (≥ 136 ms), the following metabolites can be demonstrated: creatine and phosphocreatine as a single peak (Cr), choline (Cho), *N*-acetyl aspartate (NAA) and—when present—lactate (Lac) and 1,2-propandiol (result of medication such as phenobarbitone). When shorter echo times are used, myo-inositol, taurine and the combined glutamate–glutamine–GABA peak can be measured (117). Given the large amounts of water in the neonatal brain, high-quality water suppression is essential for ^{1}H MRS. The concentration of the above metabolites is in the millimolar range. Absolute quantification of metabolites is difficult, therefore metabolite ratios such as Lac/NAA, NAA/Cho,

NAA/Cr or Cho/Cr are used instead (118). From ^{1}H MRS data, in infants with NE it is of particular interest cerebral lactate, a marker of anaerobic metabolism, and N-acetyl-aspartate (NAA), an abundant amino acid found mostly in neuronal bodies acting as a marker of neuronal integrity (119-121). Cerebral lactate rises and NAA falls during transient hypoxia-ischaemia; these metabolites return almost to baseline levels after successful resuscitation, only to be followed by a secondary increase in lactate and slower reduction in NAA in the hours that follow. An example of ^{1}H MRS in a normal baby and a baby following severe hypoxia-ischaemia can be found in *figure 1-0-7.* Currently, the most sensitive and specific biomarker of long-term neurodevelopmental outcome in infants with neonatal encephalopathy has been shown to be the peak area ratio of Lac/NAA in the ventrolateral nuclei of the left thalamus at TE 288 ms, between day 5 and 14 of life. This meta-analysis gathers the data from 32 studies with 860 infants with neonatal encephalopathy in total (122). Azzopardi et al (123), also confirmed in the TOBY-Xenon study that this biomarker was a good predictor of outcome after neuroprotective therapy. More recently, in a cohort of 55 infants with neonatal encephalopathy, it was shown that BGT Lac/NAA within 14 days, using an optimised metabolite fitting (Tarquin) with threonine and total NAA on ^{1}H MRS at 3T accurately predicts 2-year motor, cognitive and language outcome and may be a marker directing decisions for therapies after cooling (124). There has been also studies in healthy controls and preterm babies (125).

^{31}P MRS was one of the first MRS techniques used in neonates more than three decades ago (126). It provides complementary information to ^{1}H MRS. Generally,

for ^{31}P MRS in neonates, spectra are collected from large regions of brain. With this technique, metabolites such as high energy phosphates (phosphocreatine (PCr) and nucleotide triphosphate (NTP, mainly ATP in infants)) and inorganic phosphate (Pi), phosphomonoesters (PME) and phosphodiesters (PDE) can be detected. As it happens with ^{1}H MRS, absolute quantifications are difficult to achieve and therefore, metabolite ratios are generally calculated to analyse brain oxidative metabolism changes. In addition intracellular pH (pHi) can be calculated using the modified Henderson-Hasselbalch equation (127). In newborn infants, shortly after intrapartum hypoxia-ischaemia, cerebral energetics often appear normal on ^{31}P MRS (53). However, in infants with adverse outcome, despite adequate oxygenation and circulation, there is a decline in energy metabolites as manifested by low PCr and ATP, and an increase in Pi, in the first days of life (53-56). Examples of ^{31}P MRS in a normal baby and a baby following severe hypoxia-ischaemia can be found in *figure 1-0-7.*

Both ^{1}H MRS and ^{31}P MRS changes occur in parallel, leading to the energy disruption (reduction in PCr/EPP and NTP/EPP) and increased in lactate.

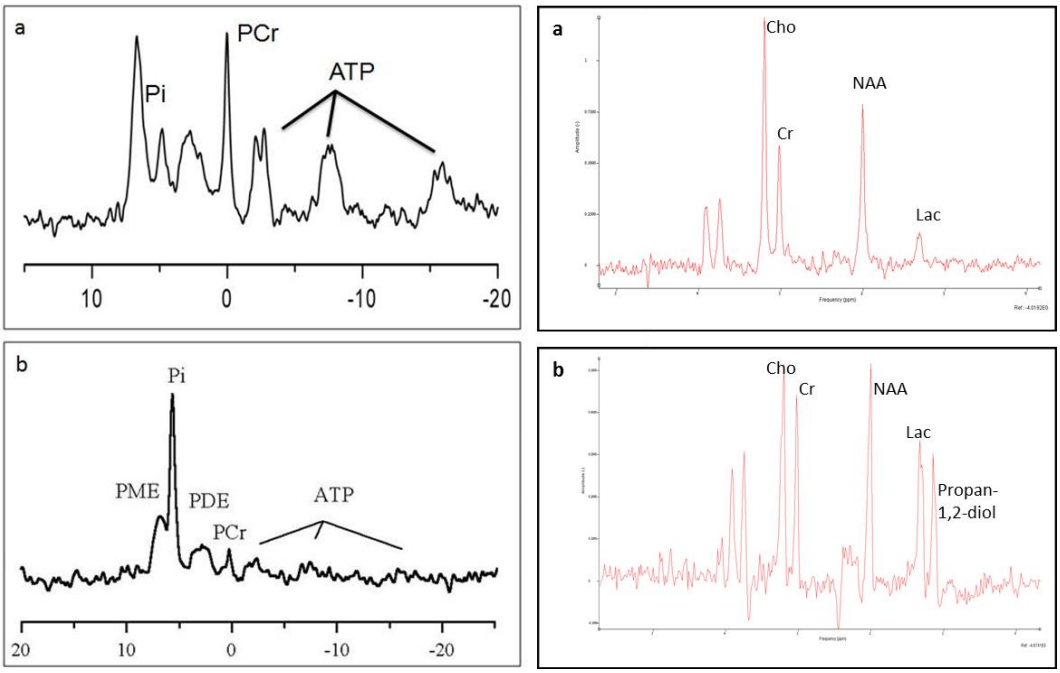

Figure 1-0-7: Representative 31P MRS (left) and 1H MRS (right) Spectra from a) a normal baby and b) a baby with severe neonatal encephalopathy (with an increased Pi peak and drop of energy metabolites on PMRS and an increased Lactate peak; there is also a propan-1,2-diol peak, which is a metabolite of phenobarbitone, appearing in those who received the medication to treat seizures)

Following initial brain acidosis, it has been observed that brain pHi becomes alkaline during this second phase of energy decline (3, 57). These metabolic changes were termed "secondary energy failure" (SEF) on the basis that they followed impaired intrapartum cerebral energy generation (resulting in transiently reduced PCr and NTP and increased Pi), which resolved following resuscitation (52) *(Figure 1-0-8)*.

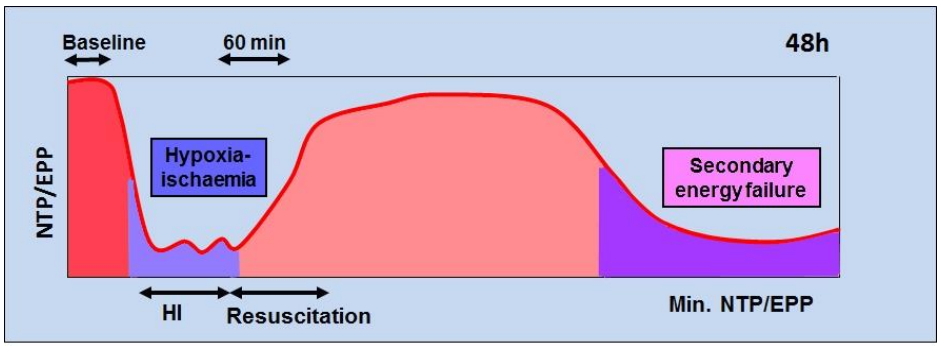

Figure 1-0-8: Schematic diagram illustrating the biphasic pattern of energy failure associated with a transient hypoxic-ischaemic (HI) insult using 31P MRS in the UCL piglet model.
NTP: Nucleotid triphosphate. **EPP**: exchangeable phosphate pool (epp=Pi + PCr + NTP).

It was assumed that SEF was consequential to a pathological mechanism initiated by intrapartum HI or/and reperfusion/reoxygenation.

1.4.7 Brain pHi changes in babies with Neonatal Encephalopathy

^{31}P MRS is the only non-invasive way to measure pHi apart from Positron Emission Tomography, which requires injection of radioactive ligands and thus not feasible in babies (128).

Using ^{31}P MRS, brain pHi is measured using the chemical shift difference of Pi (129), PCr and ATP (130-132). The titration curve of the Pi is in the physiological pH range; hence its position depends on the environmental pH to the Pi molecules. pH is calculated from the chemical shift of inorganic phosphate (δ) using a modified Henderson-Hasselbalch equation. The one used in the following studies was described by Petroff et al, and used by Hamilton et al (127, 133-135):

$$pH = 6.77 + \log_{10}[(\delta - 3.29) / (5.68 - \delta)] \quad \textbf{Equation 1}$$

The pHi value calculated from Pi is thought to reflect the pHi in dead or injured cells whereas that derived from other metabolites may reflect other cell populations. *Table 1-0-3* that I produced for the review paper published on brain pHi in hypoxia-ischaemia (49) shows studies in normal neonates and infants documenting brain pHi using ^{31}P MRS.

Reference	n	GA at birth (weeks)	Age when studied	Mean brain pHi	Localisation
Hope et al 1984	6	Median 40 (28-40)	Mean 76 h (16 h – 97 d)	7.14 ± 0.10	Surface coil
Hamilton et al 1986	18	Median 32 (28-42)	5 (1-61) days GA + PNA median 35 wks (28-42)	6.98 ± 0.34 (28 wks)	Surface coil
Boesch et al 1989	12	?	GA + PNA median 43wks (33 wks - 6 yrs) 8 were studied at 40 wks	7.08 (SD 0.1)	Surface coil
Azzopardi et al 1989	30 (data from 23)	Median 33 (24-42)	GA + PNA median 34 wks (26-42)	7.1 – no change with maturation AGA 28 wks 7.14 (±0.28) 42 wks 7.09 (±0.28) SGA 28 wks 6.97 (±0.24) 42 wks 7.19 (±0.24)	Surface coil
Laptook et al 1989	7	40+/- 1	10 examinations within the first 2 weeks after birth	7.02 ± 0.08	Surface coil
Van der Knapp et al 1990	41	Term	Mean 71 months (1 months – 16 yrs)	7.04 (95% CI 6.96 – 7.12) No significant change.	Volume localised (ISIS)
Buchli et al 1994	16[a]	Term	2-28 days GA + PNA mean 42 wks (39-44)	7.11 (±0.06)	Volume localised (ISIS)
Martin et al 1996	10[a]	Median 40 (36.3-42.1)	Median 4.3 days	7.12 (±0.05)	Volume localised (ISIS)
Robertson et al Unpublished data	3	Median 39 (38-40)	GA + PNA median 44 wks (41-64)	7.02 (±0.03)	Volume localised (ISIS)

Table 1-0-3: Studies in normal neonates and infants documenting brain pHi using 31P MRS (based on [69, 71, 78-83]) [a] Controls were healthy term newborn babies who had been hospitalised for non-neurologic reasons. GA: gestational age; PNA: postnatal age
Taken from (49).

Brain pH homeostasis in the cytosol and other cellular compartments is maintained by a dynamic, finely tuned balance between proton-extruding and proton-importing processes (136). Under physiologic conditions, the extracellular pH is ~7.4, however the cytosolic pH is more acid (~7.2). Other organelles possess their own specific pH *(Figure 1-0-9)*.

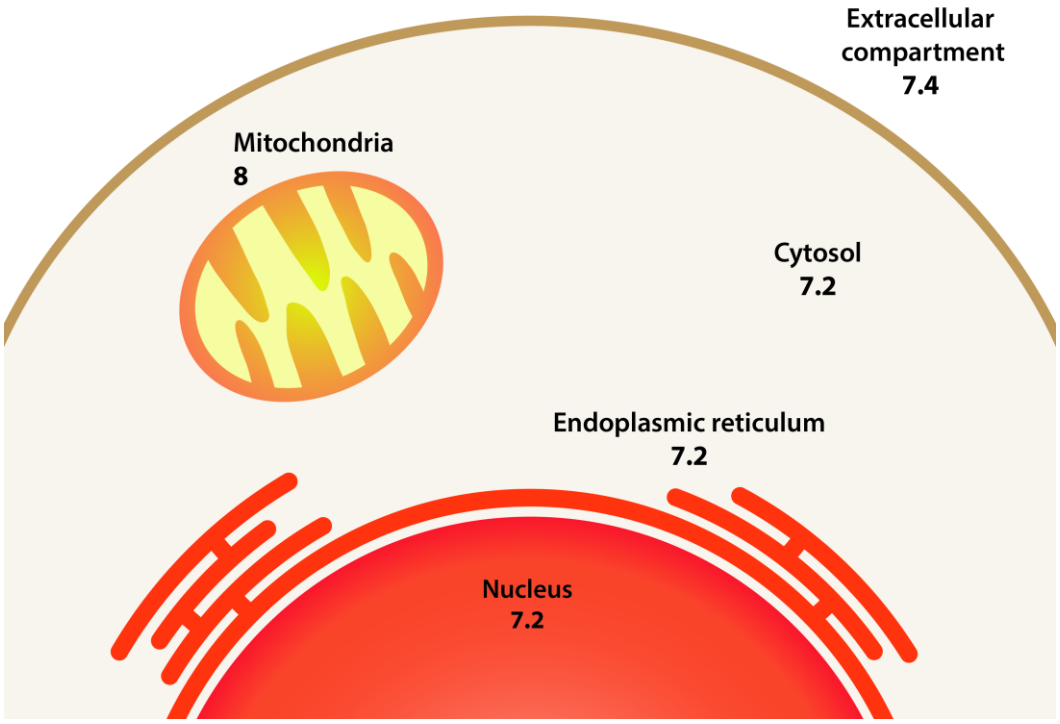

Figure 1-0-9: pH of the main cellular compartments in a prototypical mammalian cell (data collected from Casey et al (136)). Figure taken from (49). The mitochondrial pH refers to the space contained by the inner mitochondrial membrane. Under physiological conditions, the extracellular pH is slightly alkaline (around 7.4). However, even when bathed in large volumes of this heavily buffered, alkaline medium, the cytosolic pH is slightly more acidic. In fact, the cells must guard against further acidification due to the potential across the membranes (negative inside, promoting the uptake of protons and the extrusion of negative bases like bicarbonate) and to the net acid equivalents generated by various metabolic reactions (for example, ATP production in the cytoplasm by glycolysis and in mitochondria by oxidative phosphorylation).

Most of the proteins are pH-dependent to maintain their structure and function; pH plays an important part in many metabolic functions and the charge of biological surfaces affects many cellular reactions. There is a tendency for the cytosol to accumulate acid, due to the activity of the anaerobic metabolism/ glycolysis in the cytoplasm producing lactate, and to the aerobic netabolisn (oxidative phosphorylation) in the mitochondria producing CO_2. *Figure 1-0-1* represents ion transporters that contribute to regulate cytoplasmatic pHi. Protons are actively extruded from the cytosol by proton pumping ATPases,

coupling to other substrates through exchangers; the main transporter that protects cells against acidification is the Na^+/H^+ exchanger (see *section 4*).

In 2002, Robertson et al studied the pHi changes in whole brain in relation to outcome in babies with neonatal encephalopathy, in the pre-cooling era (3). In 78 babies with neonatal encephalopathy studied serially during the first year after birth (151 studies throughout the year including 56 studies of 50 infants during the first 2 weeks after birth) they demonstrated that: (i) alkaline brain pHi was associated with severely impaired outcome in babies; (ii) the degree of brain alkalosis related to the severity of brain injury on MRI and brain lactate concentration; (iii) brain alkalosis persisted for several weeks in babies with a severely impaired outcome and persistence was associated with cerebral atrophy on MRI. A brain pHi of 7.15 and above measured in the first 2 weeks after birth had a sensitivity of 71% and specificity of 92% for predicting adverse outcome.

MRI classification ≤ 2 weeks	Mean (SD) pHi at ≤ 2 weeks	n
Normal	7.04 (0.05)	10
Moderately abnormal	7.12 (0.1)	18
Severely abnormal	7.24 (0.17)	22

Table 1-0-4: Association of the severity of brain injury in MRI and mean pHi within the first 2 weeks of age. Mean (SD) brain pHi at ≤ 2 weeks of age in infants with neonatal encephalopathy classified according to the brain MRI pattern (based on data from Robertson et al (3)). There are differences statistically significant between the pHi in the group with a normal brain MRI and the pHi in the group with a severely abnormal MRI.

Table 1-0-4 published in the above mention paper (49) shows the brain pHi measured using ^{31}P MRS in infants with birth asphyxia.

In vivo data suggest that the return of pHi to normal or alkaline values may be deleterious to cells that have undergone hypoxia-ischaemia. This rebound alkalosis has been termed pH paradox and has been described in several cell types (137-139). Possible mechanisms leading to pH dependent injury include activation of phospholipases and proteases which have an alkaline pKa, onset of the mitochondrial permeability transition pore, leading to uncoupling of oxidative phosphorylation and aggravation of ATP depletion (140) and an exacerbation of excitotoxic neuronal injury due to an increased NMDA activation at alkaline pHi (141, 142). An understanding of the main transporter leading to brain alkalosis after hypoxia-ischaemia (Na^+/H^+ exchanger: NHE) therefore is important for future neuroprotection strategies.

Using magnetic resonance spectroscopy (MRS), the timing of the evolution of energy failure and changes in brain intracellular pHi have been fundamental in suggesting new avenues for neuroprotection.

Ref.	n	GA at birth (weeks)	Age when studied	Mean brain pHi	Localisation
Cady et al 1983	7 (3 birth asphyxia)	33-40	42 h – 26 d	7.2 (SD 0.1)[a] One infant studied on 5 occasions (on day 26: brain pHi = 7.4)	Surface coil
Hope et al 1984	10	38-41	8 h – 27 d (obtained in 3-6 times in each infant)	7.17 ± 0.1 at time of lowest PCr/Pi (mean age 113 h: 16h – 9d)	Surface coil
Hamilton et al 1986	27 Echodensities seen on USS (13 birth asphyxia)	Median 40 (27 – 42)	Median 3 d (8 h – 23 d)	"Tended to be raised" Values from 19 of the infants were above the regression line for normal infants; 6 were above the 95% CI.	Surface coil
Laptook et al 1989	1	36	1.5 d, 8 d, 15 d, 9 m	7.3 – 7.4	Surface coil
	5	38 ± 2	Within first 2 wks after birth	7.14 (± 0.12) Significantly different from the normal infants when other ^{31}P metabolites showed no difference	
Azzopardi et al 1989	61 (all infants)	27 – 42	3 d (0 - 23)	7.14 ± 0.27 (n=61)	Surface coil
	40 infants with asphyxia	40 (31-42)	3 d (1 - 10)	7.16 ± 0.19 (n=36)	
Martin et al 1996	23	Median 40 (36.9 – 41.9)	Median 3 d (NNS 1 - severe)	7.21 (±0.16)	Volume localised (ISIS)
			Median 5.5 d (NNS 2 – moderate)	7.09 (±0.04)	
			Median 3 d (NNS 3 – mild)	7.10 (±0.08)	
Robertson et al 1999	43	Median 39.5 (36 - 42)	77 examinations: 25 within 2 wk age 16 between 2–4 wk 25 between 4-30 wk 11 when > 30wk old	At time of lowest PCr/Pi (within first 2 wks of age): 7.23 (±0.07) – abnormal outcome group 7.08 (±0.04) – normal outcome group	Volume localised (CSI)
Robertson et al 2002	78 35 (+ 43 presented above)	39.5 (SD 1.6) (36-42)	151 examinations within the first year after birth. 50 infants' studies within 2 wks of age.	At time of lowest PCr/Pi (within first 2 wks of age): 7.28 (±0.15) – 23 infants with severe outcome or died 7.11 (±0.09) – normal outcome group	Volume localised (ISIS)

Table 1.0-5: Studies in infants with birth asphyxia documenting brain pHi measured by 31P MRS (based on [47, 48, 66, 69, 71, 80, 89, 90]) Taken from (49).

a. The pHi was taken from a heterogeneous group of infants including infants with congenital muscular dystrophy and with meningitis. The author noted there was no evidence of intracellular acidosis in infants with birth asphyxia and stated that the pHi was similar in infants with birth asphyxia to those without. On close examination, however, infants with birth asphyxia tended to have a more alkaline pHi.

NNS – neonatal score. NNS1 – severe NE; NNS 2 – moderate NE; NNS 3 – mild NE.
GA: gestational age; PNA: postnatal age; m: month; wk: week; d: day; h: hour.

Part 5: Na+/H+ Exchangers

This section has already been published in the review paper titled "Na^+/H^+ exchangers and intracellular pH in perinatal brain injury" (49). The Na^+/H^+ exchangers (NHE) are a family of ion integrate membrane transport proteins involved in maintaining a normal intracellular pH (pHi) and cell volume in many mammalian cell types (143, 144), by extruding protons from, and taking up sodium ions into cells in an electroneutral manner (1:1 stoichiometry) *(Figure 1-0-1)*.

To date at least ten NHE isoforms (NHE1 to NHE10) have been identified in mammals (145). NHE10 was recently described as an osteoclast-specific member of NHE family, regulating osteoclasts differentiation and survival (146). NHE1-5 are expressed on the plasma membranes in various types. NHE6-9 reside on intracellular organellar membranes of the endosomal-trans Golgi network (147, 148). NHE isoforms have similar membrane topologies, with an N-terminal membrane domain consisting of 12 predicted transmembrane segments and a more divergent C-terminal cytoplasmic domain (136, 148).The NHE 1 isoform has been studied closely and is present at the cell surface of most cells, especially plasma membranes. It is the most abundant isoform in the central nervous system (CNS) (149, 150). NHE1 plays a crucial role in protecting cells from internal acidification – acting together with bicarbonate-transporting systems – and restoring cell volume to steady-state levels (151).

Intracellular acidosis is the major stimulus that regulates NHE1 activity. As the H^+ concentration of the cytosol rises, there is a sharp increase in the activity of the transporter. Near-maximal velocity is achieved in approximately one pH unit (Hill coefficient > 1), thereby minimising exposure of the cytoplasm to excess acidification (152, 153).

In addition to responding to intracellular acidification, various signals can alter the NHE1 internal pH sensitivity, such as hormones, mitogens and physical stimuli (e.g. mechanical stretch and hyperosmolarity), modulating its state of phosphorylation (136, 144, 154-158).

The exchange activity is more active at alkaline pH values due to a shift of the set point by phosphorylation of the residues. It is also regulated at the transcriptional level, supporting the control at mRNA levels and at protein production level (159, 160). An alkaline cytoplasmic pH (pHc) is thought to provide a permissive environment for the progression of diverse cellular processes, including changes in cell shape (161), adhesion (162), migration (163, 164), chemotaxis (165, 166) and proliferation (167-169).

1.5.1 Effect of hypoxia-ischaemia on NHE

Reductions in blood flow with ischaemia and reduction in oxygen supply with hypoxia decrease the supply of oxygen required to maintain tissue ATP levels, especially in excitable organs such as the heart and brain that have a high demand for energy. As ATP stores are depleted, lactate, pyruvate and protons accumulate due to anaerobic metabolism of glycogen stores. The accompanying

cytoplasmic acidification causes hyperactivation of plasma membrane NHE1 leading to accumulation of intracellular Na^+. The Na^+ overload reverses the mode of operation of Na^+–Ca^{2+} exchange, driving excess Ca^{2+} into the cell. The resulting elevation in intracellular Ca^{2+} concentration, and subsequent activation of a neurotoxic cascade, with stimulation of proteases, phospholipases, and formation of oxygen and nitrogen free radicals, precipitating series of deleterious effects, including altered membrane excitability and contractility, generation of toxic free radicals, cellular hypertrophy, apoptosis and necrosis — events that result in cell death (170, 171). Activation of NHE also leads to the rapid normalization of pHi during reperfusion after HI (136, 145, 172, 173).

Removal of external Na^+ or reducing the external pH attenuates the post-anoxia alkalization (174). When ATP levels fall to 35% of control in isolated CA1 neurons during chemical anoxia, NHE activity is reduced by 44%. Thus, activation of NHE function appears to be dependent upon ATP energy levels which support phosphorylation of the protein.

1.5.2 NH Exchanger blockade and neuroprotection in neonatal models

Although the NHE activation is essential for the restoration of physiological pH, hyperactivation of NHE1 in neurons, in response to the metabolic acidification associated with an ischaemic/hypoxic insult (137, 175-178), disrupts the intracellular ion balance, causing intracellular Na^+ and Ca^{2+} overload (179) which eventually leads to cell death. There is experimental evidence in vitro and in vivo

that ion transporter inhibitors (especially NHE inhibitors) are neuroprotective (*Table 1-0-6*).

Table 1-0-6: Preclinical studies. Brain pH and NHE blockers in perinatal brain injury (based on [51, 94, 95, 91, 96-101, 90, 102-107]).
Abbreviations: NHE: Na^+/H^+ exchanger; NHE-1: isoform 1 of NHE; NCX1: Na^+/Ca^{2+} exchanger-1; BBB: blood-brain barrier.
MIA: N-methyl-isobutyl-amiloride **(**inhibitor of NHE**); EIPA:** N-(N-ethyl-N-isopropyl)-amiloride **(**highly potent derivative of amiloride for the non-selective inhibition of the NHE system in various cell types); **SM-20220:** *N*-(aminoiminomethyl)-1-methyl-1*H*-indole-2-carboxamide methanesulfonate **(**a highly selective and specific NHE-1 inhibitor, 50 times more potent than EIPA); **HOE-642:** cariporide mesilate or 4-isopropyl-3-methylsulfonylbenzoyl-guanidine methanesulfonate (a selective NHE-1 inhibitor); **S1611** (a selective NHE-3 inhibitor); **Harmaline** (a non-amiloride NHE-5 inhibitor).
NTP/PME: Nucleotide triphosphate /phosphomonoester; **Lac/NAA:** Lactate / NAA ratio.
RTNn: retrotrapezoid nucleus neurons; **NTSn:** nucleus tractus solitarii neurons; **LCn:** locus coeruleus neurons.
Taken from (49).

Paper	Species	Model, study design	NH exchanger blocker	Results
In vitro studies				
Vornov 1996	Ex-vivo Rodent 17-d rat foetuses (Harlan Sprague-Dawley) 10-12 cells.	-Neuronal tissue culture model of **ischemia** (18-19 d culture) from embryonic 17-day rat foetuses -20 min ischaemia with metabolic inhibition: K cyanide + 2-DG. - Injury quantified using LDH liberation.	-**Group 1:** ischemic conditions vs. prolonged ischemia (30min) -**Group 2:** Incubation with NHE blockers at normal pH_e (**dimethylamiloride** 100 microM & 300 microM and **harmaline** 100 microM & 300 microM) slowed pH_i recovery	-Profound **protective effects: ↓** pH_e during 1sth recovery. Still after prolonged insult (30 min, despite loss protective effects NMDA receptor antagonist MK-801) =>suggesting **protective effects** due to **intracellular acidosis**. - 1st demonstration of protective effects of blocking NHE in cerebral ischemia model (block during recovery); worst injury if pH_i normalises fast. =>Protective effects acidosis from **suppressing pH-sensitive mechanisms** of injury or from **blocking Na entry** (NHE).
Matsumoto 2004	Ex-vivo Rodent 1-d old rats Culture of cortical neurons	-Hypercapnia (5% CO2) for 10 -14 d, then cortical neurons cultured on glass-based dishes -Staining: assess glutamate-induced neuronal death. -Neurons morphological change (contrast microscope) -Ca^{2+}_i concentration and pH_i by fluorescence imaging	-Some given **SM-20220 0.3 to 30 nmol/L** 20 min **pre-**glutamate exposure; or **MK-801** (NMDA receptor antagonist)	- SM-20220: ↓ glutamate-induced neuronal death over 6h (300µmol/L), inhibited post-glutamate exposure (500µmol/L): acute cellular swelling, persistent ↑ $[Ca^{2+}]i$ and intracellular acidification. -All events glutamate-induced were MK-801-inhibited →death by excitotoxicity. => Neuroprotection: inhibit persistent ↑$[Ca^{2+}]i$ & acidification in excitotoxicity
Robertson 2005	Ex-vivo Rodent 14- and 7-d models of rat pups Brain slices	-Progressive energy decline after **HI insult** in rat brain slice neonatal model; P^{31}& H^1 MRS 350µm slice -**7-d-old** rat pups brain slices perfused in KHB: i) at 37°C; ii) at 32°C; and **14-d-old** slices perfused for 8 h in similar solutions and then NHE blocker	-**14-d-old** rat pups brain slices perfused for 8 h: i) at **37°C** in KHB; ii) at **32°C** in KHB; iii) at **37°C in HEPES** buffer, iv) **1mM amiloride** at 37°C in HEPES	-No gestational age effect on energy decline between 7-d and 14-d model. - Brain slice model underwent secondary energy failure (at 5 h: alkaline pHi, ↓ PCr/Pi and ↑ lactate/NAA, and ↓ NTP/PME, at 37°C). **- Changes were delayed with hypothermia** (32°C) **or amiloride** (pH_i acidified and NTP/PME was preserved, at baseline and at 5 h.).
Kersh 2009	Ex-vivo Rodent 3-15-d old Sprague-Dawley rat both sex Brain slices.	-Hypercapnia (15% CO_2) -NH_4Cl-induced acidification in brainstem neurons from chemosensitive regions of neonatal rats (brainstem slices from RTNn, NTSn and LCn), pH-sensitive fluorescent-dye+ fluorescence microscopy.	-DMSO-vehicle -Amiloride 1-2 mM concentration -HOE 642 1 microM concentration -S1611 5 microM concentration. -EIPA 100-500 microM concentration	-pHi recovery mediated by different pH-regulating transporters in neurons from different chemosensitive regions (NHE-1 in RTNn; NHE-1 and NHE-3 in NTSn; Na- and HCO_3-dependent transporter in LCn), but recovery suppressed by hypercapnia in all neurons (maintained acidic pH)
Liu 2010	Ex-vivo Rodent 1-3-d neonatal mice Glial cultures	- Isolation of mixed primary glial cultures in neonatal mice. - Activation of microglia after lipopolysaccharide or oxygen and glucose deprivation and reoxygenation.	-Group 1: untreated. -Group 2: HOE 642	-**HOE 642** abolished pH_i regulation in microglia basal conditions. -**Activation of microglia accelerated pH_i regulation** (**↑ pH_i**, ↑ Na^+_i and **Ca^{2+}_i**, and production of superoxide anion (SOA) and cytokines (CK)). -HOE 642 abolished pH_i regulation, ↓ production SOA, CK and $_iNOS$. **-Hypothesis**: **NHE-1** to **maintain microglial pH_i** homeostasis allowing for sustained NADPH oxidase function and "respiratory" burst.
In vivo studies				
Ferimer 1995	Rodent 13 Wistar rats	Cardiac arrest (KCl) in rats followed by resuscitation 7 mins later in untreated vs MIA.	MIA **Controls** (untreated).	-MIA delays normalization of brain pHi after cardiac arrest in rats. -**MIA**: **↓ cardiac pH** in rats post-arrest +15min reperfusion -MIA **doesn't** change pH_i from non-ischemic value.
Phillis	Rodent	-Ischaemia: 20 min occlusion carotid arteries	**-Group 1** (n=9)**:** aCSF (vehicle= control)	-**Inhibition of NHE prevented activation of phospholipases (suppress ↑** some

2000	21 Sprague-Dawley rats	(group3 30 min), with EEG (flat). Then 40min reperfusion. -Cortical superfusate (bilaterally every 10min): free fatty acids (FFA), lactate & glucose levels.	-Group 2 (n=6): EIPA 25 microM topical (cortex) 35 min pre & during ischaemia **-Group 3** (n=6)**:** 30 min ischaemia.	FFA**)** that usually occurs during reperfusion post-cerebral ischemia. **-EIPA: Lactate** levels ↑ more rapidly during reperfusion than controls, **significantly lower** by end of experiment.
Pilitsis 2001	Rodent 24 Sprague-Dawley rats	-Cerebral ischaemia (20 min carotid arteries occlusion). -Measurement of phospholipase activation by efflux of FFA in the ischemic/reperfused rat cx cortex.	-Group 1: SM-20220 20 microM topical (cortex) pre & during ischaemia (n=13) - Group 2: C**ontrol** (ischaemia) (n=11)	-↓significantly ischemia-evoked efflux of FFAs: importance NHEs in **eliciting FFA efflux** -**Inhibition** may be essential for **neuroprotection** in ischemia-reperfusion injury
Kendall 2006	Rodent 47 mice 7-d [adult C57/Bl6 female and males bred inhouse]	- HI: 2h left carotid artery occlusion followed after by moderate (30 min) or severe (1 h) hypoxia (8% O_2). -Outcome at 48 h: viable tissue in injured hemisphere (severe HI) or injury score & TUNEL stain (moderate)	-Group 1: MIA 2.5 mg/kg (in acetic acid and saline) intraperitoneal -Group 2: 0.9% Saline equivalent volume Given 8 hrly starting 30 min before HI.	-MIA neuroprotective when commenced before HI (no weight difference). -**Severe insult**: significant **neuroprotective** (↑forebrain tissue survival) -**Moderate insult**: ↓ damage **hippocampus (**injury score & TUNEL-+ve cells) -MIA **↓ neutrophil count** and hence brain swelling after HI**.**
Rocha 2008	Rodent 3-4 –m old Mice male Swiss-Webster	-Metabolic stress and dopaminergic damage in mice caused by mitochondrial inhibitor malonate. - Dialysate levels of DA and metabolites for 1h prior drug delivery (baseline) and afterwards, every 20 min.	-Group 1: HOE-642 0.3, 1 & 3 mmol/min dialized intracerebral (striatum) 20 min-periods, separated by drug washout ≥1h -Group 2: EIPA -Group 3: only Malonate (control).	-**HOE-642 pre**-treatment: **↓**malonate-induced **DA overflow** and **↓ striatal DA content, without** ↓ intensity metabolic stress or subsequent DAergic axonal damage **-Absence NHE1 on nigrostriatal DAergic neurons** (although NHE isoforms 1-5 expressed in striatum and midbrain) suggests **HOE-642** effects on striatal DA overflow via **NHE1 on other cell types** or via **multiple NHE isoforms.**
Hwang 2008	Rodent 6 m Mongolian gerbils (Meriones unguiculatus)	-HI by 5 min bilateral occlusion common carotid arteries. -Staining for delayed neuronal death and immunohistochemistry for NHE1 (at 30 min, 3h, 12h and 1-,2-,3-, 4- and 5-days following surgery). -Locomotor activity was monitored for 10 days post-insult.	**-Group 1: normal (**Sham: same surgical procedure but NO ischaemia) -Group 2: vehicle (saline given). **-Group 3: EIPA 5 mg/kg and 10 mg/kg** OD for 3-9 d after ischaemic surgery, starting **30 min post-ischaemic** surgery.	-**Sham** group: **weakly** NHE1 immunoreactivity in CA1 region. -↑NHE protein level **in CA1** region **from 2d post-HI**; activation NHE1 in **CA1 glial** cells from **2 -3d post-HI;** in **CA1 pyramidal neurons** & **glial** cells(astrocytes) from**4d** -EIPA potently protected CA1 pyramidal neurons from ischemic injury, and ↓ activation of astrocytes and microglia in ischemic CA1 region. -EIPA significantly ↓ locomotor hyperactivity 1 day after HI. -**EIPA** blocked NCX1 reactivity in CA1 region after transient forebrain ischemia -Hypothesis: role of NHE1 in delayed death. NHE inhibitors protect neurons from ischemic damage.
Shi 2011	Rodent 136 mice -NHE-$1^{+/-}$ heterozygous mouse colony SV129/BlackSwiss -Wild type SV129/Black Swiss mice -NHE-1 $^{+/-}$ & $^{+/+}$ litter mate males	-Transient focal cerebral ischaemia and reperfusion (I/R) by 60 min occlusion of left MCA. -Activated microglial cells were identified by their expression of two microglial marker proteins (CD11b and Iba1) and by their transformation from a "ramified" to an "amoeboid" morphology.	**-Group 1: vehicle control** (equivalent volume of saline intraperitoneal)**.** **-Group 2: HOE 642 0.5 mg/kg intraperitoneal** at 30 min prior to the onset of reperfusion, and then daily up to 1-7 d during reperfusion.	-Immediate ↑ **microglial** activation **ipsilateral to ischemia** in NHE-$1^{+/+}$ brains at 1 h I/ 1h R (gradually ↓ during 6-24 h). Then sharp ↑ **microglial activation peri-infarct** area and ↑ proinflammatory **CK** at **3 d** after I/R. -**HOE 642** or **NHE-1 $^{+/-}$** mice: **less microglia activation**, less NADPH oxidase activation, ↓ **proinflammatory** response at **3-7 d** post- I/R. Blocking NHE-1 significantly ↓ microglial phagocytosis in vitro. -↑↑ NHE-1 protein expression in activated microglia and astrocytes. NHE-1 inhibition ↓ microglial proinflammatory activation following I/R.

Ferrazzano 2011	Rodent 44 Wild-type controls (NHE-1$^{+/-}$), NHE-1 genetic knockdown mice (NHE-1 $^{+/-}$)	-Transient focal cerebral ischemia by 30-60 min occlusion of left MCA induced in wild-type controls (NHE-1 $^{+/+}$), NHE-1 genetic knockdown mice (NHE-1 $^{+/-}$), and NHE-1 $^{+/+}$ mice treated with HOE-642. -Brain MRI (diffusion DWI and T2 weighted)	Randomised to: **-Group 1: HOE 642 0.5 mg/kg intraperitoneally:** 30 min **pre**-reperfusion or 1h **post**-reperfusion. Then at 24 and 48h after reperfusion. -Group 2: control (Saline as vehicle).	- Significant protection in NHE1 $^{+/-}$ mice. In DWI (sensitive early marker): lesion from 1h post-reperfusion, ↓in NHE-1$^{+/-}$. In T2 imaging: NHE-1$^{+/-}$ significantly smaller infarct at 72h vs. NHE-1$^{+/+}$mice - HOE642 pre-reperfusion or during early reperfusion: ↓ ischemic damage (remains protective given during early reperfusion!). =>Therapeutic potential for inhibition NHE-1 in cerebral ischemia.
Cengiz 2011	Rodent 9-days-old 46 C57BL/6J mice	-30 min unilateral ligation of the left common carotid artery, plus exposure to hypoxia (8% O_2 for 55 min). -Histology, immunohistochemistry (neurodegeneration and microtubule-associated protein 2 (MAP2)) and motor and spatial learning assessment at 4-8 weeks of age after HI.	Randomised to: -Group 1 (n=13): HOE 642 0.5 mg/kg intraperitoneal: 5min pre-HI, 24&48hpost -Group 2 (n=10): control (Saline) pre/posttreatment **-Group 3** (n=13)**: HOE-642 posttreatment** (10min, 24 and 48h post-HI) -Group 4 (n=10): control (Saline) posttreatment.	Inhibition of NHE-1: neuroprotective in neonatal HI brain injury. - **Control** brains 72 h post-HI: neurodegeneration in hippocampus, striatum, and thalamus ipsilateral; loss MAP2 expression. NHE-1 protein upregulated in specific astrocytes. Motor-learning deficit seen at 4 wks age -**HOE 642**: better **preserved** morphologic **hippocampal** structures, **less neurodegeneration** and ↑MAP2 expression. Inhibition of NHE-1 **↓ neurodegeneration** in **acute** stage HI and improved striatum-dependent **motor and spatial learning at 8 wks** of age after HI. =>NHE-1-mediated disruption of ionic homeostasis contributes to striatal and CA1 pyramidal neuronal injury after neonatal HI.
Helmy 2011	Rodent 6-d old 159 Male Wistar rat pups	-60 min of asphyxia by hypoxia 9%, or hypercapnia 20%, or both combined. Then normal restoration of room air or graded re-establishment of normocapnia (↓ CO_2 levels 20% to 10% 30 min, then 5% further 30 min, and room air) -Monitoring with EEG recording and pH-sensitive microelectrodes.	Some in each group: **MIA 2.5 mg/kg intraperitoneally** 30 min **pre**-asphyxia **-Group 1** (60min hypoxia 9% then 21%) **-Group 2** (60min hypercapnia 20%) **-Group 3** (asphyxia: CO_2 20% + O_2 9%) **-Group 4** (asphyxia like group 2 and then graded re-establishment of normocapnia) -Group 5: controls (room air only).	-**Recovery** from asphyxia followed by large **seizure burden** and ↑ **brain pH**. -Graded restoration of normocapnia after asphyxia strongly suppresses alkaline shift in brain pH and seizure burden. -MIA pre-insult: virtually blocked seizures.
Helmy 2012	Rodent 6-7-d old Male Wistar rat pups	-60 min of asphyxia by hypoxia 9% and hypercapnia 20%. Then normal restoration or graded re-establishment of normocapnia (↓ CO_2 levels 20% to 10% 30 min, then 5% further 30 min, and room air) -Monitoring with EEG recording, pH-sensitive microelectrodes, and histology.	5 pups in each group: MIA 2.5 mg/kg intraperitoneally 30 min pre-HI A few: Amiloride 2.5 mg/kg intraperitoneally 30min pre-asphyxia. **-Group 1** (asphyxia CO_2 20% + O2 9%, then room air) **-Group 2** (asphyxia like group 1 and then graded restoration normocapnia)	-Neocortical neurons in vivo: biphasic pH changes acid-alkaline response. -Graded restoration normocapnia: strongly suppress alkaline overshoot. -Parallel ↑ pH_e and pH_i levels post-HI indicates **net loss acid equivalents** from brain tissue **not attributable to** BBB **disruption** (lack of ↑Na fluorescein extravasation into brain and EEG characteristics of BBB). -MIA: abolition net efflux acid equivalents from brain across BBB, and suppression seizure (sz) activity. -Post-asphyxia seizures: attributable to enhanced NHE-dependent net extrusion acid equivalents across BBB and consequent brain alkalosis. - BBB-mediated pH regulation: new approach prevention & therapy neonatal sz.
Robertson 2013	Piglet 18 white male <24 h-old	-Transient global cerebral HI (bilateral occlusion common carotid arteries). -P^{31} & H^1-MRS before, during and up to 48 h after HI. Tissue injury (histology/immunohistochemistry) at 48 h.	Randomized to: -Saline placebo **-3 mg/kg iv MIA** 10 min **post**-HI & 8 hrly.	-MIA starting 10 min after severe HI: neuroprotective in this perinatal model: ↓ brain Lac/NAA, cell death (in cerebral cortex, thalamus, and white matter) and microglial activation (in pyriform and mid-temporal cortex).

Amiloride was the first drug described as NHE inhibitor. There are two major classes of pharmacological NHE inhibitors. One class includes amiloride and its derivatives by double substitution of the nitrogen of the 5-amino group: DMA (dimethylamiloride), EIPA (N-(N-ethyl-N-isopropyl)-amiloride), MIA (N-methyl-isobutyl-amiloride) and HMA. They are non-selective inhibitors of the NHE system in various cell types, and EIPA is highly potent. Another class of inhibitors includes the derivatives of the benzylguanidines such as HOE 694, HOE 642 (cariporide mesilate or 4-isopropyl-3-methylsulfonylbenzoyl-guanidine methanesulfonate), eniporide and BIIB-513 which selectively inhibited NHE1. The replacement of the pyrazine ring of amiloride by a pyridine ring or by a phenyl increased the potency and the NHE selectivity. In the last two decades several bicyclic guanidines were prepared: zoniporide, MS-31038, SM-20220, SM-20550, SMP-300, KBR9032, BMS-284640, T-162559, TY-12533, S-3226 or SL-591227 (143). Of these, HOE 642 is extremely potent, being 105 times more specific for NHE1 vs. NHE3 (169); and zoniporide is very potent too and 150 fold selective for NHE1 vs. the other isoforms. S1611 and S3226 are two selective NHE-3 inhibitors. Harmaline is a non-amiloride NHE-5 inhibitor.

During in vitro cerebral ischaemia, NHE inhibitors (DMA; harmaline (137), SM-20220 (179), amiloride (180) and HOE-642 (176, 178, 181)) had a protective effect, in terms of delayed pHi normalization both in neuronal cells and in astrocytes (137, 180-183), inhibition of microglia (181) and less intracellular calcium accumulation (178, 179). This anoxia-induced alkalization was also ameliorated in NHE -/- CA1 neurons. In parallel, cell death was reduced in wild

type neurons treated with HOE 642 or in NHE1-/- neurons in cultured mouse cortical neurons undergoing 3 h oxygen-glucose deprivation (OGD) and 21 h reoxygenation (from ~70% to 40-50%) (178).

Vornov et al (137), described that pHi decreased by 0.2 pH units, but then recovers when inhibition was removed in rat cortical neuronal cultures undergoing metabolic inhibition for 20 min. NHE1 inhibitors, dimethylamiloride or harmaline, significantly reduced the post-inhibition pHi recovery, showing less brain injury in these compared to those with a fast pHi normalization.

As mentioned above, NHE1 activity also affects cellular Na^+ levels. A small but significant (~2 fold) increase in neuronal intracellular concentration of Na^+ ($[Na^+]i$) results after 2 h OGD, reaching to ~7 fold increase during 1 h reoxygenation. HOE 642 attenuated the rise in $[Na^+]i$ following OGD. NHE1-/- neurons did not exhibit significant increase in $[Na^+]i$. This supports that NHE1 activity is elevated upon reoxygenation (174, 177). Three hours of OGD and 21h reoxygenation lead to cell death in ~ 70% of the NHE1+/+ neurons. However, cell death is significantly reduced in wild type neurons treated with HOE 642 or in NHE1-/- neurons (178).

In vivo studies mainly in rodents have found that NHE1 inhibitors reduce brain injury in HI models (184) and decrease infarct size in a focal ischaemia model (178). In NHE1 heterozygous mice they found –similar to those NHE+/+ mice treated with HOE 642- significant decrease in infarct size of around 30% compared with normal NHE+/+ mice following middle cerebral artery occlusion (MCAO) (178). It implies that the disruption of Na+ and Ca2+ homeostasis

contributes to ischaemic neuronal damage. These studies firmly demonstrate the dominant role of NHE1 among other NHE isoforms in cerebral ischemic brain damage.

Other studies show neuroprotection in ischemic models. SM-20220 (N-(aminoiminomethyl)-1-methyl-1H-indole-2-carboxamide methanesulfonate), a highly selective NHE1 inhibitor, given intravenously 1 h after MCAO significantly reduces the extent of cerebral edema and Na+ content after 2 h ischemia and 4 h reperfusion and infarct volume after 22 h reperfusion (185). SM-20220 decreases infarct size in both transient and permanent MCAO models. Importantly, the reduction of infarct size improves when the treatment is delayed for 5, 30, or 60 min after the onset of ischemia (185). SM-20220 leads to ~ 50% decrease in infarct size at 72 h reperfusion. Several studies showed same results of reducing infarct volume and brain oedema using other NHE blockers *Kitayama et al* (186) with FR-183998; *Touret et al (187)* with sabiporide given pre and/or post-ischaemia (188).

Some NHE blockers (SM-20220 (189) and MIA *(184))* have been found to reduce the number of neutrophils in the ischemic hemisphere. Suzuki et al (189) studied the effect of SM-20220 administered intravenously as a bolus immediately after occlusion of the middle cerebral artery (MCA) in a rat model, followed by a continuous infusion over 2.5 hours. The infarct area was measured using hematoxylin–eosin staining at 72 h after occlusion, and neutrophils in the brain were immuno-stained with anti-myeloperoxidase. SM-20220 statistically significantly attenuated cerebral infarct volume, water content, and the

neutrophil accumulation at 72 h after the MCA occlusion and ameliorated neurological deficits. Several investigators (190, 191) have reported that activated neutrophils are involved in the development of cerebral damage induced by ischaemia, being a major source of oxygen radicals during reperfusion following focal cerebral ischaemia. It is known that intracellular pH regulates the activation of neutrophils, and NHE inhibitors attenuate neutrophil activation. SM-20220 (NHE inhibitor) prevented cerebral ischemic damage and oedema from progressing in rats post-MCA occlusion. A possible mechanism may be due to the inhibition of neutrophil accumulation. Moreover, Horikawa et al showed that SM-20220 attenuates leukocyte adhesion and migration in the mesenteric artery (192) and improves endothelial dysfunction (193). Leukocytes are important in the acute inflammatory reaction, and their activation is believed to contribute to ischaemia-induced brain injury (190, 194). These findings support that NHE inhibitors not only can prevent ischaemia-reperfusion injury by their ion kinetics effect (avoiding the increase in intracellular Na^+ and the cascade that follows), but also by the attenuation of leukocytes-endothelium cell interactions (adhesion and migration) induced by ischaemia-reperfusion. Adherent leukocytes are thought to cause injury by blocking capillaries (195) and through vasoconstriction (190), and migrated leukocytes induce tissue injury by releasing biochemical mediators, such as reactive oxygen species, as mentioned above (191).

Moreover, NHE1 blockers (EIPA and HOE 642) (175, 181, 196, 197) reduced microglial activation post-HI and hence the microglial phagocytosis and

astrocytosis in CA1 region. *Cengiz et al(197)* found that HOE 642 given either pre-hypoxia-ischaemia or starting 10 min after the insult reduces neurodegeneration in the acute stage in hippocampus, striatum and ipsilateral thalamus, and improved the striatum-dependent motor and spatial learning skills at 8 weeks.

NHE1 inhibitors are neuroprotective in astrocytes in a similar way to neurons. The intracellular Na+ overload is substantially mediated through activation of the ERK 1/2 pathways (183). In a more severe model of in vitro ischemia, cultured astrocytes were superfused with a solution which mimics the ionic composition of the ischemic extracellular space (a hypoxic, acidic, ion shifted ringers (HAIR) solutions at 37^{o}C) (198, 199). Exposure to HAIR caused a rapid decline in astrocyte pHi. This is consistent with the finding that NHE1 activity is inhibited by low extracellular pH (pHe) (200). When exposed to normal buffer again, astrocytes rapidly alkalised and a significant rebound of pHi over the baseline took place (199). *Bondarenko et al (199)* have reported that HAIR and reoxygenation leads to ~ 40% cell death in astrocytes, which is significantly reduced in the presence of NHE blockers such as EIPA or HOE 694 during HAIR and reoxygenation, or during reoxygenation alone.

NHE inhibitors also preserve neurological functions. In a model of ischaemia and hypothermia in piglets, *Castellá et al* (201) observe a rapid neurological recovery in the ones receiving HOE 642 just at the onset of cooling. Several studies (175, 202) demonstrate that EIPA not only protects gerbil hippocampal neurons from ischemic injury but also reduces the magnitude of the ischemia-induced locomotor hyperactivity at both 24 h and 6 days reperfusion. Ischemic injury to

the gerbil forebrain produces an increase in locomotor activity which is related to the degree of pyramidal neuronal damage in the CA1 region of the hippocampus (175, 203). In another Mongolian gerbil model, the consciousness recovery time improved significantly (lower neurological scores at 2 h reperfusion) following a 30 min transient global cerebral ischemia in those treated with SM-20220), compared to the vehicle group (204). This improvement in neurological deficit persists until 24 h reperfusion.

In summary, NHE blockers or genetically modified NHE1 -/- are neuroprotective in animal models. They reduce the alkalinisation of the cell (inhibition of phospholipases and kinases (202, 205) and delayed secondary energy failure (180)), and decrease the calcium and sodium intracellular overload, reducing cell oedema and cell damage. They attenuate inflammatory state, and suppress microglial activation, especially in hippocampal regions (pyramidal neurons of the CA1 area in rodents) (175) and in striatum and ipsilateral thalamus in a focal ischaemia model (197). Improved functional outcome also follows NHE blockade (197).

1.5.3 NH exchanger blockade in the piglet model of perinatal asphyxia

In the piglet model, ^{31}P MRS can be used as a biomarker. *Robertson et al* (206) used MIA started from 10 min after severe perinatal asphyxia, and 8 hourly thereafter. Out of 18 male piglets < 24 h old which underwent transient global cerebral ischaemia by occluding both common carotid arteries and hypoxia, half were randomized to MIA and the other half to a saline placebo.

Immunohistochemistry was undertaken to investigate the cerebral effects of the NHE inhibitor. ^{1}H MRS demonstrated that MIA decreased thalamic Lac/NAA compared with placebo, correlating on ^{31}P MRS with improved cerebral energy metabolism. In the MIA group, brain injury histology scores and microglial activation (in pyriform and mid-temporal cortex) were reduced. Treatment with MIA starting 10 min after hypoxia-ischaemia was neuroprotective in this perinatal asphyxia model. The use of clinically relevant MRS biomarkers and reduced cell death in a large animal model of perinatal asphyxia is an important step towards the clinical translation of NHE inhibitors. It is important to assess whether NHE blockade would augment hypothermic neuroprotection in this devastating disease. There is no evidence whether hypothermia would affect this mechanism.

Part 6: Brain pHi and seizures

This section has been published with the above mentioned paper (49) and plays a key role in the interpretation of the results from the study presented in *Chapter 3*, assessing the relationship between brain pHi and seizure burden in newborn infants with a diagnosis of neonatal encephalopathy.

1.6.1 Relation between brain pHi and seizures

Neonatal seizures are the most common manifestation of neurological disorders in the newborn period and neonatal encephalopathy is the most frequent cause of seizures at term. As described in Part 3, in the aEEG section, some studies

show that the duration of electrographic seizures in newborn babies is associated with worse MRI appearances (207) and poor neurodevelopmental outcome (208). Newborn babies with NE as a cause of seizures tend to have a higher seizure burden than those with a stroke (208). Increased morbidity and mortality, brain injury and poor neurodevelopmental outcome have been associated with a higher seizure burden (87, 208-214). Therefore addressing neonatal seizures is a priority, but current drugs are largely ineffective and are not free of serious side effects on the neonatal brain (215-217).

Therapeutic hypothermia not only improves outcomes of babies with NE by reducing the rate of death and disability at 18 months of age, but it also appears to reduce seizure burden (92). Cooling appears either to act directly to reduce seizure burden or to augment the action of conventional anticonvulsants. Xenon seems to enhance this effect of reducing seizure burden when given together (218). The data is consistent with those from preclinical models (92).

There is however still an unresolved controversy whether seizures worsen outcome by themselves or whether they are associated to those with a more severe degree of encephalopathy, hence the higher mortality and morbidity (90, 219). The molecular and cellular mechanisms underlying birth-asphyxia seizures are unknown but understanding the seizure-triggering mechanisms plays a key role in the design of novel therapeutic strategies.

A profound acidosis (blood pH 7.00 or lower) at the time of birth is an essential criteria in the diagnosis of perinatal asphyxia (220, 221). However, post-asphyxia seizures do not coincide with the maximal blood acidosis but are typically first

observed during the recovery period after a delay, that usually ranges in human babies from 2 to 16 h (222). A wide range of observations have shown that changes in extra- and intracellular pH exert a strong modulatory effect on brain excitability under normal and pathophysiological conditions, whereby an alkalosis enhances excitability while an acidosis has an opposite effect (5, 223-229). The immature brain appears to be particularly sensitive to changes in pHi. Recent experiments have shown that changes of 0.05 pH units on neonatal hippocampal slices have a profound effect on endogenous network activity (229).

Helmy et al (5) showed in a rat pup model of neonatal birth asphyxia that post-asphyxic seizures were directly caused by cortical pH recovery and subsequent alkalosis. They studied four groups of rats exposed for 60 min to: a) hypoxia (9% O_2) followed by return to normocapnia and normoxia (room air); b) hypercapnia (20% CO_2) and then back to room air; c) asphyxic condition (simultaneous hypoxia 9% and hypercapnia 20%) followed by room air (fast restoration of normocapnia); and d) asphyxic condition as in previous group, followed by a 'graded restoration of normocapnia' (CO_2 from 20 to 10% for 30 min and then to 5% for a further 30 min and finally virtually zero or room air). Some pups received the NHE inhibitor, MIA, intraperitoneally 30 min before asphyxia. Brain pH and oxygen were measured using intracortical microelectrodes, and blood pH, lactate, CO_2, O_2 and ionized calcium were monitored too. Seizures were diagnosed clinically and using intracranial electroencephalography. The baseline EEG activity in the group of pups exposed to hypercapnia or asphyxic conditions

was strongly suppressed, whereas all the pups with abrupt restoration of normocapnia after asphyxia developed pronounced EEG seizure activity. These data are consistent with the evidence that acidosis suppresses neuronal excitability and alkalosis does the opposite (225, 230-232), and that pH plays a key role in modulating neuronal survival after trauma (where acidosis is generally protective) (223, 233, 234). There was a robust correlation between brain alkalosis and seizure burden during the recovery from the asphyxia-induced acidosis. The subsequent alkaline overshoot reached values well above the normal brain pH level (+0.40 pH units), similar finding to previous studies in rats (184), piglet (52, 206) and human newborn (3, 57). However, no studies have been performed since the introduction of therapeutic hypothermia. Restoration of normocapnia in a graded way showed a dramatic decrease (85%) in the cumulative post-asphyxia seizure burden when compared with abrupt restoration of normocapnia group. The conclusion that seizures were triggered by brain alkalosis was supported by (1) the much higher seizure burden seen on abrupt restoration of normocapnia, when brain pH was much more alkaline, versus graded restoration strategy; (2) the rapid termination of seizures observed when applying 5% CO2 as such; and (3) the dramatic reduction in seizures by MIA. In addition, *Schuchmann et al* (235) demonstrated, in a model of febrile seizures, that a rise in brain pH (respiratory alkalosis from hyperthermia) was accompanied by seizure activity. Seizures were abolished by suppressing alkalosis with 5% ambient CO_2. The injection of sodium bicarbonate at higher doses (5 mmol/kg) in neonatal rat pups closely mimicked the effects of

hyperthermia and increased behavioural seizure activity, although these were also blocked by 5% ambient CO_2. A 'graded restoration of normocapnia' strategy in the resuscitation of newborn babies with perinatal asphyxia is highly recommended in view of these results and may reduce seizures and hence improve outcome.

In line with this, recent guidelines (236) encourage minimising the exposure to hypocapnia or hyperoxia in the respiratory management of infants with NE treated with therapeutic hypothermia, and avoiding the use of alkaline buffers.

Furthermore, regarding the deleterious effect of hypocapnia in NE following hypoxia-ischaemia, several studies support in recent years its association with neurological impairment (237-240). Pappas et al (237) showed, in the secondary analysis of the NICHD randomised trial of therapeutic hypothermia for moderate to severe NE, that the risk of death and adverse neurodevelopmental outcome increased when infants had lower pCO_2 values and/or higher cumulative exposure to pCO_2 below 4.7 kPa within the first 12h of life. Similarly, Lingappan et al (238) found, in a post-hoc analysis of CoolCap trial, that an unfavourable outcome was more likely with lower pCO_2 levels, in a dose-dependent manner. Szakmar et al (239) showed that in infants with moderate-severe NE who underwent therapeutic hypothermia, the time spent hypocapnic (pCO_2<4.7 kPa) was an independent predictor of brain injury on MRI. However, in the group of infants with mild encephalopathy, the time in hypocapnia had no effect on the risk of brain injury. Hypocapnia can exacerbate brain injury due to cerebral vasoconstriction and reduced cerebral blood flow, decrease in oxygen supply,

and increasing oxygen demand (236, 241). Recently, the HENRIC feasibility and safety trial (Hypoxic-Ischaemic Encephalopathy Therapy Optimisation in Neonates for Better Neuroprotection with Inhalative CO_2) (242) has shown that administering a gas mixture of 5% CO_2 and 95% air, for 12h, through the patient circuits to infants ventilated during cooling, if the temperature-corrected pCO_2 was below 5.3 kPa, was feasible and safe, and helped in preventing hypocarbia. A larger randomised trial investigating the efficacy of controlled normocapnia through 5% CO_2 inhalation on long- term neurodevelopmental outcomes are required.

1.6.2 NHE blockade and seizure reduction

In an effort to explore the mechanisms of post-asphyxia brain alkalosis, *Helmy et al (243)* used the rat pup exposed to one hour of asphyxia (simultaneous hypoxia and hypercapnia). In one group, pups breathed air after asphyxia and in the second normocapnia was achieved in a graded manner as described before (5). Some of the pups received methyl isobutyl-amiloride (MIA) intraperitoneally 30 min before asphyxia. Brain pH was measured in vivo using a two-photon imaging of intracellular pH in neocortical neurons and both body and brain pH using proton-sensitive microelectrodes. Blood-brain barrier (BBB) permeability was assessed using intraperitoneal sodium fluorescein. Seizure burden was assessed both behaviourally and using EEG. They found intraneuronal alkalosis after asphyxia, with a time course and sensitivity to graded restoration of normocapnia that were similar to what was described before for extracellular

alkalosis (5). The post-asphyxia brain alkalosis is generated in the absence of a rise of pH in blood. Thus, the increase in both extracellular and intracellular pH recorded in the brain implies an enhanced net loss of acid equivalents from brain tissue across the blood–brain barrier. It was demonstrated not to be attributable to a disruption of the BBB by the lack of increased sodium fluorescein extravasation into the brain, and by electrophysiological characteristics of the BBB. This proves a strict compartmentalisation of brain extracellular pH by the BBB under normal conditions and in response to asphyxia in this model. The electrode recordings of pH in the brain and trunk showed a net efflux of acid equivalents from the brain across the BBB, which was abolished by the NHE inhibitor MIA, suppressing the post-asphyxia rebound alkalosis of the brain extracellular pH without having any significant effect on the weight of the pups. Remarkably, MIA also abolished post-asphyxia seizures (reduced seizure burden by 88%) when applied pre-insult in rat pups (5, 243) and ameliorated brain injury when applied before hypoxic-ischemic conditions in neonatal mice (184). These findings support the conclusion that activation of NHE in the BBB leads to brain alkalosis and consequent seizures.

Therapeutic hypothermia is now standard care for infants in the developed world with moderate to severe neonatal encephalopathy (244). It is unknown whether NHE inhibition combined with therapeutic hypothermia might augment hypothermic neuroprotection after perinatal asphyxia or not. Some in vitro studies suggest that moderate hypothermia (reducing temperature from 37 to 20°C) itself increases NHE activity (245, 246) whilst others suggest that

hypothermia produces a partial inhibition of NHE activity (247). If hypothermia inhibits partially NHE or even more if it increases NHE activity, the combined effects of an NHE inhibitor with hypothermia could significantly augment hypothermic neuroprotection especially as they act on separate pathways. Importantly, studies suggest that the potency of NHE blockade under hypothermic conditions is not influenced by a change in temperature (247) and NHE blockade was beneficial in a perfused heart model even after hypothermic ischaemia (248). Pre-clinical large animal studies of the potential augmentation of mild therapeutic hypothermia combined with NHE blockade are high priority.

NHE inhibitors have been used in humans. The most used has been amiloride, which has an oral formulation, indicated as an adjunct therapy (potassium sparing diuretic) to thiazide or loop diuretics for oedema in heart failure, and hepatic disease (where potassium conservation is desirable) (249). While studies have not documented paediatric-specific problems, the safety and efficacy of amiloride have not been established in children. There is neonatal dosage for it (100-200 mcg/kg twice daily) on the BNFC (British National Formulary For Children from the National Institute for Health and Care Excellence – NICE), although it is not licensed for use in children. There are also local protocols for infant and children, like the one at Great Ormond Street Hospital. Onset of action is around 2h post-administration, diuretic peak effect occurs at 6-10h, and persists for around 24h. Amiloride is not ototoxic, being the main adverse effects hyperkalaemia, hyponatraemia, gastrointestinal disturbances, metabolic acidosis, and transient deranged renal function. Rimeporide, an NHE-1 inhibitor

which has shown a good safety and tolerability profile so far in adults (250), was on a phase Ib trial in children between 6 and 11 years old with cardiomyopathy in Duchenne Muscular Dystrophy (251). The NHE inhibitors cariporide and eniporide have also been used safely in adults with evolving myocardial infarction and those at risk of it (252). NHE inhibitors are a potential neuroprotective therapy for infants with neonatal encephalopathy, but further preclinical trial of their effects combined with cooling, and safety trials in newborn infants are still required.

Part 7: Brain perfusion following perinatal hypoxia-ischaemia

As described in the pathophysiology section, brain tissue's viability depends on the delivery of glucose and oxygen, and clearance of the products of metabolism; thus, brain perfusion is crucial. Cerebral blood flow (CBF) represents the rate of blood delivery to a tissue volume. High metabolism requirements in the brain are due to its main role: the generation of the electrical activity, which is required for neuronal signalling. Since there is no reserve store of oxygen and glucose, the continuous blood flow is crucial to guarantee the continuity of the brain function. Geiger and colleagues demonstrated in a rodent model that over 80% of the energy in brain regions such as the hippocampal axons is expended by postsynaptic potentials (253, 254). Grey matter – consisting predominantly of neuronal cell bodies – has a higher metabolic need, therefore, cerebral blood

flow requirements, compared to white matter – consisting mainly of myelinated axons – with a much lower metabolic demand, and cerebral blood flow consequently. This explains a much greater susceptibility of the grey matter regions (basal ganglia and thalami especially) to a sudden hypoxic-ischaemic insult (102). Cerebral blood flow is partly determined by vascular resistance, being affected by changes in arterial oxygenation and CO_2 levels, degree of acidosis, potassium and glucose levels, adenosine, nitric oxide (NO), arachidonic acid and its derivatives, sympathetic and parasympathetic pathways, and drugs (such as morphine, midazolam, etc.). See *table 1-0-7* for main mechanisms of autoregulation (based on (255)).

Autoregulation of CBF is the ability of the brain to maintain relatively constant blood flow despite changes in perfusion pressure (256), being particularly well developed in the brain. Cerebral ischaemia occurs when cerebral perfusion pressure falls below the lower limit of autoregulation (50). A reduction in CBF is compensated by an increase in oxygen extraction from the blood (257).

Agent	Function	Vasodilatation ↑ CBF	Vasoconstriction ↓ CBF
paO_2	Substrate of oxidative glucose metabolism	↓ [O_2] (if pO2<6.7kPa)	↑ [O_2]
$paCO_2$	Products of oxidative glucose metabolism	↑ [CO_2]	↓ [CO_2]
Acidosis (H^+)		Acidosis (arterial smooth muscle action)	Alkalosis
K^+	Neuronal signalling regulation	↑ (relaxes arterioles muscle)	↓ (mild vasoconstriction)
Glucose	Substrate of energy metabolism	Hypoglycaemia	↑
Adenosine	Energy metabolism and neuronal activity	↑	n/a
NO	Product of glutamate receptor activity and inflammatory cascade	↑	n/a
Arachidonic acid and derivatives	Inflammation / infection and pain.	↑ PGI_2, PGE_2, PGD_2	↑ $PGF_{2\alpha}$, TXA_2
Sympathetic pathway	Neural pathway	Block	Activation ⊕
Parasympathetic pathway		Activation ⊕	Block

Table 1.0-7: Summary of some mechanisms involved in autoregulation of CBF(255)
paO_2: partial pressure arterial of oxygen; $paCO_2$: partial pressure arterial of carbon dioxide; H^+: proton; K^+: potassium; NO: nitric oxide; PGI_2: prostaglandin I_2; PGE_2: prostaglandin E_2; PGD_2: prostaglandin D_2; $PGF_{2\alpha}$: prostaglandin $F_{2\alpha}$; TXA_2: thromboxane A_2.

Acute *hypoxia* causes increase in CBF via direct effects on vascular cells of cerebral arteries and arterioles (opening of K^+-ATP channels on smooth muscles with drop in ATP, causing hyperpolarisation and vasodilation; and increasing NO and adenosine production locally, also promoting vasodilation). Chronic hypoxia increases CBF by its effect on capillary density.

Carbon dioxide serves as one of the fundamental regulators of CBF. *Hypercapnia* causes vasodilation by a direct effect of extracellular H^+ on vascular smooth muscle; and in some species also due to prostanoids and NO production (255).

Changes in pH cause a direct relaxation (acidosis) or contraction (alkalosis) of the smooth muscle. Some studies suggest that pCO_2 acts independently of and/or in conjunction with altered pH (258).

Hyperkalaemia causes vasodilation due to hyperpolarization of the vascular smooth muscle (VSM) cells (Na^+-K^+ pump and/or activation of the inwardly rectifying Kir channels), and endothelium-dependent relaxation (259).

Hypoglycaemia triggers increases in CBF to improve glucose supply to the brain. This occurs by astrocytes releasing vasodilators (prostaglandins and epoxyeicosatrienoic acids) in a Ca^{2+}-dependent manner, leading to dilation of brain arterioles and increase CBF (260).

Adenosine in the brain is a dilator of pial vessels in the dog, cat, and rat. It is released when there is a mismatch between supply and demand, like moderate hypotension, during profound ischaemia, with sustained hypoxia, and also during bicuculline-induced seizures (261). If the effects of adenosine are blocked with receptor antagonists, the vasodilation is also reduced (262).

Factors that increase intracellular calcium activate endothelial NOS (responsible for conversion of L-arginine to *NO* and citrulline by the cerebral endothelium), diffusing to the VSM, where it causes vasodilation primarily by activation of soluble guanyl cyclase. This, in turn, increases the levels of cyclic guanine monophosphate (cGMP), that activates protein kinase G, causing the relaxation of VSM (in part opening BK-Ca^{2+} channels and reducing intracellular calcium).

In endothelial cells, *arachidonic acid (AA)* metabolism produces vasoactive products (less involvement of this pathway in the brain than in peripheral

endothelium). AA lipid precursors (substrates for cyclooxygenase (COX), lipoxygenases, and cytochrome P450 monooxygenases) are produced by activation of the calcium-dependent enzyme phospholipase A_2 (hydrolysing cellular lipid membranes). Products of the COX pathway can be vasodilating or vasoconstricting in nature, as shown in the table above.

Although the contribution of the autonomic nervous system to CBF control is unclear, previous studies have helped to understand their role (263).

During a hypoxic-ischaemic event, the adrenergic sympathetic activation – once the duration and severity have overrun the mechanisms of autoregulation to preserve the heart and brain's perfusion (as described in the initial sections of this chapter) – causes then a vasoconstriction and hypoperfusion to the brain.

Following hypoxia-ischaemia, severe alteration of brain metabolism and physiology are observed (264), being associated with specific abnormalities in blood flow such as vasoparalysis (80). As described in Part 3, in the cranial ultrasound section, it has been described that following neonatal encephalopathy, there is a loss of autoregulation of cerebral blood flow (CBF), with a low resistance index (RI) (79, 80). An increased CBF is found in babies who have suffered a more severe insult, using cranial ultrasound scan (76, 77), near-infrared spectroscopy (NIRS) (79, 265), and MR techniques, such as arterial spin labelling (ASL) (7, 266). This so-called 'luxury perfusion syndrome' or hyperaemia is characterized by increased CBF relative to the metabolic needs of the brain. The term was coined in 1960s in adults with various brain pathologies and mainly stroke patients (267). It is likely to be initiated by abnormal metabolism (268),

such as lactic acidosis, and loss of vessels' tone (264). This hyperperfusion restores high-energy phosphates that lead to delayed cell death (7, 269) and is associated with poor outcome (79, 80, 270). During hypothermia, it has been shown using cranial ultrasound scan that RI is less predictive, possibly due to vasoconstriction secondary to cooling, but this was reversed once hypothermia was stopped and vasodilatation was seen once the child was rewarmed (78).

Arterial Spin Labelling is a non-invasive MR imaging technique capable of both imaging and quantifying blood perfusion, or CBF, by using water as an endogenous, freely diffusible tracer (271). In ASL, arterial blood water is magnetically labelled then imaged (*figure 1-0-10*). A first stage involves magnetically labelling arterial blood water (protons) below the region of interest (ROI) by a applying a radiofrequency (RF) inversion pulse. As a result, an inversion of the net magnetisation of blood water is achieved (arterial blood is magnetically labelled). A second stage involves taking an image after a period of time (called post-labelling delay) when the labelled blood flowed into the ROI and exchanged with tissue water. The inverted spins within the blood water alter total tissue magnetisation, reducing MR signal and image intensity. A control image needs to be performed without labelling. The signal generated by static tissue is identical in control and label condition, hence a perfusion-weighted image can be produced by subtracting the labelled image and the control one. Multiple repetitions are needed to improve the signal to noise ratio (SNR), as the signal difference between labelled and control images is only 0.5-1.5% in adults (272).

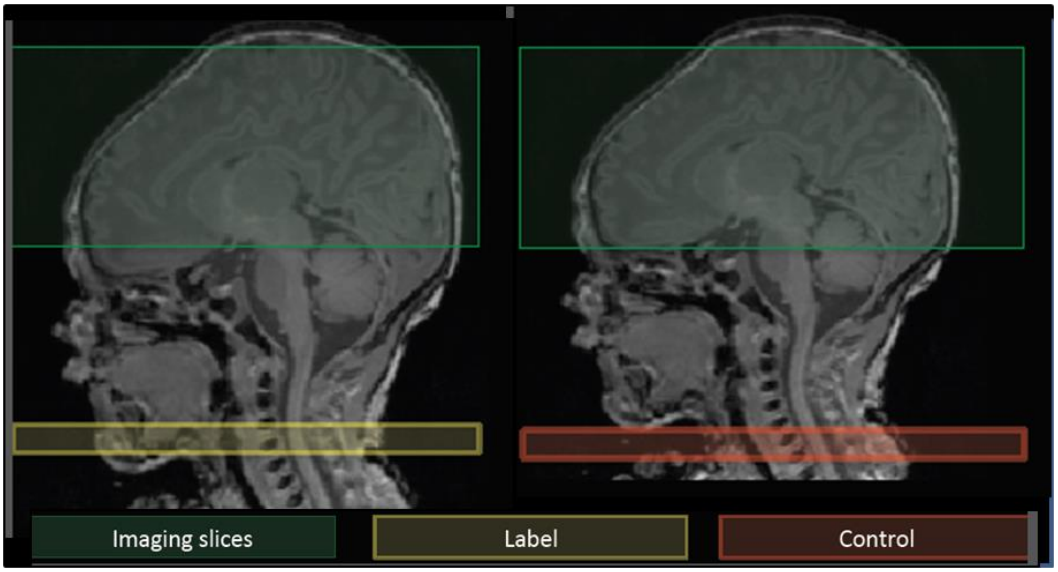

Figure 1-0-10: Schematic diagram of pCASL acquisition. *Left* is the acquisition of labelled image after a delay between the labelling (in yellow labelling plane in the neck at the bifurcation of the carotid arteries) and the acquisition of the flow into brain tissue within the ROI (green box). *Right* is the acquisition of the control image (in red control RF pulse and ROI in the green box). Figure courtesy of Dr Magdalena Sokolska (6).

Several labelling methods exist, such as continuous ASL, pulsed ASL (PASL) and pseudo-continuous ASL (pCASL) (272). The latter (pCASL) was introduced in the last 15 years (273) using a train of pulses accompanied by gradients to invert flowing spins in a "pseudo-continuous" manner. In the study performed at University College London Hospital (UCLH) – described in chapter 4 – pCASL labelling technique is used, achieving higher SNR (6). Few studies have studied cerebral blood flow in neonates following hypoxia-ischaemia, and hyperperfusion appeared in areas with subsequent injury in conventional MRI (7, 274-276), suggesting that hyperperfusion can be a marker for delayed injury. There have been no studies investigating the relationship between brain pHi and cerebral blood flow.

Part 8: Summary, Scope, and Objectives

Perinatal hypoxic-ischaemic brain injury in term babies is still a significant problem throughout the world. Therapeutic hypothermia has improved outcome, especially of those with a moderate insult. However, unfortunately, around half the infants who receive therapeutic hypothermia still have abnormal outcomes. Experimental data suggest that the addition of another agent to cooling may enhance overall protection either additively or synergistically. Experimental data have demonstrated a key role of brain intracellular pH (pHi) – both during and post-insult – and neonatal seizures in the pathophysiology of brain injury. The Na^+/H^+ exchangers are crucial in maintaining pHi and ion homeostasis and in microglial activation in some areas of the brain. NHE inhibitors are a promising neuroprotective tool in animal models, reducing cell death, seizure burden and brain injury with improvement of functional outcome. However, no studies have been performed in newborn infants with neonatal encephalopathy since the introduction of therapeutic hypothermia to prove that rebound alkalosis is occurring, and if so, that it is still related to outcome. Furthermore, no studies have shown the relationship between seizure burden and rebound brain alkalosis following hypoxia-ischaemia. The aim of the first study (Chapter 3) is to address the relationship between localised brain pHi and seizure burden, and between brain pHi and prognosis (both with other prognostic tools and with long term outcome).

Additionally, the loss of autoregulation following a hypoxic-ischaemic insult has been described but little is known about its pathophysiology. We aim to assess the relationship between brain pHi changes in brain perfusion with a sub-study of these infants with neonatal encephalopathy who underwent hypothermia, using arterial spin labelling (ASL) (Chapter 4).

Lastly, little is known about the physiology of acid-base equilibrium in the brain intra-insult. The aim of the third study (Chapter 5) is to investigate the relationship between the severity, duration, and rate of recovery from acidosis during hypoxia-ischaemia, and energy metabolite ratios at 1h post-insult measure in the brain of a preclinical model of perinatal asphyxia.

Chapter 2: General Material and Methods for ^{31}P MRS in newborn infants

Part 1: Clinical research preparation

Baby Brain Study is a research project focusing on newborn infants at risk of brain injury. The aim was to better understand the role of brain pHi, energy metabolism and cerebral blood flow in brain injury. The population of interest for this thesis is infants with neonatal encephalopathy following hypoxia-ischaemia who undergo therapeutic hypothermia. The standard of neurocritical care at UCLH includes daily examination, continuous EEG from admission, daily cranial ultrasound scans, MRI and proton MRS post-rewarming, and neurodevelopmental follow-up until 2 years of age. The Baby Brain Study added extra further neuromonitoring (NIRS) and neuroimaging investigations (phosphorus MRS and Arterial Spin Labelling), while they were having their clinical scan, to better understand the pathophysiology during the 'secondary energy failure' phase in neonates in the post-cooling era. There were three substudies within the Baby Brain Study. The first aimed to answer whether intracellular brain pH (pHi) was still a good predictor of outcome despite the introduction of cooling; the role that brain pHi had in neonatal seizures post-hypoxia-ischaemia; and the relationship between brain pHi and other markers of outcome. The second substudy aimed to understand the relationship between brain pHi and cerebral blood flow studied with ASL. The third substudy aimed to

understand whether brain metabolism measured with a new bedside NIRS system (cytochrome oxidase) was a good predictor of outcome, and its relationship with other markers of outcome. This thesis includes the first two substudies. The third study, based on NIRS, was part of the doctoral thesis of Dr S. Mitra.

Ethical permission was granted by the NRES Committee London (National Research Ethics Service) - Bloomsbury (REC reference 13/LO/0225) following IRAS application and further presentation of Baby Brain Study protocol, Parents' information leaflet version 4.1 (*Appendix 1*) and Consent form version 4.1 (*Appendix 2*), all prepared by the author. The latter attended the committee on March 2013, and approval was granted further few minor amendments. University College London Hospital R&D approval (R&D reference 13/0013) was also granted in April 2013.

Extended scanning time was arranged (extra 30 min to the 60 min clinical scanning appointments) with a "research time" application to the 3T Committee for the cases where we can perform both phosphorus (^{31}P) MRS and arterial spin labelling (ASL, to assess brain perfusion).

Part 2: ^{31}P MRS sequence optimisation

A purpose made birdcage multinuclear phosphorus-31 coil specified to be used within the Lammers® incubator was manufactured by Rapid Biomedical® and

delivered to University College London Hospital (UCLH) (*figure 2-0-1*) in December 2013 to perform these studies.

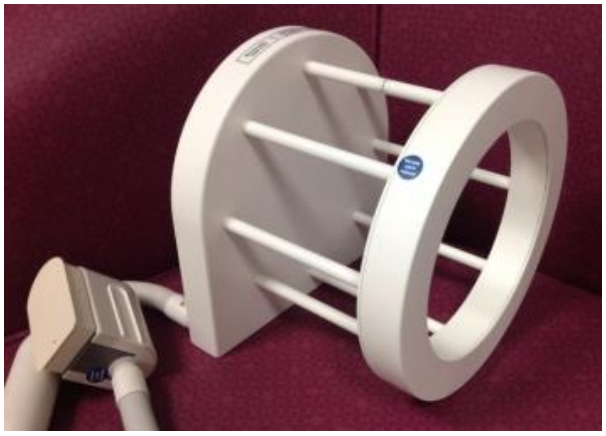

Figure 2-0-1: 31-Phosphorus coil made by Rapid Biomedical®

In collaboration with David Price (Medical Physics at UCLH), the calibration of the coil, safety checks and sequence development were performed to be used in newborn infants within an MR conditional incubator in the 3T MR scanner.

3.3.1 Safety checks

The safety requirements determined by Rapid Biomedical® for the phosphorus coil were recommended for it to be used with humidity above 30% and FiO_2 below 25%. These limits are designed to exclude the possibility of an electrical discharge.

After measurements with an oxygen probe during the phantom experiments and checking the conditions at the end of clinical scans in babies with different supplementary oxygen requirements, I produced the guideline for "Rapid Biomedical® coil use within the Lammers® incubator" (*Appendix 3*).

3.3.2 Phantom work

The following phantoms were used for coil performance validation and sequence optimisation:

1. **Phantom 1:** Philips Healthcare® **Sphere B** (10cm diameter)

   80 ml Methylphosphonic acid: 313 mM P(OH)20(CH_3)

2. **Phantom 2:** Adenosine triphosphate (ATP) Phantom (500 ml flask), using the following:

   ATP 10mM + 0-phosphoryethanolamine (PEA) 10 mM + NaCl solution 150mM, plus a buffer (6.350 gr K_2PO_4 and 1.913 gr KH_2PO_4). The ATP and PEA concentrations are similar (if a little higher) to those expected in neonatal brain whilst the inclusion of PE provides a similar range of chemical shifts (PEA to β-ATP) that will be of interest in the neonatal brain. Therefore, this phantom can be used for sequence optimisation.

3. **Phantom 3:** Coil calibration phantom replicating the one used by Rapid Biomedical®, using the following components: H_3PO_4 (phosphoric acid 80%, Sigma Roche®), $NiSO_4$ (nickel sulphate, Sigma Roche®) and NaCl (sodium chloride or saline). Two bottles were prepared:

   - 3.75g $NiSO_4$ x $6H_2O$ + 5g NaCl, in 1000 ml H_2O (plastic bottle), for mimicking the coil loading of a neonate

   - 80% phosphoric acid, in 15 ml glass vial, for signal

   We used them as one, placing the vial on top of the loading bottle.

Figure 2-0-2: Phantom work with the Rapid Biomedical® 31-phosphorus coil in the 3T Philips® scanner

3.3.3 Calibration

Using the calibration phantom, we performed a series of pulse-acquire experiments to check the factory calibration of the coil. The power supplied to the coil is controlled by scaling factors held in a calibration file installed on the scanner computer. The scaling factors should control the power applied to the coil in such a way that the scanners nominal 180° RF pulse is equal to the true 180° RF pulse yielding zero signal and maximum signal is obtained for a flip angle of 90°.

3.3.4 Sequence optimization

Offset frequency:

The offset frequency chosen was -270 Hz to set the centre of the spectrum between the ɣ- and α-ATP peaks. The RF pulse bandwidth was adequate (e.g not losing signal at the edges of the range).

Localised ^{3}P MRS

One of the aims of this study is to obtain localised pHi data. There were two options for spatially localised ^{31}P spectroscopy:

i) Image selected in vivo (ISIS):

ISIS is used as a localisation sequence to acquire metabolite information in single voxel or double voxel. Double voxel ISIS is appealing because it might allow the acquisition of pH information in two distinct regions of the brain for the same scan time however there are certain constraints limiting double voxel use in the neonatal brain on the Philips Healthcare® scanner (*figure 2-0-3*), as the two voxels need to be of the same dimensions and aligned. For anatomical reasons it would be difficult to obtain a voxel big enough to achieve an adequate SNR but small enough to fit both, separately, on the basal ganglia and thalami (BGT) and the white mater (WM).

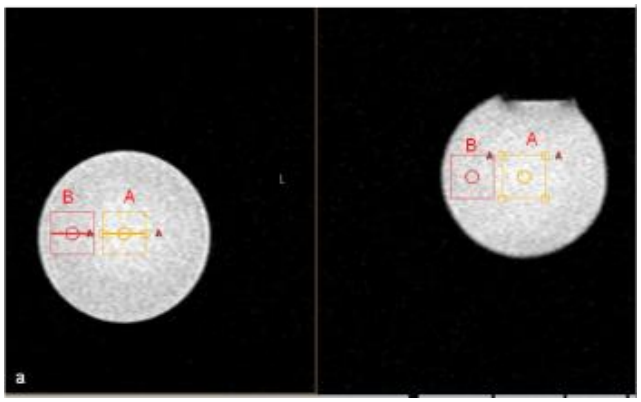

Figure 2-0-3: Double acquisition ISIS using the TP phantom: 2 voxels of the same size (25 x 25 x 25mm) and aligned on the ATP phantom.

The ISIS method generates three 180° pulses prior to a 90° pulse, after which the free induction decay (FID) is recorded. Specific slice-selective 180° pulses are combined and the FID's added or subtracted to generate a spectrum (277).

An advantage of the ISIS method is that the magnetisation before the final 90° pulse is held predominantly along the longitudinal axis and so T2 relaxation effects are relatively small. This explains the value of this technique for ^{31}P data acquisition because some phosphorus metabolites such as ATP have short T2 values. See *table 2-0-1* for T_1 and T_2 values for each metabolite.

			PME			Pi			PDE			PCr			γ-ATP			α-ATP			ß-ATP		
			T_1	T_2	mM	T_1	T_2	mM	T_1	T_2	mM	T_1	T_2	mM	T_1	T_2	mM	T_1	T_2	mM	T_1	T_2	mM
Roth (1989)		2.0T	1420		4.0	1450		2.0	1320		11.5	3140		4.9	650			850			800		2.5
Luyten (1989)		1.5T	2740			1470		2.6	1640			3290		4.3	1360		3.5	970		5.7	1030		3.0
Merboldt (1990)		2.0T	4000	70		2500	80	1.0	2000	20		3000	150	5.0	700	30	3.3	700	30	4.0	1000	20	3.3
Bottomley (1992)		1.5T			3.2			1.4			12.4			4.6									2.8
Jung (1993)		1.5T														89			84			62	
Lara (1993)		2.0T	1700	33	3.0	1400	81	0.7	1300	11	10.9	2700	390	2.7	600	17		1000	28		700	15	2.9
Matson (1993)		2.0T			2.3			1.2			7.0			3.1									2.3
Buchli (1994)	GM	2.35T			3.1			1.0			10.1			3.1									2.9
	WM	2.35T			4.3			1.3			14.2			2.9									2.9

Table 2-0-1: Absolute metabolite concentration, T1 and T2 in the brain obtained by 31P MRS. T_1 and T_2 in ms. Adapted from (278).

The disadvantage of ISIS is that eight acquisitions are required to accomplish the full spatial localisation; therefore, the sequence is vulnerable to patient movement occurring between these data collections. For a repetition time (TR) of 2-3 seconds the 8 acquisitions would be completed in 16 to 24 seconds. This defined as a single measurement. Sufficient measurements can then be acquired to give adequate spectral signal to noise when summed.

The advantage here is that while nothing can be done about motion within the 8 ISIS acquisitions it is possible to deal with the effects of motion between measurements. In the case of severe motion, a measurement can be discarded. In the case of less severe motion the phase and frequency errors can be corrected.

We decided to collect the maximum number of measurements by minimising the TR. Although the longer the TR the more signal, due to potential motion artefacts in newborn infants it would be beneficial to have a greater number of shorter repetitions. This meant that the spectra were not fully relaxed (apart from the first measurement) but there were more repetitions available for averaging. Moreover, considering the short Pi T_1 value (around 1.4s at 2T), a shorter TR is adequate.

ii) Chemical shift imaging (CSI):

CSI is an extension of MR spectroscopy, allowing a matrix of voxels to be collected each providing a spectrum. Potentially this provides a much more detailed localisation than ISIS where we are limited to a single voxel. For 2D CSI, a slice selection step is then followed by phase encoding and a spectrum is recorded at each phase encoding step. The phase encoding process is relatively time consuming. For a TR of 4 seconds and a matrix of 10 x 10 mm the scan time is around 6 minutes 40 seconds. CSI is very vulnerable to motion-related artefacts at any time during the acquisition. As an 'all or nothing' technique there is no scope for the partial rejection of corrupted data (277).

Figure 2-0-4 shows in the bottom the spectra from Voxel 34 with a high SNR. On the left a very large Pi peak is predominant but when Pi is filtered out from the spectra, we can see good phenylethanolamine and ATP peaks.

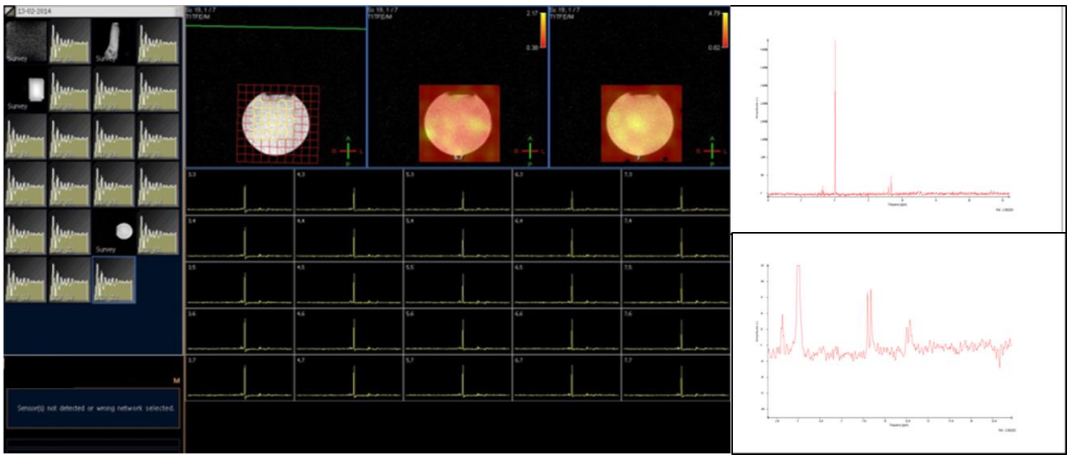

Figure 2-0-4: ^{31}P MRS Spectra using CSI from one of the voxels in the middle of the ATP phantom. (FOV 120 x 120, 10 x 10 voxels, voxel size 12 x 12 x20 mm; TR 4000ms, NSA 2) **Top:** with a high Pi and relatively small Pet and ATP peaks in comparison. **Bottom:** focusing on the ATP peaks. High SNR.

Increasing SNR: proton decoupling and Nuclear Overhauser Enhancement (NOE)

In ^{31}P MR spectroscopy nearby protons couple with phosphorus nuclei giving rise to peak splitting. By irradiating on the proton channel during FID collection decoupling can be achieved causing these multiplets to collapse back into narrower higher amplitude singlets (279). Since in-vivo proton-phosphorus coupling is weak, the benefits are not dramatic and most noticeable for phosphodiesters. Furthermore, pH measurements involve the chemical shift between 2 singlets (PCr and Pi) not greatly affected by proton- phosphorous coupling.

Energy transfer between protons and the ^{31}P nuclei can be used to give an additional signal boost called Nuclear Overhauser Enhancement (NOE) (279). By irradiating protons with the proton channel – before the FID is collected – the energy pumped into the protons can create an increased population difference

in the observed nucleus and therefore an increased signal intensity. The amount of NOE enhancement is T1 dependent so if the pathology alters T1 the amount of NOE may change. This may make comparison of metabolite ratios difficult.

The Rapid Biomedical® phosphorus coil has not been designed with the necessary filters to be used in conjunction with proton decoupling using the scanner's proton RF channel. Hence, proton decoupling generates artefacts in the phosphorus spectra.

We did several experiments using broadband NOE, both standardised Waltz 8 and Waltz 16 pulses. There was a slight amplitude increase when using NOE at mix times of 3500ms (B1 max had to be increased to 2), achieving the best SNR but reaching borderline SAR levels of 80%.

Similar experiment was performed with NOE using 2D CSI with a shorter TR (more like in vivo range) on the ATP phantom, with a slight increase signal.

Although NOE improved the signal, with an optimal value at around 2500 ms, there is an increase SAR and duration of the scan. Moreover, as mentioned above, signal enhancement is T1-dependent. Therefore, if the pathology changes T1 of the metabolite it might also change the amount of NOE, causing changes in metabolite ratios difficult to interpret. The decision at this point was not to use NOE for this study.

3.3.5 Baby Brain Study ^{31}P MRS: noise detection and sequence type

The first two babies were recruited into the study in March 2014. In both cases 2D CSI and ISIS were performed before deciding which one we would continue obtaining for the rest of the study.

The signal to noise from these infants' spectra was very poor. When analysing back the ATP phantom spectra, when ^{31}P MRS was performed within the Lammers® incubator, it was possible to see a deterioration of the SNR although less obvious because of the very high signal within the phantom. Following a series of experiments, it was demonstrated that both the Lammers® incubator battery and the Lammers® incubator monitoring (pulse oximeter and temperature) caused significant noise on the Spectra. I ordered a new MR conditional monitoring (Nonin 7500FO® Pediatric Fiber Optic MRI conditional Pulse oximeter, Nonin Medical, Inc., Minnesota, USA), which didn't create any interference with the ^{31}P MRS. From this point, I added to the guideline that during the ^{31}P MRS sequence, the Lammers® incubator ought to be completely turned off (both the trolley's battery and the head monitoring screen), with the monitoring being performed exclusively by the Nonin 7500FO® MR conditional. The ventilator and the Faraday cage for the Braun® pumps did not cause interference.

In May 2014, the first successful ^{31}P MRS using the Rapid Biomedical® phosphorus coil was performed, both with a 2D CSI and a single voxel ISIS over the BGT. Data with a good SNR was obtained from both techniques (*figure 2-0-5 and 2-0-6*). The maximum time available for ^{31}P MRS sequence was 10 - 15 min.

As mentioned above, the strategy followed with ISIS was to use the minimum TR possible to maximise the number of measurements. Although it is expected that partial T1 recovery will occur depending on the T1 of the different metabolites, signal will be detected by summing several measurements.

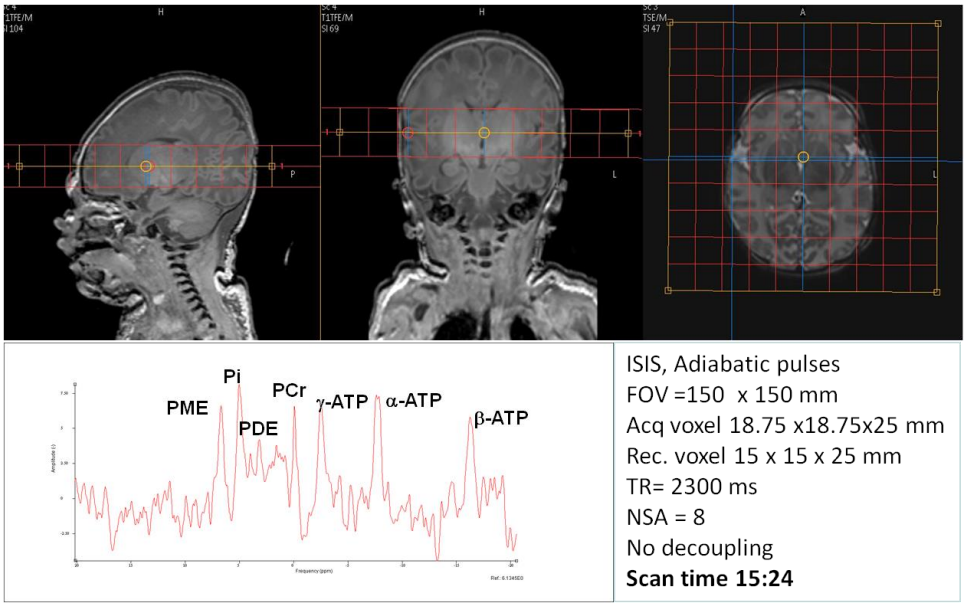

Figure 2-0-5: Localised brain ^{31}P MRS Spectra obtained with 2D CSI.

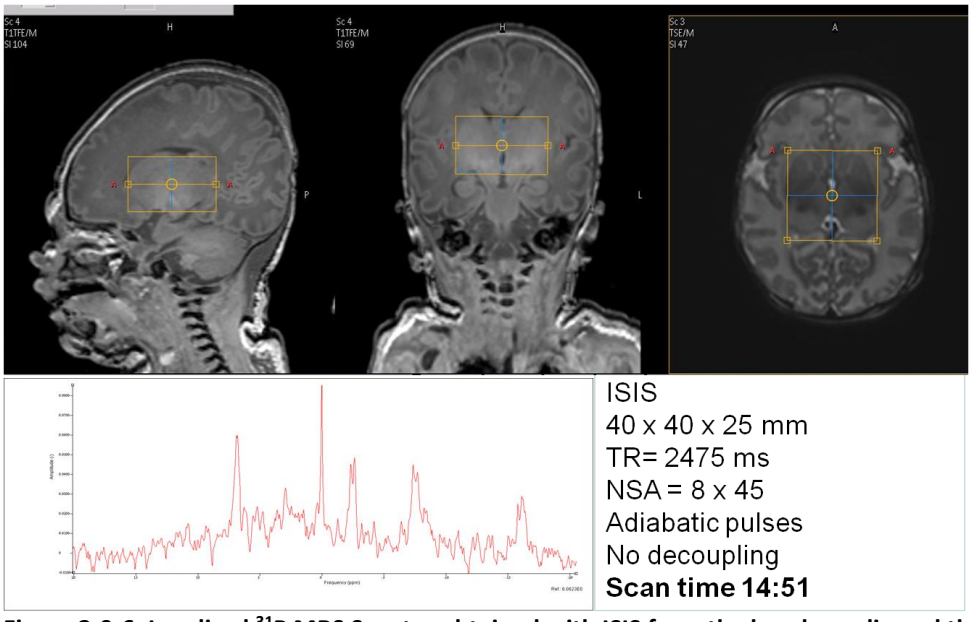

Figure 2-0-6: Localised ^{31}P MRS Spectra obtained with ISIS from the basal ganglia and thalami.

Initially, following these results we decided to continue performing CSI sequences for all babies in view that the SNR was very good, and more information was obtained (multivoxel), providing a more localised brain pHi calculation. The consecutive two infants who had ^{31}P MRS CSI performed had a very poor signal, likely due to some motion.

In view of these results, we decided that ISIS was the best localising phosphorus spectroscopy method to use with the current conditions. Although CSI provides a better localisation (multivoxel), providing a more localised brain pHi; ISIS allows us to localise to the basal ganglia and thalami (area expected to be more affected following an acute hypoxic-ischaemic event), within a reasonable acquisition time and with the benefit of being significantly more robust to motion. The central position of the voxel and the way the baby's head is immobilised – within a plastic coil-shape device of the same diameter than both the proton and the phosphorus coil – means that any movement occurring will effectively cause small rotations of the voxel relative to the baby's brain, rather than large translational shifts.

Since September 2014, we have performed only ISIS on all the babies, with a voxel covering both basal ganglia and thalami. The acquisition time for this sequence is 14:51 min. Scanning time was reduced for clinical reasons in 7 babies by reducing the number of repetitions from 8 x 45 to 8 x 35 or 25. Parameters used can be found in the guideline (Appendix 3):

Geometry: Nucleus P31 Offset frequency -270 Hz Coil selection: MC-Rapid-BM-MN Dual coil: no Preparation coil: Q-Body VOI orientation: transverse VOI size AP (mm): 40 RL (mm): 40 FH (mm): 25 Samples: 2048 Spectral BW: 3000	*Contrast:* Scan type: spectroscopy Scan mode: SV Technique: FID VOI selection: volume Method: ISIS Echoes: 1 TE: shortest RF pulse set: adiabatic TR: 2475 ms Shim: PB-auto PB order: second B1 mode: default Gradient mode: max PNS mode: low SAR: <5%
Motion: NSA: 8 Phase cycles: 8 *Dyn/angio:* Dynamic study: individual Dyn scans: 45 Dyn scans time: shortest ASL: no	*Postprocessing:* Receiver attenuation: 8 Reference tissue: WM Shifted metabolite: none.

3.3.6 Data analysis

Phosphorus (^{31}P) spectroscopy data is processed using the jMRUI software (280). It contains a suite of pre-processing functions such as apodisation, zero-filling, truncation, and phasing. It also offers a number of fitting algorithms such as AMARES (advanced method for accurate, robust, and efficient spectral fitting)

(281). AMARES is a non-linear-least-squares (NLLS) quantitation algorithm. It is time-domain based fitting damped exponential functions to the free induction decay (FID).

Then zero- and first-order phase corrections were applied manually on all spectra and set the 0 ppm reference to coincide with phosphocreatine (PCr) peak (see *figure 2-0-7*).

The fit can be constrained by applying prior knowledge, such as allowed ranges for peak frequencies and line widths, and specific constraints on j-coupling constants, phases, and relative amplitudes between peaks within a multiplet.

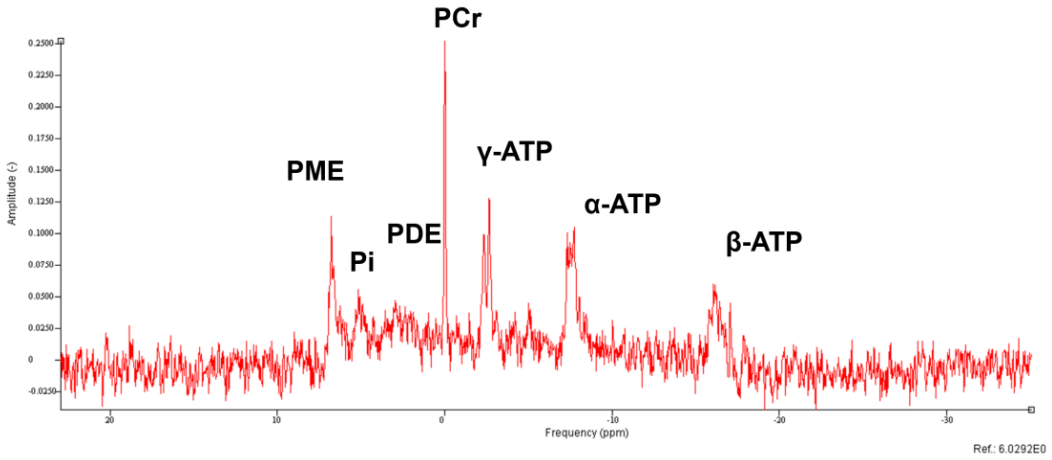

Figure 2-0-7: ^{31}P Spectra after apodization to 5 Hz and zero-order phase correction. PCr is set as 0 ppm reference.

I have used the AMARES fitting algorithm, with prior knowledge, within the jMRUI software to then fit the spectroscopy data. I have analysed each of the babies' ^{31}P MRS individually. The amplitude of each metabolite was obtained. In our time-domain free induction decay (FID) data-fitting template, we modelled PCr (phospho-creatine), Pi (inorganic phosphate), PME (phosphomonoesters,

primarily phosphocholine and phospho-ethanolamine), GPE (glycerophospho-ethanolamine), GPC (glycerophospho-choline), and α-, β-, and γ-ATP (adenosine triphosphate). The AMARES algorithm generates an estimated spectrum based on the individual components. This estimated spectrum is then subtracted from the original to yield a residue. The original, estimate, individual components and residue are displayed in 4 windows, showed in *figure 2-0-8*.

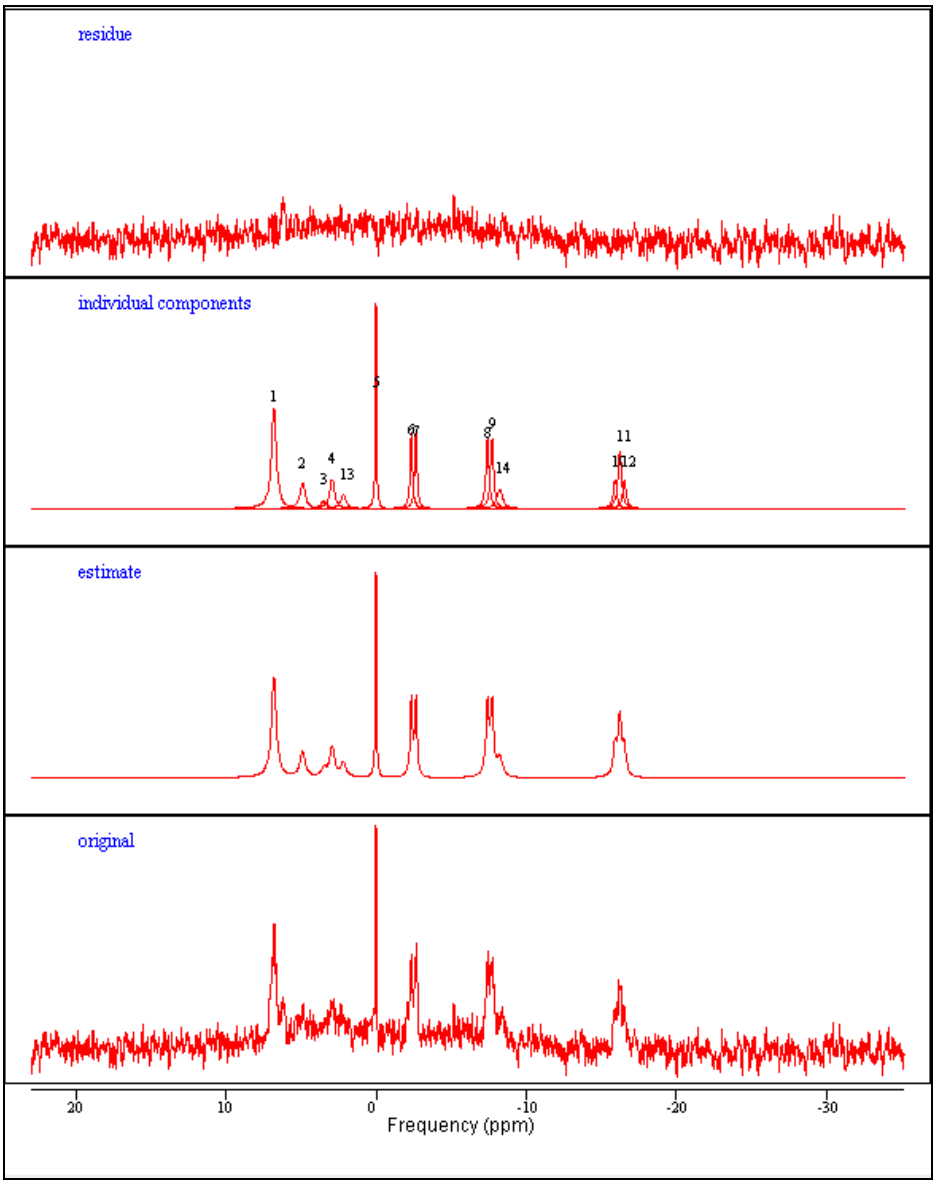

Figure 2-0-8: ^{31}P Spectra with (from top to bottom): residue, individual components, estimated and original spectra, without apodization.

Brain pHi can be calculated using the chemical shift of pH-sensitive metabolites on ^{31}P MRS. The Henderson-Hasselbalch equation describes the derivation of pH as a measure of acidity in biological and chemical systems:

$$pH = pKa + \log_{10}[(\delta - \delta^{+})) / (\delta^{0} - \delta)] \quad \textbf{Equation 1}$$

where pKa = -log Ka, and Ka is the proton dissociation equilibrium constant for the phosphoryl-moiety, δ^{+} and δ^{0} are the ^{31}P chemical shifts of the phosphoryl-moiety in the respective protonated and unprotonated forms, and δ is the chemical shift of the metabolites of interest (282).

Thus pHi measurement is derived from peak positions, using the modified Henderson-Hasselbalch equation described by Petroff et al (127). I have used the following, where δ is the chemical shift of Pi relative to PCr (Pi frequency in ppm – PCr frequency in ppm):

$$pHi\ (Hamilton) = 6.77 + \log_{10}[(\delta - 3.29) / (5.68 - \delta)]\ (135) \quad \textbf{Equation 2}$$

$$pHi\ (Robertson) = 6.75 + \log_{10}[(\delta - 3.27) / (5.69 - \delta)]\ (3) \quad \textbf{Equation 3}$$

To increase the confidence in the findings, I also determined brain pH using the chemical shift of Pi relative to α-ATP, where δ is the corrected Pi relative to α-ATP at -10.05ppm (Pi frequency in ppm + (-10.05 – [$\alpha_1 + \alpha_2$]/2)):

$$pHi\ (Raghunand) = 6.85 + \log_{10}[(\delta - 0.58) / (3.14 - \delta)]\ (132) \quad \textbf{Equation 4}$$

At physiological pH, Pi exists primarily in the forms of $H_2PO_4^-$ and HPO_4^{2-}. If α-ATP is set at -10.05 ppm, then the fast exchange of ^{31}P nuclei between these two forms results in a single resonance being observed between 0.58 ppm and 3.14 ppm, with the exact location of the resonance being determined by the relative amount of the two forms. Furthermore, the relative amount of these two forms

is determined by pH (132). It has been shown that the Pi signal originates primarily from the intracellular space in tumours (283).

Energy metabolite ratios were calculated from the ROI (region of interest):

- Pi/PCr (as a marker of neuronal death when Pi is high, hence the ratio is increased)
- ATP/Pi+PCr+ATPtotal (as a marker of brain oxidative metabolism, with a decrease in energy levels in infants with a more severe insult and who underwent secondary energy failure).

One of the difficulties of measuring brain pHi with ^{31}P MRS is to ensure a good fit, especially of Pi and PCr peaks used in the Henderson-Hasselbalch equation. This becomes challenging in infants with a less severe picture of HIE, due to a low SNR for Pi peak. We have considered different options to increase SNR as discussed previously. We have also worked on improving the fit, mainly optimising the prior knowledge used. Initially, prior knowledge based on 14 peaks was used, with a single Pi peak (*tables 2-0-2, 2-0-3 and 2-0-4)*.

Peak	Peak name	Frequency (ppm)	Line Width (Hz)
1	PME	6.79	10.0
2	Pi	4.99	15.0
3	GPE	3.54	10.0
4	GPC	2.84	10.0
5	PCr	0.0	10.0
6	ATPgamma1	-2.29	10.0
7	ATPgamma2	-2.53	10.0
8	ATPalpha1	-7.36	10.0
9	ATPalpha2	-7.66	10.0
10	ATPbeta1	-16.02	10.0
11	ATPbeta2	-15.83	10.0
12	ATPbeta3	-15.75	10.0
13	PEP	2.1	10.0
14	NADH	-8.29	10.0

Table 2-0-2: Prior knowledge for AMARES within jMRUI, based on 14 peaks: Starting values. PME (phosphomonoesters, primarily phosphocholine and phosphor-ethanolamine), Pi (inorganic phosphate), GPE (glycerophospho-ethanolamine), GPC (glycerophospho-choline), PCr (phosphor-creatine), γ-, α- and β-ATP (adenosine triphosphate), PEP (phosphoenol pyruvate) and NADH (reduced nicotinamide adenine dinucleotide).

	Peak name	Amplitude	Relative phase	Frequency (ppm)	Line Width (Hz)	Shape
1	PME	Estimated	Fixed ratio – GPC*1.0	Soft constraints – 6.7-7.1	Soft constraints – 0.0-20.0	Fixed-Lorentzian
2	Pi	Estimated	Fixed ratio – GPC*1.0	Soft constraints – 4.5 – 5.3	Soft constraints – 0.0-20.0	Fixed-Lorentzian
3	GPE	Estimated	Fixed ratio – GPC*1.0	Soft constraints – 3.5 – 3.7	Soft constraints – 0.0-20.0	Fixed-Lorentzian
4	GPC	Estimated	Estimated	Soft constraints – 2.9 – 3.1	Soft constraints – 0.0-20.0	Fixed-Lorentzian
5	PCr	Estimated	Fixed ratio – GPC*1.0	Soft constraints – -0.1 – 0.1	Soft constraints – 0.0-20.0	Fixed-Lorentzian
6	ATPgamma1	Estimated	Fixed ratio – GPC*1.0	Soft constraints – -2.4 - -2.2	Soft constraints – 0.0-20.0	Fixed-Lorentzian
7	ATPgamma2	Fixed-ratio – ATPgamma1*1.0	Fixed ratio – GPC*1.0	Fixed shift – ATPgamma1+ -16.0	Fixed-ratio – ATPgamma1*1.0	Fixed-Lorentzian
8	ATPalpha1	Estimated	Fixed ratio – GPC*1.0	Soft constraints – -7.45 - -7.25	Soft constraints – 0.0-20.0	Fixed-Lorentzian
9	ATPalpha2	Fixed-ratio – ATPalpha1*1.0	Fixed ratio – GPC*1.0	Fixed shift – ATPalpha1+ -16.0	Fixed-ratio – ATPalpha1*1.0	Fixed-Lorentzian
10	ATPbeta1	Fixed-ratio – ATPbeta2*0.5	Fixed ratio – GPC*1.0	Fixed shift – ATPbeta2+ 16.0	Fixed-ratio – ATPbeta2*1	Fixed-Lorentzian
11	ATPbeta2	Estimated	Fixed ratio – GPC*1.0	Estimated	Estimated	Fixed-Lorentzian
12	ATPbeta3	Fixed-ratio – ATPbeta2*0.5	Fixed ratio – GPC*1.0	Fixed shift – ATPbeta2+ -16.0	Fixed-ratio – ATPbeta2*1	Fixed-Lorentzian
13	PEP	Estimated	Fixed ratio – GPC*1.0	Soft constraints – 1.8 - 2.2	Soft constraints – 0.0-20.0	Fixed-Lorentzian
14	NADH	Estimated	Fixed ratio – GPC*1.0	Soft constraints – -- -8.2 - 0.0	Soft constraints – 0.0-20.0	Fixed-Lorentzian

Table 2-0-3: Prior knowledge for AMARES within jMRUI: Prior knowledge.

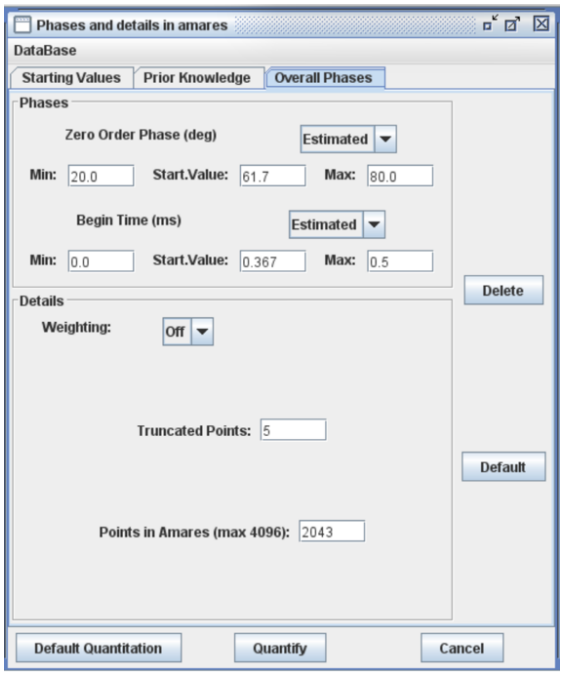

Table 2-0-4: Prior knowledge for AMARES within jMRUI: Overall Phases.

There was a group of infants for which their Pi fit wasn't accurate visually. Prior knowledge considering 4 Pi peaks was deemed to be more appropriate, as it would be more likely to detect the Pi peaks from the different compartments, each shifting slightly depending on pH in each compartment (see *tables 2-0-5, 2-0-6 and 2-0-7)*.

Peak	Peak name	Frequency (ppm)	Line Width (Hz)
1	ATPgamma1	-2.59	25.0
2	ATPgamma2	-2.69	25.0
3	ATPalpha1	-7.59	25.0
4	ATPalpha2	-7.69	25.0
5	ATPbeta1	-16.35	25.0
6	ATPbeta2	-16.15	25.0
7	ATPbeta3	-16.54	25.0
8	NAD	-8.06	25.0
9	PCr	0.0	25.0
10	GPC	2.89	25.0
11	GPE	3.48	25.0
12	Pi	5.16	25.0
13	Pi2	4.88	25.0
14	PME	6.74	25.0
15	PCh	6.43	25.0
16	UDP	-9.61	25.0
17	Pi3	4.59	25.0
18	PME2	5.99	25.0
19	Pi4	4.29	25.0

Table 2-0-5: New Prior knowledge for AMARES within jMRUI, based on 19 peaks: Starting values.

	Peak name	Amplitude	Relative phase	Frequency (ppm)	Line Width (Hz)	Shape
1	ATPgamma1	Estimated	Fixed ratio – PCr*1.0	Soft constraints – -3.5 - -1.6	Soft constraints – 1.0-100.0	Fixed-Lorentzian
2	ATPgamma2	Fixed-ratio – ATPgamma1*1.0	Fixed ratio – PCr*1.0	Fixed shift – ATPgamma1+ -17.0	Fixed-ratio – ATPgamma1*1.0	Fixed-Lorentzian
3	ATPalpha1	Estimated	Fixed ratio – PCr*1.0	Soft constraints – -7.75 - -6.85	Soft constraints – 1.0-100.0	Fixed-Lorentzian
4	ATPalpha2	Fixed-ratio – ATPalpha1*1.0	Fixed ratio – PCr*1.0	Fixed shift – ATPalpha1+ -17.0	Fixed-ratio – ATPalpha1*1.0	Fixed-Lorentzian
5	ATPbeta1	Estimated	Fixed ratio – PCr*1.0	Soft constraints – -17.49 - -14.49	Soft constraints – 1.0-100.0	Fixed-Lorentzian
6	ATPbeta2	Fixed-ratio – ATPbeta1*0.5	Fixed ratio – PCr*1.0	Fixed shift – ATPbeta1+ 17.0	Fixed-ratio – ATPbeta1*1	Fixed-Lorentzian
7	ATPbeta3	Fixed-ratio – ATPbeta1*0.5	Fixed ratio – PCr*1.0	Fixed shift – ATPbeta1+ -17.0	Fixed-ratio – ATPbeta1*1	Fixed-Lorentzian
8	NAD	Estimated	Fixed ratio – PCr*1.0	Soft constraints – -8.49 – 7.75	Soft constraints – 1.0-60.0	Fixed-Lorentzian
9	PCr	Estimated	Estimated	Soft constraints – -0.5 – 0.5	Soft constraints – 1.0-60.0	Fixed-Lorentzian
10	GPC	Estimated	Fixed ratio – PCr*1.0	Soft constraints –2.8 – 3.0	Soft constraints – 1.0-60.0	Fixed-Lorentzian
11	GPE	Estimated	Fixed ratio – PCr*1.0	Soft constraints – 3.3 – 3.5	Soft constraints – 1.0-60.0	Fixed-Lorentzian
12	Pi	Estimated	Fixed ratio – PCr*1.0	Soft constraints – 4.0 – 4.5	Soft constraints – 1.0-60.0	Fixed-Lorentzian
13	Pi2	Estimated	Fixed ratio – PCr*1.0	Soft constraints – 4.0 – 5.3	Soft constraints – 1.0-60.0	Fixed-Lorentzian
14	PME	Estimated	Fixed ratio – PCr*1.0	Soft constraints – 6.0-7.0	Soft constraints – 1.0-60.0	Fixed-Lorentzian
15	PCh	Estimated	Fixed ratio – PCr*1.0	Soft constraints – 5.8 – 6.5	Soft constraints – 1.0-60.0	Fixed-Lorentzian
16	UDP	Estimated	Fixed ratio – PCr*1.0	Soft constraints – -9.99- -8.99	Soft constraints – 1.0-100.0	Fixed-Lorentzian
17	Pi3	Estimated	Fixed ratio – PCr*1.0	Soft constraints – 4.0 – 4.9	Soft constraints – 1.0-60.0	Fixed-Lorentzian
18	PME2	Estimated	Fixed ratio – PCr*1.0	Soft constraints – 5.65 - 6.2	Soft constraints – 1.0-60.0	Fixed-Lorentzian
19	Pi4	Estimated	Fixed ratio – PCr*1.0	Soft constraints – 3.1 – 4.6	Soft constraints – 1.0-60.0	Fixed-Lorentzian

Table 2-0-6: New Prior knowledge for AMARES within jMRUI, based on 19 peaks: Prior knowledge.

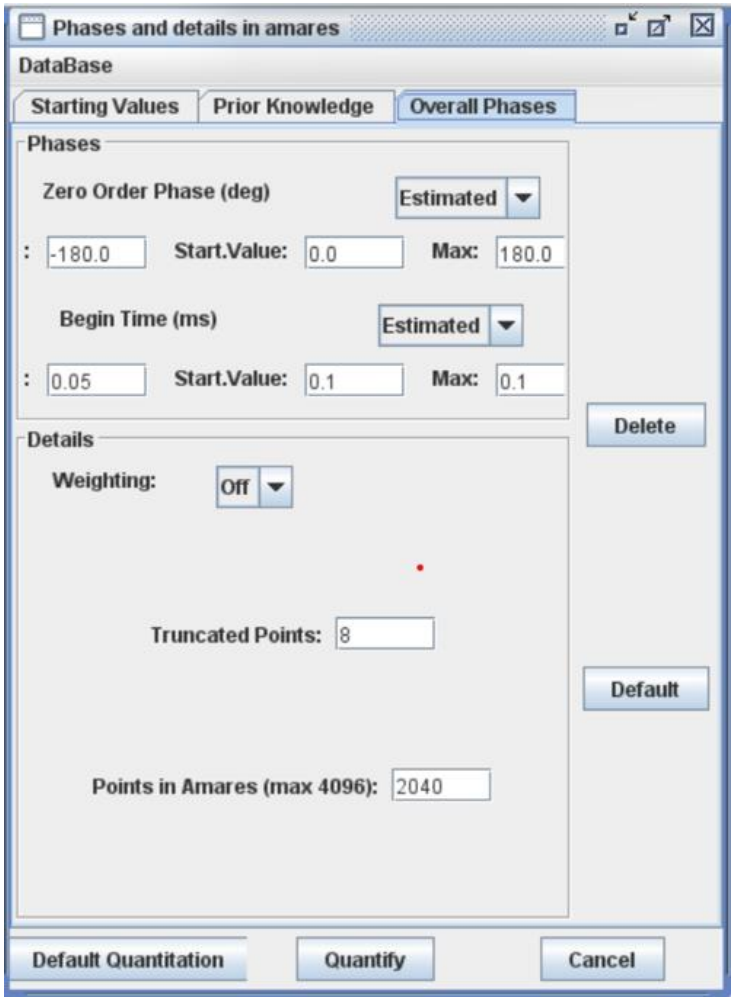

Table 2-0-7: New Prior knowledge for AMARES within jMRUI: Overall Phases.

The fit improved especially in 5 infants with a low Pi peak. This was assessed subjectively by getting a better fit around the frequency of Pi (4.5 – 5.3ppm) and by getting less residue. *Figure 2-0-9* shows an example of ^{31}P MRS Spectra from an infant with low SNR for Pi. In the close-up look at the fitting around 5ppm (where Pi peak is expected), the Pi fitting, using the second set of prior knowledge (peaks 12, 13, 17 and 19 within the circled area in the bottom right), looked more similar to the original spectra compared to the Pi fitting, using the previous set of prior knowledge (peak 2 within the circled area in the bottom left).

Pi frequency, used to measure chemical shift, was calculated using an amplitude weighted-average of the 4 Pi peaks frequencies (weighted Pi frequency = ([Pi1 freq. * Pi1 ampl.] + ([Pi2 freq. * Pi2 ampl.] + ([Pi3 freq. * Pi3 ampl.] + ([Pi4 freq. * Pi4 ampl.]) / (Pi1 ampl. + Pi2 ampl. + Pi3 ampl. + Pi4 ampl)).

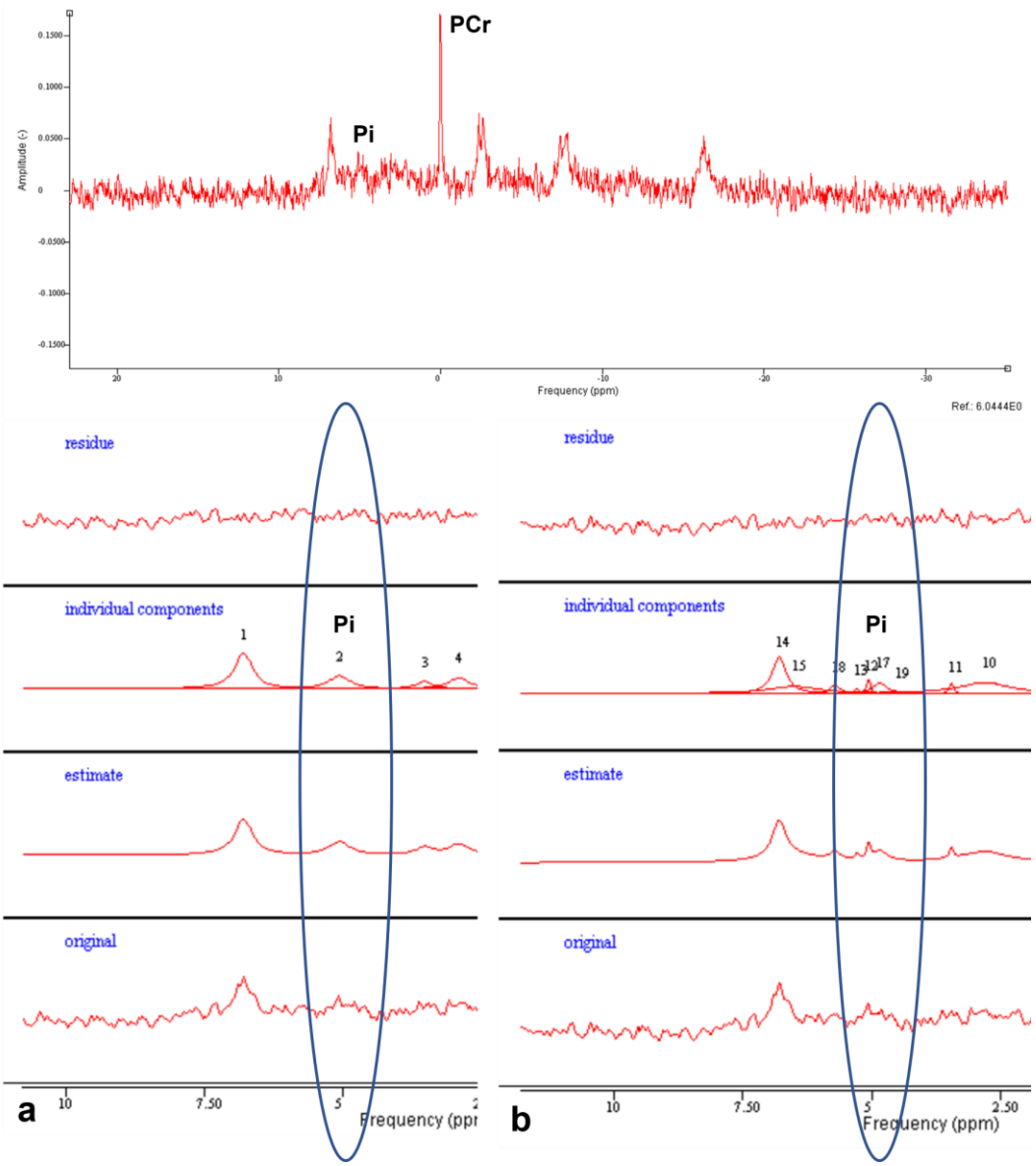

Figure 2-0-9: Spectra from a newborn infant with a low Pi peak. (*Top*) Spectra with reference 0 ppm set on the PCr peak. **(*Bottom Left*)** Close-up to the fitting around where we expect the Pi peak (between 4 and 5.3 ppm), **using the initial prior knowledge with one Pi peak (peak number 2). (*Bottom right*)** Close-up to the fitting around where we expect the Pi peak (between 4 and 5.3 ppm), **using the second prior knowledge with 4 Pi peaks (peaks number 12, 13, 17 and 19).** The pHi calculation was 7.22 with the fit on the left and 7.08 with the fit on the right.

For ^{1}H MRS, the dynamic spectra were summed off-line after phase and frequency correction and rejection of motion-corrupted data. MRS analysis was performed using Tarquin (284). The following metabolites were fitted: Choline (Cho), Creatine (Cr), Lactate (Lac), Threonine (Thr)(285), N-acetyl aspartate (NAA) and N-acetyl-aspartyl-glutamate (NAAG); lipids and macromolecules were not included. On long echo time (TE), the proximity of the methyl resonances of Lactate and Threonine, at 1.31ppm and 1.32ppm respectively, mean that with conventional MRS they are not independently resolvable in in-vivo spectra. By including Thr, in addition to lactate, in the spectral analysis, the goal was to improve the spectral fit in the region around 1.3 ppm in cases where lactate is raised (124, 286). Hence, the peak area ratios for LacT/tNAA (Lactate plus Threonine to total NAA [NAA+NAAG]) was calculated, and a cut-off point of 0.39 was considered as predictor of outcome, as published by Mitra et al. (124) *Figure 2-0-10* shows and example of ^{1}H MRS analysed with Tarquin for one infant with a good prognosis and one with a unfavourable prognosis.

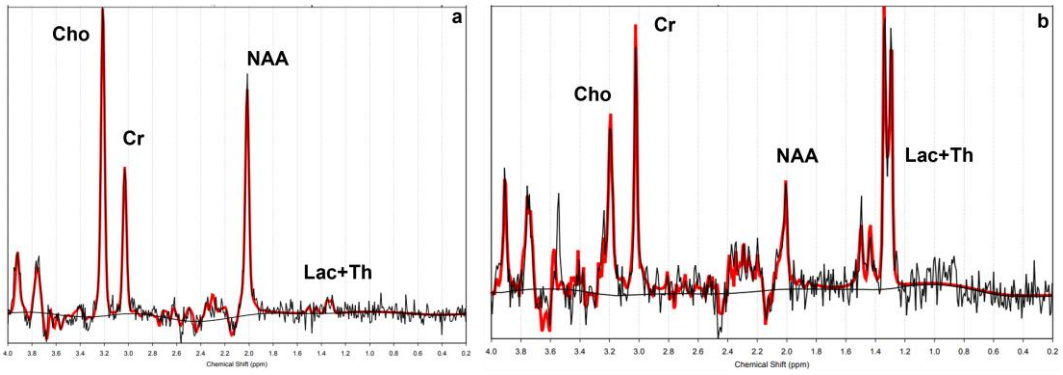

Figure 2-0-10: 1H MRS Spectra (PRESS, TE 288ms) on the left thalamus of the BGT of a newborn infant analysed with Tarquin. Cho: choline (cell membrane marker); Cr: creatine (energy metabolism); NAA: N-acetyl-aspartate (main neuronal marker); Lac: Lactate (product of anaerobic glycolysis; Th: threonine (similar frequency to Lac). On the left **(a)**, **Spectra of an infant following mild HIE**: high NAA peak and low Lac peak. On the right **(b)**, **Spectra of an infant following severe HIE**: low NAA peak and high Lac peak.

Part 3: Study recruitment

Since end of May 2014, I approached 78 families with an infant admitted to the neonatal unit at University College London Hospital (UCLH) at risk of brain injury. The flow-chart shows recruitment and exclusion numbers into the Baby Brain Study for ^{31}P MRS. Of the 71 who consented, 23 were excluded from the studies due to: i) poor quality of the data/different PMRS sequence (n=5); ii) withdrawal of consent (n=4); iii) unable to use the 3T scanner due to software issues or amplifier out of service (n=12); iv) running out of scanning time for research sequences (n=2). Useful phosphorus spectroscopy data has been acquired from 48 infants of them (see *flowchart in figure 2-0-11*). For the purpose of this study, only infants with neonatal encephalopathy secondary to hypoxia-ischaemia and who underwent therapeutic hypothermia were included (n=43). The other five were excluded due to different baseline diagnosis (1 with final diagnosis of stroke, 1 preterm 33+5 weeks who was not cooled, 2 with neonatal seizures who were not cooled and 1 ex-preterm baby with a cardiac arrest around term-time corrected, who was not cooled).

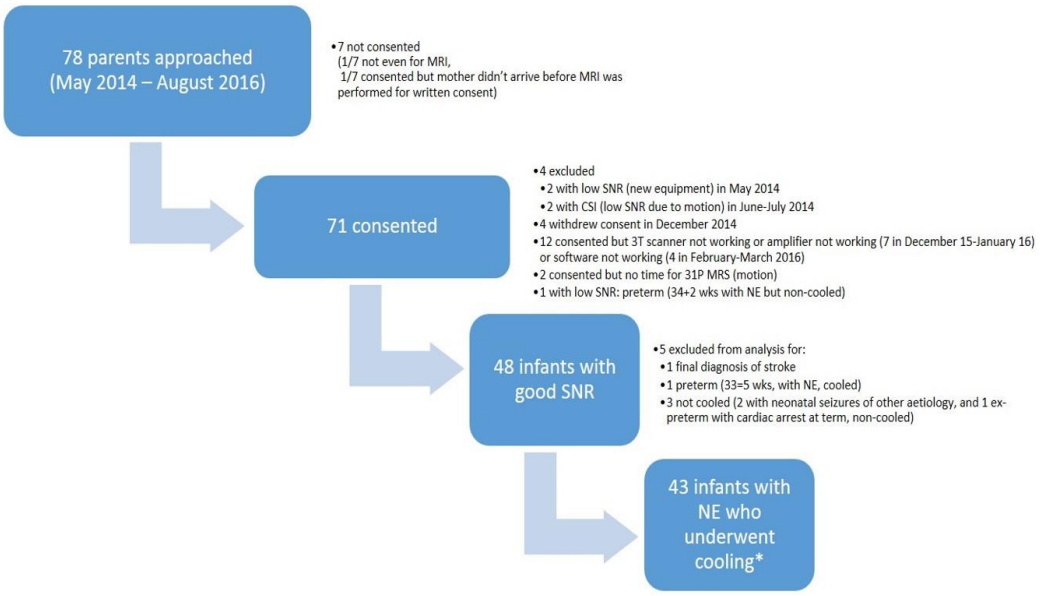

Figure 2-0-11: Flowchart of consenting process and numbers recruited into the Baby Brain Study

*One infant born in good condition but had a postnatal collapse at 1h of age and fulfilled all the rest of criteria for cooling, therefore, included in the analysis.

Chapter 3: Brain pHi and seizure burden in newborn infants with neonatal encephalopathy

Introduction

Perinatal hypoxic-ischaemic brain injury in term babies is still a significant problem throughout the world. Unfortunately, despite the introduction of therapeutic hypothermia, around half the infants still have abnormal outcomes (1, 30). Experimental data suggest that the addition of another agent to cooling may enhance overall protection either additively or synergistically.

The first "in man" phosphorus-31 (^{31}P) magnetic resonance brain spectrum was obtained at University College London (UCL) in 1983 in a preterm infant following perinatal asphyxia (126). This and later studies in babies (53, 54) and piglets (52) were significant landmarks in our understanding of the biphasic nature of energy failure during and after hypoxia-ischaemia. The decline in brain energy measured in the days and hours after birth strongly correlated with neurodevelopmental outcome and head growth (54); however, since the 1980s there have been few studies using ^{31}P MRS as outcome biomarker in babies following asphyxia, as this is not routinely available on clinical scanners.

^{31}P MRS can also provide measurement of brain intracellular pH (pHi) which may be vital to our understanding of the response to hypoxia-ischaemia and lead to possible new avenues of neuroprotection; there is no other non-invasive way to

measure pHi apart from Positron Emission Tomography, which requires injection of radioactive ligands (i.e. Carbon-11-labeled dimethyloxazolidinedione ([11C]DMO)) (128) and, hence, not feasible in babies. Brain pHi can be measured using the chemical shift difference of inorganic phosphate (Pi) (129), phosphocreatine (PCr) and adenosine triphosphate (ATP) (287). The pHi value calculated from Pi (the chemical shift between Pi and PCr) is thought to reflect the pHi in dead or injured cells whereas that derived from other metabolites may reflect different cell populations.

Over a decade ago, an important shift in brain pHi was observed using whole brain ^{31}P MRS. 78 babies with neonatal encephalopathy (NE) in the precooling era were studied serially during the first year after birth (3). The findings were: (i) brain alkalosis magnitude related to brain injury severity on MRI and brain lactate concentration; (ii) brain alkalosis persisted for several weeks in babies with a severely impaired outcome.

More recently, an important relation between seizures and brain alkalosis has been observed by the Helsinki group (5, 243). In their rodent model, recovery from asphyxia was followed by a large seizure burden that was tightly paralleled by a rise in brain pHi. Graded restoration of normocapnia (by adding 10% or 5% CO_2) or the application of N-methyl-isobutyl amiloride – Na^+/H^+ exchange (NHE) inhibitor – suppressed the alkaline shift in brain pHi and strongly suppressed seizures. NHE inhibitors are a promising neuroprotective tool in animal models, reducing cell death, seizure burden and brain injury with improvement of functional outcome (5, 49, 175, 178, 179, 184, 186, 196, 197, 201, 204-206, 243,

288, 289), as described in our literature review (49). More recently, they showed in their rat model of asphyxia that carbonic anhydrase inhibitors, which induce systemic acidosis, also blocked post-asphyxia seizures (290).

Brain pHi is thus likely to be an important biomarker, but no studies have been performed in babies since the work done in 2002 (3).

The **aim** of this chapter is to study babies who underwent therapeutic hypothermia and determine if (i) localised deep grey matter pHi predicts outcome based on the following biomarker: thalamic peak area ratio Lactate + Threonine to total N-acetyl aspartate (LacT/tNAA) obtained by proton (^{1}H) MRS (122); (ii) alkaline brain pHi correlates with seizure burden on EEG; (iii) localised deep grey matter pHi can predicts clinical outcome; and (iv) the relationship between brain pHi and other markers of outcome.

Patients and Methods

Ethical permission was granted by the NRES Committee London (National Research Ethics Service) - Bloomsbury (13/LO/0225) and UCL Hospital (UCLH) R&D approval (13/0013). Parental written informed consent was obtained prior to every examination (*Appendix 1 and 2*).

3.2.1 Patients and study design

To calculate the sample size needed for this study, data from the 2002 pHi study (3) was used – where infants were divided into two groups (mild and

moderate/severe) based on clinical findings (MRI) –. A difference of 0.1 pH units between groups would be of interest and in previous studies a standard deviation (SD) of around 0.1 pH units was seen in these groups. With an 80% power and 5% significance, the number of infants required in each brain MRI group is 21, to determine differences between these groups and find a threshold pHi that best predicts outcome. Thus, we need a total of 42 subjects.

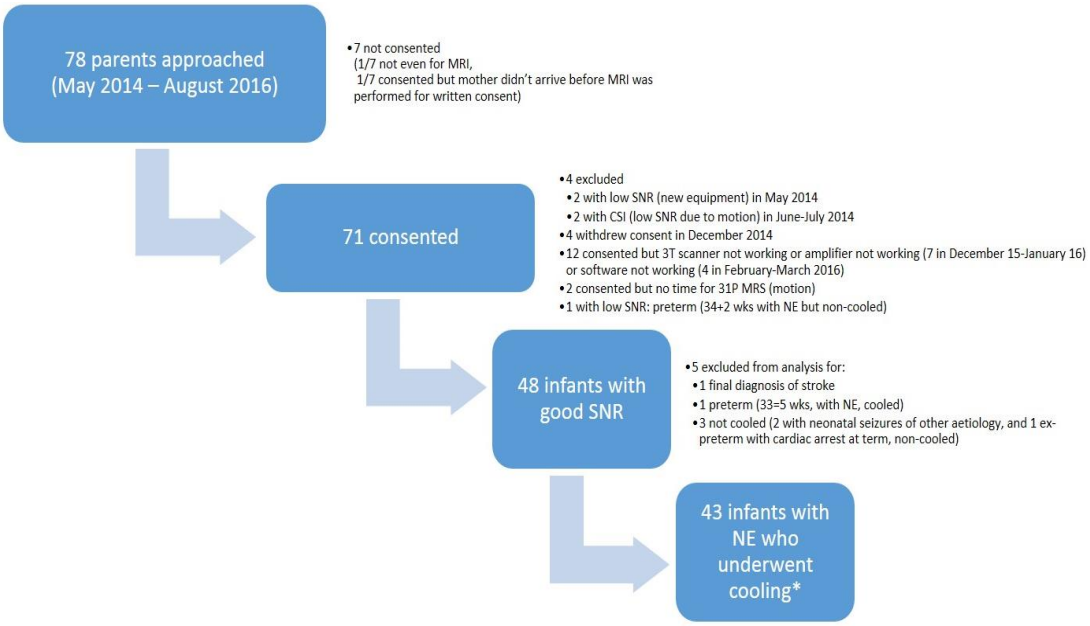

Figure 3-0-1: Flowchart of consenting process and numbers recruited into the Baby Brain Study
*One infant born in good condition but suffered postnatal collapse at 1h of age, fulfilling all the rest of cooling criteria, therefore, included in the analysis.

Of the 48 infants with good quality phosphorus MRS data who consented into the study, 5 were excluded due to having a different diagnosis than NE or didn't undergo cooling (1 with final diagnosis of stroke, 1 preterm 33+5 weeks who was not cooled, 2 with neonatal seizures who were not cooled and 1 ex-preterm baby with a cardiac arrest around term-time corrected gestational age, not cooled).

Forty-three newborn infants with NE presumed secondary to perinatal hypoxia-ischaemia who fulfilled current criteria for therapeutic hypothermia (17) were

enrolled prospectively at UCLH, London, United Kingdom between May 2014 and August 2016 (see recruitment flowchart *figure 3-0-1*). Mean gestational age (SD; range) was 39.8 weeks (SD 1.7; range 35.3-41.9) and mean birth weight of 3368g (SD 597; range 2250–4910). Neonates with congenital anomalies, genetic syndromes, or those with aetiology of NE different from hypoxia-ischaemia were excluded from the present analysis. They all received therapeutic hypothermia. *Table 3-0-1* shows descriptive characteristics of the cohort.

	N	Mean ± SD	Median	Range
GA (weeks)	43	39.8± 1.7	40	35.3 – 41.9
Birth weight (gr)	43	3368 ± 597	3334	2250 – 4910
Gender (M:F)	23:20			
Inpatient/outpatient	17/26			
Apgar score (5 min)	41	4.0 ± 2.7	4	0 – 10[1]
Apgar score (10 min)	35	4.8 ± 2.7	4	0 – 10[1]
Blood pH within 1st hour (including cord)	41	6.94 ± 0.14	6.95	6.60 – 7.25
Blood BE within 1st hour (including cord)	35	-18.0 ± 5.4	-16.9	-31.8 - -5.3
Lactate within 1st hour (including cord)	27	13.4 ± 3.4	13	7.2 – 20
Intubated during resuscitation	39/43			
Cardiac massage	12/43			
Drugs during resuscitation	7/43			
Age at target temperature	37	3.3 ± 2.3	3	0.5 - 10.5
Duration cooling	43	70.8 ± 11.8	72	22 – 96[2]
Death	2/43			

Table 3-0-1: Descriptive characteristics of the cohort of newborn infants with NE
[1]One born in good condition and suffered a postnatal collapse, fulfilling cooling criteria
[2]Therapeutic hypothermia stopped earlier in one baby because of very mild clinical picture. One baby re-cooled for extra 24h due to seizures during rewarming.

Clinical data was collected: perinatal markers of asphyxia, sentinel events (e.g., placental abruption, uterine rupture, cord prolapse, other cord accident or shoulder dystocia), and multiorganic failure's symptoms (*tables 3-0-2* and *3-0-3*).

Some data was unavailable regarding foetal CTG and presence of sentinel events, mainly in infants transferred ex-utero to UCLH. 18/43 infants presented with a sentinel event and 31/38 with signs of foetal distress. Regarding multiorgan failure, over two thirds of the infants presented with at least one other organ affected (the most frequent was renal impairment/olyguria). Those with more severe NE presented with more than one other organ affected. In this cohort, no children had genetic or metabolic abnormalities supected (exclusion criteria). Those who presented with low blood sugar, were investigated with a hypoglycaemia screen, with no abnormalities found in any of them and the cause being the low glucose intake due to fluid restriction. Most babies were ventilated (41/43) during therapeutic hypothermia due to the use of sedation, in line with the publication that showed no protective effect in an animal model of asphyxia when subjects were undesated during cooling (70). Only 16/43 had increased ventilation or oxygen requirements.

	Frequency
Fetal distress	31/38 (80%)
Unspecific decelerations on CTG	23/29 (79.3%)
Flat HR on CTG	1/38
Fetal tachycardia on CTG	1/38
Fetal bradycardia on CTG	19/35
Sentinel events	
Uterine rupture	1/43
Placental abruption	4/43
Cord prolapse	1/43
Cord accident	5/40
Shoulder dystocia	8/40

Table 3-0-2: Summary of antenatal signs of foetal distress and/or sentinel events. Cord accident includes cord prolapse or tight cord around the neck. 18/43 infants had one sentinel event explaining the hypoxia-ischaemia.

Multiorganic failure	Frequency
Hypotension	23/40
Thrombocytopenia	14/43
Coagulopathy	19/43
Oliguria	30/43
Pulmonary impairment	16/43
Others	
Sepsis (markers elevation and treated at least 5 days antibiotics)	13/43
Hypoglycaemia	5/43
Prognosis (breastfeeding/oral feeding at 8-10 days of life)	31/43

Table 3-0-3: Clinical co-morbidities and prognostic factors. Hypotension requiring inotropes. Coagulopathy requiring blood products. Oliguria (less than 1ml/kg/h). Hypoglycaemia (<2mmol/dL).

3.2.2 Imaging

MR imaging and spectroscopy (MRI/MRS) were performed at a mean age of 5 days (SD 1.4; range 3-8) using a 3T MR system (Philips Medical Systems®, Best, The Netherlands). Infants were transported in an MR conditional incubator with integrated monitoring (pulsioximetry) and a ventilator, required by most of them: a Lammers® incubator. MRI and proton (^{1}H) MRS were obtained using a double-tuned neonatal birdcage coil specific to be used within a Lammers® incubator; these are part of the routine care imaging of infants with neonatal encephalopathy who undergo therapeutic hypothermia. The following sequences were used in the protocol:

- High-resolution T1-weighted 3D anatomical scan (MP-RAGE)
- T2-weighted TSE imaging anatomical scan (3mm slice thickness)
- Multi-direction (32 directions) Diffusion tensor-like imaging (DTI)
- Single voxel proton spectroscopy (water suppressed PRESS, repetition time/echo time (TR/TE) = 2288/288ms, voxel size 15x15x15mm, dynamic series of 16 spectra were acquired each with 8 averages, scan time ~7min): allows measurement of different metabolites in a voxel localised mostly on the left ventrolateral nuclei of the thalami. The peak-area ratio of thalamic Lactate + Threonine to total N-acetyl aspartate (LacT/tNAA) is the current validated biomarker of outcome (122, 124).

These 43 babies had an extra “research” sequence: localised phosphorus (^{31}P) MRS. A purpose made birdcage multinuclear phosphorus-31 coil specified to be

used in newborn infants within a Lammers® incubator was manufactured by Rapid Biomedical® for this study and delivered to UCLH (see *Chapter 2* for sequence optimisation). Scan acquisition time was 14 minutes 51 seconds: ISIS, pulse sequence, with a voxel size of 40x40x25mm along RL x AP x SI directions (RL: Right-Left; AP: Anterior-Posterior; SI: Superior-Inferior), TR = 2475 ms, scan number 8 x 45, and sample size 2048. The sequence was shortened in 7 occasions by reducing the number of repetitions (25-40 x 8 repetitions). Full description of the sequence can be found in *Chapter 2*. The ISIS sequence was implemented without proton decoupling, and the centre of frequency of the RF pulse was set between ɣ- and α-ATP. The voxel was placed using the structural T1 and T2 sequences in the three planes (sagittal/coronal/axial). Prior to the ^{31}P MRS sequence, a survey was run with the body coil to adjust the voxel positioning if there had been any minor displacement of the head during the coil replacement. Proton coil and phosphorus coil have the same inside diameter and slide on top of a coil-shape plastic model where the baby's head is fixed with foams placed lateral to each ear (*figure 3-0-2*).

Figure 3-0-2: Head placement within the in-built 1H MRS coil in the Lammers® Incubator.

3.2.3 Data processing

For ^{1}H MRS, the dynamic spectra were summed off-line after phase and frequency correction and rejection of motion-corrupted data. MRS analysis was performed using Tarquin (284). The following metabolites were fitted: Choline (Cho), Creatine (Cr), Lactate (Lac), Threonine (Thr) (285), N-acetyl aspartate (NAA) and N-acetyl-aspartyl-glutamate (NAAG); lipids and macromolecules were not included. It was described a significant residual when the signal around 1.3ppm was high (124), and often, the fit was improved by including Thr in the basis set (124, 286). Hence, the peak area ratios for LacT/tNAA (Lactate plus Threonine to total NAA [NAA+NAAG]) was calculated.

For ^{31}P MRS, during pre-processing, the spectra were manually corrected for phase and frequency shifts and fitted using the Advanced Magnetic Resonance (AMARES) (281) algorithm implemented in the jMRUI software package (280). The software performs the Fourier transformation of the time-domain data. Zero- and first-order phase corrections were performed manually on all spectra and the 0 ppm reference was set on the phosphocreatine (PCr) peak (see *figure 3-0-3*). The fit can be constrained by applying prior knowledge, such as allowed ranges for peak frequencies and line widths, and specific constraints on j-coupling constants, phases, and relative amplitudes between peaks within a multiplet (see *Chapter 2*). In our time-domain free induction decay (FID) data-fitting template, we modelled: PCr, Pi (4 peaks), PME (phosphomonoesters, primarily PCh [phosphocholine] and phosphoethanolamine), GPE (glycerophosphoethanolamine), GPC (glycerophosphocholine), NADH (reduced

nicotinamide adenine dinucleotide), UDP (uridin diphosphates) and γ_1-, γ_2-, α_1-, α_2-, β_1-, β_2- and β_3-NTP (nucleotide triphosphate). The prior knowledge was adjusted for certain cases to ensure a good fit of the spectra with minimal residue. Pi frequency was calculated as the amplitude-weighted Pi frequency of the 4 Pi peaks (Weighted Pi frequency= ([Pi1 frequency x Pi1 Amplitude] + [Pi2 frequency x Pi2 Amplitude] + [Pi3 frequency x Pi3 Amplitude] + [Pi4 frequency x Pi4 Amplitude]) / (Pi1 amplitude + Pi2 amplitude + Pi3 amplitude + Pi4 amplitude)).

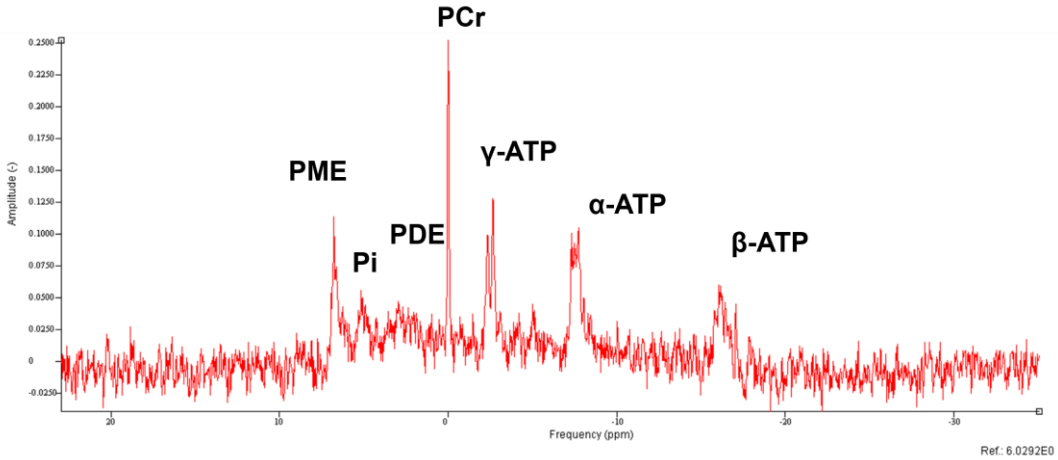

Figure 3-0-3: ^{31}P Spectrum after apodisation to 5 Hz and zero-order phase correction.

Measurement of pHi is derived from peak positions, using the Henderson-Hasselbalch equation – where δ is the chemical shift of Pi relative to PCr:

$$\text{pHi (Hamilton)} = 6.77 + \log_{10}[(\delta - 3.29) / (5.68 - \delta)] \quad (135) \qquad \textbf{Equation 1}$$

$$\text{pHi (Robertson)} = 6.75 + \log_{10}[(\delta - 3.27) / (5.69 - \delta)] \quad (3) \qquad \textbf{Equation 2}$$

To increase the confidence in the findings, I also determined brain pHi using the chemical shift of Pi relative to α-ATP, where δ is the corrected Pi relative to α-ATP at -10.05ppm (Pi frequency in ppm + (-10.05 – [α_1 + α_2]/2):

$$\text{pHi (Raghunand)} = 6.85 + \log_{10}[(\delta - 0.58) / (3.14 - \delta)] \quad (132) \qquad \textbf{Equation 3}$$

Correlation between the 3 equations was analysed and, for the purpose of the study, the Hamilton pHi calculation was used (135).

The total duration of the MRI/MRS scan is around 1h. The examination was performed either during natural sleep ('feed-and-wrap' technique) or after sedation with oral chloral hydrate (30-50 mg/kg) or morphine infusion in those who were ventilated.

MRI scans were scored with an expert neuroradiologist using a previously validated scoring system: the NICHD NRN MRI (291) score. It has been validated to predict death or IQ at 6-7 years of age following hypothermia for NE (*table 3-0-4*). Newborn infants were grouped into 3 degrees of severity of injury: normal (score 0), mild (1A and 1B) and moderate-severe injury (2A, 2B and 3).

Score	Description
0	Normal MRI
1A	Minimal cerebral lesions only
1B	More extensive cerebral lesions only
2A	Any basal ganglia thalami (BGT), anterior limb of the internal capsule (ALIC) or posterior limb of the internal capsule (PLIC), or watershed infarction
2B	2A with additional cerebral lesions
3	Hemispheric devastation

Table 3-0-4: NICHD MRI scoring system (291).

3.2.4 aEEG/EEG acquisition

Multichannel twelve-lead EEG monitoring (NicoletOne EEG/LTM®, Natus, Care Fusion, Wisconsin, USA, or Nihon Kohden Neurofax EEG-1200®, Rosbach, Germany) was acquired from admission (around 1-7h of life, depending whether inborn or outborn) and until the baby was completely rewarmed and free of seizures (at least 86h from the beginning of therapeutic hypothermia). Filtered

amplitude-integrated EEG recordings were classified according to the pattern classification (292). *Table 3-0-5* shows the different pattern of aEEG background activity described, at epochs between 0-6 hours from the start of therapeutic hypothermia –being time 0 when target temperature reached 33-34°C–, 6-12 hours, 12-24 hours, 24-48 hours, 48-72 hours, rewarming period (72-86 hours) and after rewarming. The presence of sleep-wake cycling was also scored during these time epochs.

Score	Pattern classification	Description	
		Upper margin	Lower Margin
0	Continuous normal voltage (CNV)	> 10 µV	> 5 µV
1	Discontinuous normal voltage (DNV)	> 10 µV	Mostly > 5 µV
2	Burst suppression (BS)	Up to 25 µV	< 5 µV
3	Continuous low voltage (CLV)	< 10 µV	< 5 µV
4	Flat trace or isoelectric (Flat)	< 5 µV	< 5 µV

Table 3-0-5: aEEG background activity pattern classification (292).

Fifteen patients presented with electrical seizures. Seizure burden was calculated by the author, annotating on the raw EEG the beginning and end for each seizure and then calculating the total duration of seizures in minutes. In case of doubts, consensus was reached with an EEG expert (Dr. Sean Mathieson).

3.2.5 Clinical outcome data

Two newborn infants died within the first week of life. Thirty-six children were assessed for their neurodevelopmental outcome at 3, 6, 12 and 24 months of age, as part of their clinical follow-up, led by Dr Angela Huertas-Ceballos. Five children were lost to follow-up (11.6%), which is below rates described in other studies (293).

At 24 months (range 21-36), the Bayley Scales of Infant Development, Third Edition was used for assessment (Bayley III) (294). It has five scales (cognitive, language (receptive and expressive), motor (fine and gross motor), social emotional and adaptative behaviour). Raw scores are transformed into a composite score, where the mean is 100 (SD 15). Combined cognitive and language composite score (CB-III) was calculated too as the average between the two of them.

Outcomes were categorised as normal (n=28), mild (n=4) or severe (includes moderate-severe, n=6) (*table 3-0-6*). The same categorisation was done taking into consideration the CB-III and Motor composite scores.

Outcome severity at 2 years of age	
Normal	Bayley-III Composite score within 1SD (**≥85**)
Mild	**One domain** affected with a Composite score between 2SD and 1SD below the mean (**70-84**)
Severe	• **Death** • **Any one domain** with a Composite score below 2SD (**<70**) • **At least 2 domains** with a Composite score between 2SD and 1SD below the mean (**70-84**)

Table 3-0-6: Outcome severity at 2 years of age based on Bayley-III assessment (294-296).

There were 4 patients in the severe group who didn't have Bayley-III Composite Scores: 2 who died in the neonatal period and 2 infants who were seen in clinic with very severe disability, but Bayley-III was not achievable (children with cerebral palsy who required physical assistance for mobility, plus learning difficulties, plus other added disabilities). In the normal group, there was an infant without scores because the last Bayley-III assessment was done at 12 months (not comparable with the 2 year-outcome) but further clinic letters showed normal development.

3.2.6 Statistical Methods

Analyses were performed using IBM SPSS Statistics 28.0, SPSS Inc., Chicago IL. Descriptive data summaries were generated using means and standard deviations (or medians and inter-quartile range) for quantitative variables, and frequency distributions (total number and frequency) for qualitative variables.

Bivariate analyses were performed to study association between the different prognostic tools and, also, with long-term outcomes using Pearson correlation (or Spearman correlation for categorical values).

Prior to comparing two groups and due to the small sample size within groups, normality tests were performed (Kolmogorov-Smirnov and Shapiro-Wilks) (297, 298). In those where normality was assumed, the difference in means was analysed using a t-Student test for independent samples. The Levene's test for Equality of Variances was performed beforehand to interpret results. If normality couldn't be assumed, a U-Mann Whitney test was performed.

The cut-off point used to compare infants with low-high pHi was 7.16, based on previous studies (3), and when comparing infants with low-high thalamic LacT/tNAA, it was 0.39 (124).

A t-Student test for paired samples was used when comparing pHi calculated using different equations. Statistical significance was considered when p value was <0.05 (95% confidence interval [C.I.]).

The predictive ability of prognostic markers was explored estimating sensitivity and specificity (95% confidence interval [C.I.]).

3.3.1 Deep grey matter pHi and ^{1}H MRS

There was a significant positive association between infants with NE who presented with a higher LacT/tNAA (worse prognosis) and a more alkaline BGT pHi (p<0.001) (see *Figure 3-0-4).*

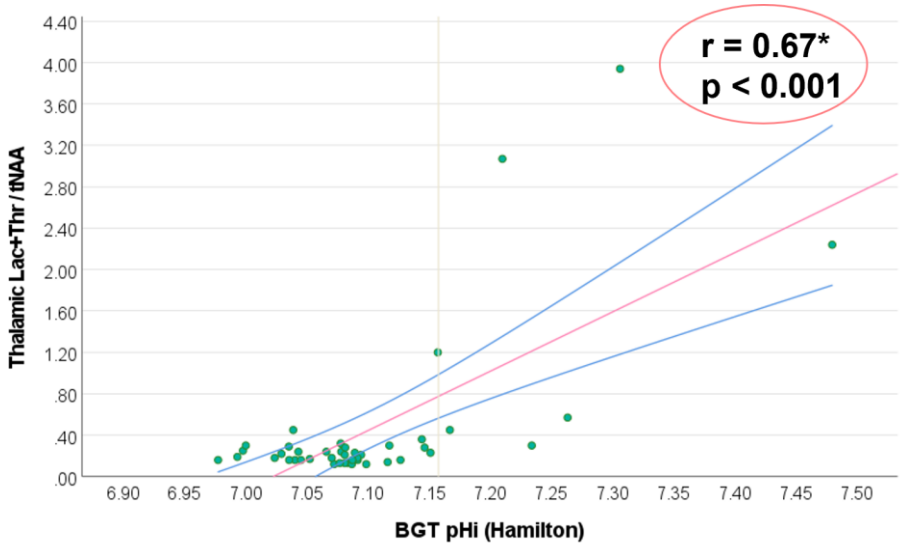

Figure 3-0-4: Correlation between BGT pHi and thalamic LacT/tNAA in 43 infants with NE

A cut-off value for LacT/tNAA of 0.39 was used, where infants with a LacT/tNAA above 0.39 are more likely to have a poor neurodevelopmental outcome (124). When comparing mean BGT pHi within these 2 groups, there was a significant difference (p=0.012) – infants more likely to have an unfavourable outcome present with a more alkalotic pHi on the BGT – (*table 3-0-7, figure 3-0-5*).

	BGT pHi (mean [SD])	n
Lac/tNAA < 0.39	7.08 (0.05)	36
Lac/tNAA ≥ 0.39	7.23 (0.14)	7

Table 3-0-7: Mean (SD) of deep grey matter pHi within the first 2 weeks of life in infants classified by LacT/tNAA from ^{1}H MRS (124).

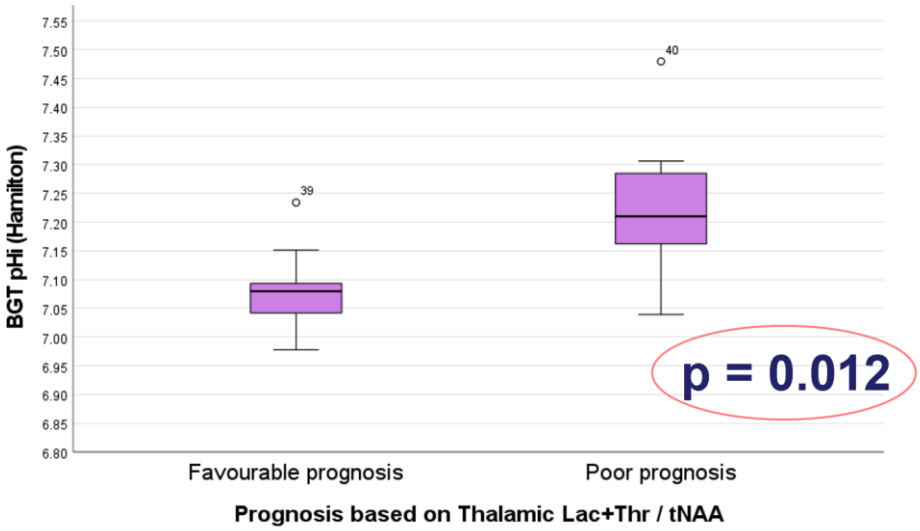

Figure 3-0-5: Boxplot for deep grey matter pHi within the first 2 weeks of life in infants classified by thalamic LacT/tNAA (median, 1st, and 3rd quartiles [box] and ±1.5 interquartiles [whiskers])

3.3.2 Deep grey matter pHi and electroencephalograhy

The BGT pHi and electroencephalographic examinations of 43 infants with NE who underwent cooling are summarised in *table 3-0-8*. Fifteen of them had seizures. The mean for seizure burden was 39 min (SD 96, range 0-530 min).

There was a positive association between a more alkalotic BGT pHi and a higher seizure burden (p<0.012) (*figure 3-0-6*).

EEG data	Frequencies
Seizure burden (in min) Mean ± SD (range)	39 ± 96 (0 – 539)
Background pattern aEEG at 0-6h	CNV: 16 / 37 (43.2%) DNV: 5 / 37 (13.5%) BS: 1 / 37 (1.6%) CLV: 1 / 37 (1.6%) Flat: 14 / 37 (37.8%)
Background pattern aEEG at 24-48h	CNV: 22 / 43 (51.1%) DNV: 14 / 43 (32.6%) BS: 3 / 43 (7%) Flat: 4 / 43 (9.3%)
Background pattern aEEG at 48-72h	CNV: 21 / 43 (48.8%) DNV: 17 / 43 (39.5%) BS: 1 / 43 (2.3%) Flat: 4 / 43 (9.3%)
Background pattern aEEG at rewarming	CNV: 17 / 40 (42.5%) DNV: 18 / 40 (45%) BS: 1 / 40 (2.5%) Flat: 4 / 40 (10%)
Background pattern aEEG post-rewarming	CNV: 24 / 39 (61.5%) DNV: 11 / 39 (28.2%) Flat: 4 / 39 (10.3%)
SWC recovery	3/43 (7%) by 24 hours 7/43 (16.2%) by 48 hours 9/43 (20.9%) by 72 hours 15/39 (38.5%) after rewarming

Table 3-0-8: Summary of electroencephalographic data. aEEG: amplitude integrated EEG; SWC: sleep wake cycle. CNV: continuous normal voltage; DNV discontinuous normal voltage; BS: burst suppression; CLV: continuous low voltage; Flat: isoelectric trace.

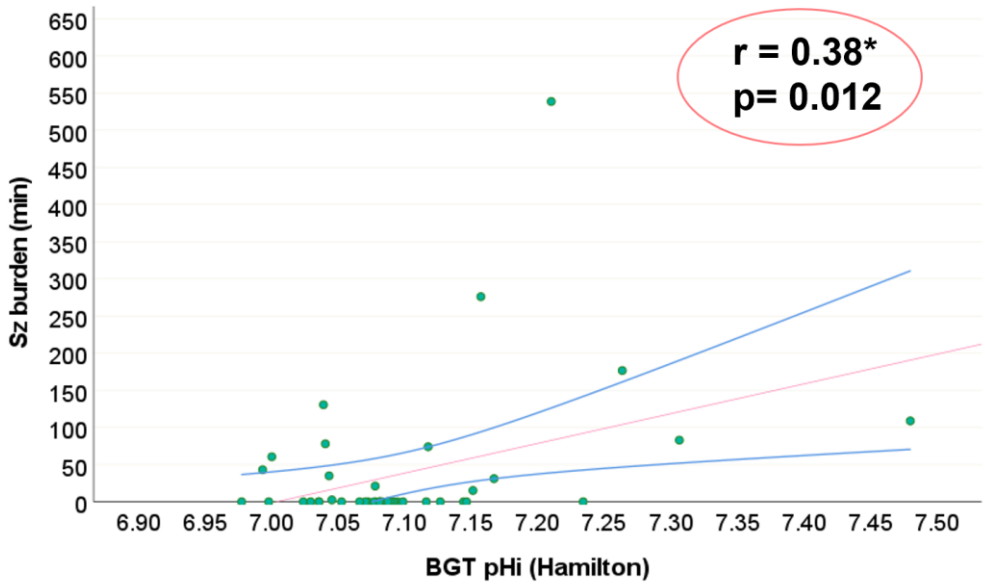

Figure 3-0-6: Correlation between deep grey matter pHi and seizure burden.

Regarding aEEG background activity, *figure 3-0-7* shows the boxplot for median pHi in the different groups of background activity (with first and third quartile [box]; ±1.5 interquartile [whiskers]). When comparing the group with a mild-normal aEEG background (CNV or DNV) vs moderate-severe changes (BS, CLV or flat), there were statistically significant differences in mean BGT pHi (p=0.005 at 24-48 hours; p= 0.01 at 48-72 hours) and between ranks at 0-6h (p=0.005) (*table 3-0-9*).

	Mean pHi (SD)		p value
	Normal-mild aEEG	Moderate-severe aEEG	
aEEG background at 0-6h	7.06 (0.04) n=21	7.16 (0.12) n=16	**0.009***
aEEG background at 24-48h	7.07 (0.05) n=36	7.24 (0.12) n=7	**0.005***
aEEG background at 48-72h	7.08 (0.05) n=37	7.28 (0.12) n=5	**0.01***

Table 3-0-9: Mean (SD) of deep grey matter pHi within the first 2 weeks of life in infants according to aEEG background activity at different time points. Comparison of mean pHi between the group normal-mild aEEG background (CNV and DNV) and moderate severe aEEG background (BS, CLV and flat trace) (84).

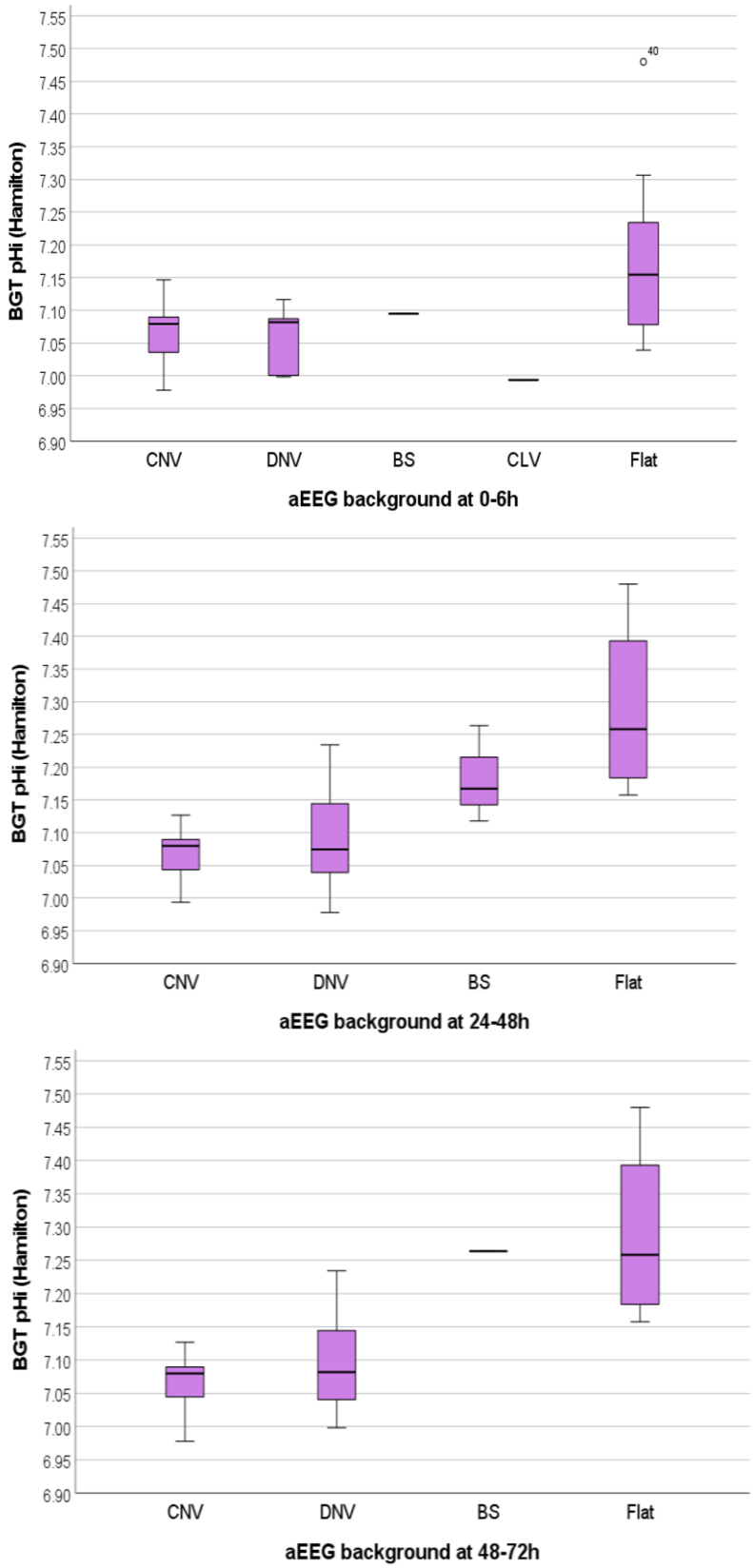

Figure 3-0-7: Comparison of medians between BGT pHi and aEEG background activity at 3 different time points: 0-6h (top)**, 24-48h** (middle) **and 48-72h** (bottom)**.** (median, 1st and 3rd quartiles [box] and ±1.5 interquartiles [whiskers])

3.3.7 Deep grey matter pHi and MR Imaging

Examining the MRI and ^{31}P MRS data, there was a statistically significant difference in mean BGT pHi between those with normal-mild changes on the MRI and those with a moderate-severe pattern of injury on the MRI (p=0.002). *Table 3-0-10* shows a summary of the pHi data classified according to MRI degrees of severity using the NICHD scoring system (291); and *figure 3-0-8* shows the box-plot with median BGT pHi in these 3 groups.

MRI severity	BGT pHi (mean [SD]) Min.-Max.	n
Normal MRI	7.07 (0.04) 6.98 – 7.15	26
Mild changes on MRI	7.08 (0.04) 7.04-7.15	5
Moderate-severe changes on MRI	7.17 (0.14) 7.00-7.48	12

Table 3-0-10: Mean (SD) of deep grey matter pHi within the first 2 weeks of life in infants classified according to brain MRI severity

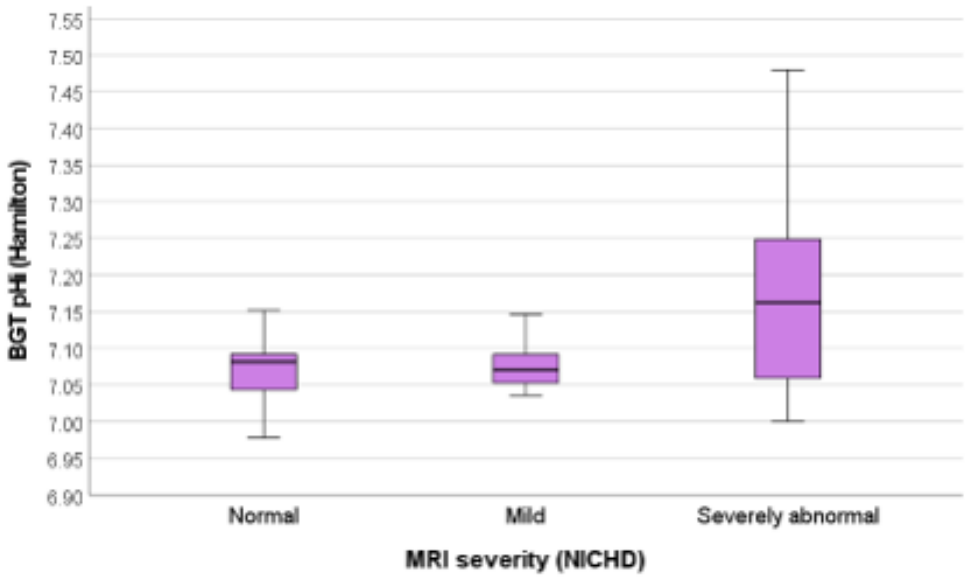

Figure 3-0-8: Boxplot for median deep grey matter pHi classified according to MRI severity in infants with NE who underwent cooling. (median, 1st and 3rd quartiles [box] and ±1.5 interquartiles [whiskers])

3.3.8 Energy metabolites ratios and BGT pHi

^{31}P MRS data of these 43 infants showed a significant positive association between Pi/PCr ratio and pHi in the deep grey matter, and a significant negative association between NTP/total phosphates components ratio and pHi (*figure 3-0-9*).

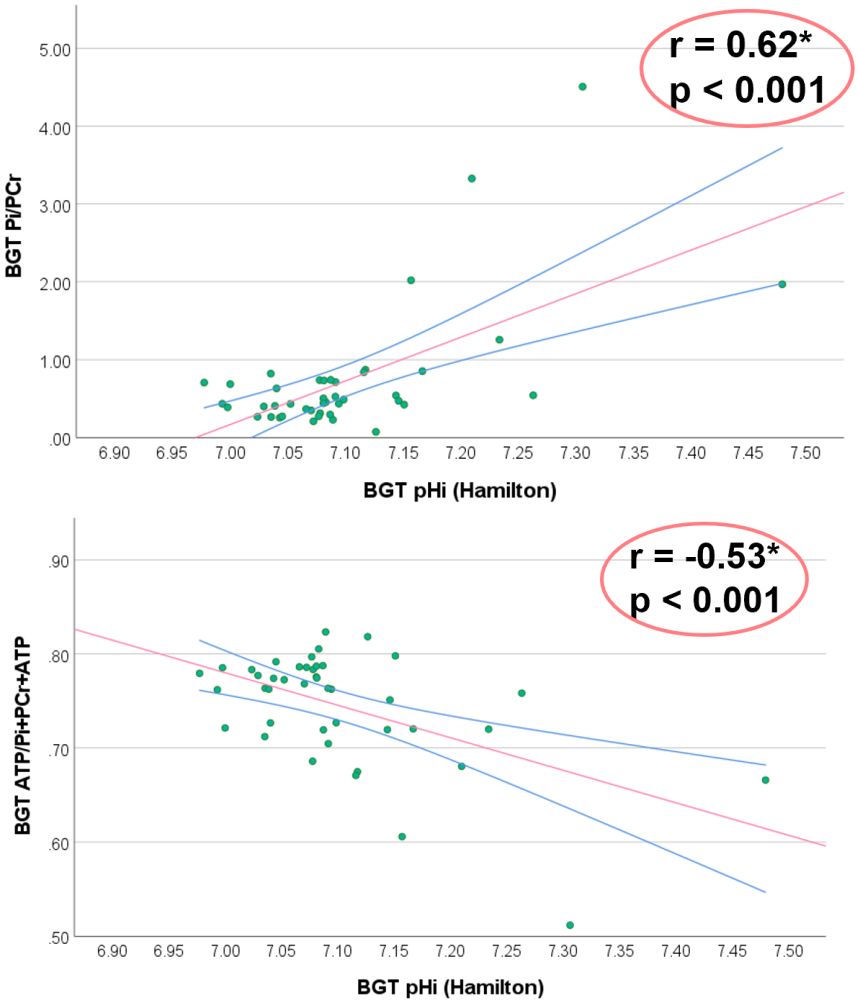

Figure 3-0-9: Correlation between deep grey matter intracellular pH and *(top)* Pi/PCr ratio; and *(bottom)* NTP/total phosphates pool (Pi + PCr + ATP).

3.3.9 Clinical outcome at 2 years of age and BGT pHi

In addition, I have looked at neurodevelopmental outcome at 2 years of age. A summary for the children in this cohort is shown in *table 3-0-11*.

Outcome severity at 2 years	n	
Normal	**28**	
Mild	**4**	**1** with mild **Cognitive** impairment (Composite 70-84) **3** with mild **Language** impairment (Composite 70-84)
Severe	**6**	**2 died** in the neonatal period **2** severe **Cerebral Palsy** and **severely disabled** (unable to undergo Bayley-III) **1** with mild **Motor** and severe **Cognitive** impairment **1** with severe **Cognitive** impairment (Compositev <70) (unable to have Language scale assessed).
Lost-to-follow-up	**5**	

Table 3-0-11: Summary of neurodevelopmental outcomes at 2 years of age.

When looking at Bayley-III Composite Scores, there was no significant association between deep grey matter pHi and Cognitive (n=33), Language (n=30), Motor (32) and CB-III (n=30) for this cohort ($p>0.05$). When categorising for severity of outcome, including 5 infants without Composite Scores (one with good outcome, two infants who died and two with severe disabilities but no Composite Scores), there were 38 infants. According to outcome severity, there was a significant association between a more alkalotic brain pHi within the first 2 weeks of life and a more severe neurodevelopmental outcome at 2 years of age ($p<0.032$) (see *figure 3-0-10, bottom)*.

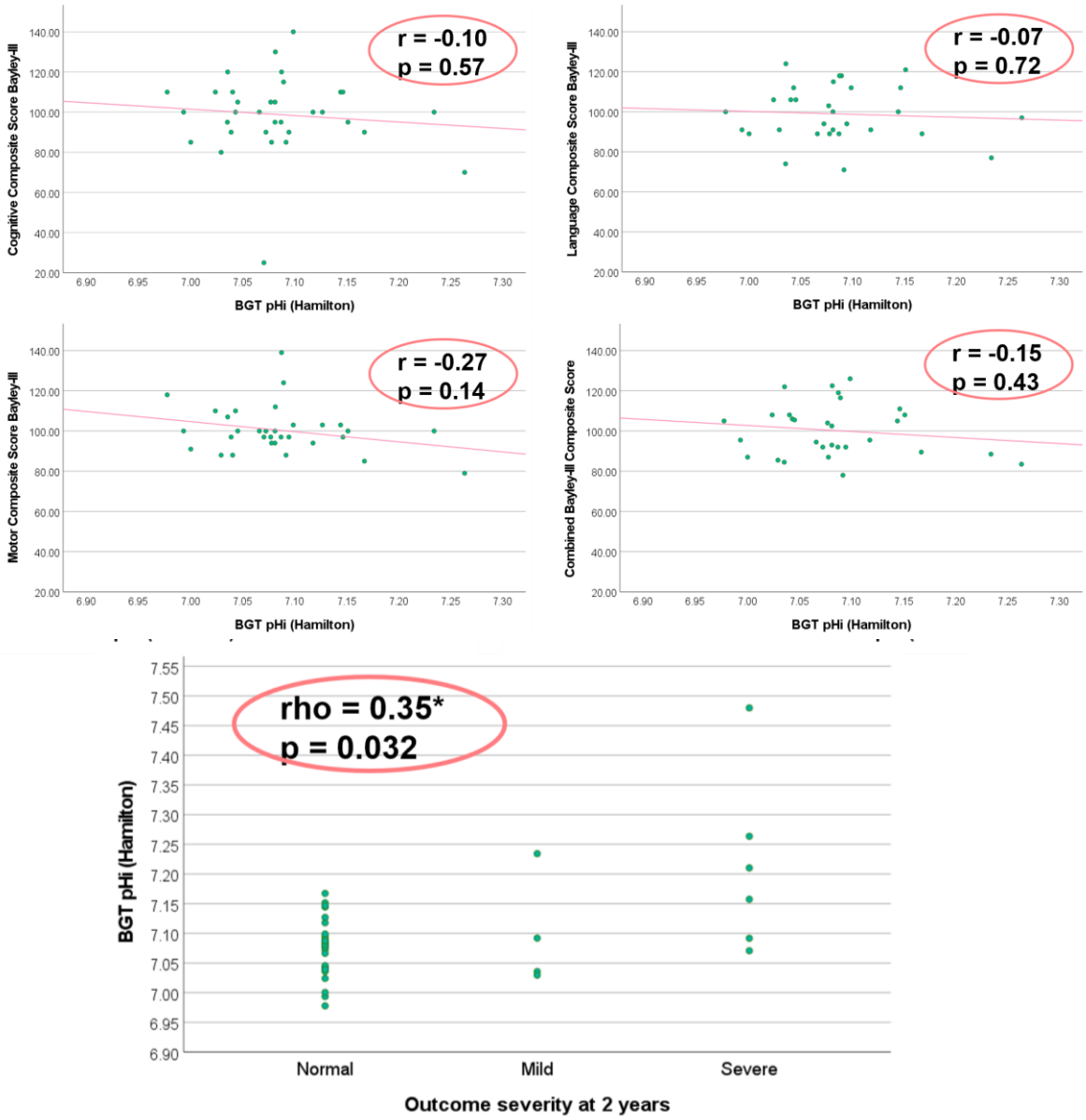

Figure 3-0-10: Correlation between deep grey matter pHi and neurodevelopmental outcome data at 2 years. ***(Top row)*** a) Cognitive Composite Score; b) Language Composite Score**;** ***(Middle row)*** c) Motor Composite Score Bayley-III; d) Combined Bayley-III Composite Score; ***(Bottom row)*** e) BGT pHi according to outcome severity at 2 years of age (normal, mild and severe).

There was a statistically significant difference in mean BGT pHi between those with a normal outcome at 2 years and those with an adverse one (p=0.038). *Table 3-0-12* shows a summary of the pHi data classified according to severity of neurodevelopmental outcome at 2 years of age.

Neurodevelopmental outcome at 2 years	BGT pHi (mean [SD]) Range	n
Normal	7.08 (0.05) 6.98 – 7.17	28
Mild	7.10 (0.10) 7.03-7.23	4
Severe	7.21 (0.15) 7.07-7.48	6

Table 3-0-12: Mean (SD) of deep grey matter pHi within the first 2 weeks of life in infants classified according to neurodevelopmental outcome severity at 2 years of age.

3.3.10 Predictors against the biomarker of outcome

Finally, I have looked at the prognostic tools available from MRI/MRS (severity of pattern of injury, BGT pHi and BGT energy metabolites ratios) and EEG (seizure burden and background pattern at different time points), compared with the current biomarker of outcome (thalamic LacT/tNAA). They all showed a statistically significant correlation, as presented in *figure 3-0-11*.

When looking at the categorical variables, there were statistically significant differences in LacT/tNAA according to the classification of brain MRI severity (comparing between mild-moderate changes vs severe MRI changes, $p<0.001$) and for aEEG background (comparing normal-mild (CNV, DNV) vs moderate-severe background (BS, CLV, Flat)) at 0-6, 24-48 and 48-72 hours (all three $p<0.001$).

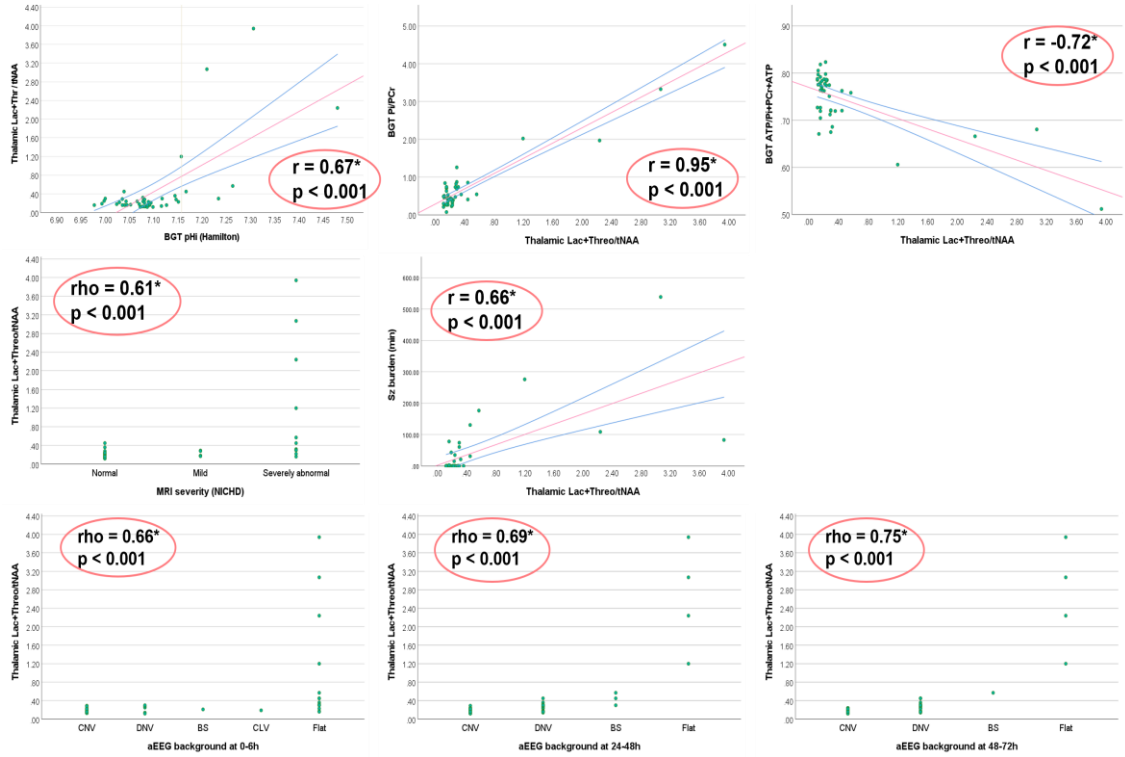

Figure 3-0-11: Correlation between the different prognostic tools and LacT/tNAA: ***(Top row)*** a) BGT pHi; b) Pi/PCr; c) NTP/total phosphates components; ***(Middle row)*** d) Severity of MRI; e) Seizure burden; ***(Bottom row)*** f) aEEG background at 0-6h; g) aEEG background at 24-48h; h) aEEG background at 48-72h.

When looking at clinical outcomes, in this cohort there is a significant negative association between LacT/tNAA and Motor Composite Scores (n= 32) and the Combined Bayley-III Score (average between Cognitive and Language Composite, n=30). When grouping outcomes as normal-mild vs severe - including those who didn't have a Bayley Score but had a severe outcome, like death and severe cerebral palsy – there was a significant association between a higher LacT/tNAA and a more severe clinical outcome (n=38) (*figure 3-0-12*).

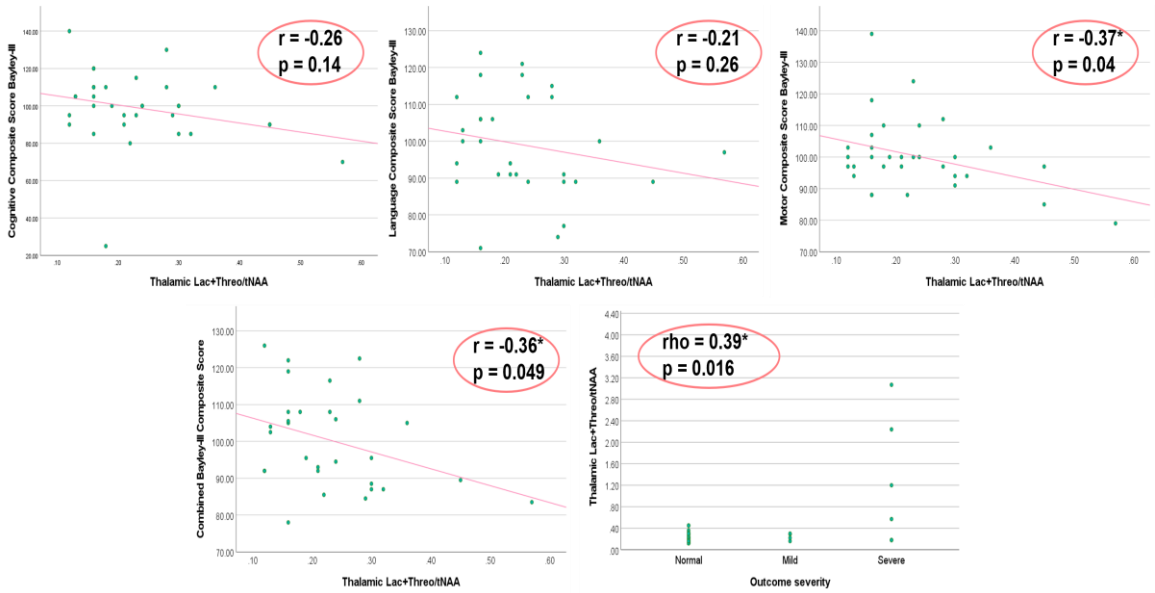

Figure 3-0-12: Correlation between the neurodevelopmental outcome using Bayley-III and LacT/tNAA: a) Cognitive Composite Score; b) Language Composite Score; c) Motor Composite Score; d) Combine Bayley-III Composite Score; e) Outcome severity.

Discussion

3.4.1 Deep grey matter alkalosis: prognostic tool for neurodevelopmental outcome

Localised brain pHi is a marker of outcome in infants who underwent cooling. Infants with a LacT/tNAA ≥ 0.39 are more likely to have a poor neurodevelopmental outcome (124). Six out of seven babies with an unfavourable prognosis in this cohort presented with a BGT pHi above 7.16. A BGT pHi ≥ 7.16 measured in the first 2 weeks after birth has a sensitivity of 85.7% (95% C.I. 71.4–100%) and specificity of 97.2% (95% C.I. 91.7–100%) for predicting adverse outcome, which is a better performance than published using whole brain phosphorus spectroscopy in the pre-cooling era (3). There are 0.15 points

difference between pHi in infants with good and poor prognosis. In this cohort, the 'normal' pHi mean value within the BGT was 7.08 for 36/43 infants with a LacT/tNAA < 0.39 and 7.07 when considering 26/43 infants with a normal MRI scan – consistent with normal values published previously, between 7.02 and 7.12, using a volume localised technique (ISIS) (56, 115, 299).

However, there are significant limitations to use ^{31}P MRS in a clinical setting as a prognostic tool. Firstly, it is not a widely available technique, requiring a separate coil and significant physics expertise to process and analyse the data. Secondly, there is a limitation in accurately fitting Pi peak, especially in the less severe infants. Pi/PCr is a marker of neuronal death when Pi peak is high, hence, the ratio is high. When looking at the individual spectrum, infants with a less severe picture had a low amplitude Pi peak and the signal-to-noise ratio (SNR) was low (*figure 1-0-13 and 1-0-14*). In these cases, it is more difficult to accurately fit Pi peak, required to calculate pHi. That would explain why Pi/PCr ratio (favourable prognosis baby with a low Pi and high PCr peak) correlated more strongly with LacT/tNAA (r 0.95, p<0.001) than pHi did (r 0.67, p<0.001). Equally, this would make the association between Pi/PCr and BGT pHi weaker (r 0.62, p<0.001). Different methods were discussed to increase SNR, like discarding noise (300), or truncating the end of the FID (free induction decay), or apodisation (application of spectral smoothing function), which could potentially improve the data slightly. To increase signal, a bigger voxel can be used (e.g., whole brain ^{31}P MRS), compromising localisation. Another option was trying to improve the fitting. Previous study used the average of two Pi chemical shifts when more than one

peak was detected in the chemical shift area of Pi (3). As described in Chapter 2, the 'prior knowledge' with 19 peaks (including 4 Pi peaks) has improved the fitting in our dataset, but SNR is a limitation to be considered.

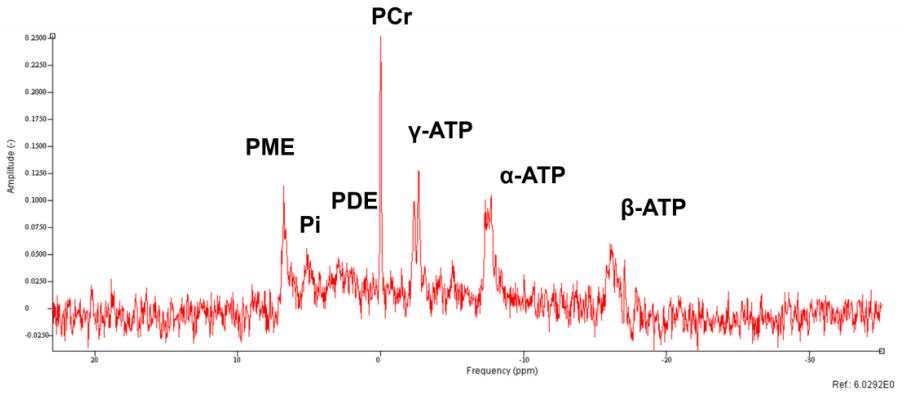

Figure 3-0-13: ^{31}P MRS Spectra from one infant with discrepancy between BGT pHi and LacT/tNAA (pHi=7.23; LacT/tNAA=0.3).

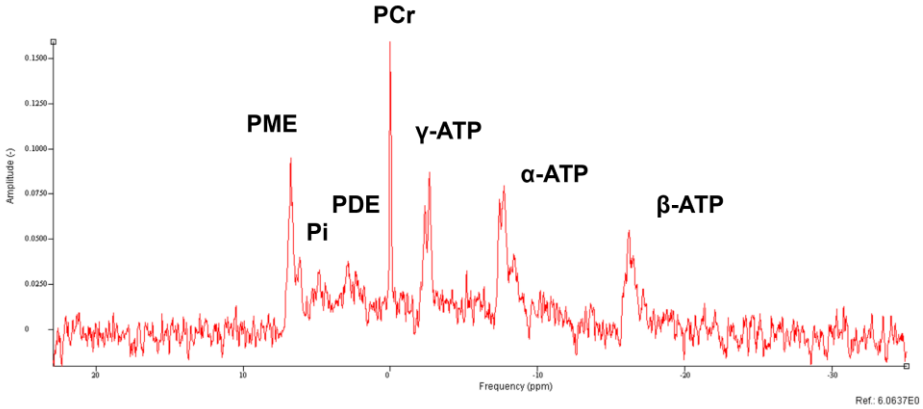

Figure 3-0-14: ^{31}P Spectra from one infant with low Pi peak: lower SNR (pHi=7.00; LacT/tNAA=0.25)

In addition, correlation between some of the different equations to calculate pHi from in-vivo ^{31}P MRS were calculated. *Figure 3-0-15* shows that there was a perfect correlation between the equation published by Hamilton et al (135) and Robertson et al (3), as expected; and a strong correlation with that from Raghunand et al (132). However, all three take into account the Pi chemical shift, and the latter over-calculated pHi by 0.14 points compared to the other two

equations. Hence, normal pHi values would be higher when using the equation published by Raghunand, and the BGT pHi cut-off point to predict an adverse outcome would be at 7.3.

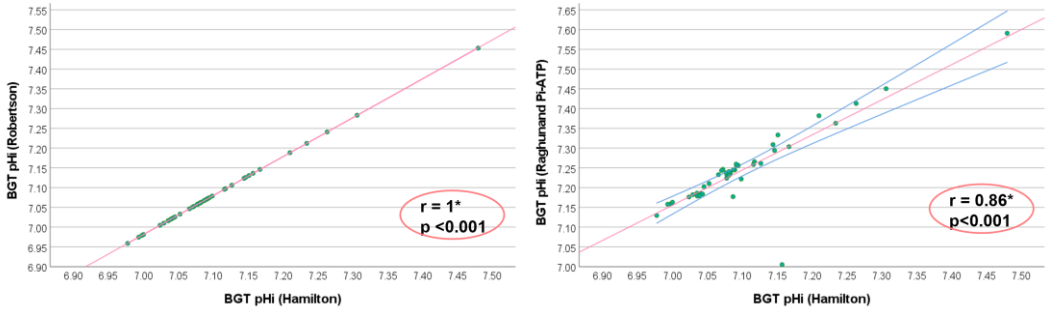

Figure 3-0-15: Correlation between BGT pHi using three different equations. (Left) Equation 1 vs Equation 2, using both chemical shift between Pi/PCr; **(Right)** Equation 1 vs 3, the latter considering chemical shift between Pi and α-ATP.

1.4.1 Alkalosis and increased seizure burden

There was a significant association between having a more alkalotic BGT pHi within the first 2 weeks of life and a higher seizure burden within the first 90h in infants with NE who underwent therapeutic hypothermia. Excluding the outlier with a very high seizure burden, there was still a significant positive correlation (r=0.40, p=0.01). This is described for the first time in newborn infants. According with preclinical data available (5, 243), this finding suggests that avoiding this rebound alkalosis could reduce seizure burden and improve neurodevelopmental outcome. An alkaline pHi has been shown to enhance excitability while acidosis has an opposite effect (5, 223-229). The immature brain appears to be particularly sensitive to changes in pHi. Although we are not measuring pHi at the time seizures occur, we know from previous studies that this rebound alkalosis tends to happen within the first 6-12h, correlating with seizures in time

(5). Furthermore, we know from clinical data that rebound alkalosis persists for even weeks following the insult (3). Hence it is plausible to consider that infants found to have a more alkalotic pHi at the time of the MR scan were likely to have an alkalotic pHi already at the time seizures started. In addition, it has been postulated that pH plays a key role in modulating neuronal survival after trauma (where acidosis is generally protective) (223, 233, 234). A 'graded restoration of normocapnia' strategy in the resuscitation of newborn babies with perinatal asphyxia - trying to avoid a fast shift of pH and the rebound alkalosis - is highly recommended in view of these results and may reduce seizures, improving outcome (5). This data supports the recommendation from recent guidelines (236) that encourages minimising the exposure to hypocapnia or hyperoxia in the respiratory management of infants with NE treated with therapeutic hypothermia, and avoiding the use of alkaline buffers, avoiding a rebound alkalosis. Extra CO_2 inhalation has been trialed as feasible and safe in a small cohort of newborn infants who underwent cooling (242), being another potential avenue for neuroprotection, restoring gradually normocapnia and avoiding hypocapnia (241).

There is a well-established knowledge that the use of Na^+/H^+ exchanger (NHE) inhibitors, such as amiloride, has shown to improve outcome in preclinical model of hypoxia-ischaemia (49, 76, 178, 179, 184, 188, 197, 201, 202, 205, 206, 289, 301). NHE inhibitors should be explored in a preclinical model combined with therapeutic hypothermia to monitor safety levels and pharmacokinetics during cooling, and to prove if, given in addition to therapeutic hypothermia, they

reduce seizures and add neuroprotection. Also, there has been a more recent study in their rat model of asphyxia, exploring the use of carbonic anhydrase inhibitors (to reduce brain pH) which found that electrographic post-asphyxia seizures were suppressed (290), this is another potential avenue.

1.4.3 Neurodevelopmental outcome

There was a significant association between localized deep grey matter pHi measured withing the first 2 weeks of life and the severity of the neurodevelopmental outcome at 2 years of age. A DGM pHi ≥ 7.16 measured in the first 2 weeks after birth has a sensitivity of 66.7% (95% C.I. 20.5-100%; 4 out of 6 infants with a severe outcome) and specificity of 93.8% (95% C.I. 85.2–100%; 30 out of 32 infants with a normal-mild outcome) for predicting their neurodevelopment. However, when looking into the Composite Scores, there was no significant associations. Although the number of lost-to follow-up data is not too large (n=5, 11% of the cohort) compared to other studies (302, 303), it is significant for this study size. Moreover, the fact that 5 extra infants didn't have the Bayley-III performed (4 of which had an adverse outcome) makes the statistical analysis using Composite Scores underpowered. This substantial proportion of data missing and at differential rates between the two severity groups becomes a threat to the internal validity of the Composite Scores analysis.

1.4.4 Other prognostic markers

Furthermore, in this cohort we found consistently with previous publications that brain MRI severity, seizure burden and the aEEG background activity at different time-points are good markers of prognosis in babies who had NE and cooling. In line with a previous study by Thoresen et al (84), we found that aEEG background showed a stronger association with prognosis at 48 hours of age than within the first 6h and at 24h of age, if infants received therapeutic hypothermia. With cooling, children with good prognosis may take longer to have aEEG background activity normalised. The fact that all these babies were receiving medication such as morphine while being cooled might also play a role in the delay recovering a more continuous background activity.

As described in previous studies (122, 124), there was a strong association between LacT/tNAA and the severity of outcome. Looking at the Composite Scores, there was a significant association between a higher LacT/tNAA and a lower Motor Composite Score and a CB-III Composite Score in this cohort. Like with BGT pHi, a thalamic LactT/tNAA ≥ 0.39 measured in the first 2 weeks after birth has a sensitivity of 66.7% (95% C.I. 20.5-100%; 4 out of 6 infants with a severe outcome) and specificity of 93.8% (95% C.I. 85.2–100%; 30 out of 32 infants with a normal-mild outcome) for predicting their neurodevelopment. These values are lower than those described in our previous retrospective study of 55 infants with NE who underwent therapeutic hypothermia and had neurodevelopmental outcome at 2 years of age (124), probably due to sample size.

Future work

The most exciting finding from this study is the correlation shown between seizure burden during the first 4 days of life and deep grey matter alkalosis at the time of the MR scan between day 3 and 8 of life. This finding is described for the first time in infants and could have potential therapeutical implications. The output from this chapter is being written for publication.

Following the completion of the PhD, it would be interesting to test in a preclinical model of hypoxia-ischaemia the effect of NHE inhibitors – both in reducing seizure burden and improving outcome – in conjunction with hypothermia. If successful, the next step would be to consider a multicentre randomised control clinical trial in infants with neonatal encephalopathy and therapeutic hypothermia, using amiloride. Although amiloride has been used in infants as a potassium sparing diuretic, further phase I clinical trials would need to assess safety in children with NE, side effects, dosage, and timing. Also, amiloride exists for oral administration in children, so intravenous administration options would need to be explored. Another potential avenue is the inhalation of 5% carbon dioxide through the ventilator to ensure a gradual restoration of normocapnia, potentially preventing seizures in infants with neonatal encephalopathy, and improving their outcome. Although a small safety study was done in ten infants, larger randomised control trials would need to test this.

Chapter 4: Brain pHi and brain perfusion in newborn infants with neonatal encephalopathy

Introduction

Brain perfusion described by cerebral blood flow (CBF) is part of the aetiology of hypoxia-ischaemia (HI) and suffers significant alterations in its regulations following the insult. Since there is no brain reserve store of oxygen and glucose, a continuous blood flow is crucial to guarantee the continuity of brain function (304). Grey matter – predominantly neuronal cell bodies – has higher metabolic needs, and therefore, CBF requirements, compared to white matter – mainly myelinated axons – with a much lower metabolic demand, and CBF consequently. This explains a much greater susceptibility of the grey matter regions (basal ganglia and thalami especially [BGT]) to a sudden HI insult (102).

Auto-regulation of CBF is the ability of the brain to maintain relatively constant blood flow despite changes in perfusion pressure (256), protecting it from hypo- and hyperperfusion (305). This constant blood flow is maintained through neural, hormonal, and metabolic mechanisms. Cerebral ischaemia occurs when cerebral perfusion pressure falls below the lower limit of auto-regulation (50). A reduction in CBF is compensated by an increase in blood oxygen extraction (257). During a prolonged and severe enough HI event, the adrenergic sympathetic activation causes a vasoconstriction and hypoperfusion to the brain.

Following HI severe alteration of brain metabolism and physiology are observed (264), being associated with specific abnormalities in blood flow such as vasoparalysis (80). An increased CBF is found in babies who have suffered a more severe insult from day 1, using cranial ultrasound scan (76, 77), near-infrared spectroscopy (NIRS) (79, 265), and MR techniques, such as arterial spin labelling (ASL) (6, 7, 266, 274-276). This so-called 'luxury perfusion syndrome' or 'reperfusion syndrome' is characterized by increased CBF relative to the metabolic needs of the brain. It is likely to be initiated by abnormal metabolism (268), such as lactic acidosis, and loss of vessels tone (264). This hyperperfusion restores high-energy phosphates that lead to delayed cell death (secondary energy failure) (269) and are associated with poor prognosis (79, 80, 270).

In a previous study performed at UCLH, the sequence was optimised for neonates and a processing framework created for detailed analysis, with regions of interest for ASL (6). We showed in a cohort of 17 infants with neonatal encephalopathy (NE) (6, 266), that those with an unfavourable prognosis (n=3) – Lac/NAA peak area ratio > 0.3 (122) – presented with hyperperfusion in different areas of the brain, being statistically significant for the lentiform nuclei (*figure 4-0-1*). Other studies showed also that CBF using ASL would increase the predictive power of Lac/NAA, when used in combination (7).

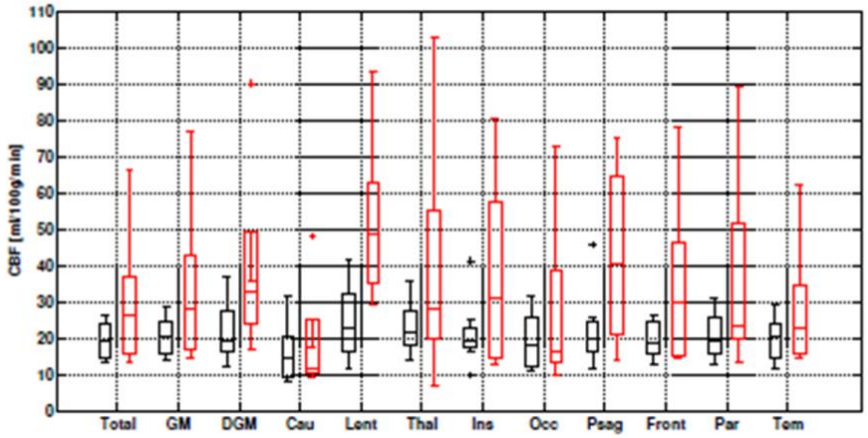

Figure 4-0-1: Comparison between regional CBF for different areas of the brain depending on the likelihood of good prognosis (black, with Lac/NAA<0.3) or bad one (red). From (6, 266).

On the other hand, ^{31}P MRS can provide unique information such as brain intracellular pH (pHi) that may lead to possible new avenues of neuroprotection as described in *Chapter 3*. In this sub-study, in addition to localised deep grey matter (DGM) pHi, regional CBF will also be assessed using pCASL. Any relationship between DGM pHi and brain perfusion in infants with neonatal encephalopathy (NE) is unclear. It is possible that not only hyperperfusion contributes to the rebound alkalosis (306), that occurs in infants with a poor prognosis, by removing excess carbon dioxide; but also it will be related to energy metabolism, by restoring high energy phosphates and leading to delayed cell death (269).

The **aim of this study** is to investigate, in newborn infants with NE who underwent therapeutic hypothermia, the association (i) between localised deep grey matter pHi and rCBF; (ii) between rCBF and the current updated biomarker of outcome (thalamic Lactate plus Threonine to total N-acetyl-aspartate (LacT/tNAA) peak area ratio, using a cut-off point of 0.39 (124)); and (iii) between

rCBF and neurodevelopmental outcome at 2 years of age. The hypothesis is that infants with NE with an unfavourable prognosis (LacT/tNAA ≥ 0.39) will have an increased perfusion to the basal ganglia and thalami (BGT), and this will be associated with a more alkalotic pHi in the BGT. We also expect that infants with an adverse outcome will have higher rCBF levels in the BGT.

Patients and Methods

This is a sub-study within the Baby Brain Study, hence the same 'patients and methods' selection criteria than in *Chapter 3* apply, adding an MR sequence to measure regional cerebral blood flow (rCBF) to the scanning time: pseudo-continuous arterial spin labelling MR imaging (pCASL).

Ethical and UCLH R&D approval were obtained, and parental written informed consent given prior to every examination.

4.2.1 Patients and study design

To calculate the sample size needed, data from the previous study (266) was used, where infants were divided into two outcome groups according to Lac/NAA (favourable and unfavourable prognosis). A difference of 30ml/100g/min in CBF between groups would be of interest and in previous studies a standard deviation of around 18ml/100g/min in CBF was seen in these groups (6). With an 80% power and 5% significance, the number of infants required in each group is 12, to determine differences and find a threshold CBF that best predicts outcome. Thus, we need a total of 24 subjects.

In this sub-study, 23 of the 43 newborn infants with NE secondary to perinatal HI who fulfilled criteria for therapeutic hypothermia (17) underwent ^{31}P MRS and ASL. They were enrolled prospectively at UCLH, London, United Kingdom from May 2014 to August 2016. Mean gestational age ([SD]; range) was 39.4 weeks (SD 1.5; range 36.6-41.9) and mean birth weight 3304g (SD 526; range 2350–4376). Neonates with congenital anomalies, genetic syndromes, or those with a different aetiology of NE to HI were excluded from the analysis. They all received therapeutic hypothermia from a median age of 2h of life and for a total duration of 72h – except one who was rewarmed after 22 hours because of very mild picture of NE and another who was re-cooled for extra 12 hours due to seizures during rewarming, as our standard clinical practice –. *Table 4-0-1* shows descriptive characteristics of the cohort.

	N	Mean ± SD	Median	Range
GA (weeks)	23	39.4± 1.5	40.3	36.6 – 41.9
Birth weight (gr)	23	3304 ± 526	3160	2350 – 4376
Gender (M:F)	11:12			
Inpatient/outpatient	11/12			
Apgar score (5 min)	23	4.0 ± 2.5	4	0 – 9
Apgar score (10 min)	19	5.1 ± 2.7	5	0 – 9
Blood pH within 1st hour (including cord)	22	6.91 ± 0.14	6.93	6.60 – 7.17
Blood BE within 1st hour (including cord)	19	-18.3 ± 5.3	-17.0	-31.8 - -9.2
Lactate within 1st hour (including cord)	17	13.5 ± 3.7	12.7	7.2 – 20
Intubated during resuscitation	21/23			
Cardiac massage	6/23			
Drugs during resuscitation	3/23			
Age at target temperature	20	2.7 ± 2.0	2	0.5 - 6.5
Duration cooling	23	69.22 ± 15.9	72	22 – 96[1]
Death	1/23			

Table 4-0-1: Descriptive characteristics of the subgroup of infants with NE who had ^{31}P MRS and ASL. [1]Therapeutic hypothermia stopped earlier in one baby because of very mild clinical picture. One baby re-cooled for extra 12h due to seizures during rewarming.

4.2.2 Imaging

MRI and MRS were performed at a median age of 5 days (range 4-15), with corrected gestational ages between 37.3 - 43.1 weeks, using a 3T MR System (Philips Medical Systems®, Best, The Netherlands). The same scanning protocol was used as in the previous study. MRI were scored using the NICHD scoring system (291) (together with the Neuroradiologist Dr R Gunny). ^{1}H MRS data were analysed using Tarquin and LacT/tNAA peak area ratio (Lactate + Threonine to total N-acetyl-aspartate [NAA+NAAG]) was used as biomarker of outcome (122-124)). ^{31}P MRS was analysed by the author using AMARES algorithm for jMRUI. Energy metabolite ratios and pHi calculations [equation 1 by Hamilton (135)) were obtained.

Twenty-three babies had also pCASL (pseudocontinuous ASL) performed. Protocol and data processing framework used were the ones developed by Dr. M. Sokolska , as part of her PhD (6). The labelling plane was positioned based on ToF angiography images to ensure that it was perpendicular to the feeding arteries. For this study, labelling duration was 1.7 seconds with a post-labelling delay (PLD) of 2s.

A. Data processing for pCASL

Postprocessing of the pCASL images was performed by a Physicist (Dr. Magdalena Sokolska following methodology developed as part of her PhD (6)) and CBF was calculated using Matlab. Images were corrected for motion (*figure 4-0-2*). The single compartment kinetic model was used for CBF quantification

(*equation 4*) (307) and was calculated for each baby based on haematocrit (Hct) values measured close to the time of the MRI, according to *equation 5 (308, 309)*.

$$CBF = \frac{6000 \cdot \lambda \cdot (SI_{control} - SI_{label}) \cdot e^{\frac{PLD}{T_{1,blood}}}}{2 \cdot \alpha \cdot T_{1,blood} \cdot SI_{PD} \cdot \left(1 - e^{\frac{\tau}{T_{1,blood}}}\right)} \qquad \left[\frac{ml}{100g}/min\right]$$

Equation 4

where λ is the brain/blood partition coefficient (concentration of the tracer in brain tissue relative to that of the blood)) in ml/g (1 ml/g), $SI_{control}$ and SI_{label} are time-average signal intensities in the control and label images, respectively, $T_{1,blood}$ is the longitudinal relaxation time of blood in seconds (calculated for each baby individually based on haematocrit with *Equation 5* (308)), α is the label efficiency (0.69; including background suppression efficiency of 0.95 per pulse), SI_{PD} is the signal intensity of a proton density-weighted image, and τ is the label duration (1.7s) and PLD is the post labelling delay (2s). The units are converted from ml/g/s to ml/100g/min – as usually presented in the literature – with the factor of 6000.

$$1/T_{blood} = 0.5*Hct + 0.37$$ **Equation 5**

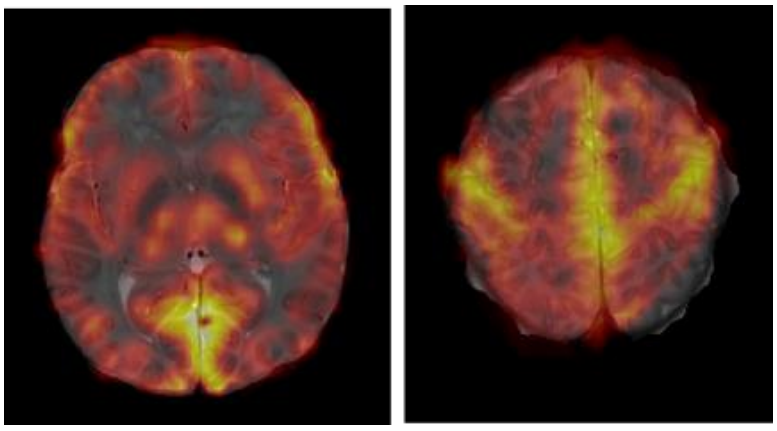

Figure 4-0-2: Example of CBF map acquired using pCASL in a baby studied. Grading colour scale, where black is equivalent to CBF of 0ml/100g/min, grades up to red (15-35ml/100g/min), orange (35-50ml/100g/min), yellow (50-70ml/100g/min) and white (>70ml/100g/min).

Regional CBF analysis was performed automatically based on available atlases (310, 311). Previous studies (6, 266, 310-312) have shown these atlases to be useful for segmentation and parcellation of high resolution data for volumetric studies, and for rCBF quantification in ASL for different regions of interest (ROI): grey matter (GM or cortex), deep grey matter (DGM), white matter (WM), cerebellum (CB), brainstem (BS), then, each GM region (frontal, temporal, parietal, occipital, cingulate and insula) and each DGM region (caudate, thalamus and lentiform nuclei).

4.2.3 Neurodevelopmental outcome data at 2 years of age

One newborn infant died within the first week of life. Nineteen children were assessed for their neurodevelopmental outcome at 3, 6, 12 and 24 months of age, as part of their clinical follow-up, led by Dr A Huertas-Ceballos. Three children were lost to follow-up (13.6%).

At 24 months (range 21-26), the Bayley Scales of Infant Development, Third Edition was used for assessment (Bayley III) (294). It has five scales (cognitive, language (receptive and expressive), motor (fine and gross motor), social emotional and adaptative behaviour). Raw scores are transformed into a composite score, where the mean is 100 (SD 15). Outcome was classified as normal, mild, and severe (see *table 4-0-2*)

Outcome severity at 2 years of age	
Normal	Bayley-III Composite score within 1SD (**≥85**)
Mild	**One domain** affected with a Composite score between 2SD and 1SD below the mean (**70-84**)
Severe	• **Death** • **Any one domain** with a Composite score below 2SD (**<70**) • **At least 2 domains** with a Composite score between 2SD and 1SD below the mean (**70-84**)

Table 4-0-2: Outcome severity classification based on Bayley-III assessments (295, 296)

4.2.4 Statistical Methods

Analyses were performed using IBM SPSS Statistics 28.0, SPSS Inc., Chicago, IL. Descriptive data summaries were generated using means and standard deviations (or medians and inter-quartile range) for quantitative variables, and frequency distributions (total number and frequency) for qualitative variables.

To analyse the association between regional cerebral blood flow (rCBF) and other prognostic tools (both DGM pHi and thalamic LacT/tNAA) bivariate analyses were performed, using Pearson correlation (or Spearman correlation for categorical values). Qualitative analysis will be performed for outcome severity due to only one infant with a severe long-term outcome.

Prior to comparing rCBF between two groups and due to the small sample size within groups, normality tests were performed (Kolmogorov-Smirnov and Shapiro-Wilks) (297, 298). In those where normality was assumed, the difference in means was analysed using a t-Student test for independent samples. The Levene's test for Equality of Variances was performed beforehand to interpret results. If normality couldn't be assumed, a U-Mann Whitney test was performed

to assess whether there was a difference in rCBF between infants with a favourable/unfavourable prognosis based on DGM pHi and thalamic LacT/tNAA.

The cut-off point used to compare infants with low-high pHi was 7.16, based on previous studies (3) and Chapter 3; and when comparing infants with low-high thalamic LacT/tNAA, it was 0.39 (124).

Statistical significance was considered when p value was <0.05 (95% confidence interval [C.I.]).

The predictive ability of rCBF as a prognostic marker were explored estimating positive predictive value, negative predictive value, sensitivity, and specificity.

Results

4.3.1 Overview of regional CBF data

Figure 4-0-3 shows MR images and rCBF maps from two infants in this sub-study, one with increase perfusion (top row) and another with lower rCBF values (bottom row).

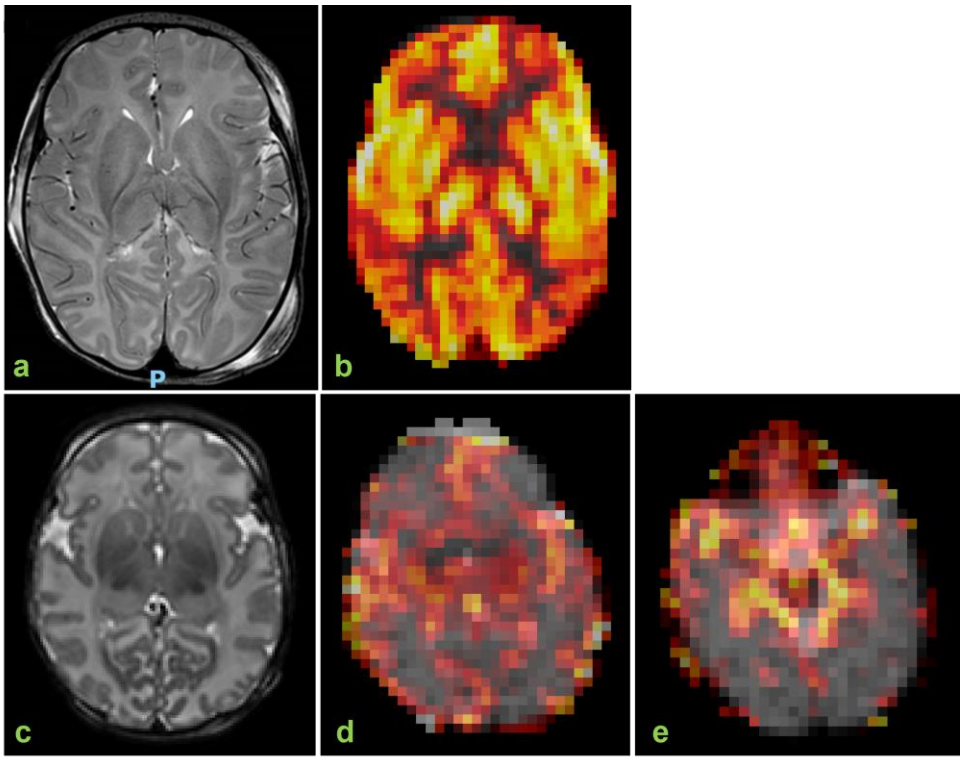

Figure 4-0-3: MRI Images and rCBF map acquired using pcASL from 2 infants. Grading colour scale, where black is equivalent to CBF of 0ml/100g/min, grades up to red (15-35ml/100g/min), orange (35-50ml/100g/min), yellow (50-70ml/100g/min) and white (>70ml/100g/min).
(*Top row*) Infant with an adverse outcome and high LacT/tNAA and pHi **a)** T2 sequence MRI. NICHD score 2B; **b)** rCBF map showing increase values of perfusion, especially in DGM and cortical regions. **(*Bottom row*)** Infant with a normal outcome and low LacT/tNAA and pHi **c)** T2 sequence MRI. NICHD score 2A; **d, e)** rCBF maps showing lower values of perfusion.

Figure 4-0-4 shows a summary of the rCBF for each region of interest in each of the 23 infants studied with neonatal encephalopathy and who underwent hypothermia.

The top graph shows the regional CBF values for each region of interest (grey matter, deep grey matter, white matter, cerebellum and brainstem, each in one colour), grouped for each of the 23 infants (on the x axis). There is only one infant with remarkably higher CBF values for most regions of interest compared to the other infants studied. Looking at the graphs below, the grey matter (GM) rCBF, deep grey matter (DGM) rCBF, and white matter (WM) rCBF to a lesser extent (middle left graph), show a more marked increase than the cerebellum

and brasintem rCBF (middle right graph). The graphs at the bottom, show the rCBF for each subregion within the GM (bottom left: frontal cortex, temporal, parietal, occipital, cingulate, and insula) and DGM (bottom right: caudate, thalamus and lentiform).

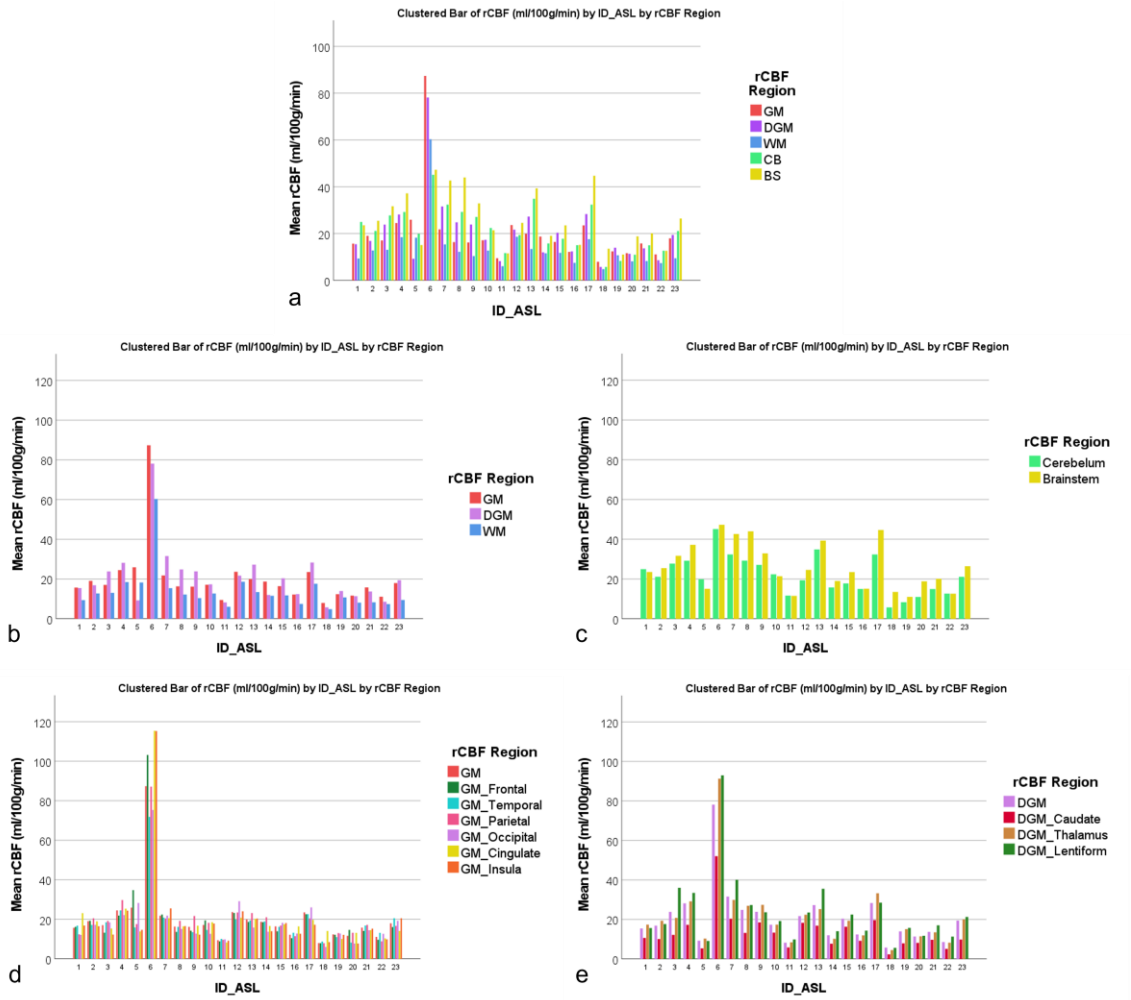

Figure 4-0-4: Summary of the regional CBF (rCBF) for each region studied for each one of the 23 infants studied. ***(Top) a)*** rCBF for the main areas in the brain. **GM:** Grey matter (cortex); **DGM:** deep grey matter; **WM:** White matter; **CB**: Cerebellum; **BS**: Brainstem. Then each cortical region and each DGM region. ***(Middle row)*** Split into two graphs: **b)** rCBF for GM, DGM and WM for each baby; and **c)** rCBF for cerebellum and brainstem. ***(Bottom row)*** **d)** rCBF for the different cortical areas (GM); and **e)** for the different DGM areas.

4.3.2 Association between rCBF and BGT pHi

We used a cut-off point of 7.16, as described in Chapter 3 and previously by Robertson et al. (3), where infants with a more alkalotic basal ganglia and thalami (BGT) pHi were more likely to have an unfavourable prognosis. In this cohort there were three infants with a high BGT pHi. Although 1 of these 3 infants had a remarkably increased CBF in all regions, except cerebellum and brainstem, there was no significant correlation between pHi and rCBF for any of the studied regions (*figure 4-0-5).*

When comparing median rCBF between these 2 groups, there were no differences found (*figure 4-0-6, table 4-0-3*). Infants more likely to have an unfavourable outcome present with wide range of CBF. Those infants with a low pHi, have more consistently CBF values between 10 and 40 ml/100g/min.

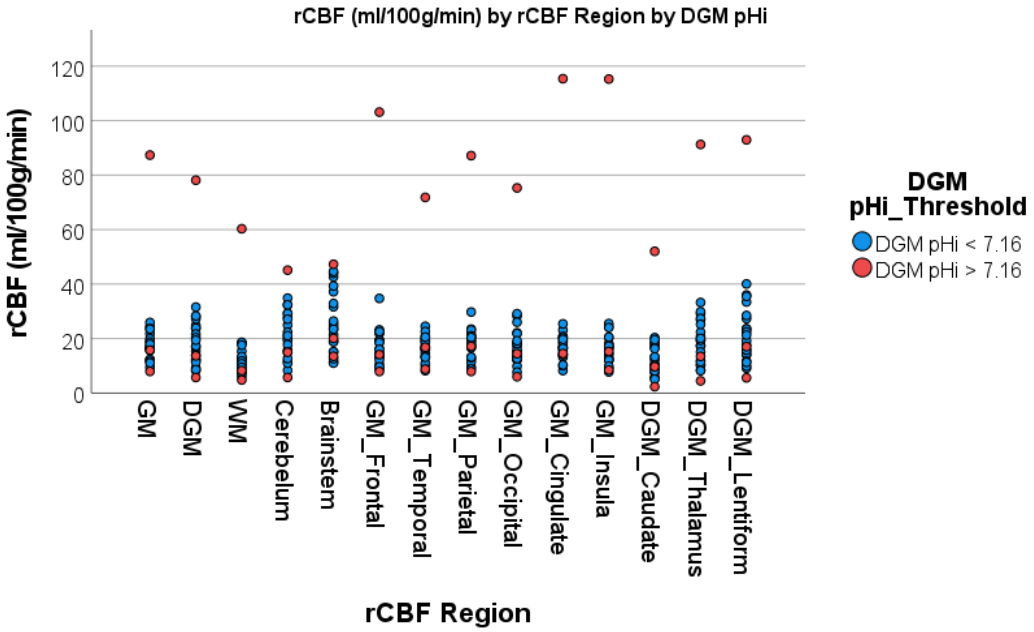

Figure 4-0-5: Cerebral blood flow (CBF) for each of the regions of interest (ROI) according to severity of deep grey matter pHi. In **red**, three infants with a more alkalotic pHi; and in **blue**, 20 infants with a lower pHi.

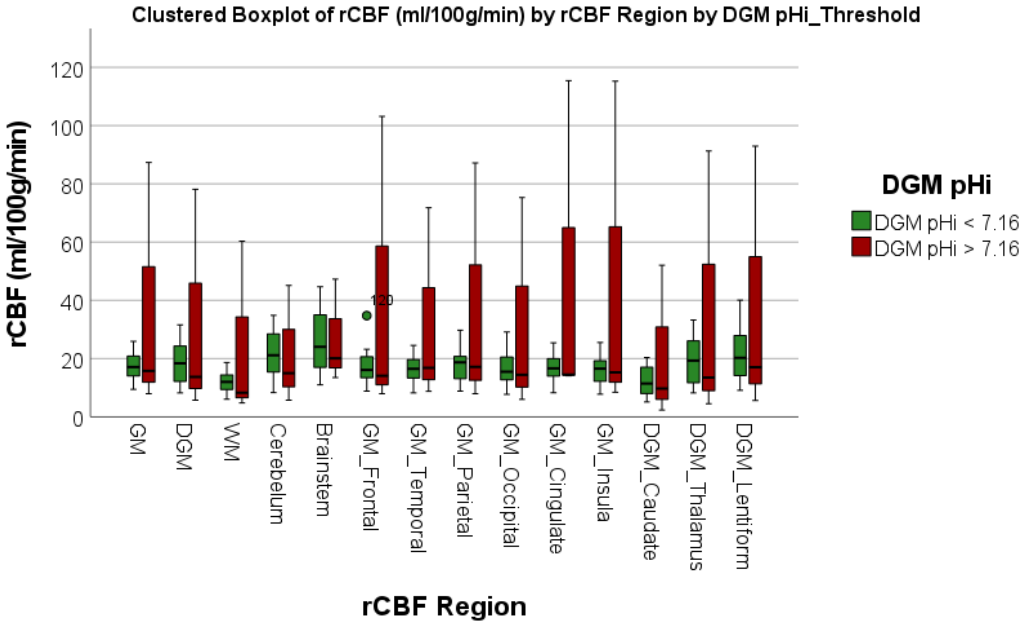

Figure 4-0-6: Clustered Boxplot for median CBF for each of the regions of interest according to BGT pHi, using the cut-off point of 7.16. The box shows median, first and third quartiles, whiskers represent the ±1.5 interquartiles.

rCBF (ml/100g/min)	DGM pHi <7.16 n=20 Mean (SD)	DGM pHi ≥ 7.16 n=3 Median (Range)
rCBF GM	17.53 (4.73)	15.78 (7.96 – 87.38)
rCBF DGM	18.74 (7.26)	13.70 (5.74 – 78.16)
rCBF WM	12.25 (3.85)	8.28 (4.81 – 60.33)
rCBF Cerebelum	21.71 (7.86)	14.99 (5.74 – 45.13)
rCBF Brainstem	26.04 (11.05)	20.10 (12.63 – 47.29)
rCBF GM_Frontal	17.20 (6.03)	14.13 (7.94 – 103.16)
rCBF GM_Temporal	16.58 (4.25)	16.82 (8.79 – 71.84)
rCBF GM_Parietal	17.84 (5.22)	17.19 (7.93 – 87.18)
rCBF GM_Occipital	16.94 (5.99)	14.46 (6.02 – 75.34)
rCBF GM_Cingulate	16.82 (4.38)	14.53 (10.32 – 115.42)
rCBF GM_Insula	16.14 (5.07)	15.28 (8.48 – 115.29)
rCBF DGM_Caudate	12.29 (5.03)	9.71 (2.36 – 52.05)
rCBF DGM_Thalamus	19.22 (7.67)	13.49 (4.50 – 91.28)
rCBF DGM_Lentiform	21.53 (9.37)	17.05 (5.61 – 92.98)

Table 4-0-3: Descriptive table of rCBF for the different regions of interest within the first 2 weeks of life in infants classified by DGM pHi from ^{31}P MRS. Mean (SD) for the low pHi group (n=20) and Median (Min-Max) for the high pHi group (n=3).

4.3.3 Association between rCBF and thalamic LacT/tNAA

A cut-off value for LacT/tNAA of 0.39 was used, where infants with a Lac/NAA above 0.39 are more likely to have a poor neurodevelopmental outcome (124). There were 3 infants with a high LacT/tNAA in this cohort (one of them with a low pHi). There was a significant positive correlation between a higher LacT/tNAA and a higher rCBF in the grey matter (r= 0.44, p=0.034), the frontal region (r= 0.47, p=0.024), the temporal region (r= 0.44, p=0.037), the parietal region (r= 0.43, p=0.041), the cingulate (r= 0.54, p=0.007), insula (r= 0.50, p=0.015), and white matter (r= 0.42, p=0.044) (*figure 4-0-7*). When excluding the two outliers from the analysis (two neonates with a high LacT/tNAA: one with a very high CBF and the other one very low), the positive association disappeared.

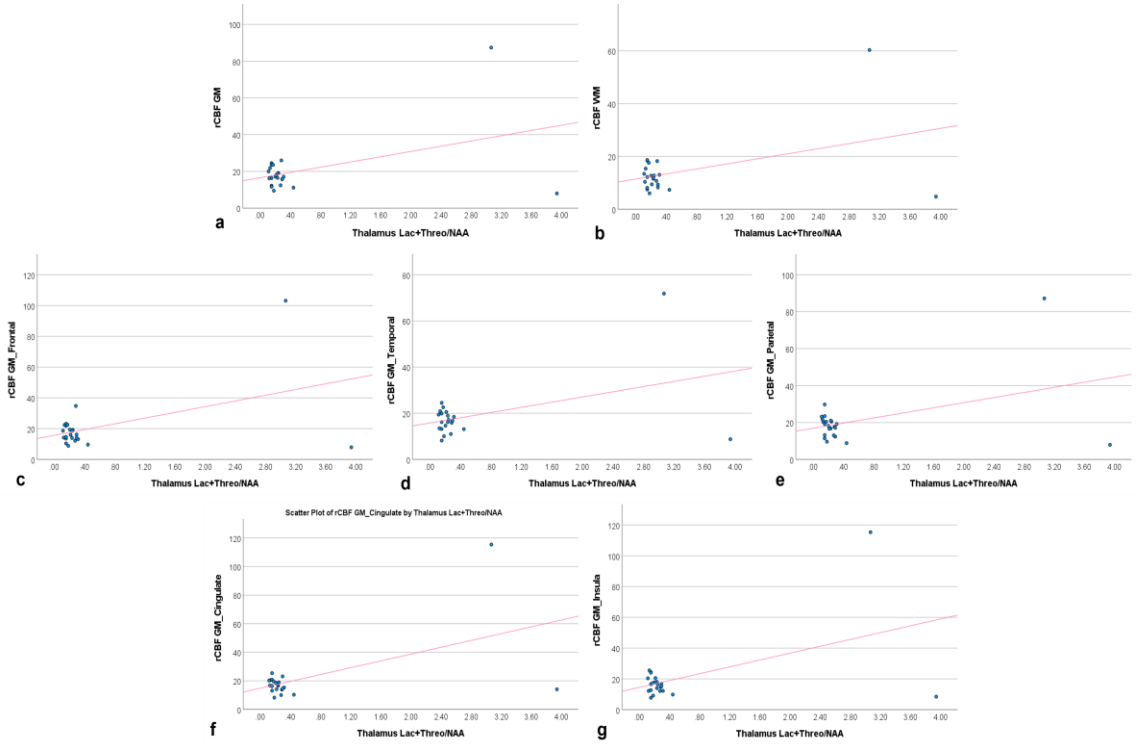

Figure 4-0-7: Correlation between thalamic LacT/tNAA and rCBF in 23 infants with NE, for the regions that showed a significant association. **a)** Grey Matter; **b)** White Matter; **c)** Frontal cortex; **d)** Temporal cortex; **e)** Parietal cortex; **f)** Cingulate; and **g)** Insula.

Figure 4-0-8 shows a summary of rCBF for each region of interest according to prognosis, based on thalamic LacT/tNAA. There was a wide range of rCBF in the three infants with a poor prognosis (red dots).

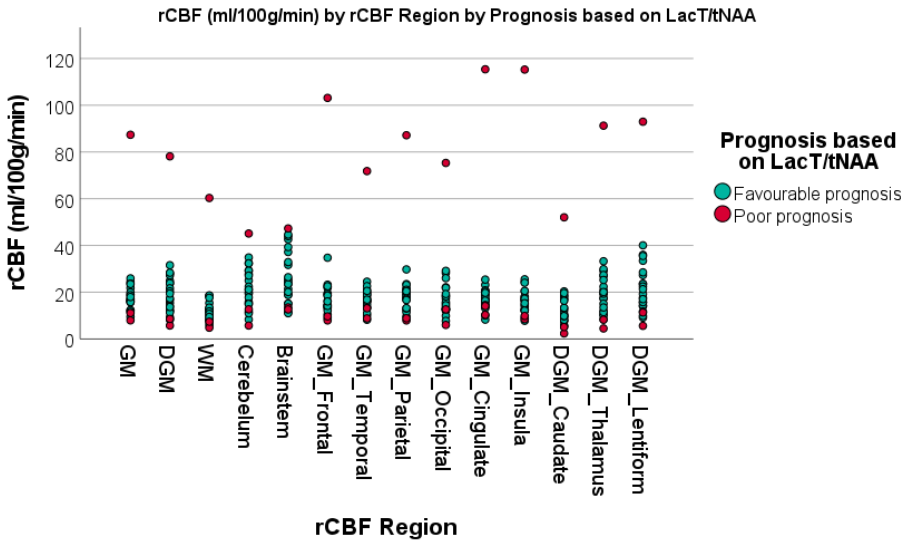

Figure 4-0-8: Cerebral blood flow (CBF) for each of the regions of interest (ROI) according to severity of thalamic LacT/tNAA. In red, three infants with a LacT/tNAA ≥ 0.39; and in green, 20 infants with a lower LacT/tNAA and better prognosis.

When comparing median rCBF for the different areas of interest between the groups with a favourable vs poor prognosis, according to thalamic LacT/tNAA, there were no differences. Again, although one baby showed remarkable hyperperfusion to most areas, the other 2 babies with a high LacT/tNAA presented low CBF (*figure 4-0-9, table 4-0-4*).

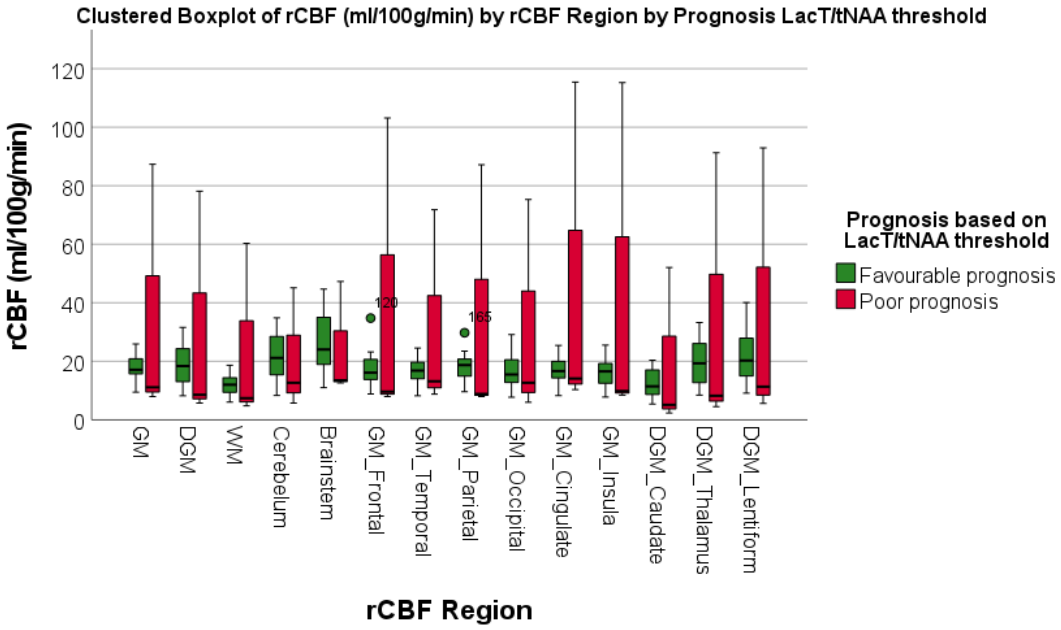

Figure 4-0-9: Clustered Boxplot for median CBF for each of the regions of interest according to likelihood of a good/bad prognosis based on ^{1}H MRS. The box shows median, first and third quartiles, whiskers represent the ±1.5 interquartiles.

rCBF (ml/100g/min) Mean (SD)	LacT/tNAA < 0.39 n=20 Mean (SD)	LacT/tNAA ≥ 0.39 n=3 Median (Range)
rCBF GM	17.77 (4.50)	11.10 (7.96 – 87.38)
rCBF DGM	18.99 (6.97)	8.59 (5.74 – 78.16)
rCBF WM	12.29 (3.79)	7.38 (4.81 – 60.33)
rCBF Cerebelum	21.82 (7.73)	12.69 (5.74 – 45.13)
rCBF Brainstem	26.41 (10.69)	13.52 (12.63 – 47.29)
rCBF GM_Frontal	17.42 (5.81)	9.65 (7.94 – 103.16)
rCBF GM_Temporal	16.76 (4.17)	13.15 (8.79 – 71.84)
rCBF GM_Parietal	18.26 (4.78)	8.86 (7.93 – 87.18)
rCBF GM_Occipital	17.03 (5.94)	12.67 (6.02 – 75.34)
rCBF GM_Cingulate	17.03 (4.15)	14.10 (10.32 – 115.42)
rCBF GM_Insula	16.42 (4.86)	9.85 (8.48 – 115.29)
rCBF DGM_Caudate	12.52 (4.78)	5.10 (2.36 – 52.05)
rCBF DGM_Thalamus	19.48 (7.36)	8.25 (4.50 – 91.28)
rCBF DGM_Lentiform	21.82 (9.13)	11.33 (5.61 – 92.98)

Table 4-0-4: Mean (SD) of rCBF for the different regions of interest within the first 2 weeks of life in infants classified by DGM pHi from ^{31}P MRS. Mean (SD) for the low LacT/tNAA group (n=20) and Median (Min-Max) for the high LacT/tNAA (n=3).

4.3.4 Association between rCBF and neurodevelopmental outcome at 2 years of age

One infant died in the neonatal period. Nineteen of the other 22 were assessed in the neurodevelopmental clinic at a median age of 24 months (range: 22-26 months). Four infants presented with a mild outcome (3 with a Language Composite Score in the mild range, between 70 and 84, between 2SD and 1SD (295, 296)) and 1 with a Cognitive Composite Score in the mild range too, between 70 and 84); and 15 infants showed a normal outcome at 2 years of age. Unfortunately, with only one infant with an adverse long-term outcome (*figure 4-0-10*), this sub-study is underpowered to undertake any further analysis.

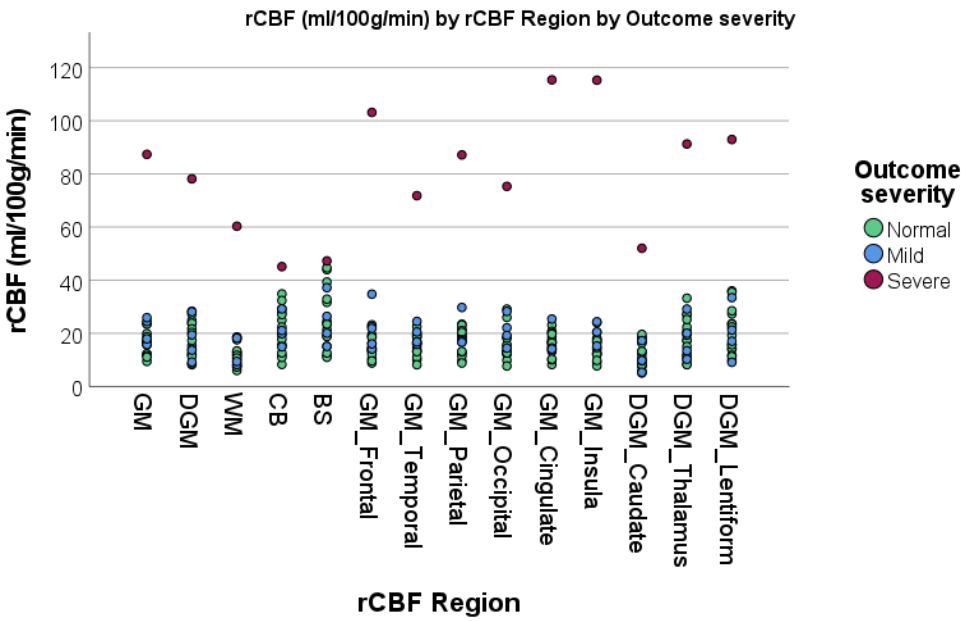

Figure 4-0-10: Cerebral blood flow (CBF) for each of the regions of interest (ROI) according to severity of neurodevelopmental outcome at 2 years of age. In **red**, one infant who died in the neonatal period; in **blue**, 4 infants with a mild outcome; and in **green,** 15 infants with a normal outcome.

There were no differences between mean CBF for the different regions for infants with a normal outcome and those with a mild outcome ($p > 0.05$). In *table 4-0-4*, there is a summary of mean (sd) of rCBF for each region of interest in the

group of infants with a normal outcome (first column, n=15), in the group with normal-mild outcome combined (second column, n=19) and the values of rCBF for the infant with a severe outcome in this cohort (third column).

rCBF (ml/100g/min)	Normal n=15 Mean (SD)	Normal-mild outcome n=19 Mean (SD)	Severe outcome n=1
rCBF GM	16.10 (4.26)	17.14 (4.74)	87.38
rCBF DGM	17.97 (6.79)	17.90 (6.85)	78.16
rCBF WM	11.37 (3.56)	11.84 (3.97)	60.33
rCBF Cerebelum	20.69 (8.38)	20.82 (7.78)	45.13
rCBF Brainstem	24.92 (11.27)	24.88 (10.68)	47.29
rCBF GM_Frontal	15.30 (4.42)	16.65 (6.07)	103.16
rCBF GM_Temporal	15.50 (4.03)	16.33 (4.24)	71.84
rCBF GM_Parietal	16.79 (4.95)	17.53 (5.28)	87.18
rCBF GM_Occipital	15.34 (5.72)	16.53 (6.06)	75.34
rCBF GM_Cingulate	16.22 (4.23)	16.38 (4.40)	115.42
rCBF GM_Insula	14.75 (4.48)	15.59 (4.68)	115.29
rCBF DGM_Caudate	12.20 (4.86)	11.85 (4.79)	52.05
rCBF DGM_Thalamus	18.37 (7.63)	18.35 (7.54)	91.28
rCBF DGM_Lentiform	20.60 (8.45)	20.52 (8.53)	92.98

Table 4-0-5: rCBF for the different regions of interest within the first 2 weeks of life in infants classified by neurodevelopmental outcome at 2 years of age. Mean (SD) for the normal (n=15), normal-mild (n=19), and CBF value for the child who died in the neonatal period (n=1).

Discussion

4.4.1 Localised brain pHi and rCBF

It has been described previously that neonatal cerebral blood flow, after a hypoxic-ischaemic event, usually, increases in the affected tissue (6, 7, 274-276). Similarly, in this cohort, the one infant with a remarkable increased CBF above normal values (6) presented an alkalotic BGT pHi. Elevated lactate and alkalosis in chronic infarctions has also been described in adults with brain infarcts,

consistently with the presence of phagocytic cells, gliosis, altered buffering mechanisms and/or luxury perfusion (313). In severe cases, the severity and duration of the insult have overrun the autoregulation mechanisms. The increase in adenosine , factors that increase intracellular calcium (which activate endothelial NOS) and other inflammatory/infectious compounds (like arachidonic acid) will cause vasodilation (255, 261).

A possible mechanism of rebound alkalosis, in addition to the ones discussed (such as NHE over-stimulation), is related to the fact that alkalosis correlates with a reduced oxygen extraction fraction and blood perfusion exceeding metabolic demands (e.g. luxury perfusion), causing alkalosis by removing excess CO_2 (306). Moreover, luxury perfusion may contribute to alkalosis per se. There is some evidence that hyperperfusion restores high-energy phosphates in neonates severely affected, leading to delayed cell death (269). During the secondary energy failure phase, an increase in Pi will happen then (as we showed the elevated Pi/PCr in the group with a poor prognosis in Chapter 3), and potentially, alkalosis, by clearing protons and products of glycolysis.

However, no significant association between localised DGM brain pHi measured within the first 2 weeks of life and regional cerebral blood flow to the different regions of interest studied was found in this sub-study. Unfortunately, statistical power is compromised due to the small number of infants in the severe hypoxia-ischaemia group, which is a **limitation** of this sub-study. There were two main reasons for this. The main challenge was adding two extra MR sequences to the clinical scan, despite the study being granted over half an hour above the

standard clinical scan (one and a half hour available per child in total). The coil needed to be changed between proton and phosphorus acquisitions within a single scanning session. This was especially difficult in ventilated babies, requiring a brief disconnection from the ventilator to slide the coils in-out. Any setback (e.g., motion during the clinical sequences and motion-tolerant sequences had to be added for clinical purposes, infant lightly sedated who started to wake up by the time of the second MR research sequence, etc) meant that on many occasions we were only able to get either ^{31}P MRS or ASL, but not both. Secondly, in the last few years, the number of severe HIE cases have fortunately decreased. This implies that the estimations made for how long it would take to recruit the number needed of infants in each group changed significantly, becoming unfeasible to recruit 12 infants into the severe prognosis group within a reasonable timeframe.

4.4.2 rCBF and prognosis

Although perfusion was increased in BGT, cortical areas and white matter in an infant with a high LacT/tNAA that later presented with unfavourable outcome; there was a wide range of rCBF in the group of infants with a poor prognosis (high LacT/tNAA), and no significant differences in median rCBF were found. This data is consistent with our prior results (266) and with the literature (7, 8, 314). 'Luxury perfusion' has been well documented in these studies and it was associated with adverse prognosis or severe outcome; but rCBF values can be

broadly spread in this group of neonates, making difficult to interpret a low rCBF in isolation from the rest of predictors of outcome. On the other hand, children with a good prognosis presented with normal/lower values of CBF consistently. Similar to the results in De Vis et al. (7), in this cohort the positive predictive value of rCBF is 100% (although only one in this group), and the negative predictive value is 90%. However, sensitivity is 30%, and specificity 100% (see *table 4-0-6*). A high CBF in certain regions in the brain (especially some cortical areas, thalamus and lentiform nuclei) will suggest a poor outcome, but a lower CBF doesn't seem to be a good predictor on its own.

	LacT/tNAA ≥ 0.39	LacT/tNAA < 0.39
rCBF > 50ml/100g/min	TP 1	FP 0
rCBF < 50ml/100g/min	FN 2	TN 20

Sensitivity= TP / (TP+FN)
Specificity= TN / (FP+TN)

PPV= TP / (TP+FP)
NPV= TN / (TN+FN)

Table 4-0-6: Calculation of sensitivity, specificity, positive predictive value and negative predictive value

Supporting this further, within the whole Baby Brain Study, there was a total group of 47 infants with NE who underwent therapeutic hypothermia and had both ^{1}H MRS and ASL, but not ^{31}P MRS (*unpublished data* yet). *Figures 4-0-11* shows how, similarly to the smaller cohort in this sub-study, there were no significant differences in mean CBF for any of the areas of interest between the group with favourable outcome (n=37) and the group with unfavourable outcome (n=10), based on Lac/NAA cut-off (122). However, as discussed above, only 2/10 infants with unfavourable outcome showed remarkable high values of rCBF (>100ml/100g/min) (*figure 4-0-12*).

Similar findings were discussed recently by the Zurich Group (314) in their initial communication, finding differences between the favourable and unfavourable outcome groups, but describing as well the wide range of CBF in the unfavourable group.

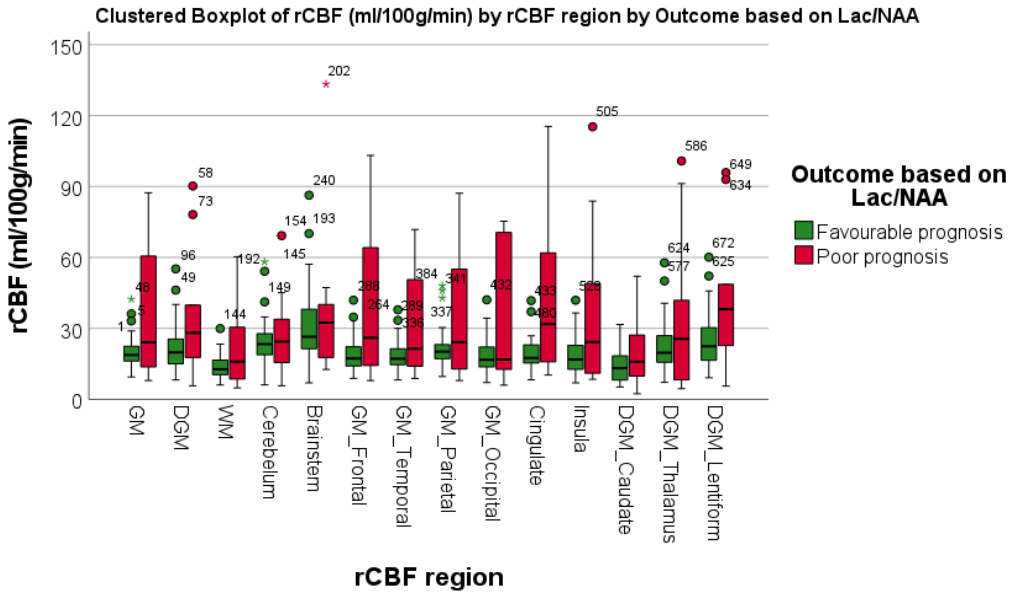

Figure 4-0-11: Clustered Box-plot for median CBF for each of the regions of interest according to likelihood of a good/bad prognosis based on ^{1}H MRS in a different group of 47 infants with NE (37 with a low Lac/NAA and 10 with a high Lac/NAA). *(unpublished data)* The box shows median, first and third quartiles, whiskers represent the ±1.5 interquartiles.

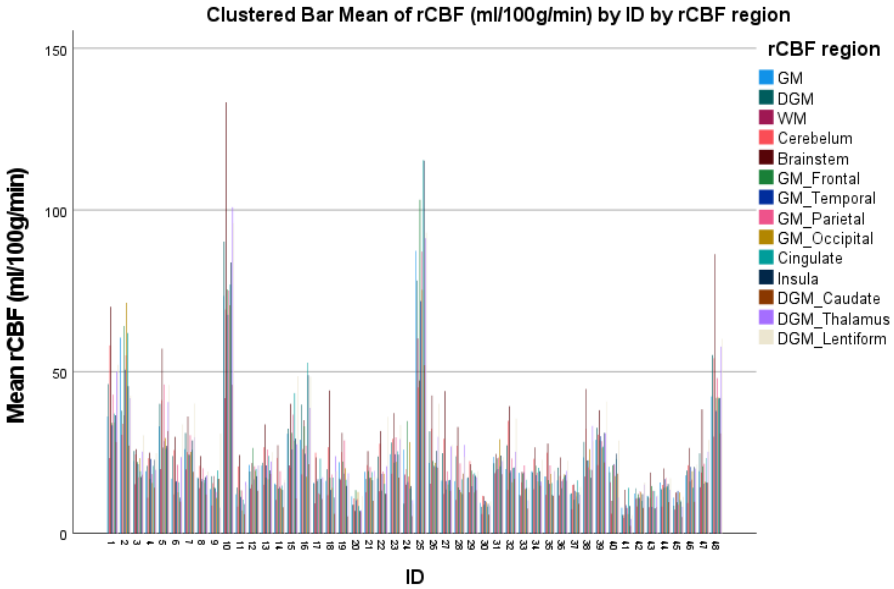

Figure 4-0-12: Summary of rCBF for each of the regions of interest for each of the infants in a different group at UCLH of 47 infants with NE *(unpublished data)***.**

There are several hypotheses for a low rCBF in those with a poor prognosis. It could be that some infants present with immediate cell death at the time of the hypoxia-ischaemia, which would be picked up on the MRI, but they lack the reperfusion excitotoxicity, whereas in others, the latter might play a larger role. Wintermark et al. (274) also found low perfusion in two infants with brain injury on MRI. Another explanation could be due to variable arterial transit time (time needed for labelling blood to travel from labelling plane to ROI) leading to underestimation of CBF values. Additionally, low blood flow velocities in the feeding arteries can reduce labelling efficiency (315), further underestimating CBF values. This will be discussed further in the case study of infant ID18.

4.4.3 Case studies: infants with high predictors of outcome

There were four infants with either a high thalamic LacT/tNAA or a high BGT pHi. *Table 4-0-7* shows a summary of other prognostic markers, including seizure burden in minutes, aEEG background classification (85) and evolution over the first 96 hours of life, MRI severity based on NICHD scoring system (291) and gestational age at scan; ^{31}P MRS prognostic markers (pHi, Pi/PCr as a marker of neuronal death, and ATP/Pi+PCr+ATP as a marker of brain oxidative metabolism and secondary energy failure (316)); ^{1}H MRS biomarker of outcome (LacT/tNAA (124)); and neurodevelopmental outcome using the Bayley-III scale at 2 years of age (294).

	rCBF	Sz burden	aEEG background	GA at scan	MRI Severity	pHi	Pi/PCr	ATP / (Pi+PCr+ATP)	LacT/NAA	Outcome Bayley-III
ID6	↑	538,72	Flat throughout	39.6 (D4)	Severe (2B)	7.21	3.33	0.68	3.07	Died
ID18	↓↓	82.91	Flat throughout	37.3 (D5)	Severe (3)	7.31	4.51	0.51	3.94	Lost-to-follow-up
ID21	↓	0	Flat, DNV by 12-24h age.	40.9 (D4)	Severe (2A)	7.23	1.26	0.72	0.3	Mild (Lang Comp 77, rest normal)
ID22	↓	130.55	Flat, DNV by 24-48h age.	42.6 (D7)	Normal (0)	7.04	0.41	0.76	0.45	Normal

Table 4-0-7: Descriptive details of prognostic markers for these 4 infants who showed any unfavourable prognostic marker. *rCBF: regional cerebral blood flow;* Sz burden: seizure burden; aEEG: integrated electroencephalogram; GA: gestational age; D; day of life at scan; MRI: MR imaging; Pi: inorganic phosphate; PCr: phosphocreatine; ATP: Adenosin triphosphate; LacT/tNAA: lactate+threonine/total N-acetyl-aspartate.

Infant ID6:

Looking in detail at the child who presented with significant brain hyperperfusion in most areas studied, interestingly, CBF in the insula, cingulate and frontal cortex reached values around 100ml/100g/min, which is well above the threshold of 50ml/100g/min postulated by De Vis et al (7). Also, the grey matter and parietal cortex, thalamus and lentiform nuclei reached values above 80ml/100g/min. This is consistent with the 'luxury perfusion' concept that occurs in infants with a poor outcome (80, 267) and to the pathophysiology of brain injury. All prognostic factors agreed in this case: flat aEEG background that never recovered, severe MRI changes (score 2B: see *figure 4-0-13*), high pHi with a high Pi/PCr and high LacT/tNAA. This infant died within the first week of life.

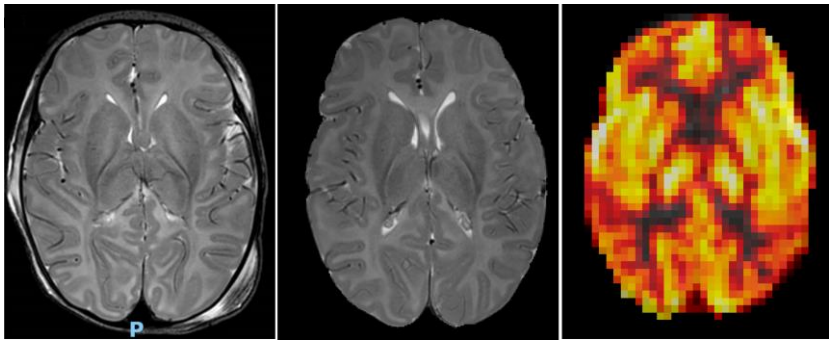

Figure 4-0-13: MRI and rCBF map from baby ID6. *T2 images*: NICHD scoring 2B and severe oedema**.** *rCBF map*: increase perfusion, especially in DGM and cortical areas.

Infant ID18

Interestingly, there is another baby with a poor prognosis (high LacT/tNAA) who presented with the lowest CBF values in all regions. The rest of the prognostic markers also agreed in this case: flat aEEG background that never recovered, severe MRI changes (score 3: see *figure 4-0-14*), high pHi, higher Pi/PCr and low energy metabolites ratio (suggestive of secondary energy failure) and high LacT/tNAA. Unfortunately, this child moved away, and no follow-up data was available.

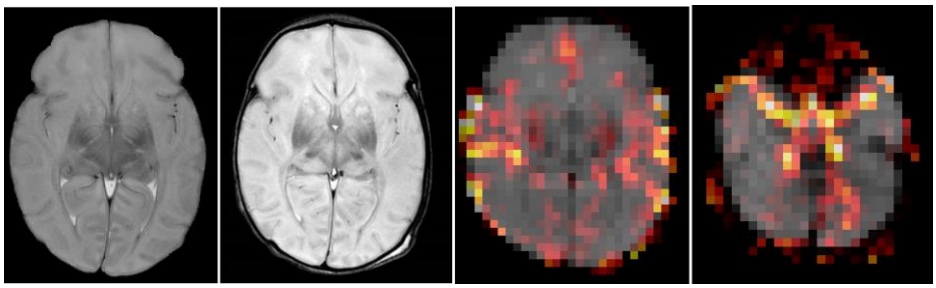

Figure 4-0-14: MRI and rCBF maps from infant ID18. *T2 MRI:* NICHD scoring 3, severe oedema and devastating brain lesions. *rCBF maps:* low brain perfusion with "labelled" blood in the large arteries of the circle of Willis.

When looking at the ASL images for this baby (*figure 4-0-15*), it looks like the "labelled" blood was still in the large brain arteries of the circle of Willis at the time of image acquisition (2sPLD), indicating much lower velocities and markedly prolonged arterial transit time (time it takes labelled blood to reach tissue parenchyma from labelling position in the neck). One potential explanation of this is severe cerebral oedema, putting pressure on vessel lumen or slowing velocity of the blood. *Figure 4-0-14* shows the lack of dark bands of vascular signal void compared with image from ID6 image (*figure 4-0-16*).

Infant ID21

This infant presented with a low LacT/tNAA, suggestive of a favourable outcome and a mild outcome at Bayley-III assessment at 2 years of age. Although he had an alkalotic brain pHi and an elevated Pi/PCr (less than previous two cases) and severe changes on the MRI, all the other predictors were reassuring: initial flat trace on the aEEG which normalised within 24h of age, higher energy metabolites ratio than the other two infants, no seizures, and low CBF.

Infant ID22

Equally, this neonate had a high LacT/tNAA, but all the other prognostic factors were reassuring: flat aEEG initially which normalised within 48 hours of life (84), normal MRI, low pHi with a low Pi peak (low Pi/PCr) and higher energy metabolite ratio than the others, and a low CBF (*figure 4-0-15)*.

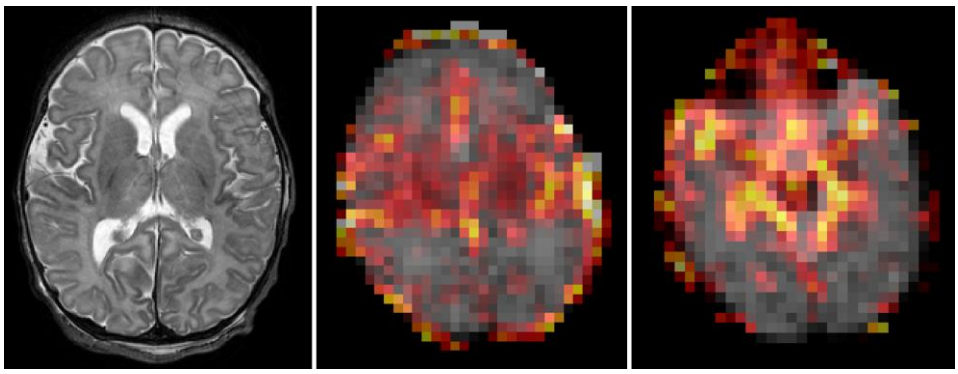

Figure 4-0-15: MRI and rCBF maps of infant ID22. *T2 MRI:* NICHD score 0. rCBF maps: lower perfusion.

In this respect, CBF can be a helpful tool used in combination with all the other predictors of outcome. When we are counselling families, we will try to narrow

prognostication options by means of using as many predictors available as possible from the clinical, imaging, and electroencephalographic data.

Future work

Despite this unconclusive study, it is likely that brain perfusion plays a role in rebound alkalosis and secondary energy failure. The infant with a high rCBF in most regions studied presented with an alkalotic DGM pHi within the first 2 weeks of life. However, the range of rCBF can be wide within the group of neonates with an alkalotic pHi. It would be interesting to analyse this further in a larger cohort. To overcome the limitation of having to perform 2 MR sequence, CBF could be measured using NIRS, and pHi using Phosphorus MRS.

The output from this chapter is being written for publication.

Chapter 5: Relationship between brain pHi during the insult and outcome in a preclinical model of hypoxia-ischaemia

Introduction

It is universally admitted that foetal or cord blood pH –measuring the acidity of the blood in the foetus around the time of delivery– is a marker of the severity of the insult: the greater the acidosis (pH<7.00) –especially if the acidosis is metabolic (base excess > 12) (317, 318) rather than hypercapnic– the greater the insult (220, 221). Acidosis is not only present in the circulation but also intracellular acidosis has been described in the piglet model of hypoxia-ischaemia (HI) using phosphorus (^{31}P) MRS (319). The degree of acidosis was proportional to the rise in intracerebral lactate due to anaerobic glycolysis. An acidotic status in the brain in the acute phase has been postulated as a mediator of injury –directly injuring neurons and glia, or disrupting cellular function by interrupting mitochondrial function (10, 12, 198, 320)–. The degree of brain injury has been associated with the duration of acidosis after asphyxia (321), but not with its severity. Other studies in vitro, using mixed neuronal and glial cell cultures, described that cell death only occurred when exposed to lactic acidosis (pH 5.2) for 1 hour (320) –more severe and prolonged than we would consider compatible with neonatal survival. The effects of reperfusion on brain pHi have been studied using animal models, showing a rapid return of brain pHi to normal following reperfusion (322), and this rapid normalisation occurred substantially

earlier than normalisation of primary energetic compounds; although time required to compensate appeared to relate to insult severity (323).

Other studies (3, 57), showed that it was not only the severity and extent of acidosis during the insult that caused damage, but also a later alkaline shift in brain intracellular pH (pHi) –despite presenting with a stable blood pH–. It is likely that post-asphyxia brain alkalosis plays an important role in cell death, as described in previous chapters. In the piglet model of HI, rebound alkalosis was not found occurring as described in human neonates or rodent models. Furthermore, the degree of acidosis may predict the magnitude and duration of alkalosis –determinant of outcome.

The **aim of this study** is to understand the physiological pH changes occurring during the insult in a piglet model of HI. The hypothesis is that piglets with a more severe injury (lower NTP/ exchangeable phosphate pool [epp] and higher Pi/PCr peak ratio at one hour after the insult) (i) would have lower brain pHi values, (ii) would remain for a longer period of time under a certain deleterious pHi threshold, and (iii) would take longer, or would fail altogether, to recover their baseline brain pHi in the following minutes after resuscitation. The correlation between blood pH and brain pHi both at baseline and at the nadir of the insult will also be analysed.

Subjects and Methods

5.2.1 Animal experiments, surgical preparation, and cerebral HI

All animal experiments were approved by the Ethics Committee of University College London (UCL) and performed according to the UK Home Office Guidelines [Animals (Scientific procedures) Act, 1986]. The study complies with ARRIVE guidelines. Twenty nine piglets, aged less than 48h, with mean (±standard deviation [SD]; range) weight 1.94kg (±0.13; 1.6 - 2.1) were anaesthetized and surgically prepared as described previously (324). Subjects showing signs of infections or with an abnormally high lactate on baseline bloods were excluded from the study. Piglets were sedated with intramuscular midazolam (0.2 mg/kg), and arterial O2 saturation was monitored (Nonin Medical, Plymouth, MN, USA). Anaesthesia was induced by Isoflurane (4% v/v) initially given through a face mask to facilitate tracheostomy and intubation and was maintained (3% during surgery and 2% otherwise), guided by peripheral oxygen saturation monitoring and the animal's response to stimulation.

Piglets were mechanically ventilated (SLE 2000 infant ventilator, Surrey, UK); ventilator settings were adjusted to maintain partial pressure of oxygen (PaO_2) and carbon dioxide ($PaCO_2$) at 8–13 kPa and 4.5–6.5 kPa, respectively, allowing for temperature correction of the arterial blood sample. An umbilical venous catheter was inserted for infusion of maintenance fluids (10% dextrose, 60 ml/kg/day), fentanyl (3–6 mg/kg/h) and antibiotics (benzylpenicillin 50 mg/kg and gentamicin 2.5 mg/kg, every 12 h). An umbilical arterial catheter was

inserted for continuous monitoring of heart rate and arterial blood pressure, and intermittent blood sampling was used to measure PaO_2, $PaCO_2$, pH, electrolytes, glucose, and lactate (Abbot Laboratories). Mean arterial blood pressure was maintained >40 mmHg, and bolus infusions of colloid (Gelofusin, B Braun Medical Ltd.) and inotropes administered if required. All animals received continuous physiological monitoring (SA instruments) and intensive life support throughout experimentation. Arterial lines were maintained by infusing 0.9% saline solution (Baxter; 1 ml/h); heparin sodium was added at a concentration of 1 IU/ml to prevent line blockage.

Both common carotid arteries were surgically isolated at the level of the fourth cervical vertebra and encircled by remotely controlled vascular occluders (OC2A, In Vivo Metric). After surgery, piglets were positioned prone in a plastic pod, and the head immobilized securely in a stereotactic frame.

Two MRI surface coils were secured to the head, and the animal was positioned into the bore of a 9.4-T Varian spectrometer for serial ^{1}H and ^{31}P MRS data acquisition. Transient hypoxia–ischaemia was induced by remote occlusion of both common carotid arteries, whilst in the MRS system, using inflatable vascular occluders; and the fractional inspired oxygen (FiO_2) was reduced to 12%. All piglets are monitored with phosphorus spectroscopy (^{31}P MRS) every 2 min, at baseline, during HI and for one-hour post-resuscitation. Cerebral energetic changes were observed and beta-nucleotide triphosphate (β -NTP; mainly ATP) peak height was continuously monitored. Similar severity of insult was performed in all subjects, standardising the β-NTP peak height fall using ^{31}P MRS.

Once the β-NTP peak height had fallen to 40% of baseline, FiO_2 was titrated to maintain it at that value for 12.5 min (325, 326). At the end of this 12.5-min period, the occluders were deflated and FiO_2 was normalized.

5.2.2 MR Methods

MRS acquisition was performed in a 9.4 Tesla Agilent® MR scanner.

^{1}H MRS was acquired at baseline, 24 and 48h after cerebral HI, from voxels located in the dorsal right white matter and in both lateral thalami (TR/TE = 5000/288ms, 128 averages). ^{1}H MRS data weren't used in this analysis because following the first hour, subjects received different interventions: control group (N=7), therapeutic hypothermia from 2h post-HI for 24h (N=10), argon 50% plus cooling, both from 2h after the insult for 24h (N=10), dexmedetomidine given at 1h post-insult (N=1) and melatonin given at 2h after the insult followed by repeated doses (N=1).

^{31}P MRS was acquired at baseline and then continuously from the beginning of the insult and for 60 minutes post-resuscitation (80-101 min; mean ± SD: 85 ± 4.74). A 7 x 5 cm elliptical transmit-receive MRS surface-coil tuned to the ^{31}P resonant frequency (162 MHz) was positioned on top of the head. ^{31}P MRS was acquired with 1 minute resolution using a non-localised single-pulse surface-coil acquisition (TR 10s, 6 summed acquisitions per spectrum). MRS data were manually corrected for phase and frequency shifts and fitted using AMARES (327) within jMRUI software (280). Prior knowledge of NTP multiplet structure was

used (fitting doublets to α- and γ-NTP and a triplet to β-NTP) but no assumption was made as to multiplet relative sizes. NTP is predominantly ATP, contributing approximately 70% of the NTP signal (328). Pi was fitted using 4 separate components and PCr with a single component. The following peak-area ratios were calculated: Pi/epp, PCr/epp, and NTP/epp where epp (exchangeable phosphate pool) = total Pi + PCr + 2*(γ-NTP) + β-NTP. NTP/epp during hypoxia–ischaemia and the first 60 min of resuscitation gave the magnitude of acute energy depletion, as described in previous studies (329).

As mentioned in *Chapter 1*, measurement of intracellular (pHi) is derived from peak positions, using the Henderson-Hasselbalch equation –where δ is the chemical shift of Pi relative to PCr –:

$$pHi\ (Hamilton) = 6.77 + \log_{10}[(\delta - 3.29) / (5.68 - \delta)]\ (135) \quad \textbf{Equation 1}$$

$$pHi\ (Robertson) = 6.75 + \log_{10}[(\delta - 3.27) / (5.69 - \delta)]\ (3) \quad \textbf{Equation 2}$$

$$pHi\ (Corbett) = 6.683 + \log_{10}[(\delta - 3.153) / (5.728 - \delta)]\ (330) \quad \textbf{Equation 6}$$

During the nadir of the insult there was a dramatic drop of high energy metabolites, such as NTP and PCr. Calculation of pHi relies on an accurate detection of both Pi and PCr chemical shifts, leading to a certain degree of inaccuracy. Hence the challenge to accurately fit PCr peak at nadir (low amplitude), risking a less accurate pHi calculation. Examples of this are in figure *5-0-1*, where there are three pHi curves pre-, intra- and post-insult for three different subjects. An increased dispersion in the pHi curve can be noticed when reaching the nadir (lowest PCr peak and least reliable fitting). Therefore, PCr chemical shift for those PCr peaks where the amplitude was below 25% of their

baseline amplitude for each subject was estimated following a predictive polynomial trace, estimated from the rest of the PCr chemical shifts from prior and after nadir (with higher amplitudes) for each subject. Once the PCr frequencies were estimated for those with peak amplitude below 25% of their baseline, chemical shift and pHi can be calculated using the 'thresholded' values of PCr chemical shift. In *figure 5-0-2*, there are the new pHi curves for the same 3 subjects, but using the thresholded PCr chemical shift, and hence smoother curve at nadir for pHi.

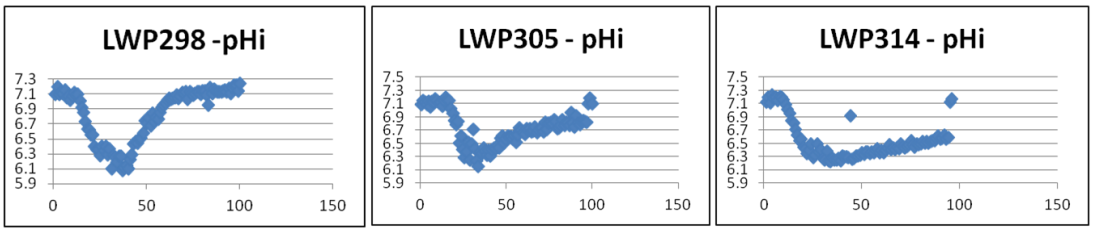

Figure 5-0-1: Examples of pHi curve pre-, intra-, and post-HI insult in three different subjects. x axis represents time in minutes.

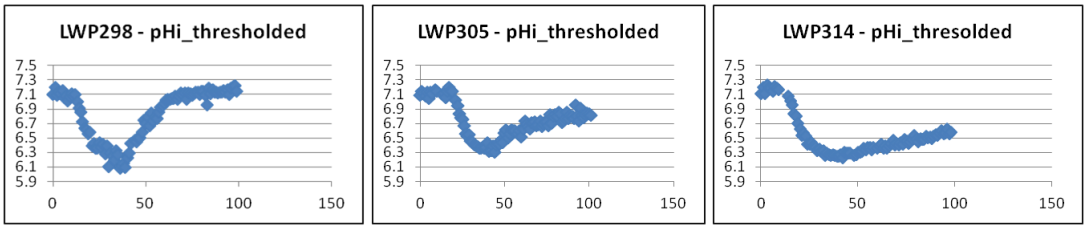

Figure 5-0-2: Examples of pHi curve in the same three piglets as above, but thresholding PCr amplitude to smooth the nadir pHi calculations. (x axis, time in minutes)

Mean baseline or initial pHi was calculated from pHi during the minutes prior to the insult. Mean titration pHi was calculated from pHi for 12.5 minutes when NTP/epp ratio remained between 30-40% of baseline levels.

NTP/epp (marker of brain energy failure) and Pi/PCr (marker of neuronal death) at 1 hour post-resuscitation were used as predictors of outcome, as described previously (329, 331, 332).

Area under the curve (AUC) for pHi plotted against time was calculated from the beginning of the insult for (i) 60 minutes, and (ii) until the end of the scanning time. Calculation of AUC was performed using the trapezoid rule (*figure 5-0-3*).

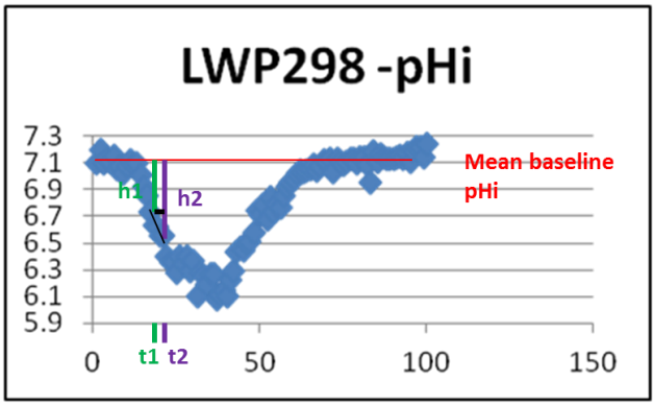

Figure 5-0-3: Calculation of area under the curve (AUC). h1= (baseline pHi)-(pHi at t1); h2= (baseline pHi)-(pHi at t2). AUC t2-t1= [h1*(t2-t1)] + [(h2-h1)*(t2-t1)/2]. Total AUC is the addition of this area for each time point.

Then the AUC for pHi was normalised dividing by the duration of the experiment for which the AUC was calculated for each subject. This reflects the actual brain exposure to pHi following a HI insult. This area under the curve is dependent on the rate at which pHi becomes acidotic and the rate of normalisation of this pHi. In a controlled insult, such as this one, the rate of pHi becoming acidotic was similar between subjects; hence the AUC depends mainly on the rate of normalisation –if normalisation occurs– of brain pHi following the insult.

The duration of each subject's brain pHi below a certain threshold –cut-off points selected were 6.3, 6.5 and 6.7, due to clinical significance– was also calculated.

5.2.3 Statistical Methods

Analyses were performed using the SAS JMP® v12.0.0 software for correlation graphs, and IBM SPSS® Statistics 22.0. Pearson correlations were calculated for

quantitative variables. Comparison of means using t-Student test for paired samples was applied when comparing brain pHi values calculated using the different equations; comparing blood and brain pH, and blood $paCO_2$, base excess and lactate with brain pHi; and comparing minimum brain pHi value reached during titration by each subject and energy metabolite ratios at one hour after resuscitation. Comparison of means between two groups – classified by AUC level or a cut-off point of time spent below a certain pHi value – was performed using t-Student test for independent samples. U-Mann Whitney was used to compare medians for 2 groups, if the groups were too small for a parametric test. Statistical significance was considered when p value was <0.05 (95% confidence intervals [C.I.]).

Results

5.3.1 Assessing the different pHi calculations: different equations and validation of thresholded PCr amplitude calculations

There was a strong correlation between brain pHi calculated using the three different equations mentioned ($r=1$, $p<0.001$), as expected. The difference in pHi mean values was less than 0.1 points when using the different equations to calculate brain pHi.

There was also a strong correlation between titration pHi calculations using the raw PCr chemical shifts, calculated by AMARES, and those using the estimated PCr values when PCr amplitude was thresholded at 25% of its baseline amplitude

to calculate more accurately PCr chemical shifts (r= 0.78, 0.78 and 0.77, for equation 1, 2 and 6, respectively, $p<0.05$ for all three). The differences between titration pHi mean values were less than 0.07 points when using the raw calculation or the "thresholded" one.

All other values inferred from these calculations –such as AUC for pHi and time below a certain pHi threshold– did also correlate strongly with those using the raw data. *Table 5-0-1* summarises brain pHi results at baseline and titration, both using the raw data and applying the threshold for PCr amplitude.

Equation 1 (Hamilton) was used for pHi calculations.

There was no correlation, as expected, between initial and titration pHi (p=0.68).

	Raw data	Thresholded PCr at 25% baseline PCr amplitude
Initial – baseline pHi		
Initial pHi (Hamilton)	7.09 ± 0.43 (7.02 – 7.17)	
Initial pHi (Robertson)	7.07 ± 0.43 (7.00 – 7.15)	
Initial pHi (Corbett)	7.01 ± 0.40 (6.94 – 7.09)	
Titration pHi		
Titration pHi (Hamilton)	6.28 ± 0.13 (6.05 – 6.58)	6.34 ±0.13 (6.07 – 6.64)
Titration pHi (Robertson)	6.27 ± 0.13 (6.05 – 6.57)	6.33 ± 0.13 (6.07 – 6.62)
Titration pHi (Corbett)	6.28 ± 0.11 (6.09 – 6.54)	6.33 ± 0.11 (6.10 – 6.59)

Table 5-0-1: Summary of brain pHi calculated with equation 1, 2 and 6, at baseline and at titration (N=29). Left column shows the calculation using the raw data for PCr chemical shift and the right column shows the values once the chemical shift has been calculated with a threshold according to PCr amplitude (25% of the baseline amplitude). This method does not affect, by definition, the calculation of baseline pHi.

5.3.2 Relation between blood pH and brain pHi

Twenty eight of 29 had blood samples taken at baseline and twenty-four at nadir (summary shown in *table 5-0-2*).

The only significant association found was between nadir blood lactate level and Pi/PCr at 1h (r=0.53, p=0.009).

There was no relationship, as expected between bloods pre-insult and those at nadir. Importantly, there was no correlation between blood pH and brain pHi, neither initially (p=0.97) nor at nadir (p=0.20). There was a significant difference between titration brain pHi and both $paCO_2$ (r=-0.53, p=0.008) and blood lactate (r=-0.47, p=0.02) at nadir.

Blood pH, initial and at nadir, don't show a significant association with injury severity –determined by Pi/PCr at 1h post-resuscitation–, in this cohort.

Bloods	Before insult (N=28)	Nadir (N=24)
pH	7.44 ± 0.10	7.34 ± 0.11
pCO2	5.77 ± 1.30	5.17 ± 1.11
pO2	15.33 ± 12.44	6.39 ± 2.82
BE	5.04 ± 4.58	-4.58 ± 4.24
Bicarbonate	28.31 ± 5.06	20.78 ± 3.09
Lactate	2.60 ± 0.71	8.78 ± 2.18

Table 5-0-2: Summary of blood gases before the insult and at nadir. Mean ± SD

5.3.3 Correlation between mean titration brain pHi and energy metabolite ratios at 1h after the insult

There was an association between mean titration acidosis during HI and NTP/epp at 1h after HI, and with Pi/PCr (*figure 5-0-4)*. These relations were not statistically significant.

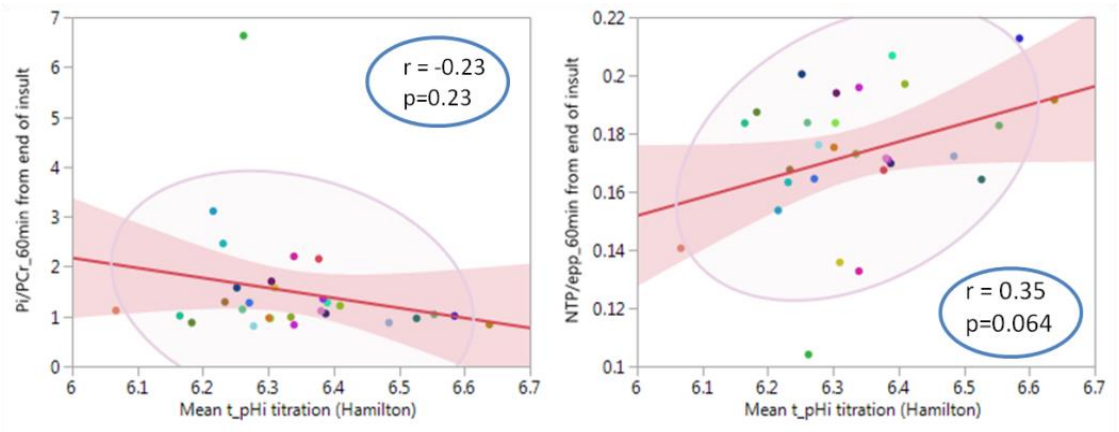

Figure 5-0-4: Correlation between titration pHi and energy metabolites ratios at 1h: (Left) with Pi/PCr and (Right) with NTP/epp at 1h

5.3.4 Relationship between minimum brain pHi and energy metabolite ratios at 1h

There was a significant association between the lowest brain pHi reached during titration and Pi/PCr at 1h post-insult, and with NTP/epp (*figure 5-0-5)*.

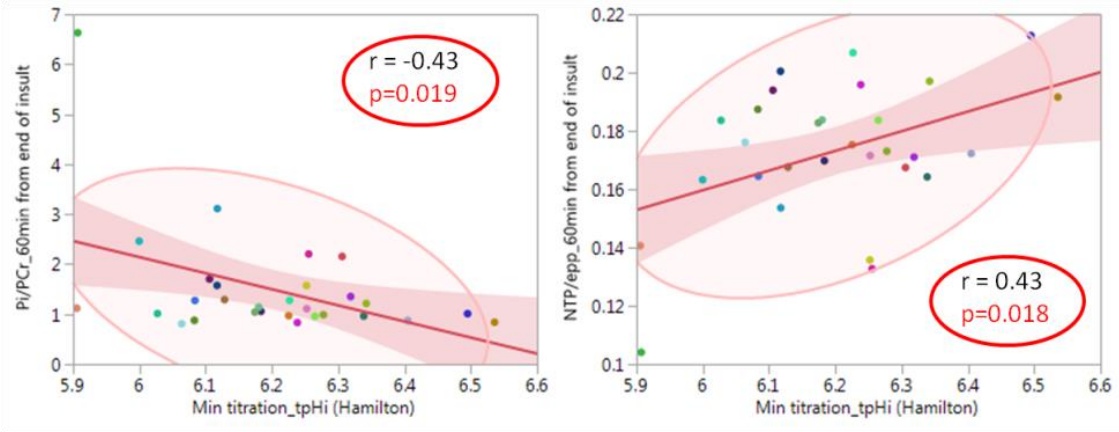

Figure 5-0-5: Correlation between minimum brain pHi reached and severity of injury measured by energy metabolite ratios: (Left) with Pi/PCr, and (Right) with NTP/epp at 1h

5.3.5 Correlation between time under pHi thresholds (6.7, 6.5 and 6.3) and energy metabolite ratios at 1h

A. Threshold of brain pHi at 6.7

There was positive correlation between duration of brain pHi below 6.7 and the degree of brain injury, measured by Pi/PCr and NTP/epp at 1h post-resuscitation (*figure 5-0-6*). Moreover, analysing the graph showing the correlation between Pi/PCr and the duration of brain pHi < 6.7, Pi/PCr does not follow a linear association. The association remains static until around 50 minutes, increasing from around 60 min.

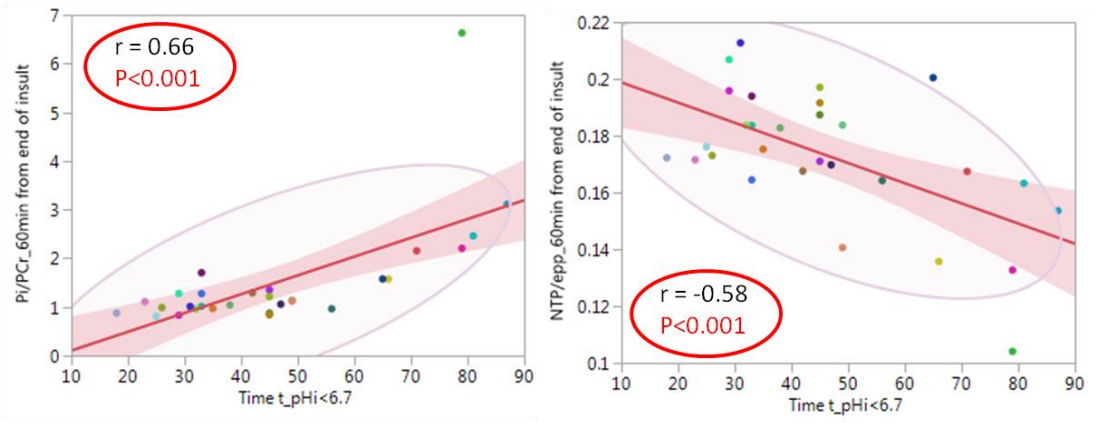

Figure 5-0-6: Correlation between time spent with a brain pHi below 6.7 and energy metabolite ratios: (Left) with Pi/PCr, and (Right) with NTP/epp at 1h

Comparing mean energy metabolite ratios at 1h post-resuscitation and depending on whether they spent *under* or *over an hour* with a brain pHi<6.7 (n=22 and n=7 respectively) there was a significant difference in median Pi/PCr (p=0.002), PCr/epp (p=0.006) and Pi/epp (p=0.002), but not significant for

NTP/epp (p=0.08). When comparing means for energy metabolite ratios between these two groups, differences were significant for all of them (*figure 5-0-7*).

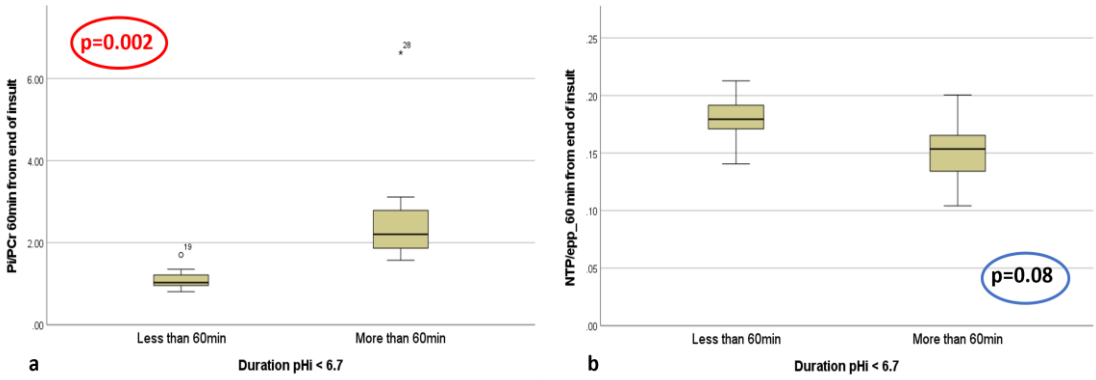

Figure 5-0-7: Boxplot for time spent below a brain pHi of 6.7, using a cut-off of 60 min and energy metabolite ratios. a: Pi/PCr; b: NTP/epp (median and quartiles)

B. Threshold of brain pHi at 6.5

Using a cut-off point for brain pHi of 6.5, there was positive correlation between duration of brain pHi below that level and the degree of brain injury, measured by Pi/PCr and NTP/epp at 1h post-resuscitation (*figure 5-0-8*). Similarly, to what occurs using the threshold of 6.7, analysing the graph showing the correlation between Pi/PCr and time spent under a brain pHi of 6.5, Pi/PCr remains static until around 40 minutes, increasing from around 45min.

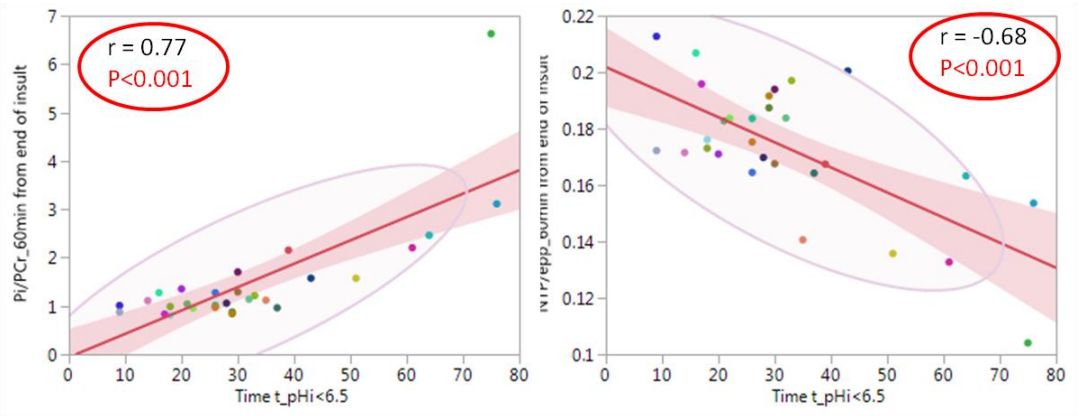

Figure 5-0-8: Correlation between time spent with a brain pHi below 6.5 and energy metabolite ratios: (Left) with Pi/PCr at 1h and (Right) with NTP/epp at 1h

Comparing median energy metabolite ratios at 1h after HI and depending on whether they spent *under* or *over 45min* with a brain pHi < 6.5 (n=24 and n=5 respectively) there was a significant difference in median Pi/PCr (p=0.017), NTP/epp (p=0.042), Pi/epp (p=0.017) and PCr/epp (p=0.042) *(figure 5-0-9.a,c)*.

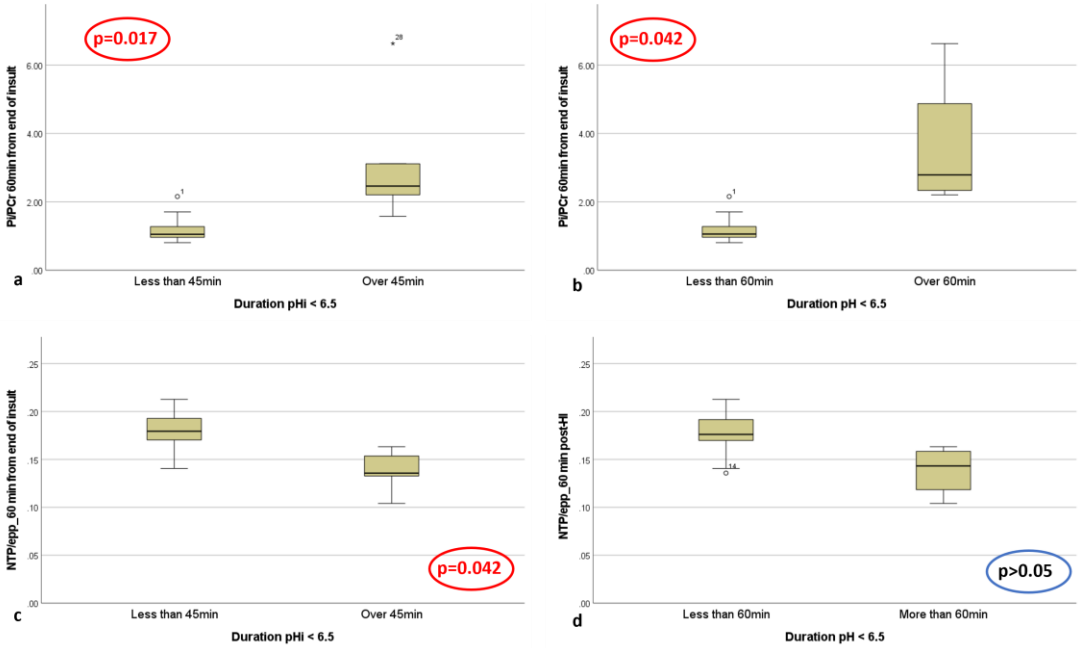

Figure 5-0-9: Boxplot for time spent below a brain pHi of 6.5, using a cut-off of 45 min (a,c) and 1h (b,d) and energy metabolite ratios. a and b: Pi/PCr median and quartiles; c and d: NTP/epp median and quartiles.

When performing the same analysis for those who spent *under or over 1 hour* with a brain pHi < 6.5 (n=25 and n=4 respectively) there was a significant difference in median Pi/PCr (p=0.042) and Pi/epp (p=0.042), but not for NTP/epp (p>0.05) (*figure 5-0-9.c,d*).

C. Threshold of brain pHi at 6.3

Finally, using a cut-off of 6.3, there was a positive correlation between duration of brain pHi below 6.3 and the degree of brain injury, measured by Pi/PCr and NTP/epp at 1h post-resuscitation (*figure 5-0-10*).

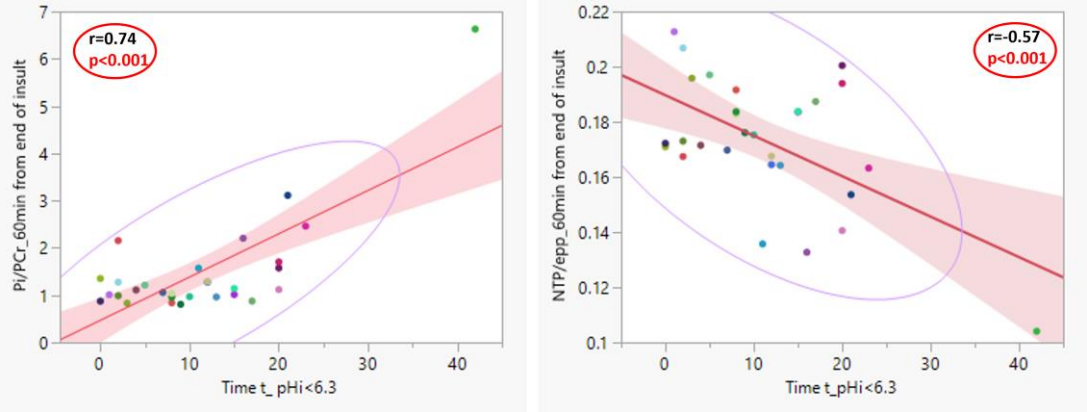

Figure 5-0-10: Correlation between time spent with a brain pHi below 6.3 and energy metabolite ratios: (Left) with Pi/PCr at 1h and (Right) with NTP/epp at 1h

Comparing median energy metabolite ratios at 1h after HI and depending on whether they spent *under* or *over 20 min* with a brain pHi < 6.3 (n=26 and n=3 respectively) there were no significant differences between medians for Pi/PCr (p=0.1), NTP/epp (p=0.2), Pi/epp (p=0.2) and PCr/epp (p=0.1) *(figure 5-0-11)*.

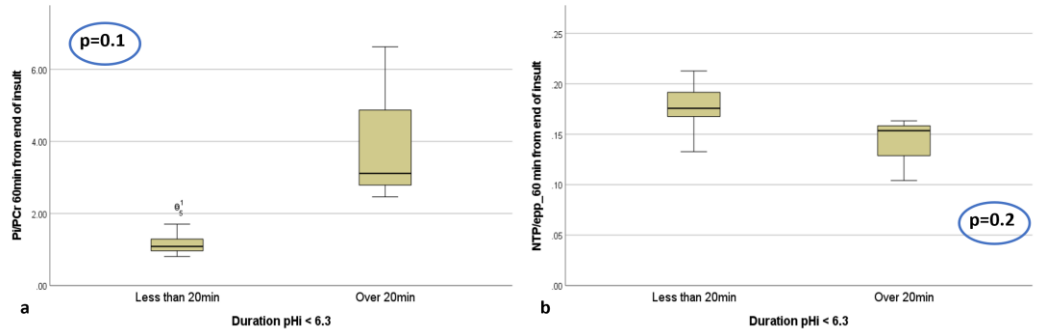

Figure 5-0-11: Boxplot for time spent below a brain pHi of 6.3, using a cut-off of 20 min and energy metabolite ratios. a: Pi/PCr median and quartiles; c: NTP/epp median and quartiles.

5.3.6 Correlation between AUC for brain pHi and Pi/PCr at one hour

There was a correlation between AUC normalised during the first hour and the severity of brain injury, measured by means of Pi/PCr and NTP/epp at 1h post-resuscitation (*figure 5-0-12.a,b*), and between AUC normalised for all the

experiment and brain injury (*figure 5-0-12.c,d*). The longer it takes to recover – if at all – a normal brain pHi, the higher Pi/PCr ratio will be, and the lower the levels of energy metabolites (NTP/epp).

Similarly, to the subgroups created for duration under a certain brain pHi value, when analysing the correlation between AUC for brain pHi for the first hour of the experiment, Pi/PCr ratio remains relatively stable until 0.6-0.7.

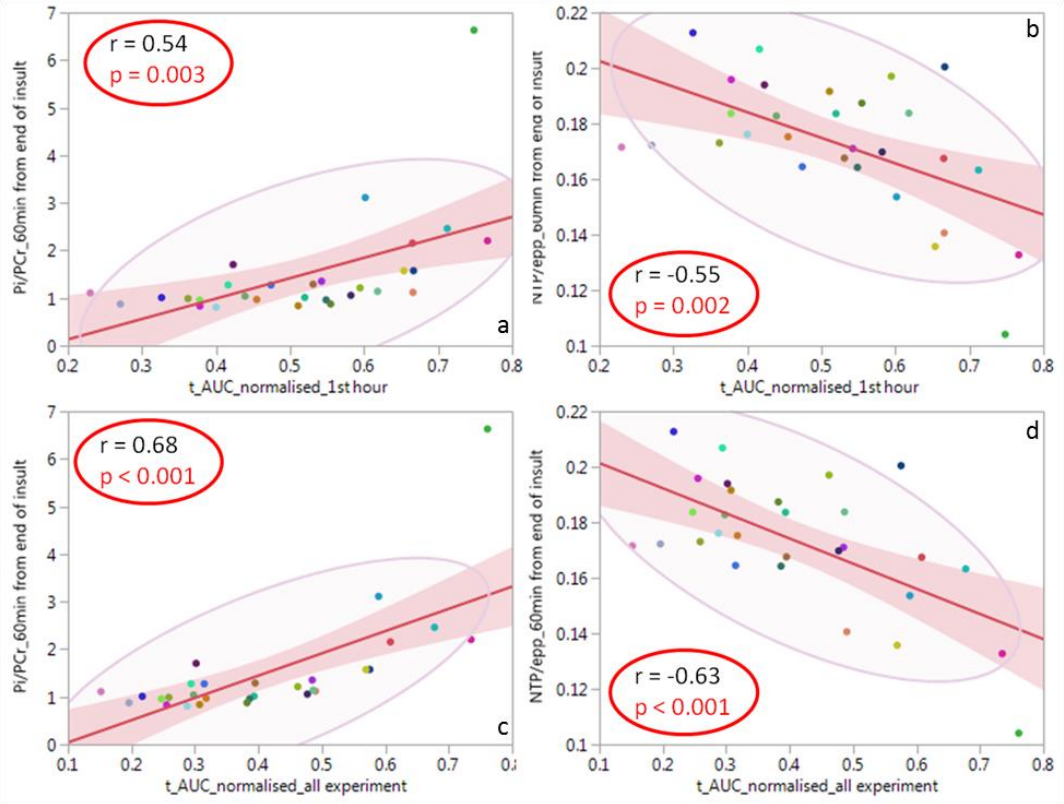

Figure 5-0-12: Correlation between AUC for pHi and energy metabolite ratios. a and **b**: AUC normalised for the first hour from the beginning of the experiment showing relationship against **(a)** Pi/PCr, and **(b)** NTP/epp. **c** and **d**: AUC normalised for the duration of the whole experiment following the insult (maximum 101min), association with **(c)** Pi/PCr, and **(d)** NTP/epp.

Therefore, when comparing between those with an *AUC normalised above and below 0.*6 (n=8 and n=20 respectively), there were significant differences for medians of Pi/PCr (p=0.002) and PCr/epp (p=0.033), but not for NTP/epp (p=0.21) (*figure 5-0-13.a,b*). Using cut-off of 0.55 for the AUC normalised for the

first hour after the insult for pHi, there was a significant difference in Pi/PCr means (p=0.04) between subjects with an AUC<0.55 (N=17) and those >0.55 (N=11); and, for NTP/epp (p=0.03). Although comparing medians, the difference was only statistically significant for Pi/PCr (p=0.02) and PCr/epp (p=0.02) (*figure 5-0-13.c,d*).

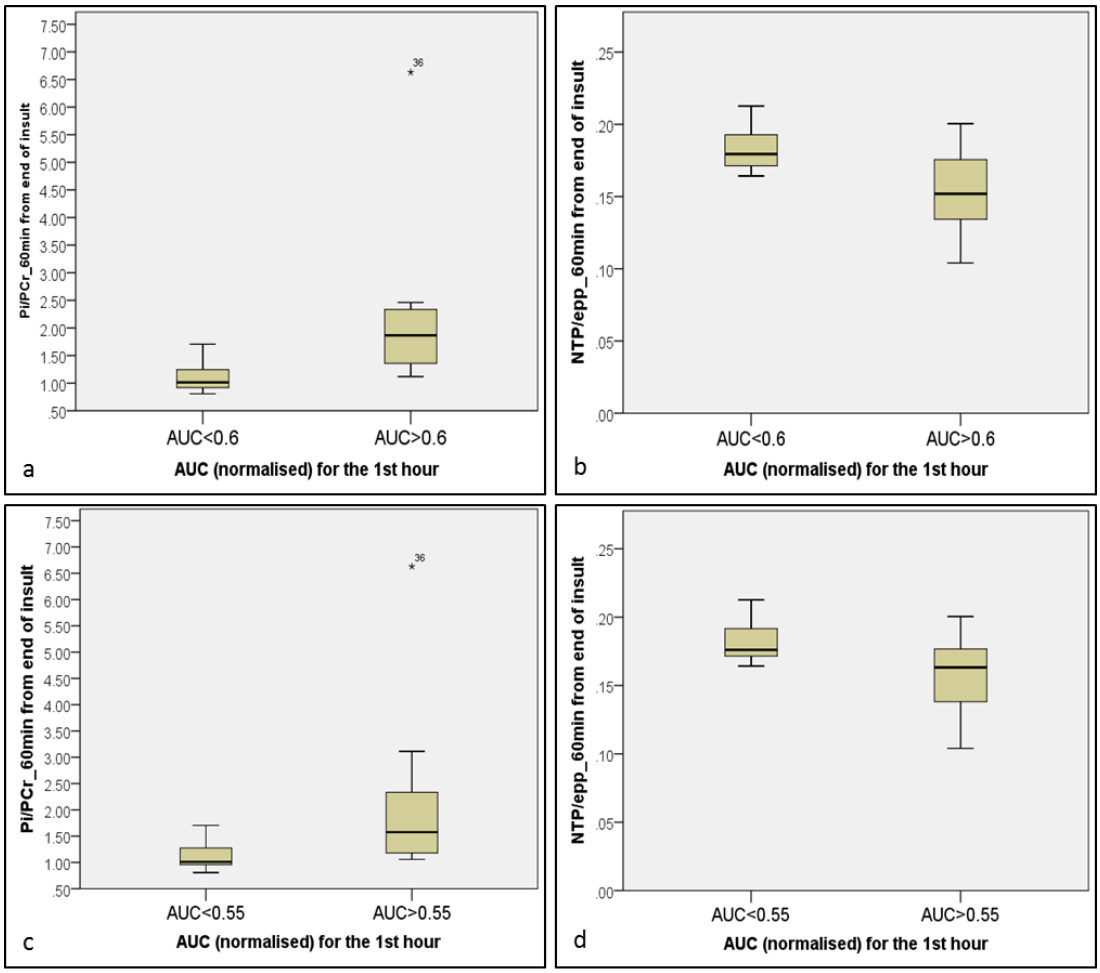

Figure 5-0-13: Boxplot for energy metabolite ratios according to two groups depending on a cut-off point for the AUC. Median and quartiles for **(a,c)** Pi/PCr and **(b,d)** NTP/epp, using a cut-off point for AUC normalised value of **(a,b)** 0.6 and **(c,d)** 0.55**.**

Discussion

The **strength** of this study is that piglet brain pHi is calculated continuously using ^{31}P MRS from the beginning of the insult until at least 1h post-resuscitation. This allows a better understanding of brain pHi evolution during HI in a preclinical model of perinatal asphyxia and its effects on cell death and energy metabolism, during the acute phase following HI. However, the **limitation** of this study is the use of Pi/PCr as a surrogate of outcome (cell death), rather than the histopathology. This was because subjects underwent different treatments afterwards (neuroprotective strategies) and that would affect results at a later point in time.

5.4.1 Relationship between blood pH and brain pHi

In this cohort of newborn piglets, there is no correlation between blood pH and brain pHi at any point of the experiment. During the titration period, this could be explained because of the nature of the insult, causing HI selectively to the brain (carotid arteries occlusion plus hypoxia), hence acidosis in the brain is likely to be more pronounced. However, this wouldn't explain the dissociation found between baseline blood pH and brain pHi.

The minimum brain pHi value found during titration in this cohort of piglets is 5.91 and minimum average brain pHi was 6.07; well below minimum blood pH values compatible with survival in newborn infants.

However, blood lactate at nadir is found to correlate well in this cohort with Pi/PCr at 1h after resuscitation; hence, lactate at nadir is a useful marker of severity of the insult during the experiments.

5.4.2 Brain pHi and energy metabolite ratios

The fact that mean pHi during titration does not show a statistically significant correlation with Pi/PCr nor with NTP/epp at 1h supports the idea that acidosis toxicity mechanisms are not just directly associated but other factors must be involved.

Interestingly, these data support that the degree of maximum acidosis (minimum pHi value reached at nadir), the length of severe acidosis (e.g. over 45min below a pHi value of 6.5) and the pattern of brain pHi buffering ability (e.g. slower rate of pHi normalisation, measured by a larger AUC) correlate well with the degree of cell death – inferred from Pi/PCr at 1h (332).

Besides, these data suggest there might be an in-vivo threshold for brain pHi under which there is a significant increase of brain injury. The correlation between duration of pHi under the threshold and brain injury is stronger when selecting a lower brain pHi threshold (r= 0.74 and 0.77 vs 0.66, for pHi threshold of 6.3 and 6.5 vs 6.7 when correlating with Pi/PCr, and r= -0.68 vs -0.58, for 6.5 and 6.7 respectively when correlating with NTP/epp). Furthermore, the duration under these thresholds seems a determinant of injury severity, with a cut-off of 45min for a pHi<6.5 showing significant differences between energy metabolite ratios at 1h. This suggests that the severity of acidosis (threshold value selected)

and the length of time spent under that specific value will be inversely correlated, suggesting that brain cells tolerate a milder degree of acidosis for a longer period before causing energy failure.

This study brings further knowledge to brain pHi evolution during HI and the association of specific factors with the severity of brain oxidative metabolism disruption. Few studies have addressed this issue with such a continuous non-invasive monitoring of brain pHi intra-insult.

Chapter 6: Conclusions

The motivation of this PhD was to improve the understanding of the role of brain intracellular pH (pHi) in the therapeutic hypothermia era, to point towards new neuroprotective therapy targets.

1 Summary of background

In Chapter 1, we gained understanding on the pathophysiology of neonatal encephalopathy following hypoxia-ischaemia, the neurotoxic cascade, cerebral energy metabolism and brain pHi changes. A systematic literature review on the role of sodium proton exchanger (NHE) in hypoxia-ischaemia is presented and the evidence both in vivo and in vitro of NHE inhibitors as potential neuroprotective agents. A study, in the pre-cooling era, showed an association between brain alkalosis and poor prognosis (3), but no studies had been done since in newborn infants. Moreover, the Helsinki group (5), had described an association, in their rodent model of asphyxia, between alkalosis and seizures. They described how seizures could be suppressed by avoiding the rebound alkalosis, either by graded restoration of normocapnia (adding a percentage of CO_2) or by administering N-methyl-isobutyl-amiloride (NHE inhibitor); and outcomes were improved too. In addition, there is an increasing body of evidence supporting that in infants with moderate to severe neonatal encephalopathy who underwent cooling, the time spent in hypocapnia is an independent predictor of brain injury on MRI (239). Hence the recommendation

to minimise exposure to hypocapnia and hyperoxia, and to avoid the use of alkaline buffers (236). The HENRIC trial (242) has shown in ten infants undergoing therapeutic hypothermia that inhaling 5% CO_2 within the first 6h of life and for a maximum of 12h, was a feasible and safe intervention for correcting hypocapnia. This could also have implications for treating seizures in this group of infants.

The pathophysiology of cerebral blood flow was also reviewed. There were few studies describing the association between hyperperfusion to the basal ganglia and thalami measured with arterial spin labelling (ASL) in infants with neonatal encephalopathy following hypoxia-ischaemia. There was very little evidence of the relationship between brain alkalosis following hypoxia-ischaemia and hyperperfusion.

2 Study set-up and Phosphorus MRS

In Chapter 2, we reviewed the steps undertaken in order to set up the clinical study called the Baby Brain Study. The Study Protocol, Parents' Information Leaflets, Parents' Consent Form were written. Ethical approval successfully obtained and NHS approval too.

A new purpose made birdcage neonatal Phosphorus coil was ordered-to-measure to fit into the neonatal MR compatible incubator. The Standard Operation Procedures on how to safely use the coil within the incubator, how to

safely switch between the proton and phosphorus coil, and other safety concerns were written.

The aim was to perform localised deep grey matter phosphorus spectroscopy, to analyse energy metabolite ratios and to calculate localised DGM intracellular pH (pHi), using the Henderson-Hasselbalch equation, using the chemical shift of pH-sensitive metabolites (Pi to PCr). The sequence was developed with the support from Medical Physics. During the initial experiments, some limitations were overcome along the way (optimising the infant's gentle head fixation during the MR scanning time, optimising low SNR, avoiding interferences from equipment, accurate fitting of the Spectra and deciding on the best 'Prior knowledge' to use for data analysis with the algorithm AMARES within jMRUI).

3 Key points from the main study: localised pHi, outcome and seizure burden

The aim of the first study (*Chapter 3*) was to analyse localised deep grey matter (DGM) pHi using phosphorus-31 spectroscopy, obtained within the first two weeks of life in 43 newborn infants with neonatal encephalopathy who underwent cooling.

The **most novel finding** from this study was the association observed between an alkaline DGM pHi on day 3 – 8 of life and seizure burden. This is the first time described in infants. Based on previous pre-clinical research, this leads to two new potential neuroprotective therapies aiming to avoid the rebound alkalosis:

NHE inhibitors and carbon dioxide inhalation to achieve normocapnia in a graded manner.

Previous research in a rodent model showed that both seizure burden and outcome improved when this rebound alkalosis was avoided (e.g., graded restoration of normocapnia or blocking the Na^+/H^+ exchangers). Clinical observational studies also support the independent deleterious effect of hypocarbia in infants with moderate - severe encephalopathy.

In this study, localised alkalosis was still a good marker of poor outcome in neonates following therapeutic hypothermia. Alkalosis was associated with other prognostic factors, such as severity of brain injury on magnetic resonance imaging (MRI), amplitude electroencephalography (aEEG) background pattern, seizure burden measured from raw EEG, and peak-area ratio Lactate+Threonine to total N-acetyl aspartate (LacT/tNAA) calculated from thalamic proton magnetic resonance spectroscopy (MRS), current biomarker of outcome. It was also associated with severity of long-term outcome.

The next step would be to test, in a preclinical model of hypoxia-ischaemia, the effect of NHE inhibitors, in conjunction with hypothermia, in reducing seizure burden and improving outcome; and that of a graded restoration of normocapnia strategy (by administering 5% CO_2) in conjunction with cooling.

The most plausible NHE inhibitor to be trialed in newborn infants is amiloride, which has already been used safely as a potassium sparing diuretic, in the context of oedemas in cardiac failure or hepatic disease. If preclinical trials support the added neuroprotective effect of NHE inhibitors to cooling, and the

reduction in seizure burden, then a phase I clinical trial would test the safety, side effects, best dose, and timing of it. Intravenous administration should be explored, as currently amiloride is available to be administered exclusively orally.

Avoiding hypocapnia is already recommended in the respiratory management of infants with neonatal encephalopathy undergoing cooling, especially if ventilated (236). Since inhaled 5% CO_2 has been administered in a small cohort of infants showing it to be safe, this is a potential feasible treatment to prevent neonatal seizures, by avoiding the rebound alkalosis, and improving outcome.

I believe phosphorus spectroscopy will remain a research tool, as its availability is limited in the clinical setting. The need for a different coil and the level of expertise required to set-up and analyse the data will limit its use in clinical practice. The calculation of pHi relies on an accurate fit of the spectra. This can be challenging in infants with a favourable prognosis, as their Pi/PCr ratio (marker of neuronal death) will be low; hence, some will present low SNR for Pi peak, making it more challenging to get an accurate frequency for Pi peak. One of the difficulties during the analysis has been to find the adequate 'Prior knowledge' that we fed the algorithm, to improve the fit. In the end, we have used 'Prior knowledge' considering 4 Pi peaks, which will take into account Pi found in the different compartments (slightly different pH and frequencies) and used an amplitude-weighted Pi frequency for calculations.

4 Key points from the sub-study

In Chapter 4 we investigated, in a sub-study of 23 infants with neonatal encephalopathy who underwent therapeutic hypothermia, the relationship between regional cerebral blood flow (rCBF), measured using pseudo-continuous arterial spin labelling (pCASL) between day 4 and 15 days of life , and brain pHi (measured with phosphorus spectroscopy), LacT/tNAA (measured with proton spectroscopy, as the current biomarker of outcome) (124), and long-term outcome.

We observed an increased DGM and grey matter perfusion in an infant with a poor prognosis (high LacT/tNAA), a more alkaline pHi and an adverse outcome (death). 'Luxury perfusion' has been well described in infants with neonatal encephalopathy and a poor prognosis. However, we observe that within the group of alkaline DGM pHi and/or high LacT/tNAA, there is a wide range of rCBF values. More studies using ASL in neonatal encephalopathy (6, 7, 274) have described this widespread distribution of rCBF within the poor prognosis group, and different hypothesis have been discussed. Hence, ASL shows to be a useful tool to predict outcome when increased regional CBF is detected. However, when a normal/lower rCBF is found, the other prognostic tools available (aEEG, MRI, HMRS) are required in addition to predict outcome.

The size of this sub-study was a limitation, especially the small number of infants with a poor prognosis, making it underpowered for statistical analysis. ASL is still an important research tool to further explore the interconnection between

hyperperfusion, metabolism and inflammation. It would be interesting to further assess the association between CBF and brain pHi, without the limitation of having to perform 2 extra research MR sequences, CBF could be assessed using NIRS instead of ASL.

5 Key points from the preclinical model of NE

In *Chapter 5,* a third study, in a pre-clinical model of neonatal encephalopathy, analysed brain pHi during hypoxic-ischaemic insult and its evolution over the next hour in 29 piglets.

We showed an association between the lowest level of brain tissue acidosis during hypoxia-ischaemia, the duration of acidosis under a certain threshold and its rate of recovery over the first hour after the insult, and energy metabolite ratios at 1h after the insult. Few studies have addressed this issue with such a continuous non-invasive monitoring of brain pHi intra-insult, providing an important insight into mechanisms of injury in the acute phase. It seems that cells have a threshold at which they reach the non-recovery phase, and the longer they spend under a certain threshold, the lower the threshold will be. Underlying infection/inflammation might affect the 'tolerance' to acidosis or might increase the severity of acidosis.

References

1. Edwards AD, Brocklehurst P, Gunn AJ, Halliday H, Juszczak E, Levene M, et al. Neurological outcomes at 18 months of age after moderate hypothermia for perinatal hypoxic ischaemic encephalopathy: synthesis and meta-analysis of trial data. BMJ. 2010;340:c363.
2. Jacobs SE, Berg M, Hunt R, Tarnow-Mordi WO, Inder TE, Davis PG. Cooling for newborns with hypoxic ischaemic encephalopathy. The Cochrane database of systematic reviews. 2013;1:CD003311.
3. Robertson NJ, Cowan FM, Cox IJ, Edwards AD. Brain alkaline intracellular pH after neonatal encephalopathy. Ann Neurol. 2002;52(6):732-42.
4. Uria-Avellanal C, Robertson NJ. Na^+/H^+ exchangers and intracellular pH in perinatal brain injury. Transl Stroke Res. 2014;5(1):79-98.
5. Helmy MM, Tolner EA, Vanhatalo S, Voipio J, Kaila K. Brain alkalosis causes birth asphyxia seizures, suggesting therapeutic strategy. Ann Neurol. 2011;69(3):493-500.
6. Sokolska M. Optimisation of Arterial Spin Labelling MRI for the assessment of perinatal brain injury.: UCL (University College London). 2017.
7. De Vis JB, Hendrikse J, Petersen ET, de Vries LS, van Bel F, Alderliesten T, et al. Arterial spin-labelling perfusion MRI and outcome in neonates with hypoxic-ischemic encephalopathy. Eur Radiol. 2015;25(1):113-21.
8. Zheng Q, Martin-Saavedra JS, Saade-Lemus S, Vossough A, Zuccoli G, Gonçalves FG, et al. Cerebral Pulsed Arterial Spin Labeling Perfusion Weighted Imaging Predicts Language and Motor Outcomes in Neonatal Hypoxic-Ischemic Encephalopathy. Frontiers in Pediatrics. 2020;8.
9. Nelson KB, Leviton A. How much of neonatal encephalopathy is due to birth asphyxia? Am J Dis Child. 1991;145(11):1325-31.
10. Robertson NJ GF. Hypoxic-ischaemic brain injury. . In: Churchill Livingstone E, editor. Rennie & Roberton's Textbook of Neonatology, fifth ed2005. p. 1114-55.
11. Kurinczuk JJ, White-Koning M, Badawi N. Epidemiology of neonatal encephalopathy and hypoxic-ischaemic encephalopathy. Early Hum Dev. 2010;86(6):329-38.
12. Volpe JJ. Hypoxic-ischaemic encephalopathy: neuropathology and pathogenesis. In: Volpe, J. (Ed.), Neurology of the Newborn. 2001 ed: Saunders, Philapdelphia; 2001. p. 497-520.
13. Okereafor A, Allsop J, Counsell SJ, Fitzpatrick J, Azzopardi D, Rutherford MA, et al. Patterns of brain injury in neonates exposed to perinatal sentinel events. Pediatrics. 2008;121(5):906-14.
14. Badawi N, Kurinczuk JJ, Keogh JM, Alessandri LM, O'Sullivan F, Burton PR, et al. Antepartum risk factors for newborn encephalopathy: the Western Australian case-control study. BMJ. 1998;317(7172):1549-53.
15. Badawi N, Kurinczuk JJ, Keogh JM, Alessandri LM, O'Sullivan F, Burton PR, et al. Intrapartum risk factors for newborn encephalopathy: the Western Australian case-control study. BMJ. 1998;317(7172):1554-8.
16. National-Institute-for-Health-and-Clinical-Excellence. Therapeutic hypothermia with intracorporeal temperature monitoring for hypoxic perinatal brain injury 2010 [updated 2012. http://guidance.nice.org.uk/IPG347/Guidance/pdf/English].
17. National Perinatal Epidemiology Unit (npeu) O. UK Toby cooling Register Clinician's handbook. Version 4. 2010 [Available from: https://www.npeu.ox.ac.uk/downloads/files/tobyregister/Register-Clinicans-Handbook1-v4-07-06-10.pdf.

18. Bona E, Hagberg H, Loberg EM, Bagenholm R, Thoresen M. Protective effects of moderate hypothermia after neonatal hypoxia-ischemia: short- and long-term outcome. Pediatr Res. 1998;43(6):738-45.
19. Thoresen M, Penrice J, Lorek A, Cady EB, Wylezinska M, Kirkbride V, et al. Mild hypothermia after severe transient hypoxia-ischemia ameliorates delayed cerebral energy failure in the newborn piglet. Pediatr Res. 1995;37(5):667-70.
20. Thoresen M, Bagenholm R, Loberg EM, Apricena F, Kjellmer I. Posthypoxic cooling of neonatal rats provides protection against brain injury. Arch Dis Child Fetal Neonatal Ed. 1996;74(1):F3-9.
21. Edwards AD, Wyatt JS, Thoresen M. Treatment of hypoxic-ischaemic brain damage by moderate hypothermia. Arch Dis Child Fetal Neonatal Ed. 1998;78(2):F85-8.
22. Gunn AJ, Gunn TR, Gunning MI, Williams CE, Gluckman PD. Neuroprotection with prolonged head cooling started before postischemic seizures in fetal sheep. Pediatrics. 1998;102(5):1098-106.
23. Edwards AD, Yue X, Squier MV, Thoresen M, Cady EB, Penrice J, et al. Specific inhibition of apoptosis after cerebral hypoxia-ischaemia by moderate post-insult hypothermia. Biochem Biophys Res Commun. 1995;217(3):1193-9.
24. Laptook AR, Corbett RJ, Sterett R, Garcia D, Tollefsbol G. Quantitative relationship between brain temperature and energy utilization rate measured in vivo using 31P and 1H magnetic resonance spectroscopy. Pediatr Res. 1995;38(6):919-25.
25. Laptook AR, Corbett RJ, Sterett R, Burns DK, Garcia D, Tollefsbol G. Modest hypothermia provides partial neuroprotection when used for immediate resuscitation after brain ischemia. Pediatr Res. 1997;42(1):17-23.
26. Gunn AJ, Gluckman PD, Gunn TR. Selective head cooling in newborn infants after perinatal asphyxia: a safety study. Pediatrics. 1998;102(4 Pt 1):885-92.
27. Gluckman PD, Wyatt JS, Azzopardi D, Ballard R, Edwards AD, Ferriero DM, et al. Selective head cooling with mild systemic hypothermia after neonatal encephalopathy: multicentre randomised trial. Lancet. 2005;365(9460):663-70.
28. Shankaran S, Laptook AR, Ehrenkranz RA, Tyson JE, McDonald SA, Donovan EF, et al. Whole-body hypothermia for neonates with hypoxic-ischemic encephalopathy. N Engl J Med. 2005;353(15):1574-84.
29. Azzopardi DV, Strohm B, Edwards AD, Dyet L, Halliday HL, Juszczak E, et al. Moderate hypothermia to treat perinatal asphyxial encephalopathy. N Engl J Med. 2009;361(14):1349-58.
30. Jacobs SE, Morley CJ, Inder TE, Stewart MJ, Smith KR, McNamara PJ, et al. Whole-body hypothermia for term and near-term newborns with hypoxic-ischemic encephalopathy: a randomized controlled trial. Arch Pediatr Adolesc Med. 2011;165(8):692-700.
31. Simbruner G, Mittal RA, Rohlmann F, Muche R. Systemic hypothermia after neonatal encephalopathy: outcomes of neo.nEURO.network RCT. Pediatrics. 2010;126(4):e771-8.
32. Miller JA, Jr., Miller FS, Westin B. HYPOTHERMIA IN THE TREATMENT OF ASPHYXIA NEONATORUM. Biologia neonatorum Neo-natal studies. 1964;6:148-63.
33. Ehrstrom J, Hirvensalo M, Donner M, Hietalahti J. Hypothermia in the resuscitation of severely asphyctic newborn infants. A follow-up study. Annals of clinical research. 1969;1(1):40-9.
34. Miller JA, Jr. New approaches to preventing brain damage during asphyxia. Am J Obstet Gynecol. 1971;110(8):1125-33.
35. Cordey R, Chiolero R, Miller JA, Jr. Resuscitation of neonates by hypothermia: report on 20 cases with acid-base determination on 10 cases and the long-term development of 33 cases. Resuscitation. 1973;2(3):169-81.

36. Duhn R, Schoen EJ, Siu M. Subcutaneous fat necrosis with extensive calcification after hypothermia in two newborn infants. Pediatrics. 1968;41(3):661-4.
37. Silverman WA, Fertig JW, Berger AP. The influence of the thermal environment upon the survival of newly born premature infants. Pediatrics. 1958;22(5):876-86.
38. Jolly H, Molyneux P, Newell DJ. A controlled study of the effect of temperature on premature babies. J Pediatr. 1962;60:889-94.
39. Day RL, Caliguiri L, Kamenski C, Ehrlich F. Body temperature and survival of premature infants. Pediatrics. 1964;34:171-81.
40. Buetow KC, Klein SW. EFFECT OF MAINTENANCE OF "NORMAL" SKIN TEMPERATURE ON SURVIVAL OF INFANTS OF LOW BIRTH WEIGHT. Pediatrics. 1964;34:163-70.
41. Wagner CL, Eicher DJ, Katikaneni LD, Barbosa E, Holden KR. The use of hypothermia: a role in the treatment of neonatal asphyxia? Pediatr Neurol. 1999;21(1):429-43.
42. Guillet R, Edwards AD, Thoresen M, Ferriero DM, Gluckman PD, Whitelaw A, et al. Seven- to eight-year follow-up of the CoolCap trial of head cooling for neonatal encephalopathy. Pediatr Res. 2012;71(2):205-9.
43. Azzopardi D, Strohm B, Marlow N, Brocklehurst P, Deierl A, Eddama O, et al. Effects of hypothermia for perinatal asphyxia on childhood outcomes. N Engl J Med. 2014;371(2):140-9.
44. Shankaran S, Pappas A, McDonald SA, Vohr BR, Hintz SR, Yolton K, et al. Childhood outcomes after hypothermia for neonatal encephalopathy. N Engl J Med. 2012;366(22):2085-92.
45. Shankaran S, Pappas A, Laptook AR, McDonald SA, Ehrenkranz RA, Tyson JE, et al. Outcomes of safety and effectiveness in a multicenter randomized, controlled trial of whole-body hypothermia for neonatal hypoxic-ischemic encephalopathy. Pediatrics. 2008;122(4):e791-8.
46. Myers RE. Two patterns of perinatal brain damage and their conditions of occurrence. Am J Obstet Gynecol. 1972;112(2):246-76.
47. Dawes GS, Duncan SL, Lewis BV, Merlet CL, Owen-Thomas JB, Reeves JT. Hypoxaemia and aortic chemoreceptor function in foetal lambs. The Journal of physiology. 1969;201(1):105-16.
48. Peeters LL, Sheldon RE, Jones MD, Jr., Makowski EL, Meschia G. Blood flow to fetal organs as a function of arterial oxygen content. Am J Obstet Gynecol. 1979;135(5):637-46.
49. Uria-Avellanal C, Robertson NJ. Na(+)/H(+) exchangers and intracellular pH in perinatal brain injury. Translational stroke research. 2014;5(1):79-98.
50. Hossmann KA. Viability thresholds and the penumbra of focal ischemia. Ann Neurol. 1994;36(4):557-65.
51. Crockard HA, Gadian DG, Frackowiak RS, Proctor E, Allen K, Williams SR, et al. Acute cerebral ischaemia: concurrent changes in cerebral blood flow, energy metabolites, pH, and lactate measured with hydrogen clearance and 31P and 1H nuclear magnetic resonance spectroscopy. II. Changes during ischaemia. J Cereb Blood Flow Metab. 1987;7(4):394-402.
52. Lorek A, Takei Y, Cady EB, Wyatt JS, Penrice J, Edwards AD, et al. Delayed ("secondary") cerebral energy failure after acute hypoxia-ischemia in the newborn piglet: continuous 48-hour studies by phosphorus magnetic resonance spectroscopy. Pediatr Res. 1994;36(6):699-706.
53. Hope PL, Costello AM, Cady EB, Delpy DT, Tofts PS, Chu A, et al. Cerebral energy metabolism studied with phosphorus NMR spectroscopy in normal and birth-asphyxiated infants. Lancet. 1984;2(8399):366-70.

54. Azzopardi D, Wyatt JS, Cady EB, Delpy DT, Baudin J, Stewart AL, et al. Prognosis of newborn infants with hypoxic-ischemic brain injury assessed by phosphorus magnetic resonance spectroscopy. Pediatr Res. 1989;25(5):445-51.
55. Cady EB, Amess P, Penrice J, Wylezinska M, Sams V, Wyatt JS. Early cerebral-metabolite quantification in perinatal hypoxic-ischaemic encephalopathy by proton and phosphorus magnetic resonance spectroscopy. Magn Reson Imaging. 1997;15(5):605-11.
56. Martin E, Buchli R, Ritter S, Schmid R, Largo RH, Boltshauser E, et al. Diagnostic and prognostic value of cerebral 31P magnetic resonance spectroscopy in neonates with perinatal asphyxia. Pediatr Res. 1996;40(5):749-58.
57. Robertson NJ, Cox IJ, Cowan FM, Counsell SJ, Azzopardi D, Edwards AD. Cerebral intracellular lactic alkalosis persisting months after neonatal encephalopathy measured by magnetic resonance spectroscopy. Pediatr Res. 1999;46(3):287-96.
58. Nagatomo Y, Wick M, Prielmeier F, Frahm J. Dynamic monitoring of cerebral metabolites during and after transient global ischemia in rats by quantitative proton NMR spectroscopy in vivo. NMR Biomed. 1995;8(6):265-70.
59. Barker P.B. BA, DeStefano N, Gullapalli R, Lin D.D.M. Clinical MR Spectroscopy. Techniques and Applications: Cambridge University Press; 2010 2010.
60. Kleuskens DG, Gonçalves Costa F, Annink KV, van den Hoogen A, Alderliesten T, Groenendaal F, et al. Pathophysiology of Cerebral Hyperperfusion in Term Neonates With Hypoxic-Ischemic Encephalopathy: A Systematic Review for Future Research. Front Pediatr. 2021;9:631258.
61. Bennet L, Tan S, Van den Heuij L, Derrick M, Groenendaal F, van Bel F, et al. Cell therapy for neonatal hypoxia-ischemia and cerebral palsy. Ann Neurol. 2012;71(5):589-600.
62. Siesjo BK, Agardh CD, Bengtsson F. Free radicals and brain damage. Cerebrovasc Brain Metab Rev. 1989;1(3):165-211.
63. Walsh BH, Boylan GB, Livingstone V, Kenny LC, Dempsey EM, Murray DM. Cord blood proteins and multichannel-electroencephalography in hypoxic-ischemic encephalopathy. Pediatr Crit Care Med. 2013;14(6):621-30.
64. Ikeda T, Yang L, Ikenoue T, Mallard C, Hagberg H. Endotoxin-induced hypoxic-ischemic tolerance is mediated by up-regulation of corticosterone in neonatal rat. Pediatr Res. 2006;59(1):56-60.
65. Kendall G, Peebles D. Acute fetal hypoxia: the modulating effect of infection. Early Hum Dev. 2005;81(1):27-34.
66. Siesjo BK, Siesjo P. Mechanisms of secondary brain injury. Eur J Anaesthesiol. 1996;13(3):247-68.
67. Northington FJ, Zelaya ME, O'Riordan DP, Blomgren K, Flock DL, Hagberg H, et al. Failure to complete apoptosis following neonatal hypoxia-ischemia manifests as "continuum" phenotype of cell death and occurs with multiple manifestations of mitochondrial dysfunction in rodent forebrain. Neuroscience. 2007;149(4):822-33.
68. Sarnat HB, Sarnat MS. Neonatal encephalopathy following fetal distress. A clinical and electroencephalographic study. Archives of neurology. 1976;33(10):696-705.
69. Thompson CM, Puterman AS, Linley LL, Hann FM, van der Elst CW, Molteno CD, et al. The value of a scoring system for hypoxic ischaemic encephalopathy in predicting neurodevelopmental outcome. Acta Paediatr. 1997;86(7):757-61.
70. Thoresen M, Satas S, Loberg EM, Whitelaw A, Acolet D, Lindgren C, et al. Twenty-four hours of mild hypothermia in unsedated newborn pigs starting after a severe global hypoxic-ischemic insult is not neuroprotective. Pediatr Res. 2001;50(3):405-11.
71. Wassink G, Lear CA, Gunn KC, Dean JM, Bennet L, Gunn AJ. Analgesics, sedatives, anticonvulsant drugs, and the cooled brain. Semin Fetal Neonatal Med. 2015;20(2):109-14.

72. Dubowitz L, Ricciw D, Mercuri E. The Dubowitz neurological examination of the full-term newborn. Ment Retard Dev Disabil Res Rev. 2005;11(1):52-60.
73. Sarkar S, Bhagat I, Bapuraj JR, Dechert RE, Donn SM. Does clinical status 1 week after therapeutic hypothermia predict brain MRI abnormalities? J Perinatol. 2013;33(7):538-42.
74. van Wezel-Meijler G, Steggerda SJ, Leijser LM. Cranial ultrasonography in neonates: role and limitations. Semin Perinatol. 2010;34(1):28-38.
75. L P. Diagnostic ultrasound for cerebral vascular diseases. In: Donald I LSe, editor. Present and Future of Diagnostic Ultrasound
Rotterdam, Kooyker1976. p. 141–7.
76. Archer LN, Levene MI, Evans DH. Cerebral artery Doppler ultrasonography for prediction of outcome after perinatal asphyxia. Lancet. 1986;2(8516):1116-8.
77. Elstad M, Whitelaw A, Thoresen M. Cerebral Resistance Index is less predictive in hypothermic encephalopathic newborns. Acta Paediatr. 2011;100(10):1344-9.
78. Skranes JH, Elstad M, Thoresen M, Cowan FM, Stiris T, Fugelseth D. Hypothermia makes cerebral resistance index a poor prognostic tool in encephalopathic newborns. Neonatology. 2014;106(1):17-23.
79. Meek JH, Elwell CE, McCormick DC, Edwards AD, Townsend JP, Stewart AL, et al. Abnormal cerebral haemodynamics in perinatally asphyxiated neonates related to outcome. Arch Dis Child Fetal Neonatal Ed. 1999;81(2):F110-5.
80. Pryds O, Greisen G, Lou H, Friis-Hansen B. Vasoparalysis associated with brain damage in asphyxiated term infants. J Pediatr. 1990;117(1 Pt 1):119-25.
81. Hellstrom-Westas L, Rosen I, Svenningsen NW. Predictive value of early continuous amplitude integrated EEG recordings on outcome after severe birth asphyxia in full term infants. Arch Dis Child Fetal Neonatal Ed. 1995;72(1):F34-8.
82. Toet MC, Hellstrom-Westas L, Groenendaal F, Eken P, de Vries LS. Amplitude integrated EEG 3 and 6 hours after birth in full term neonates with hypoxic-ischaemic encephalopathy. Arch Dis Child Fetal Neonatal Ed. 1999;81(1):F19-23.
83. van Rooij LG, Toet MC, Osredkar D, van Huffelen AC, Groenendaal F, de Vries LS. Recovery of amplitude integrated electroencephalographic background patterns within 24 hours of perinatal asphyxia. Arch Dis Child Fetal Neonatal Ed. 2005;90(3):F245-51.
84. Thoresen M, Hellstrom-Westas L, Liu X, de Vries LS. Effect of hypothermia on amplitude-integrated electroencephalogram in infants with asphyxia. Pediatrics. 2010;126(1):e131-9.
85. al Naqeeb N, Edwards AD, Cowan FM, Azzopardi D. Assessment of neonatal encephalopathy by amplitude-integrated electroencephalography. Pediatrics. 1999;103(6 Pt 1):1263-71.
86. de Vries LS, Hellstrom-Westas L. Role of cerebral function monitoring in the newborn. Arch Dis Child Fetal Neonatal Ed. 2005;90(3):F201-7.
87. Uria-Avellanal C, Marlow N, Rennie JM. Outcome following neonatal seizures. Semin Fetal Neonatal Med. 2013;18(4):224-32.
88. Menache CC, Bourgeois BFD, Volpe JJ. Prognostic value of neonatal discontinuous EEG. Pediatr Neurol. 2002;27(2):93-101.
89. Holmes GL. The long-term effects of neonatal seizures. Clinics in perinatology. 2009;36(4):901-14, vii-viii.
90. Glass HC, Glidden D, Jeremy RJ, Barkovich AJ, Ferriero DM, Miller SP. Clinical Neonatal Seizures are Independently Associated with Outcome in Infants at Risk for Hypoxic-Ischemic Brain Injury. J Pediatr. 2009;155(3):318-23.

91. Watanabe K, Miyazaki S, Hara K, Hakamada S. Behavioral state cycles, background EEGs and prognosis of newborns with perinatal hypoxia. Electroencephalogr Clin Neurophysiol. 1980;49(5-6):618-25.
92. Low E, Boylan GB, Mathieson SR, Murray DM, Korotchikova I, Stevenson NJ, et al. Cooling and seizure burden in term neonates: an observational study. Arch Dis Child Fetal Neonatal Ed. 2012;97(4):F267-72.
93. Mitra S, Bale G, Meek J, Tachtsidis I, Robertson NJ. Cerebral Near Infrared Spectroscopy Monitoring in Term Infants With Hypoxic Ischemic Encephalopathy-A Systematic Review. Front Neurol. 2020;11:393.
94. Mitra S, Bale G, Highton D, Gunny R, Uria-Avellanal C, Bainbridge A, et al. Pressure passivity of cerebral mitochondrial metabolism is associated with poor outcome following perinatal hypoxic ischemic brain injury. J Cereb Blood Flow Metab. 2019;39(1):118-30.
95. Bale G, Taylor N, Mitra S, Sudakou A, de Roever I, Meek J, et al. Near-Infrared Spectroscopy Measured Cerebral Blood Flow from Spontaneous Oxygenation Changes in Neonatal Brain Injury. Adv Exp Med Biol. 2020;1232:3-9.
96. Rutherford M, Biarge MM, Allsop J, Counsell S, Cowan F. MRI of perinatal brain injury. Pediatr Radiol. 2010;40(6):819-33.
97. Barkovich AJ, Miller SP, Bartha A, Newton N, Hamrick SE, Mukherjee P, et al. MR imaging, MR spectroscopy, and diffusion tensor imaging of sequential studies in neonates with encephalopathy. AJNR Am J Neuroradiol. 2006;27(3):533-47.
98. Cowan F, Rutherford M, Groenendaal F, Eken P, Mercuri E, Bydder GM, et al. Origin and timing of brain lesions in term infants with neonatal encephalopathy. Lancet. 2003;361(9359):736-42.
99. Ranck JB, Jr., Windle WF. Brain damage in the monkey, macaca mulatta, by asphyxia neonatorum. Experimental neurology. 1959;1(2):130-54.
100. Brann AW, Jr., Myers RE. Central nervous system findings in the newborn monkey following severe in utero partial asphyxia. Neurology. 1975;25(4):327-38.
101. Bednarek N, Mathur A, Inder T, Wilkinson J, Neil J, Shimony J. Impact of therapeutic hypothermia on MRI diffusion changes in neonatal encephalopathy. Neurology. 2012;78(18):1420-7.
102. Johnson M, Hanson GR, Gibb JW, Adair J, Filloux F. Effect of neonatal hypoxia-ischemia on nigro-striatal dopamine receptors and on striatal neuropeptide Y, dynorphin A and substance P concentrations in rats. Brain research Developmental brain research. 1994;83(1):109-18.
103. Martinez-Biarge M, Diez-Sebastian J, Rutherford MA, Cowan FM. Outcomes after central grey matter injury in term perinatal hypoxic-ischaemic encephalopathy. Early Hum Dev. 2010;86(11):675-82.
104. Groenendaal F, de Vries LS. Watershed infarcts in the full term neonatal brain. Arch Dis Child Fetal Neonatal Ed. 2005;90(6):F488.
105. Chau V, Poskitt KJ, Sargent MA, Lupton BA, Hill A, Roland E, et al. Comparison of computer tomography and magnetic resonance imaging scans on the third day of life in term newborns with neonatal encephalopathy. Pediatrics. 2009;123(1):319-26.
106. Rutherford M, Pennock J, Schwieso J, Cowan F, Dubowitz L. Hypoxic-ischaemic encephalopathy: early and late magnetic resonance imaging findings in relation to outcome. Arch Dis Child Fetal Neonatal Ed. 1996;75(3):F145-51.
107. Burns CM, Rutherford MA, Boardman JP, Cowan FM. Patterns of cerebral injury and neurodevelopmental outcomes after symptomatic neonatal hypoglycemia. Pediatrics. 2008;122(1):65-74.

108. Miller SP, Newton N, Ferriero DM, Partridge JC, Glidden DV, Barnwell A, et al. Predictors of 30-month outcome after perinatal depression: role of proton MRS and socioeconomic factors. Pediatr Res. 2002;52(1):71-7.
109. Marlow N, Rose AS, Rands CE, Draper ES. Neuropsychological and educational problems at school age associated with neonatal encephalopathy. Arch Dis Child Fetal Neonatal Ed. 2005;90(5):F380-7.
110. Barnett A, Mercuri E, Rutherford M, Haataja L, Frisone MF, Henderson S, et al. Neurological and perceptual-motor outcome at 5 - 6 years of age in children with neonatal encephalopathy: relationship with neonatal brain MRI. Neuropediatrics. 2002;33(5):242-8.
111. Gonzalez FF, Miller SP. Does perinatal asphyxia impair cognitive function without cerebral palsy? Arch Dis Child Fetal Neonatal Ed. 2006;91(6):F454-9.
112. Gadian DG, Aicardi J, Watkins KE, Porter DA, Mishkin M, Vargha-Khadem F. Developmental amnesia associated with early hypoxic-ischaemic injury. Brain. 2000;123 Pt 3:499-507.
113. Blumberg RM, Cady EB, Wigglesworth JS, McKenzie JE, Edwards AD. Relation between delayed impairment of cerebral energy metabolism and infarction following transient focal hypoxia-ischaemia in the developing brain. Experimental brain research Experimentelle Hirnforschung Experimentation cerebrale. 1997;113(1):130-7.
114. Iwata O, Iwata S, Thornton JS, De Vita E, Bainbridge A, Herbert L, et al. "Therapeutic time window" duration decreases with increasing severity of cerebral hypoxia-ischaemia under normothermia and delayed hypothermia in newborn piglets. Brain Res. 2007;1154:173-80.
115. van der Knaap MS, van der Grond J, van Rijen PC, Faber JA, Valk J, Willemse K. Age-dependent changes in localized proton and phosphorus MR spectroscopy of the brain. Radiology. 1990;176(2):509-15.
116. Peden CJ, Cowan FM, Bryant DJ, Sargentoni J, Cox IJ, Menon DK, et al. Proton MR spectroscopy of the brain in infants. J Comput Assist Tomogr. 1990;14(6):886-94.
117. de Vries LS, Groenendaal F. Patterns of neonatal hypoxic-ischaemic brain injury. Neuroradiology. 2010;52(6):555-66.
118. Groenendaal F, Veenhoven RH, van der Grond J, Jansen GH, Witkamp TD, de Vries LS. Cerebral lactate and N-acetyl-aspartate/choline ratios in asphyxiated full-term neonates demonstrated in vivo using proton magnetic resonance spectroscopy. Pediatr Res. 1994;35(2):148-51.
119. Urenjak J, Williams SR, Gadian DG, Noble M. Specific expression of N-acetylaspartate in neurons, oligodendrocyte-type-2 astrocyte progenitors, and immature oligodendrocytes in vitro. J Neurochem. 1992;59(1):55-61.
120. Graham GD, Kalvach P, Blamire AM, Brass LM, Fayad PB, Prichard JW. Clinical correlates of proton magnetic resonance spectroscopy findings after acute cerebral infarction. Stroke. 1995;26(2):225-9.
121. Graham SH, Meyerhoff DJ, Bayne L, Sharp FR, Weiner MW. Magnetic resonance spectroscopy of N-acetylaspartate in hypoxic-ischemic encephalopathy. Ann Neurol. 1994;35(4):490-4.
122. Thayyil S, Chandrasekaran M, Taylor A, Bainbridge A, Cady EB, Chong WK, et al. Cerebral magnetic resonance biomarkers in neonatal encephalopathy: a meta-analysis. Pediatrics. 2010;125(2):e382-95.
123. Azzopardi D, Chew AT, Deierl A, Huertas A, Robertson NJ, Tusor N, et al. Prospective qualification of early cerebral biomarkers in a randomised trial of treatment with xenon combined with moderate hypothermia after birth asphyxia. EBioMedicine. 2019;47:484-91.

124. Mitra S, Kendall GS, Bainbridge A, Sokolska M, Dinan M, Uria-Avellanal C, et al. Proton magnetic resonance spectroscopy lactate/N-acetylaspartate within 2 weeks of birth accurately predicts 2-year motor, cognitive and language outcomes in neonatal encephalopathy after therapeutic hypothermia. Arch Dis Child Fetal Neonatal Ed. 2019;104(4):F424-f32.
125. Hüppi PS, Fusch C, Boesch C, Burri R, Bossi E, Amato M, et al. Regional metabolic assessment of human brain during development by proton magnetic resonance spectroscopy in vivo and by high-performance liquid chromatography/gas chromatography in autopsy tissue. Pediatr Res. 1995;37(2):145-50.
126. Cady EB, Costello AM, Dawson MJ, Delpy DT, Hope PL, Reynolds EO, et al. Non-invasive investigation of cerebral metabolism in newborn infants by phosphorus nuclear magnetic resonance spectroscopy. Lancet. 1983;1(8333):1059-62.
127. Petroff OA, Prichard JW, Behar KL, Alger JR, den Hollander JA, Shulman RG. Cerebral intracellular pH by 31P nuclear magnetic resonance spectroscopy. Neurology. 1985;35(6):781-8.
128. Rottenberg DA, Ginos JZ, Kearfott KJ, Junck L, Bigner DD. In vivo measurement of regional brain tissue pH using positron emission tomography. Ann Neurol. 1984;15 Suppl:S98-102.
129. Moon RB, Richards JH. Determination of intracellular pH by 31P magnetic resonance. J Biol Chem. 1973;248(20):7276-8.
130. Williams GD, Smith MB. Application of the accurate assessment of intracellular magnesium and pH from the 31P shifts of ATP to cerebral hypoxia-ischemia in neonatal rat. Magn Reson Med. 1995;33(6):853-7.
131. Williams GD, Mosher TJ, Smith MB. Simultaneous determination of intracellular magnesium and pH from the three 31P NMR Chemical shifts of ATP. Anal Biochem. 1993;214(2):458-67.
132. Raghunand N. Tissue pH measurement by magnetic resonance spectroscopy and imaging. Methods Mol Med. 2006;124:347-64.
133. Petroff OA, Prichard JW. Cerebral pH by NMR. Lancet. 1983;2(8341):105-6.
134. Hamilton PA, Hope PL, Cady EB, Delpy DT, Wyatt JS, Reynolds EO. Impaired energy metabolism in brains of newborn infants with increased cerebral echodensities. Lancet. 1986;1(8492):1242-6.
135. Hamilton G, Allsop JM, Patel N, Forton DM, Thomas HC, O'Sullivan CP, et al. Variations due to analysis technique in intracellular pH measurements in simulated and in vivo 31P MR spectra of the human brain. J Magn Reson Imaging. 2006;23(4):459-64.
136. Casey JR, Grinstein S, Orlowski J. Sensors and regulators of intracellular pH. Nature reviews Molecular cell biology. 2010;11(1):50-61.
137. Vornov JJ, Thomas AG, Jo D. Protective effects of extracellular acidosis and blockade of sodium/hydrogen ion exchange during recovery from metabolic inhibition in neuronal tissue culture. J Neurochem. 1996;67(6):2379-89.
138. Bond JM, Herman B, Lemasters JJ. Protection by acidotic pH against anoxia/reoxygenation injury to rat neonatal cardiac myocytes. Biochem Biophys Res Commun. 1991;179(2):798-803.
139. Bond JM, Chacon E, Herman B, Lemasters JJ. Intracellular pH and Ca2+ homeostasis in the pH paradox of reperfusion injury to neonatal rat cardiac myocytes. Am J Physiol. 1993;265(1 Pt 1):C129-37.
140. Lemasters JJ, Nieminen AL, Qian T, Trost LC, Herman B. The mitochondrial permeability transition in toxic, hypoxic and reperfusion injury. Molecular and cellular biochemistry. 1997;174(1-2):159-65.

141. Traynelis SF, Cull-Candy SG. Proton inhibition of N-methyl-D-aspartate receptors in cerebellar neurons. Nature. 1990;345(6273):347-50.
142. Giffard RG, Weiss JH, Choi DW. Extracellular alkalinity exacerbates injury of cultured cortical neurons. Stroke. 1992;23(12):1817-21.
143. Masereel B, Pochet L, Laeckmann D. An overview of inhibitors of Na(+)/H(+) exchanger. Eur J Med Chem. 2003;38(6):547-54.
144. Slepkov ER, Rainey JK, Sykes BD, Fliegel L. Structural and functional analysis of the Na+/H+ exchanger. Biochem J. 2007;401(3):623-33.
145. Kintner DB, Wang Y, Sun D. Role of membrane ion transport proteins in cerebral ischemic damage. Frontiers in bioscience : a journal and virtual library. 2007;12:762-70.
146. Lee SH, Kim T, Park ES, Yang S, Jeong D, Choi Y, et al. NHE10, an osteoclast-specific member of the Na+/H+ exchanger family, regulates osteoclast differentiation and survival [corrected]. Biochem Biophys Res Commun. 2008;369(2):320-6.
147. Brett CL, Wei Y, Donowitz M, Rao R. Human Na(+)/H(+) exchanger isoform 6 is found in recycling endosomes of cells, not in mitochondria. Am J Physiol Cell Physiol. 2002;282(5):C1031-41.
148. Orlowski J, Grinstein S. Diversity of the mammalian sodium/proton exchanger SLC9 gene family. Pflugers Arch. 2004;447(5):549-65.
149. Ma E, Haddad GG. Expression and localization of Na+/H+ exchangers in rat central nervous system. Neuroscience. 1997;79(2):591-603.
150. Douglas RM, Schmitt BM, Xia Y, Bevensee MO, Biemesderfer D, Boron WF, et al. Sodium-hydrogen exchangers and sodium-bicarbonate co-transporters: ontogeny of protein expression in the rat brain. Neuroscience. 2001;102(1):217-28.
151. Rotin D, Grinstein S. Impaired cell volume regulation in Na(+)-H+ exchange-deficient mutants. Am J Physiol. 1989;257(6 Pt 1):C1158-65.
152. Aronson PS. Kinetic properties of the plasma membrane Na+-H+ exchanger. Annu Rev Physiol. 1985;47:545-60.
153. Paris S, Pouyssegur J. Growth factors activate the Na+/H+ antiporter in quiescent fibroblasts by increasing its affinity for intracellular H+. J Biol Chem. 1984;259(17):10989-94.
154. Haworth RS, Roberts NA, Cuello F, Avkiran M. Regulation of protein kinase D activity in adult myocardium: novel counter-regulatory roles for protein kinase Cepsilon and protein kinase A. J Mol Cell Cardiol. 2007;43(6):686-95.
155. Khaled AR, Moor AN, Li A, Kim K, Ferris DK, Muegge K, et al. Trophic factor withdrawal: p38 mitogen-activated protein kinase activates NHE1, which induces intracellular alkalinization. Mol Cell Biol. 2001;21(22):7545-57.
156. Malo ME, Li L, Fliegel L. Mitogen-activated protein kinase-dependent activation of the Na+/H+ exchanger is mediated through phosphorylation of amino acids Ser770 and Ser771. J Biol Chem. 2007;282(9):6292-9.
157. Tominaga T, Ishizaki T, Narumiya S, Barber DL. p160ROCK mediates RhoA activation of Na-H exchange. EMBO J. 1998;17(16):4712-22.
158. Yan W, Nehrke K, Choi J, Barber DL. The Nck-interacting kinase (NIK) phosphorylates the Na+-H+ exchanger NHE1 and regulates NHE1 activation by platelet-derived growth factor. J Biol Chem. 2001;276(33):31349-56.
159. Fernandez-Rachubinski F, Fliegel L. COUP-TFI and COUP-TFII regulate expression of the NHE through a nuclear hormone responsive element with enhancer activity. Eur J Biochem. 2001;268(3):620-34.
160. Slepkov E, Fliegel L. Regulation of expression of the Na+/H+ exchanger by thyroid hormone. Vitam Horm. 2004;69:249-69.

161. Denker SP, Huang DC, Orlowski J, Furthmayr H, Barber DL. Direct binding of the Na--H exchanger NHE1 to ERM proteins regulates the cortical cytoskeleton and cell shape independently of H(+) translocation. Mol Cell. 2000;6(6):1425-36.
162. Meima ME, Mackley JR, Barber DL. Beyond ion translocation: structural functions of the sodium-hydrogen exchanger isoform-1. Curr Opin Nephrol Hypertens. 2007;16(4):365-72.
163. Denker SP, Barber DL. Cell migration requires both ion translocation and cytoskeletal anchoring by the Na-H exchanger NHE1. J Cell Biol. 2002;159(6):1087-96.
164. Stock C, Schwab A. Role of the Na/H exchanger NHE1 in cell migration. Acta Physiol (Oxf). 2006;187(1-2):149-57.
165. Hayashi H, Aharonovitz O, Alexander RT, Touret N, Furuya W, Orlowski J, et al. Na+/H+ exchange and pH regulation in the control of neutrophil chemokinesis and chemotaxis. Am J Physiol Cell Physiol. 2008;294(2):C526-34.
166. Patel H, Barber DL. A developmentally regulated Na-H exchanger in Dictyostelium discoideum is necessary for cell polarity during chemotaxis. J Cell Biol. 2005;169(2):321-9.
167. Kapus A, Grinstein S, Wasan S, Kandasamy R, Orlowski J. Functional characterization of three isoforms of the Na+/H+ exchanger stably expressed in Chinese hamster ovary cells. ATP dependence, osmotic sensitivity, and role in cell proliferation. J Biol Chem. 1994;269(38):23544-52.
168. Pouyssegur J, Seuwen K. Transmembrane receptors and intracellular pathways that control cell proliferation. Annu Rev Physiol. 1992;54:195-210.
169. Putney LK, Barber DL. Na-H exchange-dependent increase in intracellular pH times G2/M entry and transition. J Biol Chem. 2003;278(45):44645-9.
170. Cheung JY, Bonventre JV, Malis CD, Leaf A. Calcium and ischemic injury. N Engl J Med. 1986;314(26):1670-6.
171. Siesjo BK. Pathophysiology and treatment of focal cerebral ischemia. Part I: Pathophysiology. J Neurosurg. 1992;77(2):169-84.
172. Wakabayashi S, Fafournoux P, Sardet C, Pouyssegur J. The Na+/H+ antiporter cytoplasmic domain mediates growth factor signals and controls "H(+)-sensing". Proc Natl Acad Sci U S A. 1992;89(6):2424-8.
173. Obara M, Szeliga M, Albrecht J. Regulation of pH in the mammalian central nervous system under normal and pathological conditions: facts and hypotheses. Neurochem Int. 2008;52(6):905-19.
174. Sheldon C, Church J. Intracellular pH response to anoxia in acutely dissociated adult rat hippocampal CA1 neurons. J Neurophysiol. 2002;87(5):2209-24.
175. Hwang IK, Yoo KY, An SJ, Li H, Lee CH, Choi JH, et al. Late expression of Na+/H+ exchanger 1 (NHE1) and neuroprotective effects of NHE inhibitor in the gerbil hippocampal CA1 region induced by transient ischemia. Experimental neurology. 2008;212(2):314-23.
176. Kersh AE, Hartzler LK, Havlin K, Hubbell BB, Nanagas V, Kalra A, et al. pH regulating transporters in neurons from various chemosensitive brainstem regions in neonatal rats. American journal of physiology Regulatory, integrative and comparative physiology. 2009;297(5):R1409-20.
177. Jorgensen EO, Holm S. The course of circulatory and cerebral recovery after circulatory arrest: influence of pre-arrest, arrest and post-arrest factors. Resuscitation. 1999;42(3):173-82.
178. Luo J, Chen H, Kintner DB, Shull GE, Sun D. Decreased neuronal death in Na+/H+ exchanger isoform 1-null mice after in vitro and in vivo ischemia. J Neurosci. 2005;25(49):11256-68.

179. Matsumoto Y, Yamamoto S, Suzuki Y, Tsuboi T, Terakawa S, Ohashi N, et al. Na+/H+ exchanger inhibitor, SM-20220, is protective against excitotoxicity in cultured cortical neurons. Stroke. 2004;35(1):185-90.
180. Robertson NJ, Bhakoo K, Puri BK, Edwards AD, Cox IJ. Hypothermia and amiloride preserve energetics in a neonatal brain slice model. Pediatr Res. 2005;58(2):288-96.
181. Liu Y, Kintner DB, Chanana V, Algharabli J, Chen X, Gao Y, et al. Activation of microglia depends on Na+/H+ exchange-mediated H+ homeostasis. J Neurosci. 2010;30(45):15210-20.
182. Yao H, Gu XQ, Douglas RM, Haddad GG. Role of Na(+)/H(+) exchanger during O(2) deprivation in mouse CA1 neurons. Am J Physiol Cell Physiol. 2001;281(4):C1205-10.
183. Kintner DB, Look A, Shull GE, Sun D. Stimulation of astrocyte Na+/H+ exchange activity in response to in vitro ischemia depends in part on activation of ERK1/2. Am J Physiol Cell Physiol. 2005;289(4):C934-45.
184. Kendall GS, Robertson NJ, Iwata O, Peebles D, Raivich G. N-methyl-isobutyl-amiloride ameliorates brain injury when commenced before hypoxia ischemia in neonatal mice. Pediatr Res. 2006;59(2):227-31.
185. Kuribayashi Y, Itoh N, Kitano M, Ohashi N. Cerebroprotective properties of SM-20220, a potent Na(+)/H(+) exchange inhibitor, in transient cerebral ischemia in rats. European journal of pharmacology. 1999;383(2):163-8.
186. Kitayama J, Kitazono T, Yao H, Ooboshi H, Takaba H, Ago T, et al. Inhibition of Na+/H+ exchanger reduces infarct volume of focal cerebral ischemia in rats. Brain Res. 2001;922(2):223-8.
187. Touret N, Tanneur V, Godart H, Seidler R, Taki N, Burger E, et al. Characterization of sabiporide, a new specific NHE-1 inhibitor exhibiting slow dissociation kinetics and cardioprotective effects. European journal of pharmacology. 2003;459(2-3):151-8.
188. Park HS, Lee BK, Park S, Kim SU, Lee SH, Baik EJ, et al. Effects of sabiporide, a specific Na+/H+ exchanger inhibitor, on neuronal cell death and brain ischemia. Brain Res. 2005;1061(1):67-71.
189. Suzuki Y, Matsumoto Y, Ikeda Y, Kondo K, Ohashi N, Umemura K. SM-20220, a Na(+)/H(+) exchanger inhibitor: effects on ischemic brain damage through edema and neutrophil accumulation in a rat middle cerebral artery occlusion model. Brain Res. 2002;945(2):242-8.
190. Kochanek PM, Hallenbeck JM. Polymorphonuclear leukocytes and monocytes/macrophages in the pathogenesis of cerebral ischemia and stroke. Stroke. 1992;23(9):1367-79.
191. Matsuo Y, Kihara T, Ikeda M, Ninomiya M, Onodera H, Kogure K. Role of Neutrophils in Radical Production during Ischemia and Reperfusion of the Rat Brain: Effect of Neutrophil Depletion on Extracellular Ascorbyl Radical Formation. Journal of Cerebral Blood Flow & Metabolism. 1995;15(6):941-7.
192. Horikawa N, Kuribayashi Y, Matsui K, Kawamura N, Ohashi N. Na+/H+ exchange inhibitor SM-20220 attenuates leukocyte adhesion induced by ischemia-reperfusion. Journal of cardiovascular pharmacology. 2001;37(6):668-77.
193. Horikawa N, Kuribayashi Y, Itoh N, Nishioka M, Matsui K, Kawamura N, et al. Na+/H+ exchange inhibitor SM-20220 improves endothelial dysfunction induced by ischemia-reperfusion. Japanese journal of pharmacology. 2001;85(3):271-7.
194. Tomita M, Fukuuchi Y. Leukocytes, macrophages and secondary brain damage following cerebral ischemia. Acta Neurochir Suppl. 1996;66:32-9.
195. del Zoppo GJ, Schmid-Schönbein GW, Mori E, Copeland BR, Chang CM. Polymorphonuclear leukocytes occlude capillaries following middle cerebral artery occlusion and reperfusion in baboons. Stroke. 1991;22(10):1276-83.

196. Shi Y, Chanana V, Watters JJ, Ferrazzano P, Sun D. Role of sodium/hydrogen exchanger isoform 1 in microglial activation and proinflammatory responses in ischemic brains. J Neurochem. 2011;119(1):124-35.
197. Cengiz P, Kleman N, Uluc K, Kendigelen P, Hagemann T, Akture E, et al. Inhibition of Na+/H+ exchanger isoform 1 is neuroprotective in neonatal hypoxic ischemic brain injury. Antioxidants & redox signaling. 2011;14(10):1803-13.
198. Bondarenko A, Chesler M. Rapid astrocyte death induced by transient hypoxia, acidosis, and extracellular ion shifts. Glia. 2001;34(2):134-42.
199. Bondarenko A, Svichar N, Chesler M. Role of Na+-H+ and Na+-Ca2+ exchange in hypoxia-related acute astrocyte death. Glia. 2005;49(1):143-52.
200. Mellergard PE, Ouyang YB, Siesjo BK. The regulation of intracellular pH in cultured astrocytes and neuroblastoma cells, and its dependence on extracellular pH in a HCO3-free solution. Canadian journal of physiology and pharmacology. 1992;70 Suppl:S293-300.
201. Castella M, Buckberg GD, Tan Z. Neurologic preservation by Na+-H+ exchange inhibition prior to 90 minutes of hypothermic circulatory arrest. The Annals of thoracic surgery. 2005;79(2):646-54; discussion -54.
202. Phillis JW, Ren J, O'Regan MH. Inhibition of Na(+)/H(+) exchange by 5-(N-ethyl-N-isopropyl)-amiloride reduces free fatty acid efflux from the ischemic reperfused rat cerebral cortex. Brain Res. 2000;884(1--2):155-62.
203. Gerhardt SC, Boast CA. Motor activity changes following cerebral ischemia in gerbils are correlated with the degree of neuronal degeneration in hippocampus. Behav Neurosci. 1988;102(2):301-3, 28.
204. Kuribayashi Y, Itoh N, Horikawa N, Ohashi N. SM-20220, a potent Na+/H+ exchange inhibitor, improves consciousness recovery and neurological outcome following transient cerebral ischaemia in gerbils. The Journal of pharmacy and pharmacology. 2000;52(4):441-4.
205. Pilitsis JG, Diaz FG, O'Regan MH, Phillis JW. Inhibition of Na(+)/H(+) exchange by SM-20220 attenuates free fatty acid efflux in rat cerebral cortex during ischemia-reperfusion injury. Brain Res. 2001;913(2):156-8.
206. Robertson NJ, Kato T, Bainbridge A, Chandrasekaran M, Iwata O, Kapetanakis A, et al. Methyl-isobutyl amiloride reduces brain Lac/NAA, cell death and microglial activation in a perinatal asphyxia model. J Neurochem. 2013;124(5):645-57.
207. van Rooij LG, Toet MC, van Huffelen AC, Groenendaal F, Laan W, Zecic A, et al. Effect of treatment of subclinical neonatal seizures detected with aEEG: randomized, controlled trial. Pediatrics. 2010;125(2):e358-66.
208. McBride MC, Laroia N, Guillet R. Electrographic seizures in neonates correlate with poor neurodevelopmental outcome. Neurology. 2000;55(4):506-13.
209. Lingwood BE, Dunster KR, Healy GN, Ward LC, Colditz PB. Cerebral impedance and neurological outcome following a mild or severe hypoxic/ischemic episode in neonatal piglets. Brain Res. 2003;969(1-2):160-7.
210. Haynes RL, Baud O, Li J, Kinney HC, Volpe JJ, Folkerth DR. Oxidative and nitrative injury in periventricular leukomalacia: a review. Brain pathology (Zurich, Switzerland). 2005;15(3):225-33.
211. Silverstein FS, Jensen FE. Neonatal seizures. Ann Neurol. 2007;62(2):112-20.
212. Lindstrom K, Hallberg B, Blennow M, Wolff K, Fernell E, Westgren M. Moderate neonatal encephalopathy: pre- and perinatal risk factors and long-term outcome. Acta obstetricia et gynecologica Scandinavica. 2008;87(5):503-9.

213. Bjorkman ST, Miller SM, Rose SE, Burke C, Colditz PB. Seizures are associated with brain injury severity in a neonatal model of hypoxia-ischemia. Neuroscience. 2010;166(1):157-67.
214. Stolp H, Neuhaus A, Sundramoorthi R, Molnar Z. The Long and the Short of it: Gene and Environment Interactions During Early Cortical Development and Consequences for Long-Term Neurological Disease. Frontiers in psychiatry. 2012;3:50.
215. Rennie JM, Boylan GB. Neonatal seizures and their treatment. Current opinion in neurology. 2003;16(2):177-81.
216. Evans DJ, Levene MI, Tsakmakis M. Anticonvulsants for preventing mortality and morbidity in full term newborns with perinatal asphyxia. The Cochrane database of systematic reviews. 2007(3):CD001240.
217. Rennie J, Boylan G. Treatment of neonatal seizures. Arch Dis Child Fetal Neonatal Ed. 2007;92(2):F148-50.
218. Azzopardi D, Robertson NJ, Kapetanakis A, Griffiths J, Rennie JM, Mathieson SR, et al. Anticonvulsant effect of xenon on neonatal asphyxial seizures. Arch Dis Child Fetal Neonatal Ed. 2013;98(5):F437-F9.
219. Kwon JM, Guillet R, Shankaran S, Laptook AR, McDonald SA, Ehrenkranz RA, et al. Clinical seizures in neonatal hypoxic-ischemic encephalopathy have no independent impact on neurodevelopmental outcome: secondary analyses of data from the neonatal research network hypothermia trial. Journal of child neurology. 2011;26(3):322-8.
220. Poland R, Freeman R. American Academy of Pediatrics,
and American College of Obstetricians and Gynecologists, (2002),
Relationship between perinatal factors and neurologic outcome, In:
Guidelines for Perinatal Care. Elk Grove Village, IL,1992. Poland, R. and Freeman, R. (eds.), American Academy of Pediatrics2002. 221-4 p.
221. Salhab WA, Wyckoff MH, Laptook AR, Perlman JM. Initial hypoglycemia and neonatal brain injury in term infants with severe fetal acidemia. Pediatrics. 2004;114(2):361-6.
222. Shalak L, Perlman JM. Hypoxic-ischemic brain injury in the term infant-current concepts. Early Hum Dev. 2004;80(2):125-41.
223. Siesjo BK. Cell damage in the brain: a speculative synthesis. J Cereb Blood Flow Metab. 1981;1(2):155-85.
224. Chesler M. The regulation and modulation of pH in the nervous system. Progress in neurobiology. 1990;34(5):401-27.
225. Kaila K. Ionic basis of GABAA receptor channel function in the nervous system. Progress in neurobiology. 1994;42(4):489-537.
226. Tombaugh GC, Somjen GG. Effects of extracellular pH on voltage-gated Na+, K+ and Ca2+ currents in isolated rat CA1 neurons. The Journal of physiology. 1996;493 (Pt 3):719-32.
227. Erecinska M, Deas J, Silver IA. The effect of pH on glycolysis and phosphofructokinase activity in cultured cells and synaptosomes. J Neurochem. 1995;65(6):2765-72.
228. Rehncrona S, Rosen I, Siesjo BK. Excessive cellular acidosis: an important mechanism of neuronal damage in the brain? Acta physiologica Scandinavica. 1980;110(4):435-7.
229. Ruusuvuori E, Kirilkin I, Pandya N, Kaila K. Spontaneous network events driven by depolarizing GABA action in neonatal hippocampal slices are not attributable to deficient mitochondrial energy metabolism. J Neurosci. 2010;30(46):15638-42.
230. Tang CM, Dichter M, Morad M. Modulation of the N-methyl-D-aspartate channel by extracellular H+. Proc Natl Acad Sci U S A. 1990;87(16):6445-9.
231. Tombaugh GC, Somjen GG. Differential sensitivity to intracellular pH among high- and low-threshold Ca2+ currents in isolated rat CA1 neurons. J Neurophysiol. 1997;77(2):639-53.

232. Towfighi J, Mauger D, Vannucci RC, Vannucci SJ. Influence of age on the cerebral lesions in an immature rat model of cerebral hypoxia-ischemia: a light microscopic study. Brain research Developmental brain research. 1997;100(2):149-60.
233. Simon RP, Niro M, Gwinn R. Brain acidosis induced by hypercarbic ventilation attenuates focal ischemic injury. The Journal of pharmacology and experimental therapeutics. 1993;267(3):1428-31.
234. Vannucci RC, Towfighi J, Brucklacher RM, Vannucci SJ. Effect of extreme hypercapnia on hypoxic-ischemic brain damage in the immature rat. Pediatr Res. 2001;49(6):799-803.
235. Schuchmann S, Schmitz D, Rivera C, Vanhatalo S, Salmen B, Mackie K, et al. Experimental febrile seizures are precipitated by a hyperthermia-induced respiratory alkalosis. Nat Med. 2006;12(7):817-23.
236. El-Dib M, Szakmar E, Chakkarapani E, Aly H. Challenges in respiratory management during therapeutic hypothermia for neonatal encephalopathy. Semin Fetal Neonatal Med. 2021;26(4):101263.
237. Pappas A, Shankaran S, Laptook AR, Langer JC, Bara R, Ehrenkranz RA, et al. Hypocarbia and adverse outcome in neonatal hypoxic-ischemic encephalopathy. J Pediatr. 2011;158(5):752-8.e1.
238. Lingappan K, Kaiser JR, Srinivasan C, Gunn AJ. Relationship between PCO2 and unfavorable outcome in infants with moderate-to-severe hypoxic ischemic encephalopathy. Pediatr Res. 2016;80(2):204-8.
239. Szakmar E, Munster C, El-Shibiny H, Jermendy A, Inder T, El-Dib M. Hypocapnia in early hours of life is associated with brain injury in moderate to severe neonatal encephalopathy. J Perinatol. 2022;42(7):892-7.
240. Lopez Laporte MA, Wang H, Sanon PN, Barbosa Vargas S, Maluorni J, Rampakakis E, et al. Association between hypocapnia and ventilation during the first days of life and brain injury in asphyxiated newborns treated with hypothermia. J Matern Fetal Neonatal Med. 2019;32(8):1312-20.
241. Molloy EJ, Cummins EP. Carbon dioxide as a drug in neonatology. Pediatr Res. 2021;89(5):1049-50.
242. Szakmar E, Kovacs K, Meder U, Bokodi G, Andorka C, Lakatos A, et al. Neonatal encephalopathy therapy optimization for better neuroprotection with inhalation of CO(2): the HENRIC feasibility and safety trial. Pediatr Res. 2020;87(6):1025-32.
243. Helmy MM, Ruusuvuori E, Watkins PV, Voipio J, Kanold PO, Kaila K. Acid extrusion via blood-brain barrier causes brain alkalosis and seizures after neonatal asphyxia. Brain. 2012;135(Pt 11):3311-9.
244. Higgins RD, Raju T, Edwards AD, Azzopardi DV, Bose CL, Clark RH, et al. Hypothermia and other treatment options for neonatal encephalopathy: an executive summary of the Eunice Kennedy Shriver NICHD workshop. J Pediatr. 2011;159(5):851-8 e1.
245. Zhou ZQ, Willis JS. Differential effects of cooling in hibernator and nonhibernator cells: Na permeation. Am J Physiol. 1989;256(1 Pt 2):R49-55.
246. Plesnila N, Muller E, Guretzki S, Ringel F, Staub F, Baethmann A. Effect of hypothermia on the volume of rat glial cells. The Journal of physiology. 2000;523 Pt 1:155-62.
247. Hoshino K, Avkiran M. Effects of moderate hypothermia on sarcolemmal Na(+)/H(+) exchanger activity and its inhibition by cariporide in cardiac ventricular myocytes. British journal of pharmacology. 2001;134(7):1587-95.
248. Yamauchi T, Ichikawa H, Sawa Y, Fukushima N, Kagisaki K, Maeda K, et al. The contribution of Na+/H+ exchange to ischemia-reperfusion injury after hypothermic cardioplegic arrest. The Annals of thoracic surgery. 1997;63(4):1107-12.
249. Sun Q, Sever P. Amiloride: A review. J Renin Angiotensin Aldosterone Syst. 2020;21(4):1470320320975893.

250. Porte-Thomé F, Nagaraju K, Yu Q, Tatem K, Bkaily G, Scholz W, et al. Development of Rimeporide, a sodium-hydrogen exchanger (NHE-1) inhibitor, for patients with Duchenne muscular dystrophy. Neuromuscular Disorders. 2015;25:S259-S60.
251. Previtali SC, Gidaro T, Díaz-Manera J, Zambon A, Carnesecchi S, Roux-Lombard P, et al. Rimeporide as a first- in-class NHE-1 inhibitor: Results of a phase Ib trial in young patients with Duchenne Muscular Dystrophy. Pharmacol Res. 2020;159:104999.
252. Avkiran M, Marber MS. Na(+)/H(+) exchange inhibitors for cardioprotective therapy: progress, problems and prospects. J Am Coll Cardiol. 2002;39(5):747-53.
253. Alle H, Roth A, Geiger JR. Energy-efficient action potentials in hippocampal mossy fibers. Science (New York, NY). 2009;325(5946):1405-8.
254. Magistretti PJ, Allaman I. A cellular perspective on brain energy metabolism and functional imaging. Neuron. 2015;86(4):883-901.
255. MJ C. Chapter 5, Control of Cerebral Blood Flow. The Cerebral Circulation. San Rafael (CA): Morgan & Claypool Life Sciences; 2009.
256. Paulson OB, Strandgaard S, Edvinsson L. Cerebral autoregulation. Cerebrovasc Brain Metab Rev. 1990;2(2):161-92.
257. C. I. Cerebral circulatory dysregulation in ischemia In: Ginsberg MD BJE, editor. Cerebrovascular Diseases: Cambridge, MA: Blackwell Science; 1998. p. 319–32.
258. Yoon S, Zuccarello M, Rapoport RM. pCO(2) and pH regulation of cerebral blood flow. Front Physiol. 2012;3:365.
259. Haddy FJ, Vanhoutte PM, Feletou M. Role of potassium in regulating blood flow and blood pressure. American Journal of Physiology-Regulatory, Integrative and Comparative Physiology. 2006;290(3):R546-R52.
260. Nippert AR, Chiang PP, Del Franco AP, Newman EA. Astrocyte regulation of cerebral blood flow during hypoglycemia. J Cereb Blood Flow Metab. 2022;42(8):1534-46.
261. Blood AB, Hunter CJ, Power GG. The role of adenosine in regulation of cerebral blood flow during hypoxia in the near-term fetal sheep. The Journal of physiology. 2002;543(Pt 3):1015-23.
262. O'Regan M. Adenosine and the regulation of cerebral blood flow. Neurological Research. 2005;27(2):175-81.
263. Koep JL, Taylor CE, Coombes JS, Bond B, Ainslie PN, Bailey TG. Autonomic control of cerebral blood flow: fundamental comparisons between peripheral and cerebrovascular circulations in humans. The Journal of physiology. 2022;600(1):15-39.
264. Pryds O. Control of cerebral circulation in the high-risk neonate. Ann Neurol. 1991;30(3):321-9.
265. Ioroi T, Peeters-Scholte C, Post I, Leusink C, Groenendaal F, van Bel F. Changes in cerebral haemodynamics, regional oxygen saturation and amplitude-integrated continuous EEG during hypoxia-ischaemia and reperfusion in newborn piglets. Experimental brain research Experimentelle Hirnforschung Experimentation cerebrale. 2002;144(2):172-7.
266. Sokolska M PM, Uria-Avellanal C, Bainbridge A, Cady E, Thomas D, Robertson NJ, Golay X. Combined use of arterial spin labeling and MRS to determine the severity of injury in neonates with hypoxic-ischaemic encephalopathy Proceedings of the 22nd Annual Meeting of ISMRM; 2014.
267. Greisen G. Cerebral blood flow and oxygenation in infants after birth asphyxia. Clinically useful information? Early Hum Dev. 2014;90(10):703-5.
268. Lassen NA. The luxury-perfusion syndrome and its possible relation to acute metabolic acidosis localised within the brain. Lancet. 1966;2(7473):1113-5.
269. Grant PE, Yu D. Acute injury to the immature brain with hypoxia with or without hypoperfusion. Magn Reson Imaging Clin N Am. 2006;14(2):271-85.

270. Rosenbaum JL, Almli CR, Yundt KD, Altman D, Powers WJ. Higher neonatal cerebral blood flow correlates with worse childhood neurologic outcome. Neurology. 1997;49:1035 - 41.
271. Golay X, Guenther M. Arterial spin labelling: final steps to make it a clinical reality. MAGMA. 2012;25(2):79-82.
272. Petersen ET, Zimine I, Ho YC, Golay X. Non-invasive measurement of perfusion: a critical review of arterial spin labelling techniques. Br J Radiol. 2006;79(944):688-701.
273. Dai W, Garcia D, de Bazelaire C, Alsop DC. Continuous flow-driven inversion for arterial spin labeling using pulsed radio frequency and gradient fields. Magn Reson Med. 2008;60(6):1488-97.
274. Wintermark P, Hansen A, Gregas MC, Soul J, Labrecque M, Robertson RL, et al. Brain perfusion in asphyxiated newborns treated with therapeutic hypothermia. AJNR Am J Neuroradiol. 2011;32(11):2023-9.
275. Shi H, Song D, Zhang YX, Qi M, Li HS, Tan ZS, et al. [Analysis of arterial spin labeling in 33 patients with hypoxic ischemic encephalopathy]. Zhonghua Er Ke Za Zhi. 2012;50(2):131-5.
276. Massaro AN, Bouyssi-Kobar M, Chang T, Vezina LG, du Plessis AJ, Limperopoulos C. Brain perfusion in encephalopathic newborns after therapeutic hypothermia. AJNR Am J Neuroradiol. 2013;34(8):1649-55.
277. Ordidge R, Helpern J. Image Guided Volume Selective Spectroscopy: A Comparison of Techniques for In-Vivo 31P NMR Spectroscopy of Human Brain. In-Vivo Magnetic Resonance Spectroscopy II: Localization and Spectral Editing: Springer; 1992. p. 103-17.
278. T FTaN. Understanding Spectra of 31P MRS and 1H MRS. In: Igata A AT, Fujimoto T, editor. MRS of the Brain and Neurological Disorders. Tokyo, Japan: CRC Press; 2000. p. 40.
279. T.L. J. Chapter 1: Fundamentals of NMR. In: Society B, editor. Biophysics Textbook Online (BTOL): https://www.biophysics.org/Portals/1/PDFs/Education/james.pdf; 1998.
280. Osorio-Garcia MI, Sima DM, Nielsen FU, Dresselaers T, Leuven FV, Himmelreich U, et al. Quantification of in vivo 1 H magnetic resonance spectroscopy signals with baseline and lineshape estimation. Measurement Science and Technology. 2011;22(11):114011.
281. Vanhamme L, van den Boogaart A, Van Huffel S. Improved method for accurate and efficient quantification of MRS data with use of prior knowledge. J Magn Reson. 1997;129(1):35-43.
282. Pettegrew JW, Withers G, Panchalingam K, Post JF. Considerations for brain pH assessment by 31P NMR. Magn Reson Imaging. 1988;6(2):135-42.
283. Stubbs M, Bhujwalla ZM, Tozer GM, Rodrigues LM, Maxwell RJ, Morgan R, et al. An assessment of 31P MRS as a method of measuring pH in rat tumours. NMR Biomed. 1992;5(6):351-9.
284. Wilson M, Reynolds G, Kauppinen RA, Arvanitis TN, Peet AC. A constrained least-squares approach to the automated quantitation of in vivo ^{1}H magnetic resonance spectroscopy data. Magn Reson Med. 2011;65(1):1-12.
285. Kreis R, Hofmann L, Kuhlmann B, Boesch C, Bossi E, Hüppi PS. Brain metabolite composition during early human brain development as measured by quantitative in vivo 1H magnetic resonance spectroscopy. Magn Reson Med. 2002;48(6):949-58.
286. Choi C, Coupland NJ, Kalra S, Bhardwaj PP, Malykhin N, Allen PS. Proton spectral editing for discrimination of lactate and threonine 1.31 ppm resonances in human brain in vivo. Magn Reson Med. 2006;56(3):660-5.
287. Williams G, Smith M. Application of the accurate assessment of intracellular magnesium and pH from the 31P shifts of ATP to cerebral hypoxia-ischemia in neonatal rat. Magn Reson Med. 1995;33:853-7.

288. Ferrazzano P, Shi Y, Manhas N, Wang Y, Hutchinson B, Chen X, et al. Inhibiting the Na+/H+ exchanger reduces reperfusion injury: a small animal MRI study. Front Biosci (Elite Ed). 2011;3:81-8.
289. Horikawa N, Nishioka M, Itoh N, Kuribayashi Y, Matsui K, Ohashi N. The Na(+)/H(+) exchanger SM-20220 attenuates ischemic injury in in vitro and in vivo models. Pharmacology. 2001;63(2):76-81.
290. Pospelov AS, Ala-Kurikka T, Kurki S, Voipio J, Kaila K. Carbonic anhydrase inhibitors suppress seizures in a rat model of birth asphyxia. Epilepsia. 2021;62(8):1971-84.
291. Shankaran S, Barnes PD, Hintz SR, Laptook AR, Zaterka-Baxter KM, McDonald SA, et al. Brain injury following trial of hypothermia for neonatal hypoxic-ischaemic encephalopathy. Arch Dis Child Fetal Neonatal Ed. 2012;97(6):F398-404.
292. Hellström-Westas L, Rosén I, Svenningsen N. Predictive value of early continuous amplitude integrated EEG recordings on outcome after severe birth asphyxia in full term infants. Arch Dis Child Fetal Neonatal Ed. 1995;72(1):F34-8.
293. Finder M, Boylan GB, Twomey D, Ahearne C, Murray DM, Hallberg B. Two-Year Neurodevelopmental Outcomes After Mild Hypoxic Ischemic Encephalopathy in the Era of Therapeutic Hypothermia. JAMA Pediatrics. 2020;174(1):48-55.
294. N B. The Bayley Scales of Infant and Toddler Development. 3rd Edition. San Antonio TX: Harcourt Assessment, Inc, 2006.
295. Johnson S, Moore T, Marlow N. Using the Bayley-III to assess neurodevelopmental delay: which cut-off should be used? Pediatr Res. 2014;75(5):670-4.
296. Del Rosario C, Slevin M, Molloy EJ, Quigley J, Nixon E. How to use the Bayley Scales of Infant and Toddler Development. Arch Dis Child Educ Pract Ed. 2021;106(2):108-12.
297. Kim TK, Park JH. More about the basic assumptions of t-test: normality and sample size. Korean J Anesthesiol. 2019;72(4):331-5.
298. Vetter TR, Mascha EJ. Unadjusted Bivariate Two-Group Comparisons: When Simpler is Better. Anesthesia and analgesia. 2018;126(1):338-42.
299. Buchli R, Martin E, Boesiger P, Rumpel H. Developmental changes of phosphorus metabolite concentrations in the human brain: a 31P magnetic resonance spectroscopy study in vivo. Pediatr Res. 1994;35(4 Pt 1):431-5.
300. Shi XF, Carlson PJ, Kim TS, Sung YH, Hellem TL, Fiedler KK, et al. Effect of altitude on brain intracellular pH and inorganic phosphate levels. Psychiatry Res. 2014;222(3):149-56.
301. Rocha MA, Crockett DP, Wong LY, Richardson JR, Sonsalla PK. Na(+)/H(+) exchanger inhibition modifies dopamine neurotransmission during normal and metabolic stress conditions. J Neurochem. 2008;106(1):231-43.
302. Chalak LF, DuPont TL, Sánchez PJ, Lucke A, Heyne RJ, Morriss MC, et al. Neurodevelopmental outcomes after hypothermia therapy in the era of Bayley-III. J Perinatol. 2014;34(8):629-33.
303. Finder M, Boylan GB, Twomey D, Ahearne C, Murray DM, Hallberg B. Two-Year Neurodevelopmental Outcomes After Mild Hypoxic Ischemic Encephalopathy in the Era of Therapeutic Hypothermia. JAMA Pediatr. 2020;174(1):48-55.
304. Clarke DD SL. Circulation and energy metabolism of the brain. Basic Neurochemistry Siegel G, Agrano BV, Albers RW, Molino PV. (Eds.) New York: Raven Press1989. p. 565-90.
305. Greisen G. Cerebral autoregulation in preterm infants. How to measure it--and why care? J Pediatr. 2014;165(5):885-6.
306. Fox PT, Raichle ME, Mintun MA, Dence C. Nonoxidative glucose consumption during focal physiologic neural activity. Science (New York, NY). 1988;241(4864):462-4.

307. Buxton RB, Frank LR, Wong EC, Siewert B, Warach S, Edelman RR. A general kinetic model for quantitative perfusion imaging with arterial spin labeling. Magn Reson Med. 1998;40(3):383-96.
308. Varela M, Hajnal JV, Petersen ET, Golay X, Merchant N, Larkman DJ. A method for rapid in vivo measurement of blood T1. NMR Biomed. 2011;24(1):80-8.
309. Lu H, Clingman C, Golay X, van Zijl PC. Determining the longitudinal relaxation time (T1) of blood at 3.0 Tesla. Magn Reson Med. 2004;52(3):679-82.
310. Kuklisova-Murgasova M, Aljabar P, Srinivasan L, Counsell SJ, Doria V, Serag A, et al. A dynamic 4D probabilistic atlas of the developing brain. Neuroimage. 2011;54(4):2750-63.
311. Gousias IS, Edwards AD, Rutherford MA, Counsell SJ, Hajnal JV, Rueckert D, et al. Magnetic resonance imaging of the newborn brain: manual segmentation of labelled atlases in term-born and preterm infants. Neuroimage. 2012;62(3):1499-509.
312. Cardoso MJ, Melbourne A, Kendall GS, Modat M, Robertson NJ, Marlow N, et al. AdaPT: An adaptive preterm segmentation algorithm for neonatal brain MRI. Neuroimage. 2013;65:97-108.
313. Hugg JW, Duijn JH, Matson GB, Maudsley AA, Tsuruda JS, Gelinas DF, et al. Elevated lactate and alkalosis in chronic human brain infarction observed by 1H and 31P MR spectroscopic imaging. J Cereb Blood Flow Metab. 1992;12(5):734-44.
314. O'Gorman Tuura R KR, Brotschi B, Sabandal C, Hagmann C, Latal B. Hyperperfusion on arterial spin labelling is associated with cognitive impairment in infants with neonatal hypoxic ischemic encephalopathy. ISMRM 2022 (presentation 0612); London2022.
315. Wang J, Licht DJ, Silvestre DW, Detre JA. Why perfusion in neonates with congenital heart defects is negative--technical issues related to pulsed arterial spin labeling. Magn Reson Imaging. 2006;24(3):249-54.
316. Reynolds EO, McCormick DC, Roth SC, Edwards AD, Wyatt JS. New non-invasive methods for the investigation of cerebral oxidative metabolism and haemodynamics in newborn infants. Ann Med. 1991;23(6):681-6.
317. Low JA. Intrapartum fetal asphyxia: definition, diagnosis, and classification. Am J Obstet Gynecol. 1997;176(5):957-9.
318. Low JA, Lindsay BG, Derrick EJ. Threshold of metabolic acidosis associated with newborn complications. Am J Obstet Gynecol. 1997;177(6):1391-4.
319. Penrice J, Lorek A, Cady EB, Amess PN, Wylezinska M, Cooper CE, et al. Proton magnetic resonance spectroscopy of the brain during acute hypoxia-ischemia and delayed cerebral energy failure in the newborn piglet. Pediatr Res. 1997;41(6):795-802.
320. Goldman SA, Pulsinelli WA, Clarke WY, Kraig RP, Plum F. The effects of extracellular acidosis on neurons and glia in vitro. J Cereb Blood Flow Metab. 1989;9(4):471-7.
321. Bender TM, Johnston JA, Manepalli AN, Mink RB. Association between brain tissue pH and brain injury during asphyxia in piglets. Resuscitation. 2003;59(2):243-54.
322. LaManna JC. Hypoxia/ischemia and the pH paradox. Adv Exp Med Biol. 1996;388:283-92.
323. Hoffman TL, LaManna JC, Pundik S, Selman WR, Whittingham TS, Ratcheson RA, et al. Early reversal of acidosis and metabolic recovery following ischemia. J Neurosurg. 1994;81(4):567-73.
324. Lorek A, Takei Y, Cady E, Wyatt J, Penrice J, Edwards A, et al. Delayed ("secondary") cerebral energy failure after acute hypoxia-ischemia in the newborn piglet: continuous 48-hour studies by phosphorus magnetic resonance spectroscopy. Pediatr Res. 1994;36:699-706.
325. Ezzati M, Broad K, Kawano G, Faulkner S, Hassell J, Fleiss B, et al. Pharmacokinetics of dexmedetomidine combined with therapeutic hypothermia in a piglet asphyxia model. Acta Anaesthesiol Scand. 2014;58(6):733-42.

326. Robertson NJ, Faulkner S, Fleiss B, Bainbridge A, Andorka C, Price D, et al. Melatonin augments hypothermic neuroprotection in a perinatal asphyxia model. Brain. 2012;136(1):90-105.
327. Vanhamme L, van den Boogaart A, van Huffel S. Improved method for accurate and efficient quantification of MRS data with use of prior knowledge. J Magn Reson Imaging. 1997;129:35-43.
328. Mandel P, Edel-Harth S. Free nucleotides in the rat brain during post-natal development. J Neurochem. 1966;13(7):591-5.
329. Faulkner S, Bainbridge A, Kato T, Chandrasekaran M, Hristova M, Liu M, et al. Xenon augmented hypothermia reduces early lactate/NAA and cell death in Perinatal Asphyxia. Ann Neurol. 2011;70(1):133-50.
330. Corbett RJ, Laptook AR, Nunnally RL. The use of the chemical shift of the phosphomonoester P-31 magnetic resonance peak for the determination of intracellular pH in the brains of neonates. Neurology. 1987;37(11):1771-9.
331. Bainbridge A, Tachtsidis I, Faulkner SD, Price D, Zhu T, Baer E, et al. Brain mitochondrial oxidative metabolism during and after cerebral hypoxia-ischemia studied by simultaneous phosphorus magnetic-resonance and broadband near-infrared spectroscopy. Neuroimage. 2014;102 Pt 1:173-83.
332. Cady EB, Iwata O, Bainbridge A, Wyatt JS, Robertson NJ. Phosphorus magnetic resonance spectroscopy 2 h after perinatal cerebral hypoxia-ischemia prognosticates outcome in the newborn piglet. J Neurochem. 2008;107(4):1027-35.

Appendix:

UCL Elizabeth Garrett Anderson Institute for Women's Health

University College London Hospitals NHS Foundation Trust

THE UCH BABY BRAIN STUDY

Parent information leaflet

Please read this leaflet carefully – it explains the research study we are currently doing and asks for your help. Please ask the Doctor or Nurse who explained the study if you require any further information.

Taking part is purely voluntary and whether or not you agree to join the study will not change the care you get in any way

15 March 2013 (Version. 4.1)

The Baby Brain Study at UCH

We are sorry to approach you at such a difficult time following the birth of your baby. As you will have been told it seems that your baby may have suffered from a lack of oxygen around the time of birth (sometimes called birth asphyxia) which has led to your baby's current treatment. We do not always know what has caused this, but we know that a lack of oxygen to the baby's brain can cause injury and because of this there is a chance that your baby could have a disability in the future. Cooling your baby's body and brain (called therapeutic hypothermia) improves the chances of improved outcome. Your baby may be part of a clinical trial to confirm whether administration of Xenon in addition to hypothermia improves the chances of having a better outcome.

Here at UCH for many years we have had a very active research programme to help make our care be the best it can be. We have been studying the development of brain injury in such circumstances using close monitoring of how the brain is working and also magnetic resonance imaging (which gives us a picture of the brain (MRI) and tells us about the levels of chemicals in the brain, which we call MRS or magnetic resonance spectroscopy). These studies give us the information that we use to tell you about your baby's condition. In addition, our better understanding of the mechanisms and development of brain injury has led to new treatments to protect the brain.

The detail of the pictures we get using magnetic resonance imaging (MRI) is better than all other forms of imaging such as using ultrasound. In our normal care for all babies, we assess how your baby is doing using:

- Daily examination by the doctor and nurse
- Continuous brain wave tracing (EEG or electroencephalography)
- Daily head ultrasound for at least 3 days
- MRI and MRS (see above)
- We then provide outpatient care for your baby for at least 2 years to check on development

In addition to these routine tests, we are asking your consent to do two extra things as part of our research programme:

- **Firstly, we would like to use a special light system called near infrared spectroscopy (NIRS); this is safe and simply involves shining a light against your babies' head. It is**

used in several centres to monitor the brain but we have developed the technique to use it alongside our routine EEG test.

- **Secondly we would like to make extra measurements while your baby is having the routine MRI scan.**

We believe this research may help your baby or others in the future.

What does the study mean for you and your baby?

- **Near infrared light spectroscopy**

  As well as the routine EEG, which is carried out with small sticky electrodes on the surface of the scalp (like for monitoring heart rate as shown in the picture on the left), we place two special probes, called optodes, against the scalp. These are very gentle and do not interfere with your baby's care.

  We cover them with a hat as you can see in the picture on the right below and then shine light against the scalp. We can detect this light and changes in how the light is scattered though the skull to tell us a lot about the way the brain and its circulation are working. We leave these in place for up to 5 days after birth.

  The technique is used widely across Europe to monitor the amount of oxygen in the brain but we wish to use it to tell us about the progression and recovery of the brain injury as well.

  This technique was first developed in babies in UCH many years ago and has taught us much about the way brain injury develops.

Baby with EEG monitoring (left) and NIRS probes (right).

- **<u>Extra measurements during MRI scans</u>**

  We usually perform an MRI scan around 5-14 days after birth when we are concerned about birth asphyxia. We wish to make some extra measurements at the end of the routine scan as long as your baby remains asleep and settled.

Usually, our scan takes about 45 minutes

Collecting our extra measurements takes about the same time if we can. This might mean that your baby is away from the Neonatal Unit for about 90 minutes compared to 1 hour normally.

The extra time will allow us to measure the amount of acid in the brain, to assess the blood flow within the brain and how much oxygen the brain is using.

We use a scanner (for the technically minded it is 3T Philips Achieva MR system) which is just over the bridge in the main hospital of UCH (about 150 metres from the unit). We use a very special incubator which is kept on the Neonatal Unit and has been made specially to avoid disturbing babies once they are away from the Neonatal unit (see picture right). At all times an experienced paediatrician and nurse will be with your baby when out of the unit and there is no need to move your baby from the incubator during the scan.

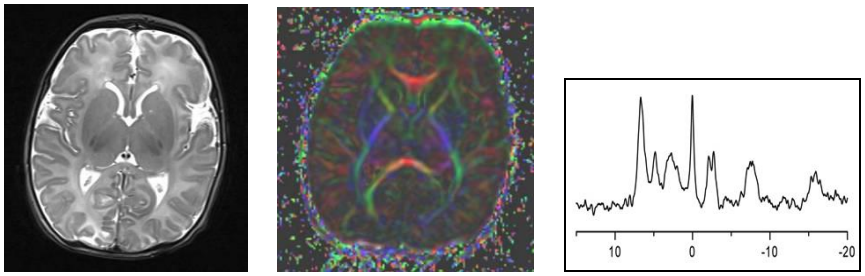

This is an example of some of the information we can collect from your baby's MRI/MRS scan; this information can help with understanding how your baby will develop. From left to right: MRI gives information on brain structure; Diffusion MRI is especially useful to find areas of injury; 31P MR Spectroscopy gives information about energy stores and recovery

Using these techniques, we wish to improve ways that we can accurately predict how your baby is likely to develop as early as possible. Every other aspect of you and your baby's care will be the same as any other baby with this condition. After going home, follow-up care will

be provided at your local hospital but we will continue to follow your baby's development in outpatients with the neurodevelopment team lead by Dr Angela Huertas.

In addition you will be invited to our 'BabyLab' where we have some special assessments that show us how babies learn, how they attend to things they see and how they behave with their mum and dad. These extra assessments are part of another study we are carrying out (led by Professor Neil Marlow) and we will ask your permission separately for this.

What do you need to do now?

After you have spoken to one of the research team and read this leaflet, please read and complete the consent form – the person talking to you about the study will also need to sign the consent form to confirm they have spoken to you about the study, so please don't sign the form until you are happy you know what the study entails.

Some Frequently Asked Questions:

Are there disadvantages or risks to taking part in the study?

As far as we know there are no risks associated with the extra measurements we propose to add to your baby's routine clinical care, other than the need to keep your baby longer in the scanner (40-45 min extra). A senior doctor and a nurse accompany your baby at all times and the scan is stopped if there are any problems. We will only do the extra measures if your baby is settled and stable after the clinical sequences. There are no risks as far as we know associated with either NIRS monitoring or with MRI scans in newborn babies, which have been used previously in other studies.

The participation is voluntary and you are free to withdraw at any time without giving any reason, without the medical care or legal rights of your baby being affected.

Are there any benefits to taking part?

This study may not be of any direct benefit to your baby, although we will use the information we get from the scans and assessments to tell you how we think your baby is progressing. If it seems to us that your baby needs extra support, we will discuss with you how we provide it.

We hope that the knowledge from this research will benefit infants with the same condition in the future.

How can you find out more about the study and about birth asphyxia?

At any time you can ask to speak to one of the team and discuss the study further.

Will my taking part in this study be kept confidential?

All information that is collected about you and your baby during the course of the research will be kept **strictly confidential**. Neither you nor your baby can be identified through the study results. All the data will be anonymised.

What will happen to the results of the research?

The results of this research will be described to other doctors at scientific meetings and will be published in medical (peer-reviewed) journals. No individual children or families will be identifiable in any of this material.

What happens to the data collected in the study?

All data are stored securely (as set out in the Data Protection Act) and not released to any third party without your explicit permission, being accessed only by authorised personnel involved in this study. Unless you give permission for us to use the records for further research or teaching they are destroyed after the results of the study have been published, but we would like to use the information in other studies we may do – in which case no personal information will be used.

Who can give me further information?

You can contact us by letter, telephone or email (see below) at any time and we will be very happy to answer any questions you may have.

You will still be attending appointments after discharge and the doctor there will be aware of the study and also able to answer questions.

All the consultants on the Neonatal Unit and not directly involved with the study are available to give you an independent view of the study if you would like to speak to someone else – the nurses looking after your baby will help you get in touch with your consultant.

Who is organising and funding the research?

The Study Director is Professor Nicola J Robertson.

Other key researchers working on the neonatal unit are Dr Giles Kendall and Dr Cristina Uria.

This study has a funding application to Action Medical Research.

In addition, the Wellcome Trust supports the research into EEG analysis and SPARKS the BabyLab. Some of the researchers are partly funded by the UCLH/UCL Clinical Biomedical Research Centre.

Who has reviewed the study?

The study was reviewed by a range of professionals during its development as we applied for funding and has been approved by the NRES Committee London - Bloomsbury (Reference 13/LO/0225) and is registered with the Research and Development Department of UCLH (Reference 13/0013).

Useful Contacts

Chief Investigator:

Professor Nicola J Robertson
020 7679 6060
n.robertson@ucl.ac.uk

UCL EGA Institute for Women's Health
Medical School Building
74 Huntley Street
London WC1E 6AU

Clinical Co-investigators:

Dr. Cristina Uria-Avellanal
Email: c.uria@ucl.ac.uk

Dr. Judith Meek
Tel: 02034478094 (Consultant's PA)
Email: judith.meek@uclh.nhs.uk

Dr. Giles Kendall
Tel: 02034478094 (Consultant's PA)
Email: g.kendall@ucl.ac.uk

What if there is a problem?

If you wish to complain, or have any concerns about any aspect of the way you have been approached or treated by members of staff you may have experienced due to your participation in the research*, National Health Service or UCL complaints mechanisms are available to you. Please ask your research doctor if you would like more information on this. In the unlikely event that you are harmed by taking part in this study, compensation may be available to you.*

If you suspect that the harm is the result of the Sponsor's (University College London) or the hospital's negligence then you may be able to claim compensation. After discussing with your research doctor, please make the claim in writing to Professor Nicola Robertson who is the Chief Investigator for the research and is based at UCL Institute for Women´s Health (see full address on previous page). The Chief Investigator will then pass the claim to the Sponsor's Insurers, via the Sponsor's office. You may have to bear the costs of the legal action initially, and you should consult a lawyer about this.

If you have a concern about any aspect of this study, you should ask to speak to a member of the study team who will do their best to answer your questions. If you remain unhappy or wish to complain formally, you can do this through the NHS Complaints Procedure. Details can be obtained from the hospital Patient Advice and Liaison Service on 020 34567898 ext 73018.

"NHS Indemnity does not offer no-fault compensation i.e. for non-negligent harm, and NHS bodies are unable to agree in advance to pay compensation for non-negligent harm."

Thank you for your help with this research

Neonatal Services

NNU Medical Secretaries

2nd Floor, North Wing

250 Euston Road

Project ID: 13/0013
REC Ref: 13/LO/0225

Patient Identification
Number for this trial: _____

Name of Researcher: Professor Nicola J Robertson

THE UCH BABY BRAIN STUDY

FORM FOR PARENTAL CONSENT

Please initial each box

1. I confirm that I have read and understand the information sheet dated 15 March 2013 (version. 4.1) for the above study. I have had the opportunity to consider the information, ask questions and have had these answered satisfactorily and have had these answered satisfactorily. ☐
2. I understand that the participation of my baby in this study (NIRS monitoring and extra sequences during MRI/MRS) is independent from other studies and I can withdraw from any of them separately at any time. ☐
3. I understand that the participation of my baby is voluntary and that I am free to withdraw at any time without giving any reason, without the medical care or legal rights of my baby being affected. ☐
4. I understand that relevant sections of my baby's medical notes and data collected during the study may be looked at by individuals from regulatory authorities or from the NHS Trust from the sponsor's representative from UCL, where it is relevant to my baby taking part in this research. I give permission for these individuals to have access to my baby's records. ☐
5. I agree that the NIRS, MRI/MRS and other MR sequences data, video recordings and EEG tracings can be used for further research and teaching purposes; the material will always be used anonymously, and my child will not be identifiable in the data used. ☐
6. I understand that I will be invited back for 3 assessments over the first year after my child was born and a last assessment will be performed at 2 years of age. ☐
7. I agree that my baby may take part in the above study. ☐

Name of Child:		
Name of Parent:	Date	Signature
Name of Person taking consent:	Date	Signature

3 copies: one to be retained by parent, one placed in the clinical notes, and one retained by the study office.
Version 4.1 15 March 2013

Guidelines for Neonatal 3T MRI Scanning

Appendix: Phosphorus-31 coil

V-XQ-030-01517

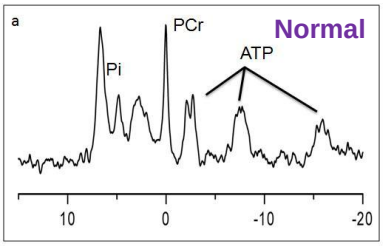

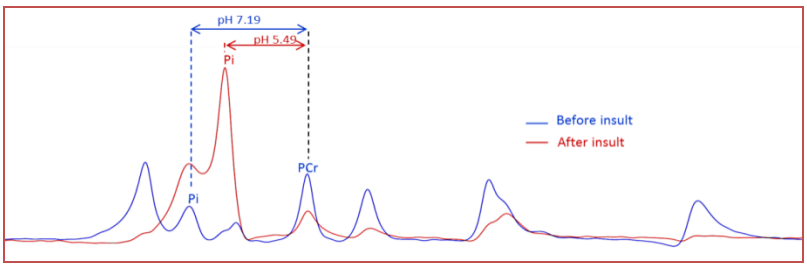

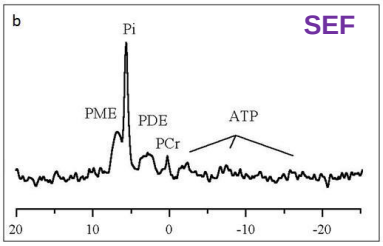

Cristina Uria-Avellanal Neonatal Neuroimaging Fellow

David Price Medical Physicist

Version 3: July 2015

Contents

1. General 3T MRI scanning guidelines

Please read the main "**Guideline for Neonatal 3T MRI scanning (Version 4, May 2012)**" for general advice regarding:

- Personnel and contact details
- Equipment and Bags
- Preparation of baby for Scan
- Scanning at 3.0 T UCLH podium 2
- Emergency Evacuation and Resuscitation
- Checklist for the Emergency Bad (Blue bag)
- MRI Patient Observation and Resuscitation paperwork
- Lammers LMT NoMag MRi Incubator
- BabyPac MRI Venrilator
- Braun Perfusor Space Syringe Pump
- Brain Infusomat Space Volumetric Pump
- Braun Space Station MRI Pump Docking Station
- Braun Clamp for Pumps (NB not MRI safe)

Neonatal Action Card – Putting out a crash call:

1. Telephone extension **2222**

2. When asked by operator, give the following information: **"Neonatal Team to 3T-MRI, main UCLH building, podium level 2"**

2. General information about Rapid ^{31}P Neonatal Head coil

a. Handling

This coil is a sensitive electronic device which has to be handled and used with appropriate care. Therefore, avoid any jolts or impacts which might have an effect on the device. **To transport the device please only carry its housing.**

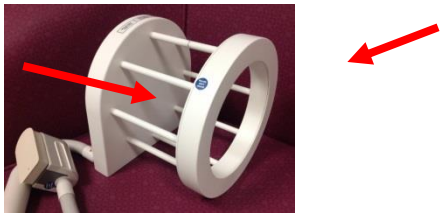

The cables and plugs connected to the device must also be treated with care. **The cables and plugs connected to the device and the trimmer bars must not be used to carry the device.**

b. Cleaning and disinfection

A moistened cloth can be used to clean the product using commercially available cleaning and disinfection solutions (e.g. alcohol-based). Do not use aldehyde or phenolic-based disinfectants. Do not use any rough or abrasive detergents, which could dissolve the surface of the housing or vanish. Although the electronic circuitry is protected against moisture, liquids should not be allowed to get into the device. Do not immerse the device. The device is not intended for sterilization.

c. Maintenance and Storage

Normal use and regular cleaning are normal maintenance requirements.

Store in a dry, cool place which is not subject to large temperature fluctuations and protect it against soiling and physical damage.

Conditions of storage and transport:

- Storage temperature: -25°C to +60°C
- Storage permissible relative humidity: 10-95%

d. Repair

Repairs may only be performed by Rapid GmbH Service or by a representative authorised by rapid GmbH.

3. Safety instructions

Classification of the Product

- Volume coil, transmit-receive; For 3.0 T Philips Achieva TX
- ^{31}P circular polarisation; Quadrature RF polarisation
- Adaptation to load: fixed tune, fixed match
- Frequency: 51.7 Hz
- Power:
    - Maximum peak: 3200 W
    - Maximum average: 10 W
- Dimensions: 200mm x 230mm x 230mm
    - Inner diameter: 170 mm
    - Outer diameter 230 mm
- Resonator length: 152 mm
- Mean coil diameter: 184 mm
- Length of connection cord: 2.8 m
- Weight: 3.25 kg

Conditions of use:

- **Patient weight:** Minimum **2.5 kg –** Maximum **10 kg**
- **For indoor use only**
- **Ambient conditions:**
    - **Working temperature range: 18-37 º C**
    - **Permissible relative humidity: 30-80%**
    - **Oxygen concentration: <25%**

      This is compatible with a ventilated baby on FiO2 ≤30%; or if free oxygen is given into the incubator, it should be ≤1.75 lpm.

Experiment checking FiO2 in the area of the coil:

	FiO2 reading in the area of the coil
1 hour with a baby ventilated with ETT on FiO2 28%	22%
15 min with free O2 into the incubator 1.75 lpm	25%
15 min with free O2 into the incubator 1.5 lpm	24.2%
15 min with free O2 into the incubator 1 lpm	23%
1 hour with free O2 into the incubator (<2 lpm)	28%
1 hour with free O2 into the incubator (3 lpm)	45%

4. Safety checks: Phantom work

The Rapid ^{31}P Neonatal head Coil has been tested on a suitable phantom (HPO4 85%, with load of NiSO4 hexahydrate 3.75gr + NaCl 5gr + 1000ml H2O) between February 6th and March 1st 2014; calibrating the coil and performing the commissioning test.

Safety checks were performed with an ATP phantom between March 19th and April 1st 2014 within the Lammers incubator for different temperature, humidiy and FiO2 conditions:

- Temperature: 27°C / 29°C / 31°C (which are the temperatures we normally set up the incubator when scanning babies)
- Humidity: 30% / 60% (we generally don't turn on the humidity but these are the reading usually when scanning a baby).
- FiO2 in the incubator: 21% / 25% (see above the guide to acknowledge how much is the FiO2 in the incubator for the amount and way of oxygen given).

The sequence was developed with an ATP phantom between February 25th and April 1st .

The coil is in good working order. And is safe to use within the Lammers incubator.

Any event of physical or other damage or malfunctions must be reported to Rapid GmbH without delay.

5. General Safety Instructions

Neonatal staff must observe babies undergoing constantly by means of personal monitoring (**Nonin Medical® 7500FO**, MR conditional monitoring which provides: HR and Saturation O2) and monitoring with equipment (temperature and humidity measurement) in such a way that in the event of an acute or imminent hazard immediate action can be taken.

Safety checks are common to the rest of the MRI examination:

- Check the baby for metal objects
- Only allow dry clothing
- Make sure there is sufficient distance between the subject and surface of the coil
- Try to avoid skin-to-skin contact between different parts of the body
- Use MR conditional monitoring, ventilation system and pump systems.
- Constantly monitor patients under sedation and unconscious patients
- Remove any unconnected devices, coils, or cables during the scan.
- **Keep the SAR (Specific Absorption Rate) monitoring system of the MR system ON at all times to ensure the safety of the patient, users, and devices** (the 31P coil does not have its own SAR monitoring system).
- The body coil must not be used to transmit while the magnet contains another coil which is in an oscillatory state at the same resonant frequency as that of the body coil.
- If the baby is sick or unstable during the MR scan, terminate the scan immediately and treatment of the patient will be initiated immediately in the side room. Resuscitaire and resuscitation trolley are prepared beforehand (see general guideline).

6. SOP specific to changing to the phosphorus coil

All babies who may undergo ^{31}P MRS will be prepared in the neonatal unit with the **"inside-coil-plastic"** in the Lammers incubator –which will keep the baby in place with the padding when coils are being changed- and the MR conditional **Nonin Medical® 7500FO monitoring** –as the Lammers monitoring needs to be turned off during ^{31}P MRS.

Although the Nonin Medical® monitor can be operated in an MR environment securely fasten (with a magnetic field of 1.5T or less, the device must be a minimum of 2 meters away from the magnet), we are **NOT introducing the monitor in the MR room**. The sensor will be disconnected when the incubator goes in the MR room and it will be thread through the wall. The monitor will be kept in the Radiographers room. During this time it can be plugged to the wall if the battery is low.

Once the clinical sequences have been completed (structural and H MRS), the doctor (neuroimaging fellow/ neonatologist, with security metal check cleared), the physicist and a radiographer will go into the scanning room.

If the baby is breathing on his own:

a) Plug off the Lammers coil and bring out the Lammers incubator, without losing the positioning.

b) Open the top lead of the Lammers and the top side door.

c) Lift slightly the Lammers' bed and pull out the lammers-coil.

d) Pass on the coil to the radiographer.

e) The physicist will pass on the phosphorus coil to you (which is kept on the grey box, on the right-hand side of the 3T scanner).

f) Lift slightly again the Lammers' bed and slide in the phosphorus coil.

g) Close both incubator's doors.

h) Turn off the Lammers incubator (button behind the screen of the incubator: bottom left) and the battery from the Lammers trolley.

i) There is no need to redo the positioning. Just press the centre button of the scanner (bottom one: the green light should light up) and bring the baby back in the scanner.

j) Once the scanner is finished, pull the bed out.

k) Change the coil back to the Lammers coil (read steps b-g, this time you can open the whole side opening).

l) Please clean the phosphorus coil (as mentioned previously) and leave it back on top of the box with the connection protected with its cap.

m) Transfer the incubator back to the Lammers trolley.

n) Turn on the Lammers monitoring and set up the temperature to what it was set to previously.

o) Turn on the trolley battery and plug in the incubator back to this battery.

p) Rest of the steps are as in the general 3T guideline.

If the baby is intubated and ventilated:

a) Plug off the Lammers coil and bring out the Lammers incubator, without losing the positioning.

b) Open the top lead of the Lammers and the whole side of the incubator.

c) Disconnect the ventilator from the ETT before sliding out the coil.

d) Lift slightly the Lammers' bed and pull out the Lammers-coil, keeping under control the ETT position.

e) Reconnect the ETT to the ventilator.

f) Pass on the coil to the radiographer.

g) The physicist will pass on the phosphorus coil to you (which is kept on the grey box, on the right-hand side of the 3T scanner) and leave in on the door ready to slide it in.

h) Disconnect the ventilator from the ETT before sliding in the coil.

i) Lift slightly the Lammers' bed and slide in the phosphorus coil.

j) Reconnect the ETT to the ventilator.

k) Close both doors and make sure the ETT is not kinked, and saturation of oxygen is adequate.

l) Turn off the Lammers incubator (button behind the screen of the incubator: bottom left) and the battery from the Lammers trolley.

m) There is no need to redo the positioning. Just press the centre button of the body coil (green-bottom one) and bring the baby back in the scanner.

n) Once the scan is finished, pull the bed out.

o) Change the coil back to the Lammers coil (read steps b-k).

q) Please clean the phosphorus coil (as mentioned previously and leave it back on top of the box with the connection protected with its cap.

p) Transfer the incubator back to the Lammers trolley.

q) Turn on the Lammers monitoring and set up the temperature to what it was set to previously. Turn on the trolley battery and plug in the incubator back to this battery.

r) Rest of the steps are as in the general 3T guideline.

If the baby is sick or unstable at any time during the MR scan, terminate the scan immediately and treatment of the patient will be initiated immediately in the side room. Equally if the baby is extubated at any point in time, bring either the incubator or the baby (depending on stability) to the side room. The Braun

Faraday cage containing the pumps will need to be wheeled out with the baby. Resuscitaire and resuscitation trolley are prepared beforehand (see general guideline).

7. Sequence in use

You will find the sequence in the structural spectroscopy folder (SURVEY and 31P MRS).

a) Run first the survey with the body-coil to check the positioning of the voxel (it should be **covering both basal ganglia and thalami**).

b) Once adjusted the position (if needed), please run the phosphorus sequence.

Set parameters are:

- ISIS, adiabetic pulse.
- TR/TE (ms): 2475 / 0.10
- NSA 8 x 45 **(can be shortened to 40-35-30; if needed to shorten the duration)**
- **Voxel size: 40 x 40 x 25 mm (this needs to be changed each time before running the sequence).**
- Length of scan: 14:51

Geometry: Nucleus P31 Offset frequency -270 Hz Coil selection: MC-Rapid-BM-MN Dual coil: no Preparation coil: Q-Body VOI orientation: transverse VOI size AP (mm): 40 RL (mm): 40 FH (mm): 25 Samples: 2048 Spectral BW: 3000	***Contrast:*** Scan type: spectroscopy Scan mode: SV Technique: FID VOI selection: volume Method: ISIS Echoes: 1 TE: shortest RF pulse set: adiabatic TR: 2475 ms Shim: PB-auto PB order: second B1 mode: default Gradient mode: max PNS mode: low SAR: <5%
Motion: NSA: 8 Phase cycles: 8 ***Dyn/angio:*** Dynamic study: individual Dyn scans: 45 Dyn scans time: shortest ASL: no	***Postprocessing:*** Receiver attenuation: 8 Reference tissue: WM Shifted metabolite: none.